

Soft-gluon resummation for high- $p_T$   
inclusive-hadron production at COMPASS



Dissertation

zur Erlangung des  
Doktorgrades der Naturwissenschaften  
(Dr. rer. nat.)  
der Fakultät für Physik  
der Universität Regensburg

vorgelegt von  
**Melanie Pfeuffer**  
aus Unterdeggenbach

Oktober 2013

Die Arbeit wurde von Prof. Dr. Andreas Schäfer angeleitet.

Das Promotionsgesuch wurde am 20. Juni 2013 eingereicht.  
Das Promotionskolloquium fand am 19. November 2013 statt.

**Prüfungsausschuss:**

Vorsitzender: Prof. Dr. F. Gießibl

1. Gutachter: Prof. Dr. A. Schäfer

2. Gutachter: Prof. Dr. W. Vogelsang

Weiterer Prüfer: Prof. Dr. K. Richter

# Contents

<b>Contents</b>	<b>i</b>
<b>Introduction</b>	<b>1</b>
<b>1. QCD as an SU(3) gauge theory</b>	<b>7</b>
1.1. The Lagrangian of QCD . . . . .	7
1.2. Asymptotic freedom . . . . .	9
1.3. Regularization and renormalization . . . . .	12
<b>2. Threshold resummation in the Drell-Yan cross section</b>	<b>17</b>
2.1. Drell-Yan: Fixed order (NLO) calculation . . . . .	18
2.2. Threshold resummation . . . . .	25
<b>3. Higher order QCD corrections and their asymptotic behavior</b>	<b>33</b>
3.1. Asymptotic series . . . . .	33
3.2. Problems with resummed exponents in physical space . . . . .	34
3.3. The Minimal Prescription formula . . . . .	39
<b>4. Threshold Resummation for single-particle inclusive cross sections</b>	<b>43</b>
4.1. The factorized cross section . . . . .	44
4.2. Refactorization of the partonic cross section . . . . .	45
4.3. Moments of the partonic cross section . . . . .	48
4.4. Soft and jet functions . . . . .	50
4.4.1. Light cone parton distribution $\Phi_{f/f}$ . . . . .	50
4.4.2. Center of mass parton distributions $\Psi_{f/f}$ . . . . .	52
4.4.3. Final-state jet . . . . .	54
4.4.4. Construction of the soft function from the eikonal cross section . . . . .	54
4.5. Resummation from factorization . . . . .	56
4.5.1. Renormalization of the hard and soft function . . . . .	57
4.5.2. Initial-state jets from the wave function ratio $\Psi/\Phi$ . . . . .	58
4.5.3. Final-state jets . . . . .	60
4.5.4. Final-state observed hadrons . . . . .	61
4.5.5. The resummed cross section . . . . .	61

<b>5. Calculation of hard, soft and anomalous dimension matrices in color space</b>	<b>65</b>
5.1. Basis of color tensors . . . . .	66
5.2. Lowest order hard and soft matrices . . . . .	72
5.2.1. Quark-antiquark annihilation processes $q\bar{q} \rightarrow q\bar{q}$ . . . . .	72
5.2.2. Gluon-gluon scattering $gg \rightarrow gg$ . . . . .	75
5.3. The soft anomalous dimension matrix . . . . .	76
<b>6. Rapidity-dependent threshold resummation for high-<math>p_T</math> hadron production</b>	<b>87</b>
6.1. Technical framework . . . . .	88
6.2. Rapidity-dependent resummed cross section . . . . .	91
6.2.1. Mellin moments and threshold region . . . . .	92
6.2.2. Rapidity-dependent resummation to next-to-leading logarithm . . . . .	93
6.2.3. Rapidity-dependent NLL exponents . . . . .	97
6.2.4. The direct contribution . . . . .	99
6.2.5. Inverse Mellin transform and matching procedure . . . . .	103
6.3. Fully rapidity-integrated resummed cross section . . . . .	105
6.3.1. Mellin moments and threshold region . . . . .	106
6.3.2. Moments of the Weizsäcker-Williams spectrum with cuts . . . . .	107
6.3.3. Fully rapidity-integrated resummed cross section to NLL accuracy . . . . .	108
<b>7. Phenomenological studies: Hadron production at COMPASS</b>	<b>115</b>
7.1. Comparison of theoretical prediction to experimental data . . . . .	115
7.2. Rapidity-dependent vs. rescaled fully rapidity-integrated resummation . . . . .	126
<b>8. Summary and Conclusions</b>	<b>133</b>
<b>A. Elements of QED and QCD: The Feynman rules</b>	<b>135</b>
<b>B. Mellin-<math>N</math> moments of Plus-distributions</b>	<b>141</b>
<b>C. Anomalous dimension-, soft- and hard- matrices</b>	<b>143</b>
<b>Bibliography</b>	<b>145</b>

# Introduction

It is rather unusual that a new result in particle physics appears at the front page of the main European and non-European newspapers. The observation of a new boson consistent with that of the predicted Higgs boson [1, 2] was able to arouse that high attention. Presently, this experiment is probably the most prominent one among numerous others performed at high-energy particle accelerators, which were set up to unravel unresolved questions and mysteries in particle physics. For instance, several measurements are made to understand protons - even though these are abundant and known for almost 100 years. Despite many years of experimental and theoretical studies with plenty of new important insights, some of their fundamental properties unveil their secrets only very slowly. Results of experiments intended to explore the spin structure of the proton back in the eighties turned out to be a great surprise and this puzzle became famous as the *nucleon's spin crisis*.

The beginnings of exploring spin-dependent observables reach back to 1922, when the concept of spin was developed to explain the measurements of Stern and Gerlach [3, 4]. Shortly after that, spin was also introduced as a fundamental observable in subatomic physics [5]. The story of the proton spin started in the late 1920s when the analysis of the specific heat [6] and of the band spectrum [7] of hydrogen molecules showed a discrepancy in quantities like their moment of inertia. Dennison [8] was able to resolve this discrepancy by concluding that the proton is a fermion of spin  $1/2$ .

With the goal of exploring the structure of the nucleon, elastic scattering experiments and in the late 1960s inelastic scattering experiments were performed. The famous SLAC (Stanford Linear Accelerator Center, USA) deep inelastic scattering experiments led to the quark parton model relying on the fact that a proton, when observed over short times, behaves as if it was built out of pointlike spin  $1/2$  particles - the quarks. More experiments followed, settled this picture and found that the quarks can occur in three different color-charges. This led to the development of quantum chromodynamics (QCD) - a non-Abelian SU(3) gauge theory of quarks and gluons and their interactions.

Soon experiments followed to investigate the spin structure of the nucleon. Polarized deep inelastic scattering experiments in the mid of 1970s should show that the proton spin is carried by its constituent partons. Therefore, polarized electrons were shot on polarized protons. First results of the SLAC experiments E80 [9] and E130 [10] showed large longitudinal double spin asymmetries as was predicted by the simple parton model. It

was thus all the more surprising that the European Muon Collaboration (EMC) at CERN found in 1988 in further measurements at a different kinematic region that only a small fraction of the proton spin is due to the quark spins [11, 12],

$$\Delta\Sigma \sim 30\%, \quad (1)$$

where  $\Delta\Sigma = \sum_q \Delta q \equiv \sum_q \int_0^1 dx [q_\uparrow(x) - q_\downarrow(x)]$  denotes the fraction of the nucleon spin due to quark spins with  $q_{\uparrow/\downarrow}(x)$  being the distributions for quarks with momentum fraction  $x$  and spin aligned (anti-aligned) to the proton spin. Contrarily to the simple quark model, the three valence quarks are only responsible for a small part of the proton spin. This puzzle of the missing spin became famous under the proton spin crisis. 25 years have passed since then and despite of several high precision experiments, the puzzle has not been resolved, yet. By angular momentum conservation the total spin of the nucleon is split not only onto the quarks but contains also a contribution from the gluon spin  $\Delta G = \int_0^1 dx \Delta g(x)$  (with  $g(x)$  the gluon helicity distribution with momentum fraction  $x$ ) and the quark and gluon orbital angular momenta  $L_q$  and  $L_g$ :

$$\frac{1}{2} = \frac{1}{2} \Delta\Sigma + L_q + \Delta G + L_g. \quad (2)$$

This is known as *spin sum rule* [13]. Like the quark spin contribution, also the gluon spin contribution is experimentally accessible and much effort on both - experimental and theoretical - side has been expended to constrain them. Several experiments like the lepton-nucleon scattering experiments HERMES at DESY (Deutsches Elektronen SYnchrotron, Hamburg), COMPASS at CERN, and the polarized proton-proton collision experiments RHIC at BNL (Brookhaven National Laboratory, Long Island) have been set up. New preliminary data at RHIC indicate a small positive contribution for  $\Delta g(x)$  over the range  $0.04 \leq x \leq 0.2$  [14] but still the errors are large and much more data are needed to determine the first moment of the gluon helicity distribution,  $\Delta G$ .

With the experiments reaching higher levels of precision, the need for high precision theoretical predictions becomes more and more urgent. The predictive power of QCD for high-energy hadronic scattering observables rests upon the ability to compute the corresponding cross section on parton level in perturbation theory. There, the quantity of interest is expanded in powers of the strong coupling constant  $\alpha_s$

$$\sigma = \sigma^{\text{LO}} + \alpha_s \sigma^{\text{NLO}} + \alpha_s^2 \sigma^{\text{NNLO}} \dots \quad (3)$$

The basic idea is that for sufficiently small expansion parameters, higher order terms should decrease with growing perturbative order. Thus the series may be truncated at some order allowing to restrict oneself on few lower order terms, but still being able to provide

a sufficiently precise approximative solution. The applicability of such a procedure typically depends crucially on the convergence behavior of the series. In case of observables in high energy experiments in the framework of perturbative QCD (pQCD), it was found that their power series are at best asymptotic. Nevertheless, in many cases this turns out to be sufficient to provide valuable information, which has impressively been shown by many perturbative calculations in the past. At the beginning of pQCD rather easy leading order (LO) calculations were performed, providing the basis only for qualitative analysis of experimental data. Quantitative predictions however require to go beyond LO, at least include next-to-leading order (NLO) contributions and thereby reduce theoretical uncertainties. Calculating also next-to-next-to leading order (NNLO) or going even to higher orders, increases the complexity of the calculation and is thus associated with immense effort or for some processes even nearly impossible with current techniques. Many theoretical effort was invested to push forward the NLO calculations for various processes offering access to the nucleon's polarized parton distributions, see for instance [15–21].

One of these are photoproduction processes in fixed-target lepton-nucleon scattering. These are of particular interest as its cross sections for high-transverse-momentum ( $p_T$ ) final states includes sizable contributions from the photon-gluon fusion subprocess  $\gamma g \rightarrow q\bar{q}$  and thus may be used to probe the nucleon's gluon distribution. The fixed target lepton scattering experiment COMPASS (and SLAC E155) makes use of this photoproduction process to constrain the polarized gluon distribution  $\Delta g$  [22]. This is hard to access in other lepton-nucleon scattering experiments like DIS and provides additional information to the polarized proton-proton-scattering at RHIC [23]. The extraction of the nucleon's gluon distribution from the experimental data is relatively complex. Photoproduction processes with quasi-real photons do not only include *direct* processes, in which the photon interacts directly with the partons of the nucleon, but the photon may also exhibit hadronic structure in the framework of QCD. Some of these *resolved* processes however depend not on the nucleon's gluon- but on its quark-distributions, which makes the overall dependence of the cross section on the gluon distributions more involved.

An interesting aspect from a theoretical point of view is due to the specific COMPASS kinematics, where the observed transverse momenta go down to  $p_T = 1 \text{ GeV}$ . Such a low hard scale brings the parton model idea and perturbative QCD to its limits and therefore allows to test the applicability of perturbative QCD at this kinematics.

An aspect that makes the COMPASS experiment quite challenging for the theoretical side is its fixed-target regime. The value of the hadron's transverse momentum over the available center-of-mass energy  $\sqrt{s}$  is relatively large, typically  $x_T = 2p_T/\sqrt{s} \gtrsim 0.1$ . Thus the partonic cross section is close to the threshold, where all available partonic center-of-mass energy is just used to produce the high-transverse momentum parton that subsequently hadronizes into the observed hadron, and its recoiling counterpart. Additional real

gluon radiation is strongly suppressed and therefore mostly constrained to the emission of soft and/or collinear gluons. This results in a strong imbalance between real and virtual gluon diagrams and the cancellation of infrared singularities leaves behind large logarithmic corrections to the leading order cross section. These are not only present in the NLO corrections, but appear also in all higher order contributions. At  $k$ th order of perturbation theory the leading logarithms are of the form

$$\alpha_s^k \ln^{2k}(1 - x_T^2), \quad (4)$$

with  $x_T$  denoting the hadronic scaling variable as before. These *threshold-logarithms* dominate the cross section in the kinematic region close to the threshold and thus have to be taken into account order-by-order. A technique that addresses these logarithms is known as *threshold resummation* and was initially developed for the Drell-Yan process [24, 25]. It was subsequently applied and extended to many other more involved partonic processes. For single-hadron production in  $pp \rightarrow hX$  [26] and for dihadron production  $pp \rightarrow h_1 h_2 X$  [27] in the fixed-target regime the resummed cross sections showed a quite substantial enhancement over the next-to-leading order ones, indicating that the NLO calculations are likely not fully sufficient. This might suggest that higher order soft-gluon contributions play also an important role for the process  $\gamma N \rightarrow hX$  in the fixed-target regime at COMPASS.

The main goal of this work is to investigate the relevance of higher-order QCD corrections of the unpolarized photoproduction reaction  $\gamma N \rightarrow hX$  in fixed-target scattering at COMPASS, where the hadron  $h$  is produced at large transverse momentum. In particular, we address large logarithmic threshold corrections to the rapidity dependent partonic cross sections, which we resum to all orders at next-to-leading accuracy and finally compare the resummed cross section to the experimental data. With a view to the polarized data, which are waiting to be analyzed also beyond NLO cross sections, it is also important to test the theoretical framework on the basis of the unpolarized measurements.

The thesis is organized as follows. Before going into details of resummation we start with a short overview of the fundamental concepts of perturbative QCD, which are vital for each perturbative calculation. In the following two chapters the Drell-Yan process will serve as introductory example to show the concept of threshold resummation. This process is particularly suitable as introductory example since its underlying partonic LO-process includes only two involved QCD particles and just consists of one channel. For comparison, in the case of hadron production we have to deal with four QCD particles and twelve different contributing channels. First, explicit expressions for the real and the virtual gluon NLO corrections of the Drell-Yan process are presented in order to demonstrate how the imperfect cancellation of their infrared singularities results in the large logarithms close to the partonic threshold. Then it is outlined how to obtain the resummed partonic cross



---

section that sums up these dominant contributions to all orders. Special emphasis is put on the asymptotic behavior of the power expansion of the resummed expression. Following the techniques developed in [28], Chap. 4 recalls how to generalize the threshold resummation for the Drell-Yan process to more complicated processes with four QCD-partons in the lowest order partonic process. Such processes appear in the resolved contribution of hadron photoproduction. While the leading soft-gluon logarithms (LL) associated with the radiative factor of each external parton are the same for QCD processes as for Drell-Yan, the next-to-leading logarithms (NLL) turn out to be different. There, the color structure of the corresponding hard scattering comes into play and influences the soft radiation near threshold. Chap. 5 is devoted to a more detailed look on some of the elements entering the resummed result. We show explicitly how to calculate these. In Chap. 6 we focus on the threshold resummation for the photoproduction of a hadron. We extend the previous work [26] by including rapidity dependence in resummation, following the technique developed in [27]. In our phenomenological studies in Chap. 7 we apply our developed resummed formalism to the fixed-target lepton-nucleon scattering experiment COMPASS at CERN [29, 30]. We study the role played by higher-order QCD corrections to the cross section close to the threshold region. Then we compare our results to the experimental data. Finally our conclusions are drawn in Chap. 8.

Parts of this work have been published in [31]. Whereas many details are omitted in the publication, we provide here all relevant formulas and details of the calculation. For a pedagogical structure of the thesis we also recall in Chap. 2 some of the results previously derived in the diploma thesis [32].



# 1. QCD as an SU(3) gauge theory

This chapter serves to give an overview of the basic concepts needed for any calculation in perturbative QCD (pQCD). This part will be rather short as there exists also a variety of textbooks on this topic. We begin with the QCD Lagrangian and show how the non-Abelian character of the gauge field results in a peculiarity of QCD: the *asymptotic freedom*. This means that the coupling constant  $\alpha_s(Q)$  decreases with growing energy  $Q$ . Another topic, one is inevitably faced with in pQCD calculations, is the regularization of infinite results. For that purpose we outline a prescription - the dimensional regularization - to handle the divergences showing up.

## 1.1. The Lagrangian of QCD

The fundamental theory of strong interactions is described by a non-Abelian Yang-Mills theory, named Quantum Chromodynamics (QCD) [33–35]. It is based on the classical Lagrangian

$$\mathcal{L}_{cl} = \sum_f^{N_f} \bar{\psi}_f (i\gamma_\mu D^\mu - m_f) \psi_f - \frac{1}{4} F_{\mu\nu}^a F^{a\mu\nu}, \quad (1.1)$$

which is invariant under Lorentz transformations and under local SU( $N$ ) gauge transformations (with  $N = 3$  for QCD) of the fermionic quark fields  $\psi_f$  with flavor  $f$  and mass  $m_f$ . There are  $N_f$  different quark fields, labeled by flavor  $f$ , interacting with the gauge fields  $A_\mu^a$  (the gluon fields). A remarkable feature of the Lagrangian, reflecting the underlying non-Abelian gauge theory, is that it includes self-interactions amongst the gauge fields through the term  $gf^{abc}A_\mu^b A_\nu^c$  in the field strength tensor  $F_{\mu\nu}^a$ ,

$$F_{\mu\nu}^a = \partial_\mu A_\nu^a - \partial_\nu A_\mu^a + gf^{abc}A_\mu^b A_\nu^c. \quad (1.2)$$

Here  $g$  is the strong coupling constant and  $f_{abc}$  are structure constants. These structure constants define the Lie algebra of the gauge group by the following commutation relation

$$[t^a, t^b] = if^{abc}t^c, \quad (1.3)$$

where the matrices  $t^a$  are a set of  $N^2 - 1$  independent generators of the group. They can be chosen such that they satisfy the normalization condition

$$\text{Tr} \left\{ t^a t^b \right\} = T_F \delta_{ab}. \quad (1.4)$$

The  $D_\mu$  in Eq. (1.1) is the covariant derivative, which ensures gauge invariance in the classical Lagrangian,

$$D_\mu = \partial_\mu - ig A_\mu^a t^a. \quad (1.5)$$

The classical Lagrangian, as given in Eq. (1.1), is constructed in such a way, that it is invariant under local gauge transformations. Due to this property, however, problems arise in its quantization. These are related to the large degeneracy between sets of gluon field configurations, which are all equivalent under gauge transformations [36]. The problems are solved by *gauge fixing* and *ghost fields*. The first mentioned term means to eliminate the freedom of the gauge transformations of the gluon fields  $A_\mu^a$ . This is achieved by adding the gauge fixing (GF) term

$$\mathcal{L}_{GF} = -\frac{1}{2\xi} (\partial^\mu A_\mu^a) (\partial^\nu A_\nu^a) \quad (1.6)$$

to the classical Lagrangian in Eq. (1.1). The gauge fixing term of the form given in Eq. (1.6) defines the set of covariant gauges. In principle, the choice of  $\xi$  is arbitrary, as it only contributes to the overall normalization and thus its value has no impact on any physical quantity. However, in order to simplify calculations, one may fix the gauge parameter  $\xi$ . A convenient choice is the *Feynman gauge*, where  $\xi = 1$ .

Another common gauge fixing density, also used in this thesis, is the *axial* or *physical gauge*. Here the gauge fixing function is defined by  $n \cdot A = 0$  with a fixed Lorentz vector  $n_\mu$ . Often, additional restrictions for the gauge vector  $n^2 = 1$  or  $n^2 = 0$  (light-cone gauge) are chosen. The corresponding gauge fixing term is

$$\mathcal{L}_{GF} = -\frac{1}{2\xi} (n \cdot A^a) (n \cdot A^a). \quad (1.7)$$

Furthermore, the choice of covariant gauges requires to add a ghost Lagrangian, which serves to eliminate the unphysical degrees of freedom of the gluon vector fields,

$$\mathcal{L}_{FP} = g f^{abc} \bar{\chi}^a \partial^\mu \left( A_\mu^c \chi^b \right) - \bar{\chi}^a \partial^\mu \partial_\mu \chi^a. \quad (1.8)$$

This method relies on the introduction of an octet of unphysical, anticommuting, fermionic scalar fields  $\chi^a$  [37], known as Faddeev-Popov ghost fields. The ghost fields ensure gauge invariance and current conservation. In contrast to covariant gauges, the axial gauge is

ghost-free.

Altogether the quantized QCD Lagrangian in the covariant gauge takes the following form

$$\begin{aligned}
 \mathcal{L}_{QCD} &= \mathcal{L}_d + \mathcal{L}_{GF} + \mathcal{L}_{FP} \\
 &= \sum_f^{N_f} \bar{\psi}_f (i\gamma_\mu D^\mu - m_f) \psi_f - \frac{1}{4} F_{\mu\nu}^a F^{a\mu\nu} \\
 &\quad - \frac{1}{2\xi} (\partial^\mu A_\mu^a) (\partial^\nu A_\nu^a) \\
 &\quad + g f^{abc} \bar{\chi}^a \partial^\mu (A_\mu^c \chi^b) - \bar{\chi}^a \partial^\mu \partial_\mu \chi^a.
 \end{aligned} \tag{1.9}$$

However, the introduction of a gauge fixing (and ghost) term brings a unlike consequence. The full quantum Lagrangian now violates the invariance under the classical local gauge transformations. This situation seems to be problematic as the formal proof of renormalization rests upon gauge symmetry. Nevertheless, one can show that  $\mathcal{L}_{QCD}$  underlies a new symmetry under extended local gauge transformations, called *BRS (Becchi-Rouet-Stora) transformations* [38]. The BRS symmetry allows to deduce generalized Ward-Takahashi identities (Slavnov-Taylor identities) [39, 40], which play a central role in the proof of the renormalizability of QCD.

## 1.2. Asymptotic freedom

As mentioned already above, the striking difference between QCD and an Abelian gauge field theory like QED resides in the non-Abelian term of the field strength tensor. It accounts for self-interactions amongst the gluons. These gluon self-interactions are mainly responsible for the property, which makes non-Abelian theories amenable for a perturbative approach: the *asymptotic freedom*. This phenomenon states that the interaction strength  $g$  becomes smaller the smaller the distance between two particles becomes. Since in pQCD we make an expansion in the strong coupling constant, small coupling constants are crucial for the applicability of perturbation theory.

How can we derive the behavior of the coupling constant? The renormalization of QCD brings in a renormalization scale  $\mu$ . Then the coupling, the masses and the gauge-fixing parameter  $\xi$  depend on the renormalization scale  $\mu$ . However the physical quantities cannot depend on the artificially introduced  $\mu$ . This implies certain constraints on the dependence of the strong coupling constant

$$\alpha_s(\mu^2) = \frac{g^2(\mu)}{4\pi}, \tag{1.10}$$

which may be written as differential equation

$$\mu \frac{d\alpha_s(\mu)}{d\mu} = \beta(\alpha_s(\mu)). \quad (1.11)$$

This differential equation is the famous *renormalization group equation*. The QCD  $\beta$ -function is perturbatively calculable

$$\beta(\alpha_s) = -\alpha_s^2 \left( \frac{\beta_0}{4\pi} + \frac{\beta_1}{(4\pi)^2} \alpha_s + \frac{\beta_2}{(4\pi)^3} \alpha_s^2 + \dots \right). \quad (1.12)$$

Its first three coefficients are given by

$$\beta_0 = \frac{11}{3}C_A - \frac{2}{3}N_f \quad (1.13)$$

$$\beta_1 = \frac{34}{3}C_A^2 - \frac{10}{3}C_A N_f - 2C_F N_f \quad (1.14)$$

$$\beta_2 = - \left( \frac{11}{9}C_F + \frac{79}{54}C_A \right) N_f^2 - \left( C_F^2 - \frac{205}{18}C_F C_A - \frac{1415}{54}C_A^2 \right) N_f - \frac{2857}{54}C_A^3$$

where  $N_f$  is the number of flavors of quarks with mass less than the energy scale  $\mu$  and  $N_c$  denotes the number of colors.  $\beta_2$  was calculated in [41] for the  $\overline{\text{MS}}$  scheme.  $\beta_3$  is also available and given in [42]. The origin of asymptotic freedom lies in the fact that  $\beta_0$  is positive, which implies that  $\beta$  is negative. The sign of  $\beta_0$  in QCD results from fermionic and - unlike QED - additional non-Abelian interactions. While fermions (in QCD given by quarks, in QED represented by leptons) in general give a positive contribution, the non-Abelian terms proportional to  $C_A$  have the opposite sign. Provided that  $N_f < 17$ , this gives an overall negative  $\beta$ . Thus, as the right hand side of Eq. (1.11) is negative for small  $\alpha_s$ , the effective coupling decreases with growing  $\mu$ .

The differential equation Eq. (1.11) is only exactly solvable at LO

$$\alpha_s(\mu^2) = \frac{\alpha_s(\mu_0^2)}{1 + \beta_0 \alpha_s(\mu_0^2) \ln(\mu^2/\mu_0^2)} \quad (1.15)$$

At next-to-leading order,  $\alpha_s(\mu^2)$  is given implicitly by

$$\begin{aligned} \ln \left( \frac{\mu^2}{\mu_0^2} \right) &= \int_{\alpha_s(\mu_0^2)}^{\alpha_s(\mu^2)} \frac{dx}{\beta(x)} = - \int_{\alpha_s(\mu_0^2)}^{\alpha_s(\mu^2)} \frac{dx}{x^2 \left( \frac{\beta_0}{4\pi} + \frac{\beta_1}{(4\pi)^2} x \right)} \\ &= - \frac{(4\pi)^2}{\beta_0^2} \int_{\alpha_s(\mu_0^2)}^{\alpha_s(\mu^2)} dx \left( \frac{\beta_0}{4\pi x} - \frac{\beta_1}{(4\pi)^2 x} + \frac{\beta_1^2}{\beta_0(4\pi)^3 + x\beta_1(4\pi)^2} \right) \end{aligned} \quad (1.16)$$

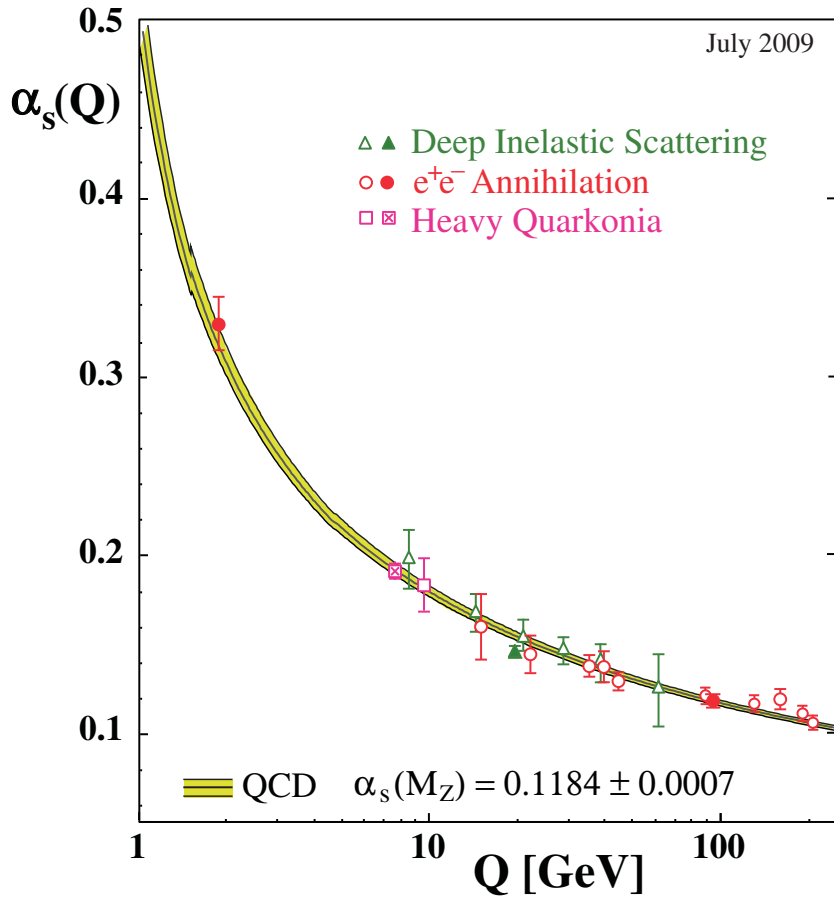


Fig. 1.1.: The running coupling constant  $\alpha_s(\mu)$ . The figure is taken from [43].

This gives

$$\beta_0 \ln \left( \frac{\mu^2}{\mu_0^2} \right) = \left[ \frac{4\pi}{\alpha_s(Q^2)} + \frac{\beta_1}{\beta_0} \ln \left( \frac{\alpha_s(Q^2)}{\beta_0 + \frac{\alpha_s(Q^2)}{4\pi} \beta_1} \right) \right]_{\mu_0^2}^{\mu^2}. \quad (1.17)$$

As soon as the value of  $\alpha_s(\mu_0^2)$  is known at one reference scale  $\mu_0$ , it is possible to solve this equation for any other scale  $\mu$  - provided that  $\mu$  is still in the perturbative region. It is common convenience to choose the reference scale as  $\mu_0 = \Lambda_{\text{QCD}}$ , the energy scale at which non-perturbative effects become important and at which the boundary condition  $\alpha_s(\Lambda_{\text{QCD}}^2) = \infty$  is used. Therefore, in terms of  $\Lambda_{\text{QCD}}$  one obtains,

$$\beta_0 \ln \left( \frac{\mu^2}{\Lambda_{\text{QCD}}^2} \right) = \frac{4\pi}{\alpha_s(\mu^2)} + \frac{\beta_1}{\beta_0} \ln \left( \frac{\alpha_s(\mu^2)}{\beta_0 + \frac{\alpha_s(\mu^2)}{4\pi} \beta_1} \right). \quad (1.18)$$

This again is an implicit equation for  $\alpha_s(\mu^2)$ . Expanding in powers of  $1/\ln(\mu^2/\Lambda_{\text{QCD}}^2)$ , yields the approximate solution

$$\frac{\alpha_s(\mu)}{4\pi} = \frac{1}{\beta_0 \ln(\mu^2/\Lambda_{\text{QCD}}^2)} - \frac{\beta_1 \ln[\ln(\mu^2/\Lambda_{\text{QCD}}^2)]}{\beta_0^3 \ln^2(\mu^2/\Lambda_{\text{QCD}}^2)} + \mathcal{O}\left(\frac{1}{\ln^3(\mu^2/\Lambda_{\text{QCD}}^2)}\right). \quad (1.19)$$

$\Lambda_{\text{QCD}}$  defines the fundamental scale parameter of the coupling in QCD. Its value must be determined from experiments and is about  $\Lambda_{\text{QCD}} \sim \mathcal{O}(200 \text{ MeV})$ , that corresponds to the mass scale of hadronic physics as the pion mass or roughly an inverse hadron size.

The solution of  $\alpha_s(\mu)$  in Eq. (1.19) illustrates the asymptotic freedom property:  $\alpha_s \rightarrow 0$  as  $\mu \rightarrow \infty$ . In experiments the prediction of the logarithmic decrease of  $\alpha_s$  with the energy could be verified over wide energy scales, as may be seen in Fig. 1.1.

The explicit relation of the coupling constant of one scale  $\mu$  to another one  $\mu_0$  is obtained by substituting

$$\Lambda_{\text{QCD}}^2 = \mu_0^2 \exp\left[-\frac{4\pi}{\beta_0 \alpha_s(\mu_0^2)}\right] \quad (1.20)$$

in Eq. (1.19), yielding

$$\alpha_s(\mu^2) = \frac{\alpha_s(\mu_0^2)}{X} \left(1 - \frac{\beta_1}{\beta_0} \alpha_s(\mu_0^2) \frac{\ln X}{X}\right), \quad \text{with } X = 1 + \beta_0 \alpha_s(\mu_0^2) \ln\left(\frac{\mu^2}{\mu_0^2}\right), \quad (1.21)$$

which is accurate to next-to-leading order.

The asymptotic freedom is one of the most basic theorems for any perturbative calculation. For this important discovery Gross, Wilczek [44] and Politzer [45] were awarded the 2004 Nobel Prize for Physics.

Now that we settled the Lagrangian for Quantum Chromodynamics and have shown the asymptotic freedom, the diagrammatic Feynman rules may be derived from the Lagrangian. They provide a systematic way to calculate amplitudes and matrix elements order-by-order in perturbation theory. We collect the Feynman rules together with some useful properties of Dirac spinors in Appendix A.

### 1.3. Regularization and renormalization

Calculating corrections to amplitudes by simply applying Feynman rules, we encounter a problem: While in leading order the calculation is straightforward and the result is finite, higher order diagrams turn out to give infinite results. In massless QCD three different kinds of divergences occur:

- **Collinear divergences**, also known as mass singularities, arise when a massless field couples with another massless field or with itself. The emission of massless particles moving collinearly to the initial on-shell massless particle produces a collinear divergence. The collinear divergences are factorized from the hard partonic scattering



cross section and absorbed in the definition of the parton distribution functions.

- ***Soft or infrared divergences*** emerge in theories including massless particles like photons in QED and gluons in QCD. Massless on-shell particles can emit particles like gluons with arbitrary low momentum. Such low momentum gluons are called *soft* gluons. The emission of soft gluons generates singularities in the matrix elements at vanishing gluon momentum. Integrating out the phase space then gives divergences. The occurrence of soft divergences are due to the setup of the theory. As we can not detect an arbitrary soft gluon experimentally, we can not distinguish the final state of a single quark  $|q\rangle$  from the final state of a quark and a soft gluon  $|qg\rangle$ . Thus, the physical observable is a quantity which contains all of these non-distinguishable contributions. And from a theoretical point of view it turns out, that adding these contributions yields a cancellation of the soft divergences order-by-order. This was first shown in QED by Bloch and Nordsieck [46] and the complete proof of the *Bloch-Nordsieck theorem* may be found in [47, 48]. In QCD there is the *Kinoshita-Lee-Nauenberg theorem* [49, 50], which reads: In a theory with massless fields, transition rates are free of the infrared divergence if the summation over the initial and final degenerate states is carried out.

A quark and an arbitrary amount of soft gluons belong to the same energy-eigenstate as a single quark and are thus degenerate. Thus, according to the Kinoshita-Lee-Nauenberg theorem the infrared divergences showing up in the calculation of single diagrams, have to cancel at the end.

- ***Ultraviolet divergences*** arise in the large-momentum limit of closed loop integrals. Physics at the general laboratory energy scale is supposed to be independent of casual fluctuations on the Planck scale  $E_{\text{Pl}} \sim 10^{19}$  GeV, a range, where gravity effects also come into play. Thus, at energy scales, at which QED and QCD are valid, high loop momentum contributions to amplitudes have to be suppressed. This procedure is called *renormalization*. Basically it proceeds in two steps. First, a regulator is introduced to identify all divergent diagrams. In the second step, a so called *counter term* Lagrangian is added to the original (unrenormalized) Lagrangian such that the ultraviolet divergences of the resulting renormalized Lagrangian are removed. The central subject of each renormalization proof is to show, that a finite number of counterterms (renormalization constants) is sufficient to cancel all the divergences in Feynman integrals at any order.

In QCD the fields are redefined by

$$A_\mu^a = Z_3^{1/2} A_{r\mu}^a, \quad \chi^a = \tilde{Z}_3^{1/2} \chi_r^a, \quad \psi = Z_2^{1/2} \psi_r \quad (1.22)$$

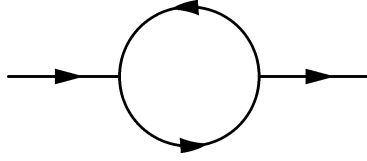


**Fig. 1.2.:** Logarithmic divergent scalar one-loop self-energy diagram

and the parameters  $g$ ,  $m$ ,  $\xi$  are redefined by

$$g = Z_g g_r, \quad m = Z_m m_r, \quad \xi = Z_3 \xi_r, \quad (1.23)$$

where  $Z_3, \tilde{Z}_3, Z_2$  and  $Z_g, Z_m$  are the gluon-field, ghost-field, quark-field, the coupling constant and the mass renormalization constants, respectively. The gauge-fixing parameter  $\xi$  is associated with the same renormalization constant  $Z_3$  as the gluon fields in order to keep the gauge-fixing term  $\mathcal{L}_{GF}$  in the same form. Also the other renormalization constants are not independent. They may be related among each other via the Slavnov-Taylor identities, which follow from the BRS-symmetry of  $\mathcal{L}_{QCD}$ .

As part of the renormalization proof, one has to specify exactly, how the renormalization constants are to be fixed. In a fixed order perturbative calculation the renormalization constants  $Z_i$  amount to a subtraction of the divergent part from the Green functions. This contains a certain amount of arbitrariness of how to define a divergent piece in a Green function, i.e., how much of the finite piece is to be subtracted together with the infinity. Therefore, a certain prescription has to be chosen.

A convenient regulator for divergent integrals in QCD is the *dimensional regularization* method, introduced by [51, 52]. The basic idea is to analytically continue the dimensionality of space-time to values  $D \neq 4$ . In this way, divergent integrals are made convergent by reducing or increasing the value of space-time dimensions. To make the idea clear, consider the scalar one-loop self-energy in Fig. 1.2. Its contribution is given by

$$S(p) = - \int \frac{d^D k}{(2\pi)^4} \frac{1}{(k^2 - m^2 + i\epsilon)[(p - k)^2 - m^2 + i\epsilon]}. \quad (1.24)$$

For  $D = 4$  dimensions, the expression is logarithmically (ultraviolet) divergent. However, the divergent behavior can be cured by reducing the number of dimensions by  $2\epsilon$  with  $\epsilon > 0$ . Then the exponent of the integrand  $\sim \frac{1}{k^4}$  is larger than the number of dimensions  $D = 4 - 2\epsilon$  in the limit of large momenta and the expression converges. The original

divergent integral results in an expression with a pole in  $\epsilon$  at  $D = 4 - 2\epsilon$ . The technique of dimensional regularization is described in [36, 53, 54] in detail.

Dimensional regularization is a very suitable regularization scheme for gauge theories, as it preserves the local symmetries in the Lagrangian such as gauge invariance. Therefore - though now in  $D$  dimensions - the structure of the QCD Lagrangian remains unaltered. The only change that is required is to replace  $g \rightarrow g\mu^\epsilon$  [52], where  $\mu$  is an arbitrary unit mass. This is necessary in order to ensure that each term in the Lagrangian density has the correct mass dimension [36].

The concept of dimensional regularization is able to tackle the ultraviolet divergences as well as infrared divergences. For infrared divergent diagrams one chooses  $\epsilon < 0$  to render them finite. As mentioned already before, their poles will cancel at each order due to the Kinoshita-Lee-Nauenberg theorem. Before the renormalization procedure is applied, the ultraviolet divergences in an  $N$ -loop amplitude manifest themselves as poles in  $1/\epsilon$ , leading to the Laurent expansion

$$\sum_{n=0}^N \left( \frac{\alpha_s}{4\pi} \right)^n \frac{C_n}{\epsilon^n} + \mathcal{O}(\epsilon), \quad (1.25)$$

where the coefficients  $C_n$  depend on the external momenta and an arbitrary mass  $\mu$ . For each order in  $\alpha_s$ , the exponent of the pole in  $1/\epsilon$  increases by one. Carrying out the renormalization procedure, removes these poles. The remaining finite renormalized result depends on which renormalization scheme is chosen. The most commonly used scheme in perturbation theory is the *modified minimal subtraction* or  $\overline{\text{MS}}$  scheme [55]. In this scheme one makes use of the fact that it is an artefact of dimensional regularization that the pole term  $1/\epsilon$  always appears in combination with the finite constants  $-\gamma_E + \ln 4\pi$ . Subtracting these terms along with the pole simplifies the result.

With these basic concepts, important for any perturbative calculation, at hand we are now ready to turn to the NLO calculation of the Drell-Yan cross section. In the following chapter we will see explicitly, where soft and collinear divergences emerge in the NLO correction.



## 2. Threshold resummation in the Drell-Yan cross section

The Drell-Yan process, the production of a lepton pair in high-energy hadron-hadron collisions, has historically been and presently still keeps on to be a process of high importance. Experimentally, massive muon pair production via the Drell-Yan process was first measured by firing a proton beam on a fixed uranium target at the Brookhaven National Laboratory [56]. Although at that time the Drell-Yan process was theoretically just known in LO, the explanation of S. Drell and T.-M. Yan [57] that the muon pair stems from the annihilation of a quark and an antiquark into a virtual photon, lead to establish the parton model to hadron collisions. It was possible to relate the results of Drell-Yan experiments to experimental results of deep inelastic lepton-hadron scattering processes through the parton distribution functions.

Since then, much effort was made on the theoretical side to calculate higher order corrections. The unpolarized [58–60], longitudinally polarized [61–64], and transversely polarized [65, 66] NLO correction were derived. Later on, the unpolarized [67–70] and longitudinally polarized [71] NNLO calculations followed. But not only higher full fixed order calculations yield a more precise theoretical understanding, there were also single terms identified giving the largest contributions in specific kinematical situations, in which the invariant mass of the lepton pair approaches the center-of-mass energy of the collision. The proof that these terms recur order-by-order and may be calculated by exponentiating lower order diagrams, opened the door to threshold resummation. The pioneering work was by [24, 25] and the generalization of how to include rapidity-dependence was derived to next-to-leading logarithmic (NLL) accuracy in [72]. In [73] the resummation has been extended to next-to-next-to-leading logarithmic order (NNLL) order.

Nowadays the Drell-Yan process is perhaps the theoretically best explored process at hadron colliders. In addition, it has large production rates and shows a clean experimental signature. The combination to be theoretically precisely calculable as well as experimentally measurable with high accuracy makes the process very suitable for a multitude of applications. It provides precise QCD tests, is used for detector calibration, provides important information on parton distribution functions, and serves as background for new physics searches. Furthermore, many of the theoretical techniques developed for the Drell-Yan process, may be taken over to other processes like the Higgs production in the gluon-

gluon fusion process [74, 75].

In the first part of this chapter we concentrate on the NLO correction of the Drell-Yan process. By looking on the real and the virtual gluon contributions separately, one can directly see how the infrared divergences cancel. However, close to the partonic threshold almost all available energy is just used to produce the lepton-pair and almost no phase space is left over to radiate additional partons. Thus the real gluon emission is restricted to soft (or collinear) gluon emission. This results in a strong imbalance between the real and the virtual gluon contributions, leading to large logarithmic terms. These terms, which also appear in higher order corrections, can be summed up via threshold resummation, a technique, which is introduced in the second section of the present chapter. As the threshold resummation of the Drell-Yan process has been already addressed in the diploma thesis [32] we will restrict here just on the most important steps and results and otherwise refer to the previous work and references therein.

## 2.1. Drell-Yan: Fixed order (NLO) calculation

We consider the production of a lepton pair with invariant mass  $M$  in a high energy hadronic collision at a center-of-mass energy  $\sqrt{s}$  of hadrons  $H_1, H_2$ . Up to power corrections  $1/M^2$  [24, 76] the Drell-Yan cross section may be factorized as

$$\frac{d\sigma(\tau)}{dM^2} = \sigma_B \sum_{a,b} \int_{\tau}^1 \frac{dx_1}{x_1} \int_{\tau/x_1}^1 \frac{dx_2}{x_2} f_{a/H_1}(x_1, \mu_f) w_{ab}(z \equiv \tau/x_1 x_2, M^2, \mu_f^2) f_{b/H_2}(x_2, \mu_f), \quad (2.1)$$

in an infrared safe, short range hard scattering function  $w_{ab}$ , which may be calculated in perturbation theory, and in the parton distribution functions  $f_{a/H_i}$ , which are non-perturbative and are fitted from experimental data. This factorization requires the introduction of a factorization scale  $\mu_f$ , on which both functions,  $w_{ab}$  and the parton distribution functions  $f_{a/H_i}$ , depend on. In principle, the specific choice of  $\mu_f$  is arbitrary. Nevertheless it should be of the order of the hard scale such that the scale dependence is minimized. The parton distribution functions  $f_{a/H_1}(x_1, \mu_f)$  and  $f_{b/H_2}(x_2, \mu_f)$  of the hadrons  $H_1$  and  $H_2$  are evolved to this scale and depend additionally on the corresponding momentum fraction  $x_{1,2}$  transferred to partons  $a$  and  $b$ . The sum in Eq. (2.1) extends over all possible partonic channels. For a fixed invariant mass  $M$  the hadronic scaling variable is given by

$$\tau = \frac{M^2}{s}. \quad (2.2)$$

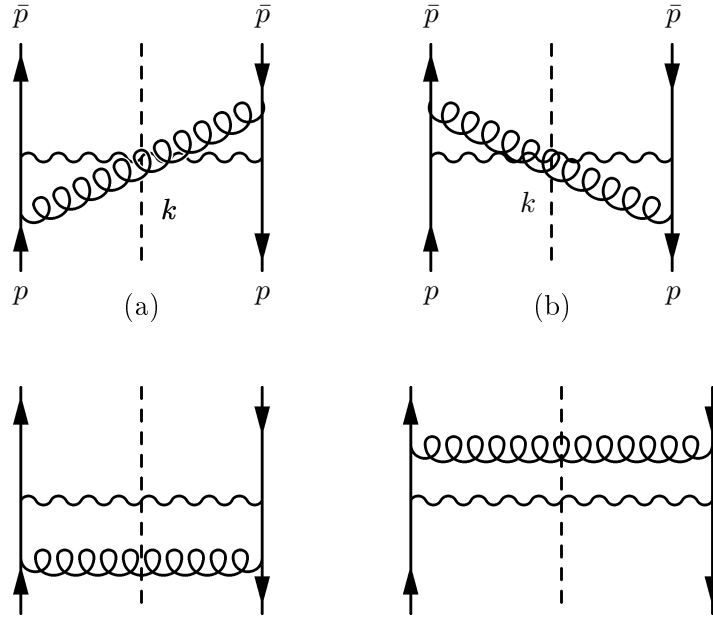


**Fig. 2.1.:** The cut diagrams  $q\bar{q} \rightarrow \gamma^* g$  for real gluon emission in the  $\mathcal{O}(\alpha_s)$  Drell-Yan process. Cut diagrams are a simple technique commonly used for the calculation of modulus squared matrix elements. All lines, which are cut by the vertical dashed line, are incoming or outgoing particles on the mass shell, whereas all other interior lines represent virtual particles. Furthermore all vertices and propagators on the right hand side of the cut have to be taken complex conjugated.

The hard scattering functions depend on the partonic analogon of this quantity,

$$z = \frac{\tau}{x_1 x_2} \equiv \frac{M^2}{\hat{s}}, \quad (2.3)$$

where the last equation serves to define the partonic center-of-mass energy  $\hat{s}$ . At leading order in perturbation theory a quark with momentum  $p$  and an antiquark with momentum  $\bar{p}$  annihilate into a photon, which in turn produces the lepton-antilepton pair. The normalization factor

$$\sigma_B = \frac{4\pi\alpha^2}{9sM^2} \quad (2.4)$$

is chosen, such that we have at leading order:

$$w_{q\bar{q}} = \delta \left( 1 - \frac{\tau}{x_1 x_2} \right). \quad (2.5)$$

Let us now consider how the diagrams look like in next-to-leading order (NLO) of perturbation theory. The  $\mathcal{O}(\alpha_s)$  corrections of the annihilation diagram include real and virtual corrections. Apart from the annihilation diagrams in NLO two further partonic channels,  $qg \rightarrow q\gamma^*$  and  $\bar{q}g \rightarrow \bar{q}\gamma^*$ , show up. However, as resummation at NLL precision has no contributions by these channels, we only will focus on the annihilation diagrams. For all

results shown, dimensional regularization in  $4 - 2\epsilon$  dimensions was used.

The real contributions of quark-antiquark annihilation into a virtual photon arise from the emission of one real gluon from the incoming quark or antiquark. Their cut diagrams are shown in Fig. 2.1. With the gluon momentum denoted with  $k$ , the total real contribution to the first order QCD correction of the four real-gluon contributions reads

$$\left. \frac{1}{\hat{\sigma}_B} \frac{d\hat{\sigma}}{dM^2} \right|_{real} = 4\alpha_s C_F \mu^{2\epsilon} \left\{ (1 - \epsilon) \left( \frac{\hat{u}}{\hat{t}} + \frac{\hat{t}}{\hat{u}} \right) + \frac{2\hat{s}M^2}{\hat{u}\hat{t}} - 2\epsilon \right\} PS_{q\bar{q} \rightarrow \gamma^* g}^{(2)} \quad (2.6)$$

in terms of the Mandelstam variables

$$\hat{s} = (p + \bar{p})^2, \quad \hat{t} = (p - k)^2, \quad \hat{u} = (\bar{p} - k)^2. \quad (2.7)$$

The scale  $\mu$  showing up in Eq. (2.6) was introduced during dimensional regularization.  $PS_{q\bar{q} \rightarrow \gamma^* g}^{(2)}$  is the two-particle phase space of the virtual photon and the gluon. In the next step this phase space integration is performed. To see the dependence on the angle explicitly, we express the Mandelstam variables in terms of

$$y \equiv \frac{1}{2}(1 + \cos \theta), \quad (2.8)$$

such that

$$\hat{s} = \frac{M^2}{z}, \quad \hat{t} = -\frac{M^2}{z}(1 - z)(1 - y) = -\sqrt{\hat{s}}|k|(1 - \cos \theta), \quad \hat{u} = -\frac{M^2}{z}(1 - z)y. \quad (2.9)$$

Then one arrives at

$$\begin{aligned} \left. \frac{1}{\hat{\sigma}_B} \frac{d\hat{\sigma}}{dM^2} \right|_{real} = & \frac{\alpha_s}{2\pi} C_F \left( \frac{4\pi\mu^2}{M^2} \right)^\epsilon \frac{1}{\Gamma(1 - \epsilon)} z^\epsilon (1 - z)^{1-2\epsilon} \int_0^1 dy (y(1 - y))^{-\epsilon} \\ & \times \left[ (1 - \epsilon) \left( \frac{1 - y}{y} + \frac{y}{1 - y} \right) + \frac{2z}{(1 - z)^2 y(1 - y)} - 2\epsilon \right]. \end{aligned} \quad (2.10)$$

This expression shows explicitly why regularization techniques are necessary. In four space-time dimensions, corresponding to  $\epsilon = 0$ , singularities show up. One can differ two types: First, the integral is divergent for  $y \rightarrow 0$  and  $y \rightarrow 1$ , which corresponds to the angles  $\theta = 180^\circ, 0^\circ$ . These singularities are known as *collinear divergence*, as they arise when the emitted gluon and the quark are moving parallel. Singularities of this kind are absorbed into the definition of the parton densities. The second type of singularities in Eq. (2.10) is the *soft divergence*. It arises when  $z \rightarrow 1$ , being equivalent to the situation when  $M^2$  approaches the partonic center-of-mass energy squared  $\hat{s}$  and only low energy gluons (soft gluons) can be emitted. This time, the divergence cannot be absorbed in the parton distribution functions, as the singular terms depend on the momentum transfer in the hard



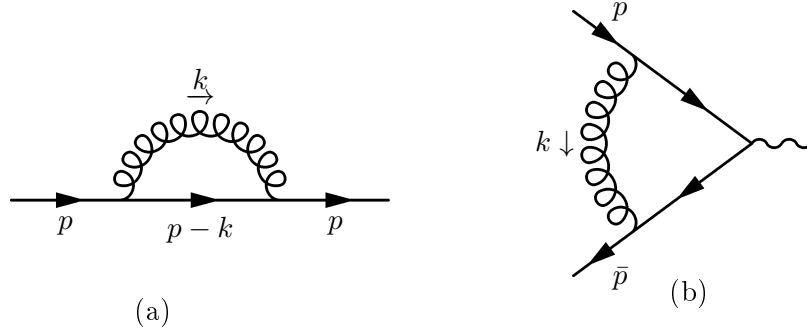


**Fig. 2.2.:** The  $\mathcal{O}(\alpha_s)$  virtual gluon correction consists of (a) the self energy contributions and (b) the vertex correction.

process and the final states. These kind of divergences have to cancel at the end of the day, after taking also the virtual contributions into account. However, we will see, that this cancellation leaves behind large logarithmic contributions at the partonic threshold. After performing the integration over the angular variable  $y$  in Eq. (2.10), we can manifesting the singular terms in a more direct way, if we make use of the plus prescription. *Plus-functions* mathematically are distributions. They are defined according to

$$f_+(x) = \lim_{\beta \rightarrow 0} \left( \theta(1 - \beta - x) f(x) - \delta(1 - \beta - x) \int_0^{1-\beta} dy f(y) \right). \quad (2.11)$$

This allows us to reveal the  $\epsilon$ -singularities completely. The real gluon contribution to the  $\mathcal{O}(\alpha_s)$  Drell-Yan cross section, neglecting again terms proportional to  $\epsilon$  reads:

$$\begin{aligned} \frac{1}{\hat{\sigma}_B} \frac{d\hat{\sigma}}{dM^2} \Big|_{real} &= \frac{\alpha_s}{2\pi} C_F \left( \frac{4\pi\mu^2}{M^2} \right)^\epsilon \frac{\Gamma(1-\epsilon)}{\Gamma(1-2\epsilon)} \\ &\times \left[ \frac{2}{\epsilon^2} \delta(1-z) - \frac{2}{\epsilon} \frac{1+z^2}{(1-z)_+} + 4(1+z)^2 \left( \frac{\ln(1-z)}{1-z} \right)_+ - 2 \frac{1+z^2}{1-z} \ln z \right]. \end{aligned} \quad (2.12)$$

We see, that the infrared divergent contribution results in a  $1/\epsilon^2$ -pole. This will cancel after adding the virtual contributions.

Now let us turn to the  $\mathcal{O}(\alpha_s)$  virtual gluon correction. As Fig. 2.2 shows, it consists of the self energy contributions and the vertex correction. Using Landau gauge ( $\xi \rightarrow 0$ ) in the gluon propagator, the self energy turns out to be zero. Even beyond that, one can show [53], that for any choice of  $\xi$  it is consistent to set the self energy equal to zero, provided that the quark line is on shell, as it is the case here. Thus it is sufficient to calculate the vertex correction. It is given by

$$\Gamma_\nu = C_F \int \frac{d^4 k}{(2\pi)^4} \frac{-i}{k^2} \frac{i}{(p-k)^2} \frac{i}{(\bar{p}+k)^2} (ig)^2 (-\tilde{\Gamma}_\nu), \quad (2.13)$$

with the definition

$$\tilde{\Gamma}_\nu = \gamma_\mu(\not{p} + \not{k})\gamma_\nu(\not{p} - \not{k})\gamma^\mu. \quad (2.14)$$

Performing the loop integral using dimensional regularization in  $D = 4 - 2\epsilon$  dimensions and assembling everything together<sup>1</sup>, the virtual  $q\bar{q}$  annihilation contribution turns out to be

$$\begin{aligned} \frac{1}{\hat{\sigma}_B} \frac{d\hat{\sigma}}{dM^2} \Big|_{\text{virtual}} &= \frac{\alpha_s}{2\pi} C_F \left( \frac{4\pi\mu^2}{M^2} \right)^\epsilon \frac{\Gamma(1-\epsilon)}{\Gamma(1-2\epsilon)} \times \\ &\times \left[ -\frac{2}{\epsilon^2} - \frac{3}{\epsilon} - 8 + \frac{2}{3}\pi^2 + \mathcal{O}(\epsilon) \right] \delta(1-z). \end{aligned} \quad (2.15)$$

Adding the real, Eq. (2.12), and the virtual correction, Eq. (2.15), yields

$$\frac{1}{\hat{\sigma}_B} \frac{d\hat{\sigma}_{q\bar{q}}^{(1)}}{dM^2} = \frac{\alpha_s}{\pi} \tilde{w}_{q\bar{q}}^{(1)} - \frac{\alpha_s}{\pi} P_{qq}^{(0)}(z) \left( \frac{4\pi\mu^2}{M^2} \right)^\epsilon \frac{\Gamma(1-\epsilon)}{\Gamma(1-2\epsilon)} \frac{1}{\epsilon}, \quad (2.16)$$

where

$$\tilde{w}_{q\bar{q}}^{(1)} = C_F \left\{ 2(1+z^2) \left( \frac{\ln(1-z)}{1-z} \right)_+ - \frac{1+z^2}{1-z} \ln z + \left( \frac{1}{3}\pi^2 - 4 \right) \delta(1-z) \right\}. \quad (2.17)$$

Note that now there is no  $1/\epsilon^2$  pole any more. This cancellation between the real and virtual diagrams reflects the cancellation of the infrared divergences. The only remaining pole terms stem from collinear divergences due to the gluon radiation parallel to the directions of the incoming quark and antiquark. These pole terms are absorbed into the parton distributions. As it was the case for renormalization, the way how to separate the hard-scattering from the parton distribution functions is not unique but depends on the choice of factorization scheme. We follow the  $\overline{\text{MS}}$  scheme [55], which uses an explicit definition of the parton distribution functions in terms of hadronic matrix elements [77]. It is given as expectation value of a number operator in the hadronic state,

$$f_{f/H}(x, \mu^2) = \int \frac{d^2\mathbf{k}_T}{(2\pi)^2} \langle H(p) | b_f^\dagger(xp, \mathbf{k}_T) b_f(xp, \mathbf{k}_T) | H(p) \rangle, \quad (2.18)$$

where the operators  $b_f(xp, \mathbf{k}_T)$  and  $b_f^\dagger(xp, \mathbf{k}_T)$  annihilate and create a parton of type  $f$  with longitudinal momentum  $xp$  and transverse momentum  $\mathbf{k}_T$  in a hadron  $H$  with momentum  $p$ . This function can not be calculated within perturbative QCD. Nevertheless, in contrast to the distribution functions of a parton in a hadron, the probability of finding a parton of type  $a$  in parton  $b$  is directly computable. We provide more details on that issue in

---

<sup>1</sup>Note that the vertex correction diagram occurs twice.

Chap. 4. For now we present the result for the one-loop calculation with  $\epsilon = 2 - D/2$  [78]

$$f_{a/b}(x, \mu, \epsilon)_{\overline{\text{MS}}} = \delta_{ab} \delta(1-x) + \frac{\alpha_s(\mu)}{2\pi} P_{ab}^{(0)}(x) \left( -\frac{1}{\epsilon} + \gamma_E - \ln 4\pi \right). \quad (2.19)$$

We see that parton-in-parton distributions depend on the Altarelli-Parisi splitting functions describing the parton splitting  $j \rightarrow i$ . These can be written in a power series in  $\alpha_s$ :

$$P_{ij}(x) = \frac{\alpha_s(\mu^2)}{2\pi} P_{ij}^{(0)}(x) + \left( \frac{\alpha_s(\mu^2)}{2\pi} \right)^2 P_{ij}^{(1)}(x) + \left( \frac{\alpha_s(\mu^2)}{2\pi} \right)^3 P_{ij}^{(2)}(x) + \dots \quad (2.20)$$

Its unpolarized and polarized first loop splitting functions  $P_{ij}^{(0)}$  were derived by [79, 80], the second loop ones by [81–87] and the third loop  $P_{ij}^{(2)}$  by [88]. Although perturbative QCD can not predict the parton distribution function from the scratch, as mentioned before, once a parton distribution function is known at one scale, it can be evolved to each other perturbative scale by means of the splitting functions. These evolution equations are known as the *DGLAP evolution equations*. Conveniently, they are presented for gluon ( $g$ ), non-singlet ( $q^{\text{NS}}$ ) and singlet ( $q^{\text{S}}$ ) combinations of quark distributions

$$q^{\text{NS}} = q_i - \bar{q}_i \quad (\text{or } q_i - q_j), \quad q^{\text{S}} = \sum_i (q_i + \bar{q}_i) \quad (2.21)$$

and are given by the differential equations

$$\begin{aligned} \frac{\partial q^{\text{NS}}}{\partial \ln \mu^2} &= \frac{\alpha_s(\mu^2)}{2\pi} P_{qq} \otimes q^{\text{NS}} \\ \frac{\partial}{\partial \ln \mu^2} \begin{pmatrix} q^{\text{S}} \\ g \end{pmatrix} &= \frac{\alpha_s(\mu^2)}{2\pi} \begin{pmatrix} P_{qq} & P_{qg} \\ P_{gq} & P_{gg} \end{pmatrix} \otimes \begin{pmatrix} q^{\text{S}} \\ g \end{pmatrix}, \end{aligned} \quad (2.22)$$

where “ $\otimes$ ” denotes a convolution  $f \otimes g = \int_x^1 \frac{dz}{z} f(z) g\left(\frac{x}{z}\right)$ .

We see that the one-loop distributions  $f_{a/b}$  of parton  $a$  in parton  $b$  in Eq. (2.19) contain the unpolarized one-loop splitting functions

$$\begin{aligned} P_{qq}^{(0)}(x) &= C_F \left[ \frac{1+x^2}{(1-x)_+} + \frac{3}{2} \delta(1-x) \right] \\ P_{qg}^{(0)}(x) &= T_F [(1-x)^2 + x^2] \\ P_{gq}^{(0)}(x) &= C_F \frac{(1-x)^2 + 1}{x} \\ P_{gg}^{(0)}(x) &= 2C_A \left[ \frac{x}{(1-x)_+} + \frac{1-x}{x} + x(1-x) \right] + \left[ \frac{11}{6} C_A - \frac{2}{3} T_F N_f \right] \delta(1-x), \end{aligned} \quad (2.23)$$

where in QCD  $C_F = 4/3$ ,  $C_A = 3$  and  $T_F = 1/2$ . Now let us compare the first order correction of  $f_{q/q} = f_{\bar{q}/\bar{q}}$  in Eq. (2.19) with the pole term in the complete first order

correction of the partonic Drell-Yan cross section in Eq. (2.16). As up to  $\mathcal{O}(\epsilon^2)$ ,

$$\left(\frac{4\pi\mu^2}{M^2}\right)^\epsilon \frac{\Gamma(1-\epsilon)}{\Gamma(1-2\epsilon)} = -\epsilon \left(-\frac{1}{\epsilon} - \ln 4\pi + \gamma_E - \ln \frac{\mu^2}{M^2}\right), \quad (2.24)$$

we see, that the term in brackets is for  $\mu^2 = M^2$  exactly twice of the pole term, which is subtracted in  $\overline{\text{MS}}$  scheme and then is part of the parton distribution function in  $\overline{\text{MS}}$  scheme. As no more additional finite terms are shifted between hard scattering functions and parton distribution functions, the  $\overline{\text{MS}}$  distribution at one-loop can be said to be defined as 'pure counterterm'.

So far, we have drawn our attention to the poles in the complete first order calculation of the Drell-Yan cross section. We have seen that the collinear divergences can be contributed to the parton distribution functions and the soft divergences cancel. So the hard scattering functions are finite now. Let us now investigate the finite piece in Eq. (2.17) in more detail. Although the soft divergent terms of the real and the virtual contributions to the cross section canceled, this cancellation was incomplete in the sense, that terms of the form

$$\alpha_s \left[ \frac{\ln(1-z)}{1-z} \right]_+ \quad (2.25)$$

are left behind. The essential aspect is how this term behaves in the threshold region, in which the invariant lepton-pair mass  $M$  approaches the total available energy, given by the partonic center-of-mass energy  $\hat{s}$ . In this limit,

$$z = \frac{M^2}{\hat{s}} \rightarrow 1, \quad (2.26)$$

most of the energy is used to produce the lepton-pair and only little phase space remains for real-gluon radiation. This imbalance yields large logarithmic corrections of the terms in Eq. (2.25) at partonic threshold. Such large contributions arise in all orders of perturbation theory in combination with the emission of an arbitrary number of soft gluons. At  $n$ th order there are contributions proportional to

$$\alpha_s^n \left[ \frac{\ln^m(1-z)}{1-z} \right]_+, \quad m \leq 2n-1. \quad (2.27)$$

The fact that large contributions like these appear in each order of perturbation theory, threatens immensely the predictive power of a fixed order calculation for the total cross section. Instead, a proper treatment of the cross section requires to sum up these logarithmic contributions to all orders. This is achieved via *threshold resummation*, a technique which is introduced in the following section.

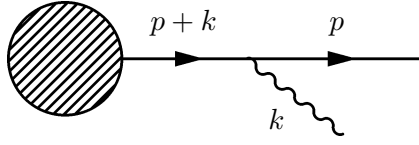


**Fig. 2.3.:** Emission of a soft gauge particle from an external particle

## 2.2. Threshold resummation

In the previous section we have seen that large logarithmic terms arise close to the partonic threshold region in the next-to-leading order calculation. These are remainders from the imperfect cancellation of infrared singularities of real and virtual gluon contributions. These threshold logarithms appear in all higher orders of perturbation theory. As they are the most dominant contribution close to the threshold it is crucial to take them into account order-by-order. It can be shown that the threshold logarithms may be resummed to all orders of perturbation theory in the *eikonal approximation*. Such a proof basically consists of three parts:

- The exponentiation of soft threshold logarithms in QED
- The inclusion of color structure (QCD)
- The factorization of the phase space.

Let us first of all introduce the eikonal approximation [89, 90]. We consider a Feynman diagram with the emission of a soft photon/gluon from an external particle with  $p^2 = m^2$  as shown in Fig. 2.3. In QED the structure of this matrix element is given by

$$\mathcal{M} = \tilde{\mathcal{M}} i \frac{(\not{p} + \not{k} + m)}{(p+k)^2 - m^2} (-ie\gamma_\mu) u(p). \quad (2.28)$$

When the photon or gluon is sufficiently soft,  $k^2$  compared to  $p \cdot k$  is small and may be neglected in the propagator denominator. Analogously  $\not{k}$  is omitted in the numerator. Making use of the Dirac equation gives

$$\mathcal{M} = \tilde{\mathcal{M}} i \frac{\not{p} + m}{2p \cdot k} (-ie\gamma_\mu) u(p) = \tilde{\mathcal{M}} \frac{i}{p \cdot k} (-iep_\mu) u(p). \quad (2.29)$$

Thus the eikonal propagator and photon-fermion vertex are given by

$$\frac{i}{p \cdot k + i\epsilon}, \quad -iep_\mu. \quad (2.30)$$

By its definition the eikonal approximation addresses the region, in which all radiation is soft compared to the hard scattering, which exactly corresponds to the threshold region.

Let us return to the task of resumming the threshold logarithms. The feature that the emission of soft gauge particles cause large perturbative effects did not appear in the Drell-Yan process for the first time. This effect was already known from QED, where also large soft logarithms emerge in the kinematic threshold region. It was proven in [91] that these logs can be exponentiated in the eikonal approximation<sup>2</sup>. However, as QCD is a non-Abelian gauge theory, the generalization from the exponentiation of soft logarithms in QED to QCD is more involved. In the Abelian theory QED the soft photons are radiated independently, while in QCD we have an additional self interaction of the gauge field with the triple and the quartic gluon coupling, which makes the situation more complex. Nevertheless, threshold resummation within QCD could be developed, first by Sterman in the soft gluon limit [24]. Catani and Trentadue [25] followed with the resummation to NLL accuracy two years later. These derivations were based on the proof in [92, 93] showing that the sum of all virtual and real eikonal gluon diagrams, labeled by  $X$ , may be reorganized in such a way that  $X$  may be written as exponential

$$X = e^Y. \quad (2.31)$$

The exponent  $Y$  contains only a specific subset of all Feynman diagrams and the contributing diagrams enter the exponent with a modified color-weight. This means, that known lower order calculations are sufficient to predict the most dominant terms of higher orders close to the threshold region.

The last missing piece towards threshold resummation is the proof of phase space factorization. It turns out<sup>3</sup>, that the phase space factorizes not in  $z$  space directly but in Mellin- $N$  momentum space, where  $N$  is the Mellin-moment conjugate with respect to  $z$ . The  $N$ -th Mellin moment of a function  $f$  is defined as

$$f^N = \int_0^1 dx x^{N-1} f(x). \quad (2.32)$$

The exponentiation of the soft-gluon effects in the Drell-Yan process are derived in terms of moments of the cross section with respect to the hadronic scaling variable  $\tau = M^2/s$ . Let us recall that  $s$  is the center-of-mass energy squared of the incoming hadrons and  $M$  denotes the invariant mass of the lepton pair. Under moments, the convolution in the Drell-Yan cross section in Eq. (2.1) factorizes into moments of the parton distributions

---

<sup>2</sup>The exponentiation of soft threshold logarithms in QED is also presented in [32].

<sup>3</sup>For more details see again for instance [32]

	LL	NLL	NNLL	...
LO	1			
NLO	$\alpha_s L^2$	$\alpha_s L$		
NNLO	$\alpha_s^2 L^4$	$\alpha_s^2 L^{\{3,2\}}$	$\alpha_s^2 L$	
$\vdots$	$\downarrow$	$\downarrow$		$\ddots$
	$h^{(1)}(\alpha_s L)$	$h^{(2)}(\alpha_s L)$		

**Fig. 2.4.:** Schematic illustration of how the threshold logarithms, arising at each order of perturbation theory, are rearranged to an exponential function.

and the partonic cross section,

$$\frac{d\sigma^N}{dM^2} = \int_0^1 d\tau \tau^{N-1} \frac{d\sigma(\tau)}{dM^2} = \sigma_B \sum_{a,b} f_{a/H_1}^N w_{ab}^N f_{b/H_2}^N, \quad (2.33)$$

with  $\sigma_B = \frac{4\pi\alpha^2}{9SM^2}$  and where the Mellin moments of the parton distributions  $f_{a/H_i}$  in the hadrons  $H_1$  and  $H_2$  and the normalized partonic cross section  $w_{ab}^N$  are defined as

$$f_{a/H_i}^N = \int_0^1 dx_i x_i^{N-1} f_{a/H_i}(x_i), \quad w_{ab}^N = \int_0^1 dz z^{N-1} w_{ab}(z). \quad (2.34)$$

The exponentiated cross section in Mellin moment space must then be inverted back to  $\tau$  space to derive the physical cross section. In principle, one has to perform a contour integration in the complex  $N$  space,

$$f(x) = \frac{1}{2\pi i} \int_{c-i\infty}^{c+i\infty} dN x^{-N} f^N, \quad (2.35)$$

where  $c$  is a real number, which is chosen such that all singularities are to the left of the contour.

Let us see how the threshold logarithms  $\ln(1-z)$  will manifest in Mellin moment space. The threshold limit  $z \rightarrow 1$  corresponds to a large  $N$  limit in Mellin moment space. By performing the Mellin transform one can show [25]

$$\int_0^1 dz z^{N-1} \left( \frac{\ln^m(1-z)}{1-z} \right)_+ = \frac{(-1)^{m+1}}{m+1} \ln^{m+1} \bar{N} + \mathcal{O}(\ln^{m-1} N), \quad (2.36)$$

where  $\bar{N} = Ne^{\gamma_E}$ . The large logs of  $(1-z)$  are translated by the Mellin transform to large logs of  $N$ . Thus at  $n$ th order in the perturbative expansion logs of the form

$$\alpha_s^n \left[ \frac{\ln^m(1-z)}{1-z} \right]_+, \quad m \leq 2n-1 \quad \longrightarrow \quad \alpha_s^n \ln^{m+1} \bar{N} \quad m \leq 2n-1 \quad (2.37)$$

will appear. The resummation deals with summing these large logarithms. Order-by-order the large logarithms of the form  $\alpha_s^n \ln^m N$  with  $m \leq 2n$  are summed and rearranged to an exponential function. This is shown schematically by:

$$\begin{aligned} \frac{\sigma^N}{\sigma_B^N} &= 1 + \sum_{n=1}^{\infty} \alpha_s^n \sum_{m=0}^{2n} \tilde{c}_{n,m} L^m = \exp \left\{ \sum_{n=1}^{\infty} \alpha_s^n \sum_{m=1}^{n+1} c_{n,m} L^m \right\} \underbrace{C(\alpha_s)}_{\text{constants}} \\ &= \exp \left\{ \underbrace{Lh^{(1)}(\alpha_s L)}_{LL} + h^{(2)}(\alpha_s L) + \alpha_s h^{(3)}(\alpha_s L) \right\} C(\alpha_s), \\ &\quad \underbrace{\hspace{10em}}_{NLL} \end{aligned}$$

where  $c_{nm}, \tilde{c}_{nm}$  denote some coefficients and  $C(\alpha_s)$  collects mainly hard virtual constants. The first double series in Eq. (2.38) stands for the ordinary expansion of an observable in a power series of  $\alpha_s$  in perturbation theory. There the power of the logarithmic terms  $L$  at  $n$ th order extend up to  $2n$ . The reorganization of terms, taking place in the next step, is the heart of the resummation. Now the maximum power of  $L$  is smaller:  $m \leq n+1$ . All the double logarithmic terms  $\tilde{c}_{k,2k} \alpha_s^k L^{2k}$  result just from exponentiating the lowest-order contribution  $c_{1,2} \alpha_s L^2$ . Then all leading logarithmic (LL) terms of the form  $\alpha_s^k L^{k+1}$  are absorbed into the function  $Lh^{(1)}(\alpha_s L)$ , whereas the next-to-leading (NLL) logarithms of the type  $\alpha_s^k L^k$  are collected in  $h^{(2)}(\alpha_s L)$ . Taking more and more subleading logarithms into account will improve the accuracy of the resummation. The procedure of reorganizing the threshold logarithms is also illustrated in Fig. 2.4.

The derivation of the resummed exponent at LL accuracy has been shown in [32] in detail. Here we present the resummation formula at NNLL accuracy<sup>4</sup> derived in [73]:

$$w_{q\bar{q}}^{\text{res},N} = \exp C_q(r_f, \alpha_s(\mu_f)) \Delta_{\text{DY}}^N, \quad (2.38)$$

where the exponent due to soft-gluon emissions is given by

$$\ln \Delta_{\text{DY}}^N = 2 \ln \Delta_q^N(M^2, \mu_f^2) + \ln \Delta_{\text{DY,int}}^N(M^2). \quad (2.39)$$

The effects of soft-gluon radiation collinear to initial state partons are organized in

$$\ln \Delta_q^N(M^2, \mu_f^2) = \int_0^1 dz \frac{z^N - 1}{1-z} \int_{\mu_f^2}^{(1-z)^2 M^2} \frac{dk_{\perp}^2}{k_{\perp}^2} A_q(\alpha_s(k_{\perp}^2)) \quad (2.40)$$

<sup>4</sup>It was shown in [94] that the constants of the Drell-Yan cross section also exponentiate.



and the large-angle soft gluon emissions are collected in the process-specific function

$$\ln \Delta_{\text{DY},\text{int}}^N(M^2) = \int_0^1 dz \frac{z^N - 1}{1 - z} D_{\text{DY}}(\alpha_s([1 - z]^2 M^2)). \quad (2.41)$$

The integrands in Eq. (2.40) and Eq. (2.41) are expanded as

$$A_q(\alpha_s) = \frac{\alpha_s}{\pi} A_q^{(1)} + \left(\frac{\alpha_s}{\pi}\right)^2 A_q^{(2)} + \left(\frac{\alpha_s}{\pi}\right)^3 A_q^{(3)} + \dots \quad (2.42)$$

$$D_{\text{DY}}(\alpha_s) = \frac{\alpha_s}{\pi} D_{\text{DY}}^{(1)} + \left(\frac{\alpha_s}{\pi}\right)^2 D_{\text{DY}}^{(2)} + \dots \quad (2.43)$$

The coefficients  $A_q^{(n)}$  are the coefficients of the  $1/[1 - x]_+$  terms of the  $n$ -loop quark-quark splitting functions  $P_{qq}^{(n-1)}(x)$  [73].

$$A_q^{(1)} = C_F, \quad A_q^{(2)} = \frac{1}{2} C_F \left[ C_A \left( \frac{67}{18} - \frac{\pi^2}{6} \right) - \frac{5}{9} N_f \right], \quad (2.44)$$

where  $C_A = 3$  and  $C_F = 4/3$  in QCD. Some years ago, the exact expression for  $P_{qq}^{(2)}$  has been completed in [88]. As it is rather lengthy, a rather accurate approximation, but with the exact  $N_f^2$  term [95] is given by [96–99]

$$64 A_q^{(3)} = (1178.8 \pm 11.5) - (183.95 \pm 0.85) N_f - \frac{16}{27} C_F N_f^2. \quad (2.45)$$

Furthermore, the first order term of  $D_{\text{DY}}(\alpha_s)$  vanishes:

$$D_{\text{DY}}^{(1)} = 0. \quad (2.46)$$

This is due to the fact, that one has at NNLO for the first time the possibility that three external QCD particles can exchange a gluon. So, large-angle soft gluon emissions will enter at NNLL first. We will see in the following two chapters that this is different for inclusive-hadron photoproduction.

The running coupling  $\alpha_s(k_\perp^2)$  in Eq. (2.40) has to be expressed in terms of  $\alpha_s(\mu^2)$  with the renormalization scale  $\mu$  according to the NLO solution of the renormalization group equation. We need Eq. (1.21) in NNLO:

$$\begin{aligned} \alpha_s(k_\perp^2) = \alpha_s(\mu_r^2) \frac{1}{X} - \alpha_s^2(\mu_r^2) \frac{\beta_1}{\beta_0} \frac{\ln X}{X} + \alpha_s^3(\mu_r^2) \left( \frac{\beta_1^2}{\beta_0^2} \frac{\ln^2 X - \ln X - 1 + X}{X^3} + \frac{\beta_2}{\beta_0} \frac{1 - X}{X^3} \right) \\ + \mathcal{O}(\alpha_s^4(\mu_r^2) [\alpha_s(\mu_r^2) \ln(k_\perp^2/\mu_r^2)]^n) \end{aligned} \quad (2.47)$$

with

$$X = 1 + \beta_0 \alpha_s(\mu_r^2) \ln(k_\perp^2/\mu_r^2). \quad (2.48)$$

For further use we define

$$b_0 = \frac{\beta_0}{4\pi} = \frac{11C_A - 2N_f}{12\pi}, \quad b_1 = \frac{\beta_1}{(4\pi)^2} = \frac{17C_A^2 - 5C_A N_f - 3C_F N_f}{24\pi^2}, \quad b_2 = \frac{\beta_2}{(4\pi)^3}, \quad (2.49)$$

which are related to the first two coefficients of the QCD  $\beta$ -function. As already mentioned above, the resummed expression is conveniently organized as

$$\ln \Delta_{\text{DY}}^N = 2 \ln \bar{N} h^{(1)}(\lambda) + 2h^{(2)}(\lambda) + \alpha_s g^{(3)}(\lambda), \quad (2.50)$$

with

$$\lambda = \alpha_s b_0 \ln N, \quad (2.51)$$

such that the first function in Eq. (2.50),  $h^{(1)}$ , collects the leading logarithmic (LL) terms. It only depends on the first-order term  $A_q^{(1)}$ . The function  $h^{(2)}$  contains the NLL contributions, which additionally need the coefficients  $A_q^{(2)}$ ,  $D_{\text{DY}}^{(1)}$ , and  $\beta_1$ . The NNLL terms are organized in the function  $g^{(3)}$ . The calculation of this function requires the knowledge of  $A_q^{(3)}$ ,  $D_{\text{DY}}^{(2)}$ , and  $\beta_2$ . Note that we present the expression for  $g^{(3)}(\lambda)$  [73] in a slightly different notation for  $A_q^{(n)}$ . The three functions read:

$$h^{(1)}(\lambda) = \frac{A_q^{(1)}}{2\pi b_0 \lambda} [2\lambda + (1 - 2\lambda) \ln(1 - 2\lambda)] \quad (2.52)$$

$$\begin{aligned} h^{(2)}(\lambda) = & -\frac{A_q^{(2)}}{2\pi^2 b_0^2} [2\lambda + \ln(1 - 2\lambda)] - \frac{A_q^{(1)} \gamma_E}{\pi b_0} \ln(1 - 2\lambda) - \frac{A_q^{(1)}}{\pi b_0} \lambda \ln \frac{M^2}{\mu_f^2} \\ & + \frac{A_q^{(1)} b_1}{2\pi b_0^3} \left[ 2\lambda + \ln(1 - 2\lambda) + \frac{1}{2} \ln^2(1 - 2\lambda) \right] \\ & + \frac{A_q^{(1)}}{2\pi b_0} [2\lambda + \ln(1 - 2\lambda)] \ln \frac{M^2}{\mu_r^2}, \end{aligned} \quad (2.53)$$

$$\begin{aligned} h^{(3)}(\lambda) = & A_1 \left\{ 8(\gamma_E^2 + \zeta_2) \frac{\lambda}{1 - 2\lambda} + \frac{b_1^2}{8\pi^2 b_0^4} \frac{1}{1 - 2\lambda} \left[ \frac{1}{2} \ln^2(1 - 2\lambda) + 2\lambda \ln(1 - 2\lambda) + 2\lambda^2 \right] \right. \\ & \left. - \frac{2b_1 \gamma_E}{b_0^2} \frac{1}{1 - 2\lambda} [2\lambda + \ln(1 - 2\lambda)] + \frac{2b_2}{b_0^3} \left[ \frac{2\lambda^2}{1 - 2\lambda} + \ln(1 - 2\lambda) + 2\lambda \right] \right\} \\ & + A_2 \left\{ \frac{8\gamma_E}{\pi b_0} \frac{\lambda}{1 - 2\lambda} - \frac{2b_1}{\pi b_0^3} \frac{1}{1 - 2\lambda} [\ln(1 - 2\lambda) + 2\lambda + 2\lambda^2] \right\} + \frac{4A_3}{\pi^2 b_0^2} \frac{\lambda^2}{1 - 2\lambda} \\ & + \ln \left( \frac{M^2}{\mu_r^2} \right) \left\{ \frac{2A_1 b_1}{b_0^2} \frac{1}{1 - 2\lambda} [2\lambda + \ln(1 - 2\lambda)] - 2 \left( 2A_1 \gamma_E + \frac{A_2}{\pi b_0} \right) \frac{2\lambda}{1 - 2\lambda} \right\} \\ & + 2A_1 \ln^2 \left( \frac{M^2}{\mu_r^2} \right) \frac{\lambda}{1 - 2\lambda} + \frac{4A_2}{\pi b_0} \ln \left( \frac{\mu_f^2}{\mu_r^2} \right) \lambda - 2A_1 \ln^2 \left( \frac{\mu_f^2}{\mu_r^2} \right) \lambda - \frac{D_{\text{DY}}^{(2)}}{4\pi b_0} \frac{\lambda}{1 - 4\lambda}, \end{aligned} \quad (2.54)$$

where

$$D_{\text{DY}}^{(2)} = C_F C_A \left( -\frac{1616}{27} + 56\zeta_3 + \frac{176}{3}\zeta_2 \right) + C_F N_f \left( \frac{224}{27} - \frac{32}{3}\zeta_2 \right) \quad (2.55)$$

and where  $\zeta_i$  denotes the Riemann zeta function  $\zeta_i = \sum_{n=0}^{\infty} \frac{1}{n^i}$ .

We recall that this expression provides the calculation of the resummed Drell-Yan cross section Eq. (2.1) in Mellin- $N$  moment space. Therefore this formula is embedded in an integration in the complex Mellin- $N$  moment space, namely the inverse Mellin transform.

$$\frac{d\sigma^{res}(\tau)}{dM^2} = \sum_{q\bar{q}} \sigma_B \int_{C_{MP}-i\infty}^{C_{MP}+i\infty} \frac{dN}{2\pi i} \tau^{-N} f_{q/H_1}^N w_{q\bar{q}}^{res,N}(r, \alpha_s(\mu)) f_{\bar{q}/H_2}^N \quad (2.56)$$

The contour has to be chosen carefully as one finds that a singularity arises when  $\lambda = 1/2$ . This corresponds to the Landau singularity  $N = N_L = \exp(1/(2\alpha_s b_0))$ . An appropriate prescription how to deal with the Landau singularity is given by the minimal prescription [100], in which the contour is chosen to lie to the left of the Landau pole but to the right of all other poles. This topic will be addressed in the following chapter in more detail.



### 3. Higher order QCD corrections and their asymptotic behavior

Diverging series are the devil's invention..

N. Abels, 1828<sup>5</sup>

The situation seemed hopeless, when Dyson [102] cast doubt on the seemingly well-established perturbative approach of QED, claiming that important perturbative series have zero radius of convergence [101]. At first, this problem has been simply ignored by the scientific community for many years. Nowadays it is well accepted that perturbative series do not have to be convergent to provide valuable information, they are at best asymptotic, which is sufficient in many cases. As we have seen for the Drell-Yan process resummation deals with summing specific contributions to all orders. Problems appear with asymptotically growing terms. How are these solved with the Minimal Prescription formalism and how does this generally fit in the concept of asymptotic series? This and a short excursion to IR-renormalons will be the topic of the present chapter. Even if we focus on the Drell-Yan process, the conclusion is general and extends beyond the Drell-Yan process.

#### 3.1. Asymptotic series

Asymptotic series play a crucial role in perturbative calculations, therefore, we will provide some basic information on asymptotic series first. It seems contradictory at a first glance, but: Asymptotic series are divergent but nevertheless give predictions for important quantities of quantum field theory, for instance the sum of Feynman diagrams. First of all let us see why.

The series  $\sum_i f_i x^i$  represents  $f(x)$  *asymptotically*, if for a given  $N$  the first  $N$  terms of the series may be made as close as desired to  $f(x)$  by making  $x$  small enough [103, 104]. To be specific, according to Poincaré [105] a divergent series is an *asymptotic expansion* of

---

<sup>5</sup>Cited following [101]

the function  $f(x)$ , if

$$\lim_{|x| \rightarrow 0} \frac{1}{x^N} \left| f(x) - \sum_{i=0}^N f_i x^i \right| = 0 \quad \text{for } N \geq 0. \quad (3.1)$$

Let us point out two important properties of asymptotic expansions:

- *Non-uniqueness*: There may exist many different asymptotic expansions for a given function  $f(x)$ . For example, as  $x \rightarrow 0$

$$\begin{aligned} \tan x &\sim x + \frac{1}{3}x^3 + \frac{2}{15}x^5 + \dots \\ &\sim \sin x + \frac{1}{2}\sin^3 x + \frac{3}{8}\sin^5 x + \dots \end{aligned} \quad (3.2)$$

- *Subdominance*: An asymptotic series does not define a function uniquely. Instead, it is an asymptotic series to a class of functions that differ from each other by subdominant functions. For instance,

$$\frac{1}{1-x} + ce^{-1/x} \sim x + x^2 + x^3 + x^4 + \dots \quad (3.3)$$

has for any constant  $c \in \mathbb{R}$  the same asymptotic expansion.

In fact, this property is essential for perturbative expansions in quantum field theory. Nonperturbative effects might come into play, which are not uniquely defined in perturbation theory. However, these are exponentially suppressed by  $\exp(-1/g)$  (with  $g$  the coupling parameter). Thus, as the perturbative expansion is an asymptotic series, the result should be independent of adding nonperturbative effects.

## 3.2. Problems with resummed exponents in physical space

Once the resummed cross section has been computed in Mellin space, it has to be transformed back to physical space by an inverse Mellin transformation as we have seen in the previous chapter for the Drell-Yan process. This task, however, is by no means obvious. The crucial point is that by transforming the resummed expression back to  $x$ -space, there is a danger to neglect formally subleading terms which however create large spurious terms with factorial growth. Although neglecting subleading terms should be formally allowed, the absence of these terms leads to a strong violation of kinematic constraints, which were satisfied in the original formulation in Mellin-space. As a consequence, the final formula for the resummed physical cross section shows large, even divergent, threshold corrections even if one is far from the threshold region.

In this subsection we want to present an explicit example, the resummed expression for the Drell-Yan process, in order to shed light on the problems one is facing in physical

**Table 3.1.:** The table shows the problems one may be confronted with when the resummed expression in Mellin- $N$ -moment space is transformed to physical space. The specific example presented here (see [100]) is the Drell-Yan process and its resummed exponent in a double log approximation (DLA) with a fixed coupling  $\alpha_s/\pi = a/(2A_i^{(1)})$ , and a leading-log (LL) approximation with a running coupling. Both of the parton distribution functions  $f_{1,2}^N$  were fixed to,  $f_1^N = f_2^N = 6/(N(N+1)(N+2))$ . Furthermore, the table shows that if the Mellin moments of the resummed expression are expanded with respect to the strong coupling and then transformed to physical space (see  $\sigma^{(k)}$  in Mellin- $N$ -moment space) the coefficients of the expansion show no factorial growth. In contrast, if the expansion is done after the transformation to physical space (see  $\sigma^{(k)}$  in physical space), factorially growing terms occur in the expansion.

		DLA - fixed coupling	LL - running coupling
		$\Delta_{\text{DLA}}^N = \exp(a \ln^2 N)$	$\Delta_{\text{LL}}^N = \exp(\ln N g_1(\alpha_s b_0 \ln N))$
Mellin- $N$ -space	$\sigma_{\text{resum}}(\tau)$	$\frac{1}{2\pi i} \int_{C-i\infty}^{C+i\infty} f_1^N f_2^N \Delta_{\text{DLA}}^N \tau^{-N} dN$ convergent <sup>6</sup>	$\frac{1}{2\pi i} \int_{C-i\infty}^{C+i\infty} f_1^N f_2^N \Delta_{\text{LL}}^N \tau^{-N} dN$ convergent
	$\sigma^{(k)}(\tau)$	$\leq \frac{1}{k!} \left( \frac{\ln(2k)}{\ln(1/\tau)} \right)^{2k} a^k$ no factorial growth	$\left( 2b_0 \ln \frac{C}{\ln 1/\tau} \right)^k \alpha_s^k$ for $k \ll \ln 1/\tau$ power behavior  $\left( 2b_0 \ln \frac{k}{\ln 1/\tau} \right)^k \alpha_s^k$ for $k \gg \ln 1/\tau$ grows faster than any power, but much slower than factorial
physical space	$\sigma_{\text{resum}}(\tau)$	$\sim \int_0^1 dx \exp[a \ln^2(1-x)]$ divergent	$\sim \int_0^1 dx \exp[l g_1(\alpha_s b_0 l)]$ with $l \approx \ln \frac{1}{1-x}$ divergent
	$\sigma^{(k)}(\tau)$	$\sim 4^k k! a^k$ factorial growth	$\sim (b_0 C_{(k)})^k k! \alpha_s^k$ for $k \leq 32$ factorial growth <sup>7</sup>

space. This example has been studied in detail in [100]. To begin with, let us recall the resummed cross section for the Drell-Yan process in  $\overline{\text{MS}}$ -scheme and in Mellin- $N$ -space,

$$\sigma^N(M^2) = f_1^N f_2^N \Delta_{\text{DY}}^N(M^2). \quad (3.4)$$

Here,  $f_{1,2}^N$  denote the Mellin moments of the parton distribution functions. For the sake of convenience, the cross section is normalized by the Born term. The threshold logs are

<sup>6</sup>For absolute convergence the contour has to be deformed as explained in the text.

<sup>7</sup>The terms of the expansion were studied numerically up to  $\alpha_s^{32}$ . The  $C_{(k)}$  are coefficients which slowly increase with  $k$ . For explicit values of these coefficients in dependence of the underlying process (gluon fusion or  $q\bar{q}$  annihilation), see [100].

resummed by the factor

$$\ln \Delta_{\text{DY}}^N = 2 \int_0^1 dx \frac{x^N - 1}{1 - x} \left[ \int_{\mu_f^2}^{(1-x)^2 M^2} \frac{dq^2}{q^2} A_i(\alpha_s(q^2)) \right], \quad (3.5)$$

with

$$A_i(\alpha_s) = \frac{\alpha_s}{\pi} A_i^{(1)} + \left( \frac{\alpha_s}{\pi} \right)^2 A_i^{(2)}, \quad (3.6)$$

where we have for the initial quark and antiquark in the Drell-Yan process,  $A_i^{(1)} = A_q^{(1)} = C_F$  and  $A_i^{(2)} = C_F \left[ C_A \left( \frac{67}{18} - \frac{\pi^2}{6} \right) - \frac{10}{9} T_R N_f \right]$ . Calculating the integral we obtain up to NLL accuracy

$$\ln \Delta_{\text{DY}}^N = \ln N h_1(\lambda) + h_2(\lambda), \quad (3.7)$$

with  $\lambda = b_0 \alpha_s \ln N$  and where the function collecting the leading logarithms is given by

$$h_1(\lambda) = \frac{A_i^{(1)}}{\pi b_0 \lambda} [2\lambda + (1 - 2\lambda) \ln(1 - 2\lambda)], \quad (3.8)$$

and where the next-to-leading function is defined in the previous chapter.

In order to point out what the problems are that may arise when transforming the Mellin- $N$ -space resummed expression into physical space, we consider the following two approximations of the NLL-resummed exponent in Eq. (3.5):

- The first one is the *double log approximation* (DLA), where one only keeps the double-logarithmic term

$$\ln \Delta_{\text{DLA}}^N = \frac{2A_i^{(1)}}{\pi} \alpha_s \ln^2 N \equiv a \ln^2 N. \quad (3.9)$$

The last equation serves to define  $a = 2A_i^{(1)}\alpha_s/\pi$ . The interesting point of this approximation is that one has no running coupling effect. Consequently there is also no Landau pole and therefore we have no ambiguities, which usually come along with the Landau pole. This approximation is not only of theoretical interest, as processes with large color factors (as one has for instance in gluon-gluon-fusion processes) and a small coupling are not far from this approximation.

- The second approximation, which will be helpful for our discussion, is the *leading-log* (LL) approximation. Here all next-to-leading terms in Eq. (3.5) are neglected and only the function  $h_1(\lambda)$  with the leading-log terms is kept:

$$\ln \Delta_{\text{LL}}^N = \ln N h_1(\lambda) \quad (3.10)$$



For the points given in the argumentation below it is not necessary to restrict oneself on the leading-log terms in Eq. (3.5), however it simplifies calculations.

For definiteness, one chooses the two parton distribution functions to be equal

$$f_1(x) = f_2(x) = (1 - x)^2, \quad (3.11)$$

which corresponds to the following Mellin moments

$$f_{1,2}^N = \frac{6}{N(N+1)(N+2)}. \quad (3.12)$$

Let us start with the resummed exponent in DLA in (3.9). To obtain a prediction in physical space the exponent is multiplied with the Mellin moments of the parton distribution functions and then an inverse Mellin transform is performed and the result,

$$\sigma^{\text{resum}}(\tau) = \frac{1}{2\pi i} \int_{C-i\infty}^{C+i\infty} f_1^N f_2^N \Delta_{\text{DLA}}^N \tau^{-N} dN, \quad (3.13)$$

is convergent<sup>8</sup>. Here, the variable  $\tau$  denotes the ratio of the squared invariant mass  $M^2$  of the Drell-Yan pair to the center-of-mass energy  $S$

$$\tau = \frac{M^2}{S} \quad (3.14)$$

Replacing  $\Delta_{\text{DLA}}^N$  by its expansion with respect to  $a$ ,  $\exp(a \ln^2 N) = \sum_{k=0}^{\infty} \frac{(a \ln^2 N)^k}{k!}$ , gives

$$\sum_{k=0}^{\infty} \sigma^{(k)} = \sum_{k=0}^{\infty} \frac{a^k}{k!} \frac{1}{2\pi i} \int_{C-i\infty}^{C+i\infty} \frac{36}{(N(N+1)(N+2))^2} \ln^{2k} N \tau^{-N} dN. \quad (3.15)$$

In [100] it is shown how to estimate an upper bound of this integral. It turns out that the  $k^{\text{th}}$ -order correction,  $\sigma^{(k)}$ , cannot grow faster than

$$\frac{1}{k!} \left( \frac{\ln 2k}{\ln \frac{1}{\tau}} \right)^{2k} a^k. \quad (3.16)$$

This shows that in the power expansion of the resummed exponent  $\Delta_{\text{DLA}}^N$  *no factorially growing terms* show up.

The interesting question that arises is whether it is possible to find a corresponding expression for Eq. (3.13) in physical space. The explicit steps for rewriting the inverse Mellin

---

<sup>8</sup>In fact, the integral with the integration contour as it stands is not absolutely convergent for large  $N$ , as  $\Delta_{\text{DLA}}^N$  grows faster than any power for large  $N$ . However, we understand by this notation, that the integration contour is deformed for instance into two straight half-lines from  $C - (i + \epsilon)\infty$  to  $C$  and then to  $C + (i - \epsilon)\infty$ . Integrating along this deformed contour makes the integral convergent (and it also does not depend on  $\epsilon$ ). The same also holds for the analogous integral in LL approximation.

transform of  $\Delta_{\text{DLA}}^N$  in a distribution which is then combined with the convolution of the parton distribution functions are shown in [100, 106]. We want to give just the final result in LL accuracy<sup>9</sup>:

$$\sigma_{\text{DLA}}(\tau) = \int_{\tau}^1 dx \exp[a \ln^2(1-x)] \frac{d}{dx} \int_{\tau/x}^1 \frac{dx_2}{x_2} f_1\left(\frac{\tau}{xx_2}\right) f_2(x_2) \quad (3.17)$$

As  $\exp[a \ln^2(1-x)]$  diverges faster than any power as  $x \rightarrow 1$ ,  $\sigma_{\text{DLA}}(\tau)$  diverges for any value of  $\tau$ .

Expanding the result in (3.17) with respect to  $a$ , we see that each term of the expansion is integrable. However, from<sup>10</sup>

$$\int_0^1 \exp[a \ln^2(1-x)] dx = \sum_{k=0}^{\infty} \frac{a^k}{k!} \int_0^1 dz \ln^{2k} z = \sum_{k=0}^{\infty} \frac{a^k (2k)!}{k!} \approx \sum_k (4a)^k k!, \quad (3.18)$$

one sees that the resulting series is an asymptotic one and diverges. Thus in order to give a prediction for the result for this asymptotic series we search for its minimal term. Here the current term is of the same size as the previous one,  $(4a)^{k-1}(k-1)! \approx (4a)^k k!$ , yielding

$$4ak = 1. \quad (3.19)$$

The error may be estimated from the left over term,

$$\delta_{\text{DLA}} = (4a)^k k! \approx (4a)^k k^k e^{-k} = e^{-\frac{1}{4a}} = \left(\frac{\Lambda}{M}\right)^{\frac{\pi b_0}{4A_i^{(1)}}}, \quad (3.20)$$

where we used  $\alpha_s b_0 = 1/\ln \frac{M^2}{\Lambda^2}$ . Although the error is power-suppressed, it may turn out, for instance for heavy flavor production via gluon fusion at fixed invariant mass of the heavy flavored pair in DIS-scheme, that the left over term is a  $(\lambda/M)^{0.16}$  correction, which is almost an order 1 correction.

To pass the last equations in review: We started with a convergent resummed expression in Mellin- $N$ -space (Eq. (3.13)). Its power expansion in Mellin- $N$ -space does not show any factorial growth (Eq. (3.16)). However, if we try to formulate resummation in physical space, we observe that its resummed analogon is a divergent integral (Eq. (3.17)), whose power expansion is a divergent asymptotic series (Eq. (3.18)). To be confronted with an asymptotic series is per se not that unusual, as one has for instance also to deal with them in ordinary perturbative calculations, where they arise due to the Landau pole in the running coupling constant. In this case, however, the approximation was explicitly chosen in such a way that there is no running coupling effect (see Eq. (3.9)). So, the asymptotic

<sup>9</sup>NLL-terms of the form  $\alpha_s^k \ln^m \frac{1}{1-x}$  with  $m \leq k$  are neglected.

<sup>10</sup>The lower limit of the integral is not relevant to draw the following conclusion.

growth, which we obtain in physical space, does not trace back to a Landau pole and infrared renormalons. Hence, they are a spurious effect resulting from neglecting certain subleading terms in the transformation to physical space. Even if this transformation is consistent with the leading-log approximation, unphysical asymptotically growing terms are created artificially.

One can repeat the preceding considerations for the full resummation formula including the effects of the running coupling [100]. This needs a prescription how to deal with the Landau singularity. According to the Minimal Prescription, which we will discuss in the next section, the integration contour is kept to the right of all singularities except for the Landau singularity. The results of the LL-approximation of the exponent (Eq. (3.10)) are listed in Table 3.1 and compared to the previous results of the DLA-approximation. As before the analogous resummed expression in physical space diverges and its perturbative expansion shows factorial growth. As in the DLA-approximation the factorially growing terms stem from neglecting subleading terms on the way of going to physical space. This can be seen from the following reason: The power expansion performed in Mellin- $N$ -space does not contain any factorially growing terms, and this *although* it includes running coupling effects now.

To conclude, we have seen two important points in this section.

- Firstly, the (naive) transformation of the resummed expression to physical space<sup>11</sup>, which we showed, introduces spurious factorial growing terms in the resummation formula.
- Secondly, even if the full resummation formula including the effects of the running coupling is considered, the power expansion in Mellin- $N$ -space (though divergent) does not grow factorially with increasing order.

### 3.3. The Minimal Prescription formula

In the previous section we stressed that it is important that the resummation formula does not introduce artificially spurious factorial terms. A widely used prescription that fulfills this requirement was developed in [100] and is known as the *Minimal prescription formula* (MP). Their formula for the resummation of threshold effects in the Drell-Yan cross section is

$$\sigma^{\text{res}} = \frac{1}{2\pi i} \int_{C-i\infty}^{C+\infty} f_1^N f_2^N \Delta_{\text{DY}}^N(M^2) \tau^{-N} dN, \quad (3.21)$$

<sup>11</sup>We want to remark at this point that there are resummation formulas in physical space based on SCET (Soft Collinear Effective Theory).

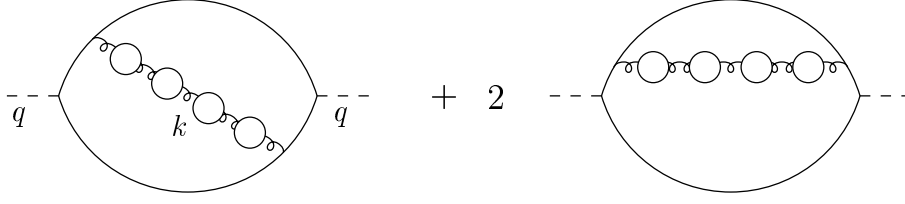


**Fig. 3.1.:** IR-renormalons in the Drell-Yan process. Figure taken from [107].

where the resummed exponent  $\Delta_{\text{DY}}^N$  is given in Eq. (3.5) and the integration contour (and in particular  $C$ ) is chosen in such a way that all singularities in the integrand are to the left of the integration contour, except for the Landau singularities at  $N = N_L$  and  $N = N_L^2$ , which lie on the positive real axis. When  $\Delta_{\text{DY}}^N$  is written as power series in  $\alpha_s$ ,

$$\Delta_{\text{DY}}^N = \sum_{k=0}^{\infty} c_k(\ln N) \alpha_s^k, \quad (3.22)$$

with coefficients  $c_k(\ln N)$  as polynomials in  $\ln N$ , then the formal power expansion of the total resummed cross section is given by

$$\sigma(\tau) = \sum_{k=0}^{\infty} \frac{1}{2\pi i} \alpha_s^k \int_{C-i\infty}^{C+\infty} f_1^N f_2^N c_k(\ln N) \tau^{-N} dN. \quad (3.23)$$

It was shown that this Minimal Prescription fulfills the following properties [100]:

- The expansion in Eq. (3.23) converges asymptotically to the MP formula.
- The coefficients of the power expansion in Eq. (3.23) do not show factorial growth.
- The best result for the “sum” of the asymptotic series in Eq. (3.23) is achieved when the series is truncated at the order at which its terms are at a minimum. The difference between this result and the full MP resummed formula is given by the truncation error

$$\delta_{\text{MP}} = e^{-H \frac{Q(1-\tau)}{\Lambda}}, \quad (3.24)$$

with  $H$  being a slowly varying positive function. This difference decreases faster than any power.

IR-renormalons - as threshold resummation - may also be related to soft gluons. So is there any connection between IR-renormalons and threshold resummation? As we have already seen in the previous section the power expansion in Eq. (3.23) admittedly is divergent due to the presence of the Landau pole. However its coefficients do not grow factorially. What about the ordinary full perturbative expansion for the Drell-Yan process? The full

perturbative expansion will show factorial growth due to the renormalon divergence, see Fig. 3.1. So while the respective power expansions of both, the resummed expression and the full perturbative result, are divergent, the full perturbative result shows factorial divergence but the power expansion of the resummed one does not. This puzzle may be solved by the argument that the leading terms of the resummed expansion do not contain this factorial growth. Thus the renormalons in a resummed expression are not given by the same contributions as the renormalons in an ordinary full perturbative expansion [100]. And, as Beneke states in [107, 108], the renormalon problem is a problem separate from soft gluon resummation.



## 4. Threshold Resummation for single-particle inclusive cross sections

The Drell-Yan process served as an introductory example to illustrate why large logarithms arise in higher orders of perturbative expansions and that these give large corrections to the leading order result close to the threshold region. These threshold logarithms may be organized in such a way that they can be resummed to all orders, despite the difficulties with QCD as a non-abelian field theory. Now the question arises whether the soft-gluon resummation as shown for the Drell-Yan process may be generalized to more complicated processes, in which four QCD-partons take part in the lowest order partonic hard scattering process. Such processes occur for the resolved contribution of hadron production, which is the main topic of this thesis. In contrast to the Drell-Yan process, their hard scatterings are themselves QCD subprocesses and therefore include color exchange. It turns out, that the leading soft-gluon logarithms associated with the radiative factor of each external parton are the same for QCD processes as for Drell-Yan. However, for the case of next-to-leading logarithms, the situation is different. There, the color structure of the corresponding hard scattering comes into play and influences the soft radiation near threshold. Nevertheless, it may be shown that also the next-to-leading logarithms may be resummed, which is the topic of the present chapter. We will see, that the combination of two different factorization methods of the partonic cross section is restrictive enough to imply the exponentiation of specific terms by making use of the ambiguity of some scales. For definiteness, we will focus on the threshold resummation for single-particle inclusive cross sections,

$$A + B \rightarrow c + X, \tag{4.1}$$

in which the hadrons  $A$  and  $B$  produce the observed photon or jet (labelled as  $c$ ).

The aim of this chapter is not to provide all details (which is unfortunately beyond the scope of this work), but to provide an overview over the general principles on which threshold resummation rests. Therefore, we want to stress and explain the basic steps on the way to soft-gluon resummation and refer to further literature otherwise.

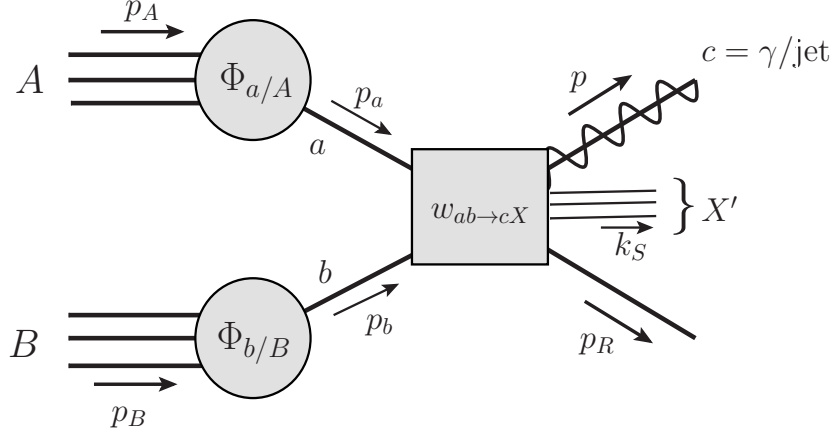


**Fig. 4.1.:** Factorization of the cross section for the hadronic process  $A(p_A) + B(p_B) \rightarrow c(p) + X(p_R + k_S)$ . “ $c$ ” denotes a photon or a jet.

## 4.1. The factorized cross section

We consider a single-particle inclusive cross section at measured momentum  $p$  and energy  $E_p$  for the hadronic process

$$A(p_A) + B(p_B) \rightarrow c(p) + X(p_R + k_S). \quad (4.2)$$

The observed particle, for instance a photon or a jet is denoted as  $c$ . Making use of the factorization theorem, which allows to separate the long-distance effects from the short-distance dynamics, the cross section may be factorized as

$$E_p \frac{d\sigma_{AB \rightarrow c+X}}{d^3p} = \frac{1}{s^2} \sum_{a,b} \int dx_a dx_b \Phi_{a/A}(x_a, \mu) \Phi_{b/B}(x_b, \mu) w_{ab \rightarrow c+X}(\hat{t}, \hat{u}, \alpha_s(\mu^2)), \quad (4.3)$$

where  $s$  denotes the center of mass energy squared. This factorization is illustrated in Fig. 4.1. The functions  $\Phi_{a/A}$  and  $\Phi_{b/B}$  in Eq. (4.3) are parton distributions in the hadron  $A$  and  $B$  respectively, evaluated at scale  $\mu$ . The hard scattering functions  $w_{ab \rightarrow c+X}$  describe the partonic process

$$a(p_a) + b(p_b) \rightarrow c(p) + X(p_R + k_S) \quad (4.4)$$

and depend on the partonic Mandelstam variables

$$\hat{s} = (p_a + p_b)^2, \quad \hat{t} = (p_a - p)^2, \quad \hat{u} = (p_b - p)^2, \quad (4.5)$$



where  $p_a = x_a p_A$  and  $p_b = x_b p_B$  are the momenta of partons  $a$  and  $b$ , respectively. The sum of these three Mandelstam variables gives the mass squared of the observed particle (or jet) plus the invariant mass squared of the QCD radiation recoiling against the observed parton  $c$ . As photons have zero mass and as mass may be neglected for light jets, we have

$$\hat{s}_4 \equiv \hat{s} + \hat{t} + \hat{u} = M_X^2. \quad (4.6)$$

In terms of this kinematic invariant the threshold region, at which all of the available energy is used to produce the observed particle, is given by the range where  $\hat{s}_4$  vanishes

$$\hat{s}_4 = 0. \quad (4.7)$$

In  $n$ th order of perturbation theory this is reflected by the appearance of singular terms

$$\alpha_s^n \left[ \frac{\ln^k(\hat{s}_4/\hat{s})}{\hat{s}_4} \right]_+ \quad \text{with } k \leq 2n - 1 \quad (4.8)$$

in the partonic cross section. The *plus-functions* are distributions

$$\left[ \frac{\ln^k(\hat{s}_4/\hat{s})}{\hat{s}_4} \right]_+ = \lim_{\Delta \rightarrow 0} \left\{ \frac{\ln^k(\hat{s}_4/\hat{s})}{\hat{s}_4} \theta(\hat{s}_4 - \Delta) + \frac{1}{k+1} \ln^{k+1} \left( \frac{\Delta}{\hat{s}_4} \right) \delta(\hat{s}_4) \right\}, \quad (4.9)$$

which arise due to the imperfect cancellation of the infrared divergences between real and virtual diagrams at the partonic threshold region, as we have seen in the Drell-Yan process.

## 4.2. Refactorization of the partonic cross section

So far we have seen that the long-distance effects (represented by the parton distribution functions) may be separated from the short-distance dynamics (partonic cross section) collected in the hard scattering functions  $w_{ab \rightarrow c+X}$  as shown in Eq. (4.3). In the next step we show that the partonic cross section itself may be further factorized, following the arguments of [109–114]. We will see that the new *refactorized* version is made up of three kinematically different parts:

- *Jet functions*, which describe soft and collinear emission of gluons along each of the incoming and outgoing hard partons.
- A *soft function* that describes the dynamics of the large-angle soft gluons interchanged between the partons.
- At last, there is a *hard function* for the hard scattering.

The interplay of these functions reproduces all singular distributions of the form Eq. (4.8) at partonic threshold. In the following we want to describe the definition and properties of these functions in greater detail.

Our starting point are the hard scattering functions  $w_{ab \rightarrow c+X}$  in Eq. (4.3). They are independent of the external hadrons. So, substituting the incoming hadrons  $A$  and  $B$  by partons, the functions  $w_{ab \rightarrow c+X}$  may be calculated in infrared-regulated perturbation theory. The basic ingredient for resummation is that the dynamics and the kinematics of the observable factorize simultaneously in the partonic threshold region of phase space near

$$s_4 = s + t + u = 0. \quad (4.10)$$

Here, the kinematic invariants are defined with respect to the overall hadronic process,

$$s = (p_A + p_B)^2, \quad t = (p_A - p)^2, \quad u = (p_B - p)^2, \quad s_4 = s + t + u. \quad (4.11)$$

In order to obtain the refactorized expression of the partonic cross section, one identifies the so-called *leading regions* in phase space. That are those regions of momentum space which produce singular leading powers of  $1/s_4$ . They are identified by investigating arising infrared divergences at higher orders in a general approach. For that, one analyzes the infrared poles in the propagators. It turns out that a *necessary* condition for a singularity is to have a *pinch* in every loop momentum component [78]. Such a pinch arises when the poles of the integrand coalesce such that the contour of the phase space integral is trapped and thus the integral might give a singular result. This condition is summarized analytically by the *Landau equations* [115, 116]. Another necessary condition for infrared divergences at finite order may be obtained by the *infrared power counting techniques*, which study whether the integrals may be bound near pinch surfaces. More details about this technique may be found in [78, 116].

With these techniques at hand, differing momentum scales in the partonic cross section may be separated as follows. The fully hard part  $H_{ab} = h_{ab}^* h_{ab}$  is given by the scattering amplitude  $h_{ab}$  and the complex conjugate amplitude  $h_{ab}^*$  and contains all virtual parton propagators that are off-shell by the order of the momentum transfer. It does not contain singular functions. The full dynamics of partons moving collinearly to the incoming partons  $a$  and  $b$  is absorbed by the jet functions  $\Psi_{a/a}$  and  $\Psi_{b/b}$ , respectively. At threshold these functions are flavor-diagonal up to finite corrections [28]. Each outgoing parton is associated with soft and collinear emissions of gluons, taken into account by the jet functions  $J$ . Here, the jet function  $J_R$  associated with the unobserved parton represents the partons recoiling against the observed parton  $c$ , with total momentum  $p_R$ . Finally, the soft function  $S_{ab}(k_S)$  collects the dynamics of soft gluons, of total momentum  $k_S$ . Both,

$H$  and  $S$ , are matrices in the space of color exchange [111, 112, 114]. The factorization as just described is schematically pictured in Fig. (4.2 (b)).

Next, we show that the kinematics of the process Eq. (4.4) may be decomposed in a way that corresponds to the refactorized expression. Let us again turn to the situation depicted in Fig. 4.1 with the incoming hadrons  $A$  and  $B$  replaced by partons  $a$  and  $b$ , respectively. Momentum conservation at parton level gives

$$xp_a + yp_b = p + p_R + k_S. \quad (4.12)$$

Furthermore, we introduce the vector  $\tilde{p}_R$  to denote the momentum of the recoiling jet at threshold. In the center-of-mass frame it is given by

$$\tilde{p}_R^\mu = (p_0, -\vec{p}) \equiv \sqrt{s}\zeta^\mu, \quad (4.13)$$

where the last equation serves to define the dimensionless vector  $\zeta^\mu$ . Squaring Eq. (4.12) we obtain near threshold and up to corrections of order  $s_4$  [28]

$$\begin{aligned} s_4 &= (1 - x_a) 2p_a \cdot \tilde{p}_R + (1 - x_b) 2p_b \cdot \tilde{p}_R + 2k_S \cdot \tilde{p}_R + p_R^2 + p^2 \\ &\equiv \left[ w_a \left( \frac{\hat{u}}{\hat{t} + \hat{u}} \right) + w_b \left( \frac{\hat{t}}{\hat{t} + \hat{u}} \right) + w_S + w_R + w_p \right] s \\ &= \left[ (1 - x_a) \left( \frac{\hat{u}}{\hat{t} + \hat{u}} \right) + (1 - x_b) \left( \frac{\hat{t}}{\hat{t} + \hat{u}} \right) + \frac{\hat{s}_4}{s} \right] s, \end{aligned} \quad (4.14)$$

where a set of dimensionless weights  $w_i$  was introduced in the second line. Note that the kinematics may be specified by  $\zeta$ . The second line of the equations splits  $s_4$  into terms which may be connected to the functions arising in the refactorized cross section and which we discussed above. The  $w_i$  provide the weights for each of these functions. As  $s_4$  they vanish at threshold. With regard to resummation, it is important that the contributions to the weight of partons within the jet functions and soft functions are independent and additive with corrections that vanish with  $s_4^2$  [117].

The third line of Eq. (4.14) represents the relation of the total  $s_4$  to the corresponding partonic quantity  $\hat{s}_4$  in the standard factorization Eq. (4.3). The standard factorization differs from the refactorized expression, as different parton distributions are used. While  $w_a$  and  $w_b$  refer to the functions  $\Psi$ , the variables  $x_a$  and  $x_b$  refer to the distributions  $\Phi$  in Eq. (4.14). Thus  $w_a \neq 1 - x_a$  and  $w_b \neq 1 - x_b$ .

The definition of the weights Eq. (4.14) enables one to rewrite the infrared-regulated par-

tonic cross section  $ab \rightarrow c + X$  at fixed  $s_4$  in the following “refactorized” way [117]:

$$\begin{aligned}
E_p \frac{d\sigma_{ab \rightarrow c+X}}{d^3p} = & \text{Tr} \left\{ H_{ab}(\hat{t}, \hat{u}) \int dw_a dw_b dw_S dw_R dw_p \right. \\
& \times \delta \left( \frac{s_4}{s} - w_a \left( \frac{\hat{u}}{\hat{t} + \hat{u}} \right) - w_b \left( \frac{\hat{t}}{\hat{t} + \hat{u}} \right) - w_S - w_R - w_P \right) \\
& \times \Psi_{a/a}(w_a, p_a, \zeta, n) \Psi_{b/b}(w_b, p_b, \zeta, n) \\
& \times J_c(w_p, p, \zeta, n) J_d(w_R, p_R, \zeta, n) S_{ab} \left( \frac{w_S s}{\mu^2}, \beta_i, \zeta, n \right) \left. \right\}. \quad (4.15)
\end{aligned}$$

This refactorized expression is illustrated schematically in Fig. 4.2 (b). The kinematic demand/restriction in Eq. (4.14) was taken into account via the delta-function. The various factors in Eq. (4.15) are evaluated in axial gauge<sup>12</sup>  $n \cdot A = 0$  with  $n^2 \neq 0$ . This choice of gauge has the advantage that collinear logarithms are factorized automatically into the jet functions [112, 116, 117]. The soft function  $S$  depends not only on  $\zeta$  and  $n$  but also on the four-velocities  $\beta_i$ , defined for a parton of type  $i$  by

$$p_i^\mu = \beta_i^\mu \sqrt{\frac{\hat{s}}{2}}, \quad (4.16)$$

at Born level.

Eq. (4.15) shows that one is able to separate not only the short-distance part from the long-distance part, but also perform further factorizations. We have terms collecting the partons that are collinear to the incoming partons. Then there are respective terms for the collinear partons in the final-state jets. Soft gluons emitted at large angles are taken into account in the soft function.

One consequence of the factorization in Eq. (4.15) is that ultraviolet divergences arise in both, the hard function  $H$  and the soft function  $S$  in such a way, that they cancel in the product. As we want to consider these functions separately, we have to deal with these extra ultraviolet divergence. They will be cancelled by renormalizing these operators.

### 4.3. Moments of the partonic cross section

We will see that the large logarithmic threshold corrections of higher orders may be organized in Mellin space in exponential functions. Therefore, in this subsection we will take moments of the standard factorized cross section in Eq. (4.3) and of the refactorized partonic cross section in Eq. (4.15) and compare them. Note that instead of a Mellin transform one may also perform a Laplace transform if one is interested in the threshold corrections. The large logarithmic contributions at  $s_4/s = 0$  correspond to the terms at large Mellin- $N$  after a transformation,  $f^N = \int_0^1 d\frac{s_4}{s} \left(1 - \frac{s_4}{s}\right)^N f(s_4/s)$ . For  $\frac{s_4}{s} \rightarrow 0$  this

<sup>12</sup>The  $n \cdot A = 0$  gauge is also often denoted as  $A^+ = 0$ .

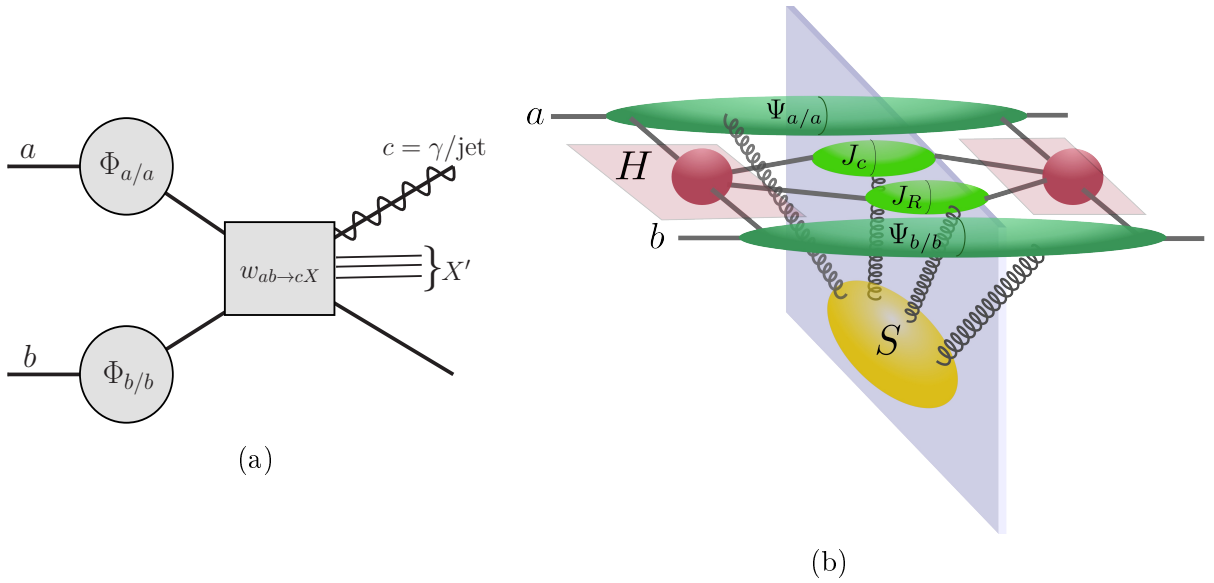


**Fig. 4.2.:** The figure shows the two approaches of factorizing the partonic cross section. In (a) it is illustrated that the same factorization properties, that hold for the hadronic cross section in Eq. (4.3) (illustrated in Fig. 4.1), hold also for infrared-regularized parton-parton scattering. In particular, the hard-scattering functions  $w_{ab \rightarrow cX}$  appearing in the factorized expressions are the same on hadron level and on parton level. In (b) the refactorized version (see Eq. (4.15)) is shown. The plane symbolizes the cut, which separates the amplitude and its complex conjugate. In this approach the partonic cross section is factorized in jet functions  $\Psi, J$  describing soft-gluon emissions off initial and final-state partons, the soft function  $S$ , and the hard function  $H$ , which is depicted as amplitude and its complex conjugate. The combination of both factorized forms is the starting point for resummation.

equals the Laplace transform  $\int_0^1 d\frac{s_4}{s} e^{-Ns_4/s} f(s_4/s)$ . The precise upper integration bound is not that important for large  $N$ .

Let us look again at the factorization of the hadronic cross section in Eq. (4.3). The same factorization properties, that hold for the hadronic cross section in Eq. (4.3) (illustrated in Fig. 4.1), hold also for infrared-regularized parton-parton scattering, i.e.  $A = a$  and  $B = b$  in Eq. (4.3). This factorization on parton level is illustrated in Fig. 4.2 (a). In particular, the hard-scattering functions  $w_{ab \rightarrow cX}$  in both factorized forms, the one on hadron level and the one on parton level, are identical. This is used, when one wants to calculate  $w_{ab \rightarrow cX}$  at fixed order of perturbation theory. The infrared-safe hard scattering function results from absorbing the initial-state collinear divergences of the partonic cross section into the light-cone distribution functions  $\Phi_{f/f}$  (see [112] and references therein). For further steps, we perform a Laplace transform with respect to  $s_4$  of this factorized partonic cross section.

The second ingredient we will use is the refactorized partonic cross section in Eq. (4.15), which we introduced in the previous subsection and which is illustrated schematically in Fig. 4.2 (b). We also take moments of this expression with respect to  $s_4$ . This gives us two expressions for the moments of the partonic cross section. By comparing these two expressions, one may deduce the following expression for the moments of the hard scattering

functions  $w_{ab}^N$ : [28, 112]

$$w_{ab}^N(\hat{t}, \hat{u}, \alpha_s(\mu^2)) = \left[ \frac{\Psi_{a/a}^{N, \frac{\hat{u}}{\hat{t}+\hat{u}}}(\frac{2p_a \cdot \zeta}{\mu}, \mu, \epsilon) \Psi_{b/b}^{N, \frac{\hat{t}}{\hat{t}+\hat{u}}}(\frac{2p_b \cdot \zeta}{\mu}, \mu, \epsilon)}{\Phi_{a/a}^{N, \frac{\hat{u}}{\hat{t}+\hat{u}}}(\mu, \epsilon) \Phi_{b/b}^{N, \frac{\hat{t}}{\hat{t}+\hat{u}}}(\mu, \epsilon)} \right] \times J_c^N(p \cdot \zeta) J_R^N(p_R \cdot n) \text{Tr} \left\{ H_{ab}(\hat{t}, \hat{u}) S_{ab}^{\frac{s}{N\mu^2}}(\beta_i, \zeta, n) \right\} + \mathcal{O}\left(\frac{1}{N}\right). \quad (4.17)$$

The first factor and the jet functions are *universal* in the sense that they do only depend on which kind of parton is involved, but they do not depend on the specific underlying process. These functions,  $\Psi/\Phi$  and  $J$ , include all the leading-log contributions, while NLL corrections are included in  $\Psi/\Phi$ ,  $J$  and  $S$ .

The fact that the moments of the hard scattering functions  $w_{ab}^N$  may be written in this factorized form, is a very important step on the way to resummation. This equation serves as starting point to solve the evolution equation of each function in Eq. (4.17). As a result one finds that the  $N$ -dependence of all functions exponentiates. This finally gives the resummed partonic cross section in moment space.

## 4.4. Soft and jet functions

In this section we will provide definitions for the jet and soft functions in terms of operator matrix elements. These definitions will enable us to organize the  $\mu$ - and  $N$ -dependence in these functions.

### 4.4.1. Light cone parton distribution $\Phi_{f/f}$

Let us start with the parton distributions  $\Phi_{i/i}$ . The operator definition for a quark in a quark and a gluon in a gluon is [78, 116], respectively:

$$\begin{aligned} \Phi_{q/q}(x) &= \frac{1}{2} \sum_{\sigma} \int_{-\infty}^{\infty} \frac{dy^-}{2\pi} e^{-ixp^+ y^-} \\ &\quad \times \langle q(p, \sigma) | \bar{q}(0^+, y^-, \mathbf{0}_{\perp}) \mathcal{P} \exp \left[ -ig \int_0^{y^-} d\lambda n \cdot A(\lambda n^{\mu}) \right] \frac{1}{2} n \cdot \gamma q(0) | q(p, \sigma) \rangle \\ \Phi_{g/g}(x) &= \sum_{\sigma} \frac{1}{4\pi x p^+} \int_{-\infty}^{\infty} dy^- e^{-ixp^+ y^-} \\ &\quad \times \langle g(p, \sigma) | F_{\mu}^+(0, y^-, \mathbf{0}) \mathcal{P} \exp \left[ -ig \int_0^{y^-} d\lambda n \cdot A(\lambda n^{\mu}) \right] F^{\mu+}(0) | g(p, \sigma) \rangle, \end{aligned} \quad (4.18)$$

where the plus and minus components are defined by  $p^{\pm} = (p^0 \pm p^3)/\sqrt{2}$ , such that  $p^2 = 2p^+p^- - p_{\perp}^2$ . Furthermore,  $n^{\mu}$  is defined as lightlike vector pointing in the opposite

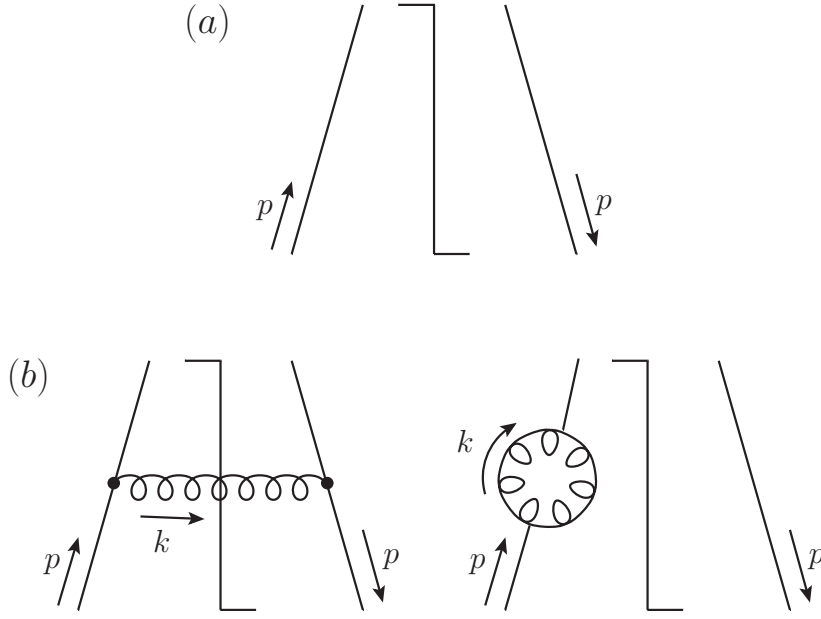


**Fig. 4.3.:** The figure shows the zeroth (a) and the first (b) order diagrams for the calculation of the distribution of a quark in a quark in  $n \cdot A = 0$  gauge. The latter ones consist of the real gluon emission diagram and the virtual gluon emission diagram.

direction as the incoming momentum  $p$ ,  $n^\mu = \delta_{\mu-}$ . With this gauge-invariant definition the physical quark and gluon fields in the matrix elements are connected via path ordered ( $\mathcal{P}$ ) exponentials (Wilson lines) along the  $n^\mu$ -light cone between the fields. The analogous definition of the distribution for antiquarks  $\Phi_{\bar{q}/\bar{q}}(x)$  is related to the quark one  $\Phi_{q/q}(x)$  by defining [116]

$$\begin{aligned}\bar{q}(x) &\equiv n \cdot \gamma q(x) \\ q(-x) &\equiv \bar{q}(x),\end{aligned}\tag{4.19}$$

in the definition of  $\Phi_{q/q}(x)$  in Eq. (4.18).

Let us recall that in the refactorized partonic cross section in Eq. (4.15) we made the choice to calculate all building blocks in the axial gauge  $n \cdot A = 0$ . In this gauge the above definitions reduce to

$$\begin{aligned}\Phi_{q/q}(x) &= \frac{1}{2} \sum_{\sigma} \int_{-\infty}^{\infty} \frac{dy^-}{2\pi} e^{-ixp^+ y^-} \langle q(p, \sigma) | \bar{q}(0^+, y^-, \mathbf{0}_\perp) \frac{1}{2} n \cdot \gamma q(0) | q(p, \sigma) \rangle_{n \cdot A=0} \\ \Phi_{g/g}(x) &= \sum_{\sigma} \frac{1}{4\pi x p^+} \int_{-\infty}^{\infty} dy^- e^{-ixp^+ y^-} \langle g(p, \sigma) | F_\mu^+(0, y^-, \mathbf{0}) F^{\mu+}(0) | g(p, \sigma) \rangle_{n \cdot A=0}.\end{aligned}\tag{4.20}$$

The zeroth and first order diagrams for the calculation of the quark in quark distribution in  $\overline{\text{MS}}$ -scheme are illustrated in Fig. 4.3 for the axial gauge. The real gluon emission

diagram in Fig. 4.3 (b) gives in  $d = 4 - 2\epsilon$  dimensions [78, 116]

$$\Phi_{f/f}^{(1)}(x, \mu, \epsilon) = \alpha_s \mu^{2\epsilon} \frac{C_F}{(2\pi)^{d-2}} \frac{2(1+x^2)}{1-x} \int \frac{d^{d-2}k_T}{k_T^2}, \quad (4.21)$$

where the divergence in the integral at transverse momentum  $k_T = 0$  reflects the collinear divergence from gluon emission. In addition, the scaleless integral shows also an ultraviolet divergence. This divergence is cured by an ultraviolet counterterm which removes all transverse momenta, that are much larger than the factorization scale and are thus unphysical [77, 78]. As there are several possibilities to define the parton distributions, one has to set one scheme. Often the  $\overline{\text{MS}}$ -scheme is chosen, in which the one-loop correction is defined as pure counterterm. Together with the virtual diagram in Fig. 4.3 (b) one obtains for the first order correction of the quark in quark distribution  $\Phi_{q/q}$  the expression

$$\Phi_{q/q}^{(1)}(x, \mu, \epsilon) = \frac{\alpha_s}{2\pi} \left( -\frac{1}{\epsilon} + \gamma_E - \ln 4\pi \right) P_{qq}^{(1)}(x), \quad (4.22)$$

which is proportional to the one-loop splitting function  $P_{qq}^{(1)}(x)$ . This gives in total

$$\Phi_{q/q}(x, \mu, \epsilon) = \delta(1-x) + \frac{\alpha_s}{2\pi} \left( -\frac{1}{\epsilon} + \gamma_E - \ln 4\pi \right) P_{qq}^{(1)}(x) \quad (4.23)$$

An analogous form holds for the gluon in gluon distribution  $\Phi_{g/g}(x)$ :

$$\Phi_{g/g}(x, \mu, \epsilon) = \delta(1-x) + \frac{\alpha_s}{2\pi} \left( -\frac{1}{\epsilon} + \gamma_E - \ln 4\pi \right) P_{gg}^{(1)}(x) \quad (4.24)$$

with the gluon-to-gluon splitting function  $P_{gg}^{(1)}(x)$ . Up to next-to-leading logarithmic accuracy  $\Phi_{g/g}$  is given by (see also [118])

$$\Phi_{g/g}(x, \mu, \epsilon) = \delta(1-x) - \frac{\alpha_s}{\pi} C_A \left[ \frac{1}{\epsilon} - \gamma_E + \ln 4\pi \right] \left( \frac{1}{1-x} \right)_+. \quad (4.25)$$

Compared to  $\Phi_{q/q}^{(1)}$ , the first order correction to  $\Phi_{g/g}$  contains an additional contributing diagram, the virtual quark pair creation diagram. It is instructive to see, how Eq. (4.24) may be calculated starting from the operator definition in Eq. (4.20). Therefore we warmly recommend [119], which provides many details for the calculation of the polarized gluon distribution.

#### 4.4.2. Center of mass parton distributions $\Psi_{f/f}$

The distributions  $\Psi_{f/f}$  in Eq. (4.17) for quarks were basically first introduced as center of mass distributions in [24]. As at threshold the total energy of the partonic process is



restricted, the parton distributions  $\Psi_{i/i}(x_i, p_i, \zeta, n)$  of partons  $i$  in parton  $i$  are defined at fixed values of momentum component  $p_i \cdot \zeta$ , what makes them different from standard light-cone parton distributions, which are defined at light-like momentum fraction. They are defined via the matrix elements [24, 112, 118],

$$\begin{aligned}\Psi_{q/q}(x, p, \zeta, n) &= \frac{1}{2N_c} \frac{p \cdot \zeta}{2\pi p \cdot v} \int_{-\infty}^{\infty} dy e^{-ixy p \cdot \zeta} \langle q(p) | \bar{q}(y\zeta) \frac{1}{2} v \cdot \gamma q(0) | q(p) \rangle_{n \cdot A=0} \\ \Psi_{\bar{q}/\bar{q}}(x, p, \zeta, n) &= \frac{1}{2N_c} \frac{p \cdot \zeta}{2\pi p \cdot v} \int_{-\infty}^{\infty} dy e^{-ixy p \cdot \zeta} \langle \bar{q}(p) | \text{Tr} \left[ \frac{1}{2} v \cdot \gamma q(y\zeta) \bar{q}(0) \right] | \bar{q}(p) \rangle_{n \cdot A=0} \\ \Psi_{g/g}(x, p, \zeta, n) &= \frac{1}{2(N_c^2 - 1)} \frac{p \cdot \zeta}{4\pi(v \cdot p)^2} \int_{-\infty}^{\infty} dy e^{-ixy p \cdot \zeta} \langle g(p) | F^{\mu\perp}(y\zeta) [v_\mu v_\nu] F^{\perp\nu}(0) | g(p) \rangle_{n \cdot A=0}.\end{aligned}\tag{4.26}$$

The first factor in each line is included due to an average over spin and color. The vector  $v$  denotes a light-like vector, pointing in the opposite direction from  $p^\mu$ . Thus, one has for  $\vec{p}$  in the  $\pm 3$  direction,  $v \cdot \gamma = \gamma^\pm$ . For definiteness, one conveniently chooses the gauge vector  $n_\mu$  as

$$p_i \cdot n = p_i \cdot \zeta \quad \text{for } i = a, b.\tag{4.27}$$

Then the densities  $\Psi_{i/i}(x_i, p_i, \zeta, n)$  are equal to the *center of mass parton distributions*, for which  $n^\mu = \zeta^\mu = \delta_{\mu 0}$  [24, 111, 112], at leading and next-to-leading logarithm [28]. A possible choice fulfilling this requirement is

$$n^\mu = \frac{p_b \cdot \zeta}{p_a \cdot p_b} p_a^\mu + \frac{p_a \cdot \zeta}{p_a \cdot p_b} p_b^\mu.\tag{4.28}$$

The matrix elements in Eq. (4.26) are calculated in axial gauge  $n \cdot A = 0$  and normalized in such a way that we have at lowest order

$$\Psi_{q/q}^{(0)}(x) = \Psi_{\bar{q}/\bar{q}}^{(0)}(x) = \Psi_{g/g}^{(0)}(x) = \delta(1 - x).\tag{4.29}$$

The first order corrections to the operator matrix elements have been calculated in  $d = 4 - 2\epsilon$  dimensions in [28]<sup>13</sup> and are to next-to-leading logarithmic accuracy given by

$$\begin{aligned}\Psi_{i/i}^{(1)}\left(x, \frac{2p \cdot \zeta}{\mu}, \mu, \epsilon\right) &= \frac{\alpha_s(\mu^2)}{\pi} C_i \left\{ - \left[ \frac{1}{\epsilon} - \gamma_E + \ln 4\pi \right] \left( \frac{1}{1-x} \right)_+ + \left( \frac{2 \ln(1-x)}{1-x} \right)_+ \right. \\ &\quad \left. + \left[ -1 + \ln \left( \frac{\hat{s}}{\mu^2} \right) + \ln(2\nu_i) \right] \left( \frac{1}{1-x} \right)_+ + \mathcal{O}(\epsilon) \right\},\end{aligned}\tag{4.30}$$

<sup>13</sup>In reference [24],  $\Psi_{q/q}^{(1)}(x)$  was calculated in temporal gauge  $A^0 = 0$ .

where  $i$  denotes quarks and gluons  $i = q, \bar{q}, g$ , with  $C_q = C_{\bar{q}} = C_F$  and  $C_g = C_A$ . We have

$$\nu_i = \frac{(\beta_i \cdot n)^2}{|n|^2}, \quad (4.31)$$

with  $n^\mu$  chosen as in Eq. (4.28) and the four-velocities  $\beta_i$  from Eq. (4.16). With these definitions, we have

$$\ln(4(p_i \cdot \zeta)^2/\mu^2) = \ln(2\nu_i) + \ln(\hat{s}/\mu^2). \quad (4.32)$$

For more detailed steps in the calculation of the polarized gluon distribution  $\Delta\Psi_{g/g}$  (which equals the unpolarized one up to NLL accuracy), we want to refer the interested reader again to [119].

Due to charge conjugation invariance the quark and the antiquark distributions are equal,  $\Psi_{q/q} = \Psi_{\bar{q}/\bar{q}}$ . The singularities showing up in the distributions in Eq. (4.30) are exactly the same as those in the light-cone parton distributions  $\Phi$  in Sec. 4.4.1. Thus, they cancel in the ratio leaving behind an infrared safe quotient.

#### 4.4.3. Final-state jet

Next, we turn to the final-state jets  $J$ . These collect the dynamics of partons moving collinearly to the outgoing parton. The final-state jets may also be defined as matrix elements. This has been done, for instance, for the resummation of threshold corrections in the context of dijet production threshold resummation in [112, 114]. Near threshold, a normalized jet function, for instance for an outgoing quark, may be defined as [112]

$$\begin{aligned} J_{f_i}^{\beta\alpha,ba}(\vec{p}_i^{(0)}, w_i, M_{JJ}, \mu, \alpha_s(\mu^2), \delta_i) &= \left(\gamma \cdot p_i^{(0)}\right)_{\beta\alpha} \delta_{ba} J_{f_i}(w_i, M_{JJ}/\mu, \alpha_s(\mu^2), \delta_i) \\ &= \sum_{\xi} 2|\vec{p}_i^{(0)}| (2\pi)^3 \delta^3(\vec{p}_i^{(0)} - \vec{p}_\xi) \delta(w_i - w(\xi, \delta_i)) \times \langle 0 | f_{\beta,b}(0) | \xi \rangle \langle \xi | \bar{f}_{\alpha,a}(0) | 0 \rangle, \end{aligned} \quad (4.33)$$

where  $M_{JJ}$  denotes the invariant mass of the two jets.  $p_i$  represents the jet momentum and  $\delta_i$  labels the opening angle of its cone. The sum extends over all states  $\xi$  with appropriate jet momentum, and which are consistent with a contribution  $w_i$  to the overall weight. Furthermore,  $f_{\beta,b}$  describes a field of flavor  $f$ , with Dirac and color indices  $\beta$  and  $b$ , respectively [112]. For the definition of gluon jets, similar considerations hold.

#### 4.4.4. Construction of the soft function from the eikonal cross section

So far, it was discussed how to define all functions in Eq. (4.17) as matrix operator elements except of one building block, the soft function  $S_{ab}$ . The soft function describes the emission of all non-collinear soft gluons and how the color exchange evolves in these emissions. This is technically handled via matrix elements of products of ordered exponentials of the

gluon field, coupled at a point representing the hard scattering [110–114]. Then gluons do not interact with physical partons, but rather with ordered exponentials. These ordered exponentials are *Wilson lines* of the corresponding color representation of the parton (quark or gluon). A general Wilson line is defined along a path  $\mathcal{C}$  in space-time, beginning at point  $z$  and ending at point  $z'$  [114],

$$W[\mathcal{C}; z', z] = \mathcal{P} \exp \left[ -ig \int_{\lambda_1}^{\lambda_2} d\eta \frac{dy(\eta)}{d\eta} \cdot A(y(\eta)) \right], \quad (4.34)$$

where the path  $\mathcal{C}$  is parametrized by the variable of integration  $\eta$ , with the endpoints  $y(\lambda_1) = z, y(\lambda_2) = z'$ .  $A(y)$  denotes the gauge field in the corresponding representation of the gauge group. In the case of a quark, the gauge fields are in the fundamental representation, for a gluon in the adjoint. These Wilson lines are a good approximation for non-collinear radiation of soft gluons by fast moving partons. For initial and final-state partons the path along which they move is a straight line, in the direction of their four-velocity  $\beta$ . Then the path with starting point  $x$  may be parametrized as  $y(\eta) = \eta\beta + x$ . For inclusive cross sections, the lines extend to infinity, either from the distant past or toward the distant future depending on whether we have an initial-state or a final-state parton. Conveniently, such Wilson lines are denoted as [112, 114]

$$\Phi_{\beta}^{(f)}(\lambda_2, \lambda_1; x) = \mathcal{P} \exp \left[ -ig \int_{\lambda_1}^{\lambda_2} d\eta \beta \cdot A^{(f)}(\eta\beta + x) \right]. \quad (4.35)$$

As before, the gauge field  $A^{(f)}$  is a matrix in the representation of the flavor  $f$ . Such Wilson lines collect the coupling of soft gluons to a single quark or hard gluon line, and also to a parton line, which connects a jet to the hard scattering [112, 120, 121]. These Wilson lines are connected at a local vertex. In this way an *eikonal nonlocal operator*  $w_I^{(f)}$  for the initial-state and final-state partons

$$a(\beta_a), b(\beta_b) \rightarrow 1(\beta_1), 2(\beta_2) \quad (4.36)$$

with four-velocities  $\beta_i$  as constructed in Eq. (4.16).

$$\begin{aligned} w_I^{(f)}(x)_{\{c_k\}} &= \sum_{d_i} \Phi_{\beta_2}^{f_2}(\infty, 0; x)_{c_2, d_2} \Phi_{\beta_1}^{f_1}(\infty, 0; x)_{c_1, d_1} \left( c_I^{(f)} \right)_{d_2 d_1, d_b d_a} \\ &\quad \times \Phi_{\beta_a}^{f_a}(0, -\infty; x)_{d_a, c_a} \Phi_{\beta_b}^{f_b}(0, -\infty; x)_{d_b, c_b}. \end{aligned} \quad (4.37)$$

The color tensor  $\left( c_I^{(f)} \right)_{d_2 d_1, d_b d_a}$  links the four Wilson lines and represents the coupling of the Wilson lines with each other in color space.

With this operator  $w_I^{(f)}$  at hand, one may define a dimensionless *eikonal cross section*

[112],

$$\sigma_{LI}^{(f),\text{eik}}(\alpha_s, \epsilon) = \sum_{\xi} \delta(w - w(\xi)) \times \langle 0 | \bar{T} \left[ (w_L^{(f)}(0))_{\{b_i\}}^\dagger \right] | \xi \rangle \langle \xi | T \left[ w_I^{(f)}(0)_{\{b_i\}} \right] | 0 \rangle, \quad (4.38)$$

where  $T$  denotes time-ordering and  $\bar{T}$  anti-time ordering. Furthermore,  $|\xi\rangle$  are a set of internal states, whose contributions to the weight are given by  $w(\xi)$ . These weights give the relevant measure of phase space near partonic threshold in the center-of-mass frame of the colliding partons.

Now let us have a look on the divergences that appear in the eikonal cross section. Besides infrared and collinear divergences, there are also ultraviolet ones because of the scale invariance of the Wilson lines [111]. Thus, the composite operator Eq. (4.37), which defines  $\sigma_{LI}^{(f),\text{eik}}$  has to be renormalized. Even after the renormalization, the eikonal cross section includes unphysical collinear divergences caused by fast-moving gluons that are collinear to the incoming, light-like eikonal lines. However one has to be careful with these gluons (real or virtual), since these are already collected in the distributions  $\Psi$ . Thus, in order to avoid double counting, they have to be separated. This may be done in quite the same way as we have done already in Eq. (4.15), where the non-collinear soft gluons were factored from collinear gluons in the moments of the (non-eikonal) partonic cross section. Therefore, the moments of  $\sigma_{LI}^{(f),\text{eik}}$  may be *refactorized* as,

$$\sigma_{LI}^{(f),\text{eik}^N} = S_{JI}^N j_a^N j_b^N j_1^N j_2^N, \quad (4.39)$$

where the  $j_i$ 's collect all collinear divergences yielding an infrared-safe soft function  $S_{JI}$ . It may be written as [114],

$$S_I^{(f)} = w_I^{(f)} \prod_{i=a,b} \frac{1}{\langle 0 | \Phi_{\beta_i}^{(f_i)}(0, -\infty; 0) | 0 \rangle} \prod_{i=1,2} \frac{1}{\langle 0 | \Phi_{\beta_i}^{(f_i)}(\infty, 0; 0) | 0 \rangle}. \quad (4.40)$$

## 4.5. Resummation from factorization

With all the work done in the last sections we are now in the position to see how the resummed expression may be derived from the factorized partonic cross section. It is a very elegant way to make use of renormalization equations. Provided that one is able to separate soft gluons from the hard scattering part, the underlying idea is that this separation is made manifest by the introduction of a specific scale. Both, the soft and the hard part depend on this scale. However, the physical cross section can not depend on it, and thus it is invariant under a transformation of this scale. This allows to derive a resummed expression in the scale dependence [114, 117].

### 4.5.1. Renormalization of the hard and soft function

To see how the soft matrix evolves, we first recall from Sec. 4.4.4 that the composite operators of the soft function  $S_{LI}^{(f)}$  need to be renormalized. For that, let us again have a look on the refactorized partonic cross section in Eq. (4.15). As the left hand side does not depend on  $\mu$ , the matrices  $H_{IL}^{(f)}$  and  $S_{LI}^{(f)}$  have to renormalize multiplicatively, with separate renormalization factors for the amplitude and the complex conjugate [110, 114, 117],

$$\begin{aligned} H_{IL}^{(f)(B)} &= \prod_{i=a,b,1,2} Z_i^{-1} \left( Z_S^{(f)-1} \right)_{IC} H_{CD}^{(f)} \left[ \left( Z_S^{(f)\dagger} \right)^{-1} \right]_{DL} \\ S_{LI}^{(f)(B)} &= \left( Z_S^{(f)\dagger} \right)_{LB} S_{BA}^{(f)} \left( Z_S^{(f)} \right)_{AI}. \end{aligned} \quad (4.41)$$

Here the  $Z_i$ 's denotes the wavefunction renormalization constants for each of the partons taking part in the hard scattering.  $Z_S^{(f),CD}$  is a matrix of renormalization constants, describing the renormalization of the soft function, i.e., of the eikonal cross section in Eq. (4.38). Furthermore the superscript  $(B)$  label the unrenormalized (bare) quantities. Based on Eq. (4.41) one may derive the following *renormalization group equation* for the soft functions  $S_{LI}^{(f)}$  [112, 114]

$$\mu \frac{d}{d\mu} S_{LI}^{(f)} = \left( \mu \frac{\partial}{\partial \mu} + \beta(\alpha_s) \frac{\partial}{\partial \alpha_s} \right) S_{LI}^{(f)} = - \left( \Gamma_S^{(f)} \right)_{LB}^\dagger S_{BI}^{(f)} - S_{LA}^{(f)} \left( \Gamma_S^{(f)} \right)_{AI} \quad (4.42)$$

The matrices  $\Gamma_S^{(f)}(\alpha_s)$  are specific to the underlying partonic process and are known as the *soft anomalous dimension matrices*. The solution of the differential equation (4.42) gives the resummation of all leading logarithms of the soft scale. For that, the soft anomalous dimension matrices have to be computed for each process. Let us recall from Sec. 4.4.4 that the soft function was defined via the eikonal cross section (4.39). Per definition the soft function is free of collinear divergences. These were factorized into the parton distributions. However it contains UV divergencies which have to be renormalized. These stem from the virtual vertex corrections to the eikonal color-dependent operators  $w_I^{(f)}(x)_{\{ck\}}$  in (4.37). Thus one computes the matrix of renormalization constants of the soft function  $Z_S^{(f)}$  in  $\overline{\text{MS}}$  renormalization scheme, taking  $\epsilon = \epsilon_{UV} = 4 - D$ , with  $D$  the number of space-time dimensions. Then, the one-loop anomalous dimension  $\Gamma_S^{(f)}$  is obtained from the residue of the UV pole contained in the matrix  $Z_S^{(f)}$ ,

$$\left( \Gamma_S^{(f)} \right)_{LI} (g) = - \frac{g}{2} \frac{\partial}{\partial g} \text{Res}_{\epsilon \rightarrow 0} \left( Z_S^{(f)} \right)_{LI} (g, \epsilon). \quad (4.43)$$

In the next chapter, we will show for an example how such a calculation is performed step-by-step. With the  $\Gamma_S^{(f)}$  given, the solution to Eq. (4.42) takes the form

$$\begin{aligned} & \text{Tr} \left\{ H^{(f)}(\hat{u}, \hat{t}, \alpha_s(\mu^2)) S^{(f)} \left( \frac{\sqrt{\hat{s}}}{N}, \alpha_s(\mu^2) \right) \right\} \\ &= \text{Tr} \left\{ H^{(f)}(\hat{u}, \hat{t}, \alpha_s(\mu^2)) \bar{\mathcal{P}} \exp \left[ \int_{\mu}^{\sqrt{\hat{s}}/N} \frac{d\mu'}{\mu'} \Gamma_s^{(f)\dagger}(\alpha_s(\mu'^2)) \right] S^{(f)}(\hat{u}, \hat{t}, \alpha_s(\hat{s}/N^2)) \right. \\ & \quad \left. \times \mathcal{P} \exp \left[ \int_{\mu}^{\sqrt{\hat{s}}/N} \frac{d\mu'}{\mu'} \Gamma_s^{(f)}(\alpha_s(\mu'^2)) \right] \right\}. \end{aligned} \quad (4.44)$$

For color-singlet processes like the case, in which parton  $c$  denotes a photon or the Drell-Yan process, in which  $S^{(f)}$  and  $\Gamma_S^{(f)}$  are  $1 \times 1$  matrices in color space, the evolution equation (4.42) simplifies to

$$\left( \mu \frac{\partial}{\partial \mu} + \beta(\alpha_s) \frac{\partial}{\partial \alpha_s} \right) S^{(f)} = -2\text{Re}\{\Gamma_s^{(f)}(\alpha_s(\mu^2))\} S^{(f)} \quad (4.45)$$

This equation can be solved by simply integrating with respect to  $\mu$  between the soft scale and the hard scale

$$S^{(f)}(\hat{u}, \hat{t}, \alpha_s(\mu^2)) = S^{(f)}(\hat{u}, \hat{t}, \alpha_s(\hat{s}/N^2)) \exp \left[ \int_{\mu}^{\mu/N} \frac{d\mu'}{\mu'} 2\text{Re}\{\Gamma_s^{(f)}(\alpha_s(\mu'^2))\} \right] \quad (4.46)$$

#### 4.5.2. Initial-state jets from the wave function ratio $\Psi/\Phi$

Next, we turn to the initial-state jet functions  $\Psi_{f/f}^N/\Phi_{f/f}^N$ , which were first derived for quarks for the Drell-Yan process [24]. They are universal in the sense that they are the same in electroweak and QCD-induced hard processes. As was shown in [24, 117], the factorization properties of Eq. (4.17) yield the exponentiation of the  $N$ -dependence for this wave function ratio. This ratio is finite, as can be seen at one-loop level from Eqs. (4.30), (4.24), and (4.24). With  $\mu = 2p_f \cdot \zeta$ , it reads [112, 122]

$$\frac{\Psi_{f/f}^N(1, \mu, \epsilon)}{\Phi_{f/f}^N(\mu, \epsilon)} = R_{(f)}(\alpha_s(\mu^2)) \exp [E_{(f)}(N, 2p_f \cdot \zeta)], \quad (4.47)$$

where in  $\overline{\text{MS}}$ -factorization scheme

$$\begin{aligned} E_{(f)}(N, M_f) = - \int_0^1 dz \frac{z^{N-1} - 1}{1 - z} \left\{ \int_{(1-z)^2}^1 \frac{dt}{t} A_f[\alpha_s(tM_f^2)] \right. \\ \left. + \bar{B}_f \left( \nu_i, \frac{M_f^2}{\hat{s}}, \alpha_s((1-z)^2 M_f^2) \right) \right\}. \end{aligned} \quad (4.48)$$

In Eq. (4.47),  $R_{(f)}(\alpha_s(M_f^2))$  is a  $N$ -independent function of the coupling. At lowest order, it can be normalized to unity [112, 122]. Furthermore, we have in Eq. (4.48)

$$\begin{aligned} A_f(\alpha_s) &= C_f \left[ \frac{\alpha_s}{\pi} + \frac{1}{2} K (\alpha_s/\pi)^2 \right], \\ \bar{B}_f \left( \nu_f, \frac{M_f^2}{\hat{s}}, \alpha_s \right) &= C_f(\alpha_s/\pi) [1 - \ln(2\nu_i) + \ln(M_f^2/\hat{s})], \end{aligned} \quad (4.49)$$

where the coefficient  $K$  is given by [123]

$$K = C_A \left[ \frac{67}{18} - \frac{\pi^2}{6} \right] - \frac{5}{9} N_f, \quad (4.50)$$

and  $C_f = C_q = C_F = 4/3$  for an incoming quark, and  $C_f = C_g = C_A = 3$  for a gluon.  $N_f$  denotes the number of flavors. The  $\nu_f$  are defined as

$$\nu_f \equiv \frac{(\beta_f \cdot n)^2}{|n^2|}, \quad (4.51)$$

with the parton velocity  $\beta_f^\mu = p_f^\mu \sqrt{2/\hat{s}}$  as defined in Eq. (4.16) and an axial gauge vector  $n$  (for a possible choice, see Eq. (4.28)). The  $\nu_f$  are related with the factorization of the cross section, as shown in Eq. (4.31) and Eq. (4.32) [28]. The gauge-dependence they express will cancel in the final resummed cross section.

Until now, the expression for moments of the ratios of the functions  $\Psi$  and  $\Phi$  were given at the scale  $\mu = 2p_f \cdot \zeta$ . General partonic cross sections, for instance with four participating QCD-partons, require to change the scale. For this purpose, one makes use of the renormalization group behavior of the parton distributions  $\Psi$  and  $\Phi$ .

The parton distribution  $\Psi$  is a composite operator and thus requires no overall renormalization [112]. It has been defined in Eq. (4.26) as product of renormalized operators. Thus, the moments of the distribution renormalize multiplicatively and the following renormalization group equation holds [112, 122]

$$\mu \frac{d\Psi_{f/f}^N(2p_f \cdot \zeta/\mu, \mu, \epsilon)}{d\mu} = 2\gamma_f(\alpha_s(\mu^2)) \Psi_{f/f}^N(2p_f \cdot \zeta/\mu, \mu, \epsilon), \quad (4.52)$$

where  $\gamma_f$  is the anomalous dimension of the field of flavor  $f$ . Therefore, we have no  $N$ -dependence in  $\gamma_f$ .

Next, we turn to the light-cone distribution  $\Phi$ . Its dependence on the factorization scale  $\mu$  depends on the choice of factorization scheme. The simplest choice is the  $\overline{\text{MS}}$ -factorization scheme, in which we have the following renormalization group equation by

definition [77, 124, 125]:

$$\mu \frac{d\Phi_{f/f}^N(\mu, \epsilon)}{d\mu} = 2\gamma_{ff}(N, \alpha_s(\mu^2))\Phi_{f/f}^N(\mu, \epsilon), \quad (4.53)$$

where  $\gamma_{ff}$  is the anomalous dimension of the color-diagonal splitting function for flavor  $f$ . The  $\gamma_{ff}$  do depend on  $N$ . As only color diagonal splitting functions are singular for  $x \rightarrow 1$ , only the flavor-diagonal evolution plays a role in the large- $N$  limit [112]. To one loop order, one has

$$\begin{aligned} \gamma_q(\alpha_s) &= \frac{3}{4}C_F \frac{\alpha_s}{\pi}, & \gamma_{qq}(N, \alpha_s) &= -\left(\ln N - \frac{3}{4}\right)C_F \frac{\alpha_s}{\pi}, \\ \gamma_g(\alpha_s) &= b_0\alpha_s, & \gamma_{gg}(N, \alpha_s) &= -(C_A \ln N - \pi b_0) \frac{\alpha_s}{\pi}, \end{aligned} \quad (4.54)$$

where  $b_0 = 4\pi\beta_0 = (11C_A - 4T_R N_f)/(12\pi)$ , with  $T_R = 1/2$  and the one-loop coefficient of the  $\beta$ -function,  $\beta_0$ .

Making use of the two evolution equations (4.52) and (4.53), the expression in Eq. (4.47) may be generalized to arbitrary scales  $\mu$ :

$$\begin{aligned} \frac{\Psi_{f/f}^N(2p_f \cdot \zeta/\mu, \mu, \epsilon)}{\Phi_{f/f}^N(\mu, \epsilon)} &= R_{(f)}(\alpha_s(\mu^2)) \exp[E_{(f)}(N, 2p_f \cdot \zeta)] \\ &\times \exp\left\{-2 \int_{\mu}^{2p_f \cdot \zeta} \frac{d\mu'}{\mu'} \gamma_f(\alpha_s(\mu'^2)) + 2 \int_{\mu}^{2p_f \cdot \zeta} \frac{d\mu'}{\mu'} \gamma_{ff}(N, \alpha_s(\mu'^2))\right\} \end{aligned} \quad (4.55)$$

This expression serves to define the resummed exponents  $\Delta_f^N(M_f^2, \mu)$  for the initial-state partons, in  $\overline{\text{MS}}$ -factorization scheme:

$$\ln \Delta_f^N(M_f^2, \mu) \equiv E_{(f)}(N, M_f) - 2 \int_{\mu}^{M_f} \frac{d\mu'}{\mu'} \gamma_f(\alpha_s(\mu'^2)) + 2 \int_{\mu}^{M_f} \frac{d\mu'}{\mu'} \gamma_{ff}(N, \alpha_s(\mu'^2)). \quad (4.56)$$

### 4.5.3. Final-state jets

The final-state jets are treated in an analogous way as the initial-state jets: It follows from the factorization properties of Eq. (4.17) that their  $N$ -dependence exponentiate [24, 117]. Unlike the initial-state jets, however, the final-state jets are independent of factorization scale. The exponential function  $J_f^N$  contains collinear emission, both soft and hard. Here



we just state the result [28, 112, 114]

$$\begin{aligned} \ln J_f^N(M^2) = \int_0^1 dz \frac{z^{N-1} - 1}{1 - z} \left\{ \int_{(1-z)^2}^{(1-z)} \frac{dt}{t} A_f[\alpha_s(tM^2)] - \gamma_f[\alpha_s((1-z)M^2)] \right. \\ \left. - \bar{B}_f[\nu_f, 1, \alpha_s((1-z)^2M^2)] \right\} + 2 \int_\mu^M \frac{d\mu'}{\mu'} \gamma_f(\alpha_s(\mu'^2)), \end{aligned} \quad (4.57)$$

where  $A_f$ ,  $\gamma_f$  and  $\bar{B}_f$  are defined as in Eq. (4.48).

There is one essential difference between this final-state jet and the initial-state jets, that is, the leading term in their exponents have the opposite sign. All of them have the same leading logarithmic contributions, collected in the function  $A_f(\alpha_s)$ , however, the final-state jets with a positive sign in (4.57) and the initial-state jets with a negative sign (see Eq. (4.48)). Consequently, the initial-state jets tend to enhance the cross section, while the final-state jets suppress it [112, 126].

#### 4.5.4. Final-state observed hadrons

Particularly with regard to the hadron production process, which is the process of our main interest and which we will study in greater detail later on, we want to consider already at this point the occurring changes, if the final parton  $c$  is a hadron rather than a photon or a jet. This parton  $c$  is “observed” such that we deal with a single-inclusive parton cross section [26]. In this situation, one is also confronted with final-state collinear singularities, which are factorized into the fragmentation functions. Thus, the procedure is similar to the initial-state partons and one ends up with essentially the same soft-gluon resummed exponent as in Eq. (4.56) [26, 127], with the initial-state factorization scale  $\mu_{fi}$  replaced by the final-state factorization scale  $\mu_{ff}$ .

#### 4.5.5. The resummed cross section

In the previous subsections we have shown step-by-step the general principles from which one derives the exponentiation of the soft function and the jet functions. Now it remains to collect the results of the previous subsections, namely (4.44), (4.56), and (4.57) and put all pieces together to obtain a resummed expression for Eq. (4.17). And here is the result

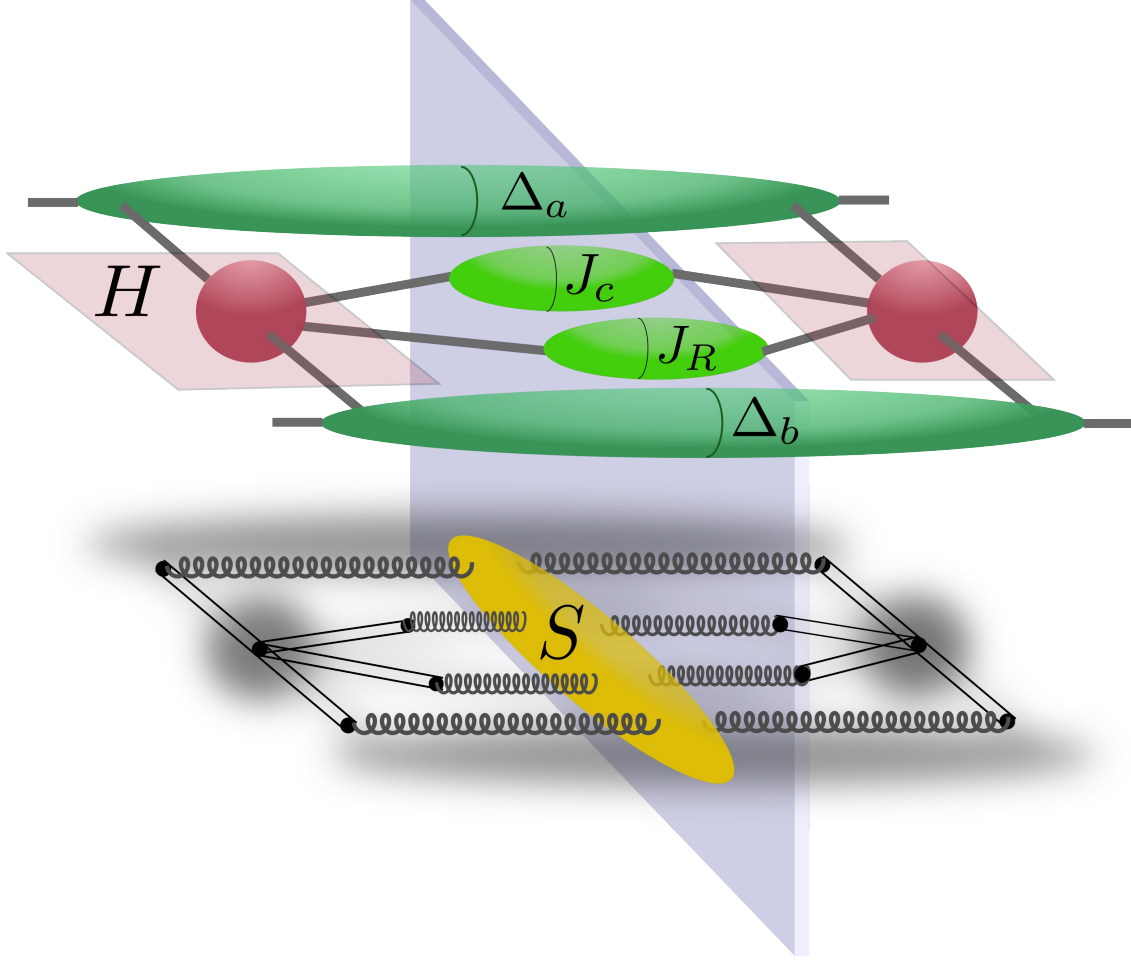


**Fig. 4.4.:** Schematic illustration of the factorization of the cross section close to threshold. The plane symbolizes the cut, which separates the amplitude and its complex conjugate. For each of the initial- and final-state partons there is a function  $(\Delta_{a,b}, J_c, J_R)$  describing soft-gluon emissions off these partons. The hard-scattering part  $H$  is depicted as amplitude and its complex conjugate. It can be completely separated from the soft function  $S$ , shown in the lower part of the figure. The double lines represent eikonal lines.

of the resummed partonic single-particle inclusive cross section:

$$\begin{aligned}
 w_{ab \rightarrow cr}^{\text{resum } N} \left( \frac{\hat{t}}{\mu^2}, \frac{\hat{u}}{\mu^2}, \alpha_s(\mu^2) \right) &= \Delta_a^{\left(-\frac{\hat{u}}{\hat{s}}\right)^N} \Delta_b^{\left(-\frac{\hat{t}}{\hat{s}}\right)^N} J_c^N(p \cdot \zeta) J_R^N(p_R \cdot n) \text{Tr} \left\{ H^{(f)}(\hat{u}, \hat{t}, \alpha_s(\mu^2)) \right. \\
 &\quad \times \bar{\mathcal{P}} \exp \left[ \int_{\mu}^{\sqrt{\hat{s}}/N} \frac{d\mu'}{\mu'} \Gamma_s^{(f)\dagger}(\alpha_s(\mu'^2)) \right] S^{(f)}(\hat{u}, \hat{t}, \alpha_s(\hat{s}/N^2)) \\
 &\quad \left. \times \mathcal{P} \exp \left[ \int_{\mu}^{\sqrt{\hat{s}}/N} \frac{d\mu'}{\mu'} \Gamma_s^{(f)}(\alpha_s(\mu'^2)) \right] \right\}. \tag{4.58}
 \end{aligned}$$

Note that if parton  $c$  is a photon, then  $J_c^N(p \cdot \zeta) = 1$ , while for a jet  $J_c^N(p \cdot \zeta)$  is given by Eq. (4.57).

We have seen that this resummed form results from general factorization properties of

the partonic cross section. For each external QCD parton, we have a radiative factor, collecting the collinear soft-gluon emissions from the respective parton. In addition to that, contributions by soft gluons emitted at wide angles are resummed by the exponentials within the trace of (4.58). Each of the functions appearing in this trace, the hard scattering functions  $H$ , the soft functions  $S$ , and the anomalous dimension matrices  $\Gamma_s$ , in general are matrices in the space of color exchange operators. As they depend on the specific underlying process, they have to be calculated for each subprocess separately. A detailed explanation how these matrices may be calculated, follows in the next chapter.



## 5. Calculation of hard, soft and anomalous dimension matrices in color space

In the previous chapter we have seen, that the resummation formula for QCD processes requires to derive the hard scattering functions  $H$ , the soft scattering functions  $S$  and the anomalous dimensions  $\Gamma_s$  for each partonic subprocess. It is instructive to make clear to oneself how to calculate these matrices. For that, each matrix has to be decomposed in its color configurations resulting in a matrix in the space of color exchange operators. In this chapter we will first of all introduce the space of color exchange operators and explain how to create a basis. This is necessary for the calculation of the hard, soft and anomalous dimension matrices, which will then be shown in detail for the quark-antiquark annihilation processes  $q\bar{q} \rightarrow q\bar{q}$ .

First of all let us introduce the notation, which we will use in this chapter. We will label the partonic subprocesses with “ $f$ ”. Furthermore, will follow [114, 126], where a genuine partonic  $2 \rightarrow 2$  process is labeled as

$$f_a(p_a, r_a) + f_b(p_b, r_b) \rightarrow f_1(p_1, r_1) + f_2(p_2, r_2). \quad (5.1)$$

The formalism is illustrated in Fig. 5.1.  $p_i$  denotes the momentum of parton  $i$ , which carries color  $r_i$ . The  $f_i$  may represent a quark, an antiquark or a gluon. The Mandelstam variables are defined as

$$\hat{s} = (p_a + p_b)^2, \quad \hat{t} = (p_a - p_1)^2, \quad \hat{u} = (p_b - p_1)^2. \quad (5.2)$$

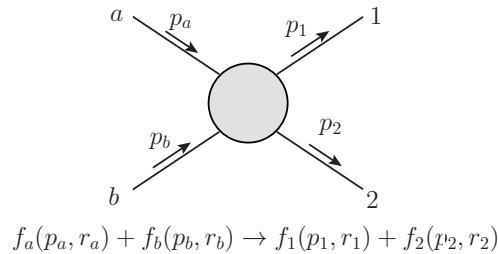


**Fig. 5.1.:** Illustration of the formalism used to calculate the lowest order hard and soft matrices for a general process.  $f_i$  may represent a quark, an antiquark or a gluon.  $p_i$  denotes the momentum of parton  $i$ , which carries color  $r_i$ .

**Table 5.1.:** Illustration of the different diagrams and their color structures for  $q\bar{q} \rightarrow q\bar{q}$ . The color structures are given in the  $\hat{t}$ -channel singlet-octet color basis:  $c_1 = \delta_{r_a r_1} \delta_{r_b r_2}$ ,  $c_2 = (t^c)_{r_1 r_a} (t^c)_{r_b r_2}$  (see Eq. (5.21)).

$q\bar{q} \rightarrow q\bar{q}$			
$q_j \bar{q}_j \rightarrow q_j \bar{q}_j$		$q_j \bar{q}_k \rightarrow q_j \bar{q}_k$	$q_j \bar{q}_j \rightarrow q_k \bar{q}_k$
$\hat{s}$ -channel $\frac{C_F}{N_c} c_1 - \frac{1}{N_c} c_2$	$\hat{t}$ -channel $c_2$	$\hat{t}$ -channel $c_2$	$\hat{s}$ -channel $\frac{C_F}{N_c} c_1 - \frac{1}{N_c} c_2$

## 5.1. Basis of color tensors

When calculating a generic partonic process, one is faced with two tasks. Firstly, one has to calculate the kinematical part of the contributing Feynman diagrams. Secondly, the color factors of each diagram have to be derived. In principle the color structure of each diagram decouples from the kinematic part in the sense that these refer to different spaces. The color structure of a diagram,  $|c\rangle$ , lives in the *color space*, which is a finite dimensional vector space. A specific partonic process requires specific color configurations of the initial-state and final-state partons.

Let us give an example: There are two contributing Feynman diagrams representing the partonic process  $q_j \bar{q}_j \rightarrow q_j \bar{q}_j$  (see Table 5.1): a  $\hat{s}$ -channel and a  $\hat{t}$ -channel diagram (with of course different kinematic terms). While both of the two channels allow for a color octet configuration<sup>14</sup> of the participating quarks and antiquarks, only the  $\hat{t}$ -channel diagram allows also for a color singlet configuration. Looking at it the other way round, this means that the process  $q_j \bar{q}_j \rightarrow q_j \bar{q}_j$  cannot be simply written as product of a kinematic term and a color factor, but it is a combination of two kinematic terms with different color structures. So, one has to keep track of the correct interplay of the kinematic part and the respective color structure. This may be done via decomposing the color structure in a basis.

In this section, we will follow the definitions and techniques of [128], where a general recipe for constructing orthogonal multiplet bases in  $SU(N_c)$  color space was developed. These will help to choose a minimal and orthogonal basis for each of the resolved partonic processes.

First of all, let us consider the color space. As we have mentioned already above, it is a finite dimensional vector space. Its dimensionality depends on the number and kind of involved partons. Let  $n_q$  be the number of outgoing quarks plus the number of incoming

<sup>14</sup>in  $\hat{t}$ -channel singlet-octet color basis (see Eq. (5.21))

antiquarks<sup>15</sup> and let  $N_g$  be the total number of incoming and outgoing gluons. Then, the color degrees of freedom of the quark states may be written as elements of  $V = \mathbb{C}^{N_c}$  and transform under the fundamental representation of  $SU(N_c)$ . Antiquark states are elements of the dual space  $\bar{V} \cong \mathbb{C}^{N_c}$  with transformations in the complex conjugate of the fundamental representation, while gluon states are elements of a real  $N_c^2 - 1$ -dimensional vector space, which can be complexified to  $A \cong \mathbb{C}^{N_c^2-1}$ , and transform in the adjoint representation. Now that we have specified the vector spaces we turn to a QCD amplitude. Its *color structure* is a tensor  $c$  of the space

$$c \in (V \otimes \bar{V})^{\otimes n_q} \otimes A^{\otimes N_g}. \quad (5.3)$$

As we have color conservation in QCD-processes, the *color space* contains only color singlets. Therefore, it is defined as color singlet subspace of  $(V \otimes \bar{V})^{\otimes n_q} \otimes A^{\otimes N_g}$ . Thus, all tensors transforming under the trivial representation of  $SU(N_c)$  span the color space.

Furthermore, as color can not be observed, one deals with color summed and averaged cross sections, respectively. They depend on the norm of the color structure

$$||c||^2 = \langle c|c \rangle, \quad (5.4)$$

where the scalar product is defined by summing over all external color indices

$$\langle c_1|c_2 \rangle = \sum_{a_1, a_2, \dots} c_1^{*a_1 a_2 \dots} c_2^{a_1 a_2 \dots}, \quad (5.5)$$

with  $a_i = 1 \dots N_c$  if parton  $i$  is a quark or antiquark, and  $a_i = 1 \dots N_c^2 - 1$  for a gluon.

Let us now provide more details about invariant tensors. Elements of the space  $V^{\otimes n_q} \otimes \bar{V}^{\otimes n_{\bar{q}}} \otimes A^{\otimes N_g}$  are made of  $n_q$  (quark) vectors  $v_j \in V$  ( $j = 1, \dots, n_q$ ),  $n_{\bar{q}}$  (antiquark) vectors  $w_k \in \bar{V}$  ( $k = 1, \dots, n_{\bar{q}}$ ), and  $N_g$  (gluon) vectors  $u_l \in A$  ( $l = 1, \dots, N_g$ ). The different vectors behave under transformations  $G \in SU(N_c)$  as:

$$\begin{aligned} v_j &\mapsto G v_j \\ w_k &\mapsto G^* w_k \\ u_l &\mapsto Ad(G) u_l. \end{aligned} \quad (5.6)$$

A tensor  $T \in V^{\otimes n_q} \otimes \bar{V}^{\otimes n_{\bar{q}}} \otimes A^{\otimes N_g}$  is called *invariant* if

$$\begin{aligned} \langle T | v_1 \otimes \dots \otimes v_{n_q} \otimes w_1 \otimes \dots \otimes w_{n_{\bar{q}}} \otimes u_1 \otimes \dots \otimes u_{N_g} \rangle = \\ \langle T | G v_1 \otimes \dots \otimes G v_{n_q} \otimes G w_1 \otimes \dots \otimes G w_{n_{\bar{q}}} \otimes Ad(G) u_1 \otimes \dots \otimes Ad(G) u_{N_g} \rangle \end{aligned} \quad (5.7)$$

<sup>15</sup>Then,  $n_q$  is also the number of incoming quarks plus the number of outgoing antiquarks.

for all transformations  $G \in \text{SU}(N_c)$  and for all vectors  $v_j, w_k, u_l$  [128]. Thus, as  $T$  transforms under the trivial representation of  $\text{SU}(N_c)$ , it is a color singlet. As the scalar product is invariant under a transformation  $G \in \text{SU}(N_c)$ , quark or antiquark lines  $\delta_{q_2 q_1}$ , gluon lines  $\delta_{g_1 g_2}$ , or the generators  $(t^g)_{q_2 q_1}$  of the fundamental representation are  $\text{SU}(N_c)$ -invariant tensors. Furthermore, the three-gluon vertices  $if_{g_1 g_2 g_3}$  and  $d_{g_1 g_2 g_3}$  are totally antisymmetric and symmetric invariant tensors respectively. Contractions and tensor products of invariant tensors are also invariant.

Our aim is to decompose each color structure into so-called *irreducible representations* and then use these in order to choose the bases. The underlying concept is comparable to the Clebsch-Gordan series of angular momentum. One makes use of the following algebraic group theoretical result: Tensor products can be classified according to their symmetry properties. Tensors with the same symmetry properties are arranged into closed (irreducible) subsets of elements, which transform into one another under the action of the group, but which do not mix with the remaining elements [129]. The term *irreducible* stems from the fact that each of the elements in a closed subset of elements will become a linear combination of elements in that same subset of elements under an arbitrary transformation within the group  $\text{SU}(N_c)$ . Later on, we will provide two examples for choosing the basis, a rather simple one which is used to explain the general procedure, followed by a more involved one.

First, we will introduce another useful mathematical tool, namely the *Young tableaux*. Young tableaux are a very pictorial method to describe the group representations of special unitary, symmetric and general linear groups. We will profit from the method to decompose a tensor product into irreducible representations. Its power lies in the fact that this approach compared to others may be rather easily generalized to arbitrary  $N_c$ . It is beyond the scope of this work to derive the mathematical theory behind the Young tableaux. We just recall the recipe for coupling two Young diagrams, see Fig. 5.2.

Let us start with quark-quark-scattering,  $qq \rightarrow qq$ , which is a rather simple example for the task of finding orthogonal basis vectors in color space. As we argued before, the color space for this process is the color singlet subspace of  $\bar{V} \otimes \bar{V} \otimes V \otimes V$ . It is two-dimensional. One possibility for the two basis vectors are the invariant tensors given by the singlet exchange in the  $\hat{s}$ - and  $\hat{u}$ -channels  $\delta_{r_a r_b} \delta_{r_1 r_2}$  and  $\delta_{r_a r_2} \delta_{r_b r_1}$ . However, we would like to decompose the color space in irreducible representations. The color content of a quark is represented by a  $\text{SU}(3)$ -triplet. Using the rules of coupling to Young-tableaux in Fig. 5.2, we may decompose the tensor product of two  $\text{SU}(3)$ -triplets as:

$$\begin{array}{c} \square \otimes \square = \square\square \oplus \begin{array}{|c|} \hline \square \\ \hline \square \\ \hline \end{array} \\ \text{3} \quad \text{3} \quad \text{6} \quad \quad \bar{3} \end{array} \quad (5.8)$$



### Coupling multiplets together

1. Draw the Young diagrams for the two multiplets, but in one of the diagrams replace the boxes in the first row with  $a$ 's, the boxes in the second row with  $b$ 's, etc.
2. Add the  $a$ 's from the lettered diagram to the right-hand ends of the rows of the unlettered diagram to form all possible legitimate Young diagrams that have no more than one  $a$  per column. In general, there will be several distinct diagrams, and all the  $a$ 's appear in each diagram.
3. Use the  $b$ 's to further enlarge the diagrams already obtained, subject to the same rules. Then throw away any diagram in which the full sequence of letters formed by reading right to left in the first row, then the second row, etc., is not admissible.
4. Proceed as in the step before with the  $c$ 's (if any), etc.

**Fig. 5.2.:** Recipe for coupling two multiplets together. Taken from the Particle Data Group [130].

Now, the procedure is as following: One constructs linear operators,

$$\mathbf{O} : V \otimes V \rightarrow V \otimes V, \quad (5.9)$$

which project onto the symmetric sextet and the antisymmetric antitriplet tensors in  $V \otimes V$ , respectively. Commonly, the  $\hat{t}$ -channel singlet-octet color basis has been chosen as

$$\begin{aligned} c_1 &= -\frac{1}{2N_c} \delta_{r_a, r_1} \delta_{r_b, r_2} + \frac{1}{2} \delta_{r_a, r_b} \delta_{r_1, r_2} \\ c_2 &= \delta_{r_a, r_1} \delta_{r_b, r_2}. \end{aligned} \quad (5.10)$$

For the sake of consistency we will also use this basis for our later calculations. However, we want to point out the advantages of using projectors. It is not that important for our case, where we have to choose color bases in Born diagrams, but it makes life much easier, when one wants to generalize the construction of color multiplet bases to higher orders and for arbitrary  $N_c$  [128].

Projectors are hermitian and chosen in such a way that they are mutually transversal

$$\mathbf{P}_j \mathbf{P}_k = \delta_{jk} \mathbf{P}_k \quad (\text{no sum over } k) \quad \forall j, k \quad (5.11)$$

Then the image of each projector is a subset of the kernel of all the others. This combined with hermiticity guarantees that they project onto mutually orthogonal subspaces, and

that the projectors are themselves *orthogonal*,

$$\langle \mathbf{P}_j | \mathbf{P}_k \rangle = 0 \quad \forall j \neq k. \quad (5.12)$$

The sum of all projection operators fulfills the *completeness relation*

$$\sum_j \mathbf{P}_j = \mathbf{1}. \quad (5.13)$$

There is a nice property of projection operators regarding the norm squared of the projector. With  $d_j$  denoting the dimension of the image of  $\mathbf{P}_j$ , the norm squared of  $\mathbf{P}_j$  is

$$\|\mathbf{P}_j\|^2 = \text{Tr}(\mathbf{P}_j^\dagger \mathbf{P}_j) = \text{Tr}(\mathbf{P}_j^2) = \text{Tr}(\mathbf{P}_j) = d_j. \quad (5.14)$$

As we will see lateron, these are exactly the elements standing on the diagonal line of the soft matrix.

Getting back to quark-quark-scattering, the projectors  $\mathbf{P}_S, \mathbf{P}_A$  can also form an orthogonal basis. Here the color space was spanned by these two projectors alone. But this is not the case for all processes. If the dimensionality  $d_j$  of a projector  $\mathbf{P}_j$  is greater than 1, the same multiplet appears several times in the decomposition of the tensor product. Then we have also linearly independent basis vectors which describe the transition from one instance of a multiplet to a different instance of the same multiplet.

Now let us turn to the more involved gluon-gluon-scattering. As starting point, we think of a basis for an arbitrary four-gluon diagram with external color indices  $r_a, r_b, r_1$  and  $r_2$ . A choice due to combinatoric considerations is

$$\begin{aligned} c_1^0 &= \text{Tr}(t^{r_a} t^{r_b} t^{r_2} t^{r_1}) & c_6^0 &= \text{Tr}(t^{r_a} t^{r_2} t^{r_b} t^{r_1}) \\ c_2^0 &= \text{Tr}(t^{r_a} t^{r_b} t^{r_1} t^{r_2}) & c_7^0 &= \frac{1}{4} \delta_{r_a r_1} \delta_{r_b r_2} \\ c_3^0 &= \text{Tr}(t^{r_a} t^{r_1} t^{r_2} t^{r_b}) & c_8^0 &= \frac{1}{4} \delta_{r_a r_b} \delta_{r_1 r_2} \\ c_4^0 &= \text{Tr}(t^{r_a} t^{r_1} t^{r_b} t^{r_2}) & c_9^0 &= \frac{1}{4} \delta_{r_a r_2} \delta_{r_b r_1} \\ c_5^0 &= \text{Tr}(t^{r_a} t^{r_2} t^{r_1} t^{r_b}). \end{aligned} \quad (5.15)$$

This set is made of the three possible singlet combinations and all constellations of traces one can build out of four generators  $t^{r_j}$ . Due to the cyclicity of the trace there are  $(N_c - 1)!$  possible traces. This initial choice of basis is illustrated in Fig. 5.3. However these nine basis vectors are not linearly independent and thus the basis is overcomplete.

The color content of a set of two gluons in SU(3) is described by the direct product of two SU(3) octets  $8 \otimes 8$ . Coupling two Young diagrams as described in Fig. 5.2 may help to

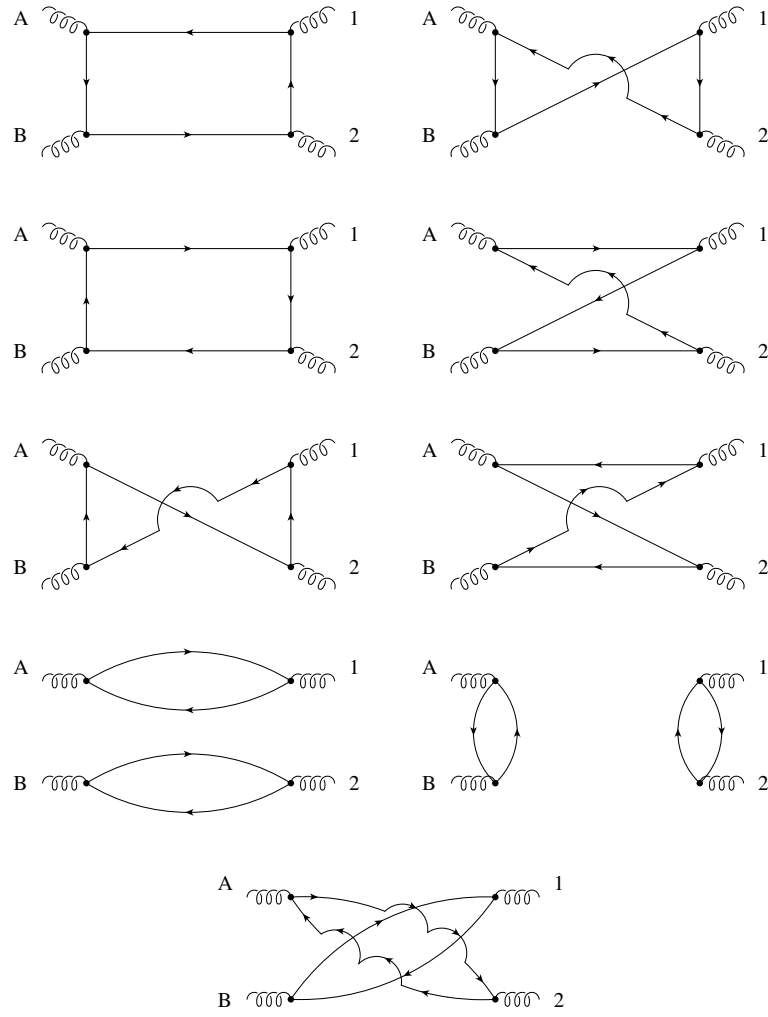


**Fig. 5.3.:** Illustration of the initial color basis for the  $gg \rightarrow gg$  process. All lines show only the color flow. The figure is taken from [114]. Note, that the notation used in the figure differs from our notation. While here capital letters label the initial-state partons, we use lower-case characters.

find the irreducible decompositions:

$$\begin{array}{c} \square & \square \\ \square & \square \end{array} \otimes \begin{array}{c} a & a \\ b & \end{array} = \begin{array}{c} \square & \square & a & a \\ \square & & b & \end{array} \oplus \begin{array}{c} \square & a & a \\ \square & & \end{array} \oplus \begin{array}{c} \square & \square & a \\ \square & a & b \end{array} \oplus \begin{array}{c} \square & a \\ b & \end{array} \oplus \begin{array}{c} \square & a \\ a & \end{array} \oplus \text{triv.} \quad (5.16)$$

$\begin{array}{cccccccc} 8 & 8 & 27 & 10 & \bar{10} & 8 & 8 & 1 \end{array}$

In literature there exist some algorithms for the construction of projectors corresponding to Eq. (5.16), some of them also for arbitrary  $N_c$ , [128, 131–134]. The  $\hat{t}$ -channel projectors

for  $N_c = 3$  are given by

$$\begin{aligned}
\mathbf{P}_1 &= \frac{1}{8} \delta_{r_a r_1} \delta_{r_b r_2} \\
\mathbf{P}_{8_S} &= \frac{3}{5} d_{r_a r_1 c} d_{r_b r_2 c} \\
\mathbf{P}_{8_A} &= \frac{1}{3} f_{r_a r_1 c} f_{r_b r_2 c} \\
\mathbf{P}_{10+\overline{10}} &= \frac{1}{2} (\delta_{r_a r_b} \delta_{r_1 r_2} - \delta_{r_a r_2} \delta_{r_b r_1}) - \mathbf{P}_{8_A} \\
\mathbf{P}_{27} &= \frac{1}{2} (\delta_{r_a r_b} \delta_{r_1 r_2} + \delta_{r_a r_2} \delta_{r_b r_1}) - \mathbf{P}_{8_S} - \mathbf{P}_1
\end{aligned} \tag{5.17}$$

Comparing these projectors to the initial basis set in Eq. (5.15), one realizes that the combinations  $c_1 = c_1^0 - c_3^0$ ,  $c_2 = c_2^0 - c_5^0$  and  $c_3 = c_4^0 - c_6^0$  are linearly independent with respect to the projectors in Eq. (5.17). The other six initial basis vectors may be written as a linear combination of only five projectors. This reflects the fact, that the initial set of basis was overcomplete. Consequently, the  $gg \rightarrow gg$  color space is spanned by the basis vectors

$$c_1, c_2, c_3, \mathbf{P}_1, \mathbf{P}_{8_S}, \mathbf{P}_{8_A}, \mathbf{P}_{10+\overline{10}}, \mathbf{P}_{27}. \tag{5.18}$$

The bases of all the other resolved processes may be derived analogously. We present a collection of their bases in Table 5.2. This table fixes our convention for the bases for the further work.

## 5.2. Lowest order hard and soft matrices

We have seen in Sec. 4.2 that we need a color decomposition of the hard scattering for each of the resolved partonic processes (labelled by “(f)”). The procedure is the following: First, one chooses a basis of color tensors,  $\{|c_i^{(f)}\rangle\}$ . Then, the Born level hard matrix,  $H_{LI}^{(f)}$  is calculated with respect to this basis. Its elements are the squares of the color-decomposed tree amplitudes. The lowest order soft matrix  $S_{LI}^{(f)}$  only depends on the definition of the basis. Its elements are given by the corresponding set of traces

$$S_{LI}^{(f)} = \text{Tr} \left[ \left( c_L^{(f)} \right)^\dagger c_I^{(f)} \right]. \tag{5.19}$$

### 5.2.1. Quark-antiquark annihilation processes $q\bar{q} \rightarrow q\bar{q}$

We start with the quark-antiquark annihilation process

$$q(p_a, r_a) \bar{q}(p_b, r_b) \rightarrow q(p_1, r_1) \bar{q}(p_2, r_2). \tag{5.20}$$

**Table 5.2.:** Basis of color structures for the resolved processes. The color space of the quark-quark processes is 2-dimensional, the color space of the quark-gluon processes is 3-dimensional, and for the gluon-gluon scattering there are even 8 basis vectors necessary. These are given in terms of  $t$ -channel  $SU(3)$  projectors for the decomposition into irreducible representations of the direct product  $8 \otimes 8$ . The projectors are given in Eq. (5.17).

$q\bar{q} \rightarrow q\bar{q}$	$qq \rightarrow qq$
$t$ -channel singlet-octet color basis	$t$ -channel singlet-octet color basis
$c_1 = \delta_{r_a, r_1} \delta_{r_b, r_2}$	$c_1 = -\frac{1}{2N_c} \delta_{r_a, r_1} \delta_{r_b, r_2} + \frac{1}{2} \delta_{r_a, r_b} \delta_{r_1, r_2}$
$c_2 = -\frac{1}{2N_c} \delta_{r_a, r_1} \delta_{r_b, r_2} + \frac{1}{2} \delta_{r_a, r_b} \delta_{r_1, r_2}$	$c_2 = \delta_{r_a, r_1} \delta_{r_b, r_2}$
$q\bar{q} \rightarrow gg$ and $gg \rightarrow q\bar{q}$	$qq \rightarrow qg$ and $\bar{q}g \rightarrow \bar{q}g$
$s$ -channel color basis	$t$ -channel color basis
$c_1 = \delta_{r_a, r_b} \delta_{r_1, r_2}$	$c_1 = \delta_{r_a, r_1} \delta_{r_b, r_2}$
$c_2 = d^{r_1 r_2 c} (t^c)_{r_b r_a}$	$c_2 = d^{r_b r_2 c} (t^c)_{r_1 r_a}$
$c_3 = i f^{r_1 r_2 c} (t^c)_{r_b r_a}$	$c_3 = i f^{r_b r_2 c} (t^c)_{r_1 r_a}$
$gg \rightarrow gg$	
$t$ -channel color basis	
$c_1 = \text{Tr} (t^{r_a} t^{r_b} t^{r_2} t^{r_1}) - \text{Tr} (t^{r_a} t^{r_1} t^{r_2} t^{r_b})$	$c_4 = \mathbf{P}_1 \quad c_7 = \mathbf{P}_{10+\overline{10}}$
$c_2 = \text{Tr} (t^{r_a} t^{r_b} t^{r_1} t^{r_2}) - \text{Tr} (t^{r_a} t^{r_2} t^{r_1} t^{r_b})$	$c_5 = \mathbf{P}_{8_S} \quad c_8 = \mathbf{P}_{27}$
$c_3 = \text{Tr} (t^{r_a} t^{r_1} t^{r_b} t^{r_2}) - \text{Tr} (t^{r_a} t^{r_2} t^{r_b} t^{r_1})$	$c_6 = \mathbf{P}_{8_A}$

One possibility to choose the basis is the  $\hat{t}$ -channel singlet-octet color basis

$$\begin{aligned}
c_1 &= \delta_{r_a r_1} \delta_{r_b r_2} \\
c_2 &= (t^c)_{r_1 r_a} (t^c)_{r_b r_2} = \frac{1}{2} \delta_{r_a r_b} \delta_{r_1, r_2} - \frac{1}{2N_c} \delta_{r_a r_1} \delta_{r_b r_2},
\end{aligned} \tag{5.21}$$

where the  $t^c$  are the generators of  $SU(3)$  in the fundamental representation. This choice of basis allows us directly to write down the lowest order soft matrix according to Eq. (5.19):

$$S^{q\bar{q} \rightarrow q\bar{q}} = \begin{pmatrix} N_c^2 & 0 \\ 0 & \frac{N_c^2 - 1}{4} \end{pmatrix} \tag{5.22}$$

The lowest order hard matrix is obtained by the squares of the color-decomposed tree amplitudes. Therefore, there is a difference, whether the flavor constellation of the produced quark-antiquark pair is identical,  $q_j \bar{q}_j \rightarrow q_j \bar{q}_j$  and  $q_j \bar{q}_k \rightarrow q_j \bar{q}_k$ , or different from the flavor of the final state quark-antiquark pair,  $q_j \bar{q}_j \rightarrow q_k \bar{q}_k$ . This is illustrated in Table 5.1. In

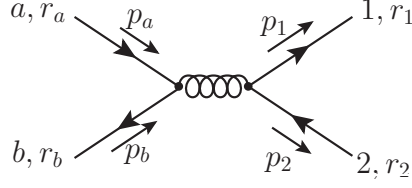


**Fig. 5.4.:** Illustration of the formalism used to calculate the lowest order hard and soft matrices for  $q_j \bar{q}_j \rightarrow q_k \bar{q}_k$ .  $p_i$  denotes the momentum of parton  $i$ , which carries color  $r_i$ .

the latter case, there is only one tree-level diagram contributing. This diagram is shown in Fig. 5.4. Its color structure is given by

$$(t^x)_{r_1 r_2} (t^x)_{r_b r_a} = \frac{1}{2} \delta_{r_1 r_a} \delta_{r_b r_2} - \frac{1}{2N_c} \delta_{r_1 r_2} \delta_{r_a r_b} = \frac{C_F}{N_c} c_1 - \frac{1}{N_c} c_2. \quad (5.23)$$

Combining with the color-decomposition of the complex conjugated diagram, averaging over the color of the incoming partons, and including also the kinematical part, yields

$$H^{q_j \bar{q}_j \rightarrow q_k \bar{q}_k} = \alpha_s^2 \frac{2}{N_c^2} \frac{\hat{t}^2 + \hat{u}^2}{\hat{s}^2} \begin{pmatrix} \frac{C_F}{N_c^2} & -\frac{C_F}{N_c^2} \\ -\frac{C_F}{N_c^2} & \frac{1}{N_c^2} \end{pmatrix}. \quad (5.24)$$

Next, let us have a look on the quark-antiquark scattering diagram,  $q_j \bar{q}_k \rightarrow q_j \bar{q}_k$ . Here the color structure is simply  $(t^x)_{r_1 r_a} (t^x)_{r_b r_2} = c_2$ . Therefore, the hard matrix has only one non-vanishing entry.

$$H^{q_j \bar{q}_k \rightarrow q_j \bar{q}_k} = \alpha_s^2 \frac{2}{N_c^2} \frac{\hat{s}^2 + \hat{u}^2}{\hat{t}^2} \begin{pmatrix} 0 & 0 \\ 0 & 1 \end{pmatrix}. \quad (5.25)$$

In contrast to these two processes, a quark-antiquark pair with identical flavor,  $q_j \bar{q}_j \rightarrow q_j \bar{q}_j$ , may be produced via a  $\hat{s}$ -channel- and a  $\hat{t}$ -channel- diagram. Thus, its hard matrix  $H^{q_j \bar{q}_j \rightarrow q_j \bar{q}_j}$  is given by  $\textcolor{red}{H}^{q_j \bar{q}_j \rightarrow q_k \bar{q}_k} + \textcolor{green}{H}^{q_j \bar{q}_k \rightarrow q_j \bar{q}_k}$  plus interference terms proportional to  $\hat{u}/\hat{s}\hat{t}$ . This gives

$$H^{q_j \bar{q}_j \rightarrow q_j \bar{q}_j} = \alpha_s^2 \begin{pmatrix} H_{11}^{q_j \bar{q}_j \rightarrow q_j \bar{q}_j} & H_{12}^{q_j \bar{q}_j \rightarrow q_j \bar{q}_j} \\ H_{12}^{q_j \bar{q}_j \rightarrow q_j \bar{q}_j} & H_{22}^{q_j \bar{q}_j \rightarrow q_j \bar{q}_j} \end{pmatrix}, \quad (5.26)$$

with

$$\begin{aligned}
H_{11}^{q_j \bar{q}_j \rightarrow q_j \bar{q}_j} &= \frac{2C_F^2 \hat{t}^2 + \hat{u}^2}{N_c^4 \hat{s}^2}, \\
H_{12}^{q_j \bar{q}_j \rightarrow q_j \bar{q}_j} &= \frac{2C_F}{N_c^3} \left( -\frac{\hat{t}^2 + \hat{u}^2}{N_c \hat{s}^2} + \frac{\hat{u}^2}{\hat{s} \hat{t}} \right), \\
H_{22}^{q_j \bar{q}_j \rightarrow q_j \bar{q}_j} &= \frac{1}{N_c^2} \left( \frac{2}{N_c^2} \frac{\hat{t}^2 + \hat{u}^2}{\hat{s}^2} + 2 \frac{\hat{s}^2 + \hat{u}^2}{\hat{t}^2} - \frac{4}{N_c} \frac{\hat{u}^2}{\hat{s} \hat{t}} \right).
\end{aligned} \tag{5.27}$$

### 5.2.2. Gluon-gluon scattering $gg \rightarrow gg$

Next, let us have a look at a more complicated process: gluon-gluon scattering. With the color basis in Eq. (5.18) (see also Table 5.2) at hand, the lowest order soft matrix may be directly derived

$$S^{gg \rightarrow gg} = \begin{pmatrix} S_{3 \times 3}^{gg \rightarrow gg} & 0_{3 \times 5} \\ 0_{5 \times 3} & S_{5 \times 5}^{gg \rightarrow gg} \end{pmatrix}, \tag{5.28}$$

where the submatrices are given by

$$S_{3 \times 3}^{gg \rightarrow gg} = \begin{pmatrix} 5 & 0 & 0 \\ 0 & 5 & 0 \\ 0 & 0 & 5 \end{pmatrix}, \quad S_{5 \times 5}^{gg \rightarrow gg} = \begin{pmatrix} 1 & 0 & 0 & 0 & 0 \\ 0 & 8 & 0 & 0 & 0 \\ 0 & 0 & 8 & 0 & 0 \\ 0 & 0 & 0 & 20 & 0 \\ 0 & 0 & 0 & 0 & 27 \end{pmatrix}. \tag{5.29}$$

The eigenvalues of the projectors on the diagonal are 1, 8, 8, 20, 27. These are exactly the number of color states belonging to each irreducible representation. The lowest order hard matrix [135], which corresponds to this basis, has block-diagonal structure,

$$H^{gg \rightarrow gg} = \alpha_s^2 \begin{pmatrix} 0_{3 \times 3} & 0_{3 \times 5} \\ 0_{5 \times 3} & H_{5 \times 5}^{gg \rightarrow gg} \end{pmatrix}, \tag{5.30}$$

with

$$H_{5 \times 5}^{gg \rightarrow gg} = \frac{1}{16} \begin{pmatrix} 9h_1 & \frac{9}{2}h_1 & \frac{9}{2}h_2 & 0 & -3h_1 \\ \frac{9}{2}h_1 & \frac{9}{4}h_1 & \frac{9}{4}h_2 & 0 & -\frac{3}{2}h_1 \\ \frac{9}{2}h_2 & \frac{9}{4}h_2 & h_3 & 0 & -\frac{3}{2}h_2 \\ 0 & 0 & 0 & 0 & 0 \\ -3h_1 & -\frac{3}{2}h_1 & -\frac{3}{2}h_2 & 0 & h_1 \end{pmatrix}, \quad (5.31)$$

and  $h_1, h_2$  and  $h_3$  defined by

$$\begin{aligned} h_1 &= 1 - \frac{\hat{t}\hat{u}}{\hat{s}^2} - \frac{\hat{s}\hat{t}}{\hat{u}^2} + \frac{\hat{t}^2}{\hat{s}\hat{u}} \\ h_2 &= \frac{\hat{s}\hat{t}}{\hat{u}^2} - \frac{\hat{t}\hat{u}}{\hat{s}^2} + \frac{\hat{u}^2}{\hat{s}\hat{t}} - \frac{\hat{s}^2}{\hat{t}\hat{u}} \\ h_3 &= \frac{27}{4} - 9 \left( \frac{\hat{s}\hat{u}}{\hat{t}^2} + \frac{1}{4} \frac{\hat{t}\hat{u}}{\hat{s}^2} + \frac{1}{4} \frac{\hat{s}\hat{t}}{\hat{u}^2} \right) + \frac{9}{2} \left( \frac{\hat{u}^2}{\hat{s}\hat{t}} + \frac{\hat{s}^2}{\hat{t}\hat{u}} - \frac{1}{2} \frac{\hat{t}^2}{\hat{s}\hat{u}} \right). \end{aligned} \quad (5.32)$$

It can be noticed that the first three basis vectors  $c_1 - c_3$  decouple from the Born cross section, as the hard scattering components in these color directions vanish.

The hard and soft matrices of the other processes may be found analogously and are given in [126] and are collected in Table C.1 and Table C.2.

### 5.3. The soft anomalous dimension matrix

In order to compute the anomalous dimension matrix we need to extract the UV divergent one loop contributions to the eikonal vertex  $w_I^{(f)}$ . The renormalization of the incoming and the outgoing light-like lines are part of the eikonal jets and have already been factorized into the corresponding wave function. Therefore in case of the soft function, we only have to deal with the UV-divergences from the vertex correction diagrams, which are shown for a generic partonic process in Fig. 5.5. For the calculation of the soft anomalous dimension matrix we need to derive the counterterms for the eikonal vertex  $w_I^{(f)}$ . They depend on the external momenta and on the axial gauge fixing vector  $n$ . With the basis color tensors  $c_I^{(f)}$  given, the eikonal vertices are given at Born level directly by

$$w_{I,Born}^{(f)} = c_I^{(f)} \quad (5.33)$$

Then the one-loop corrections follow from the Born term by multiplication with the matrix of renormalization constants  $Z_S$

$$w_{1-loop}^{(f),T} = c^{(f),T} Z_S = w_{Born}^{(f),T} Z_S, \quad (5.34)$$



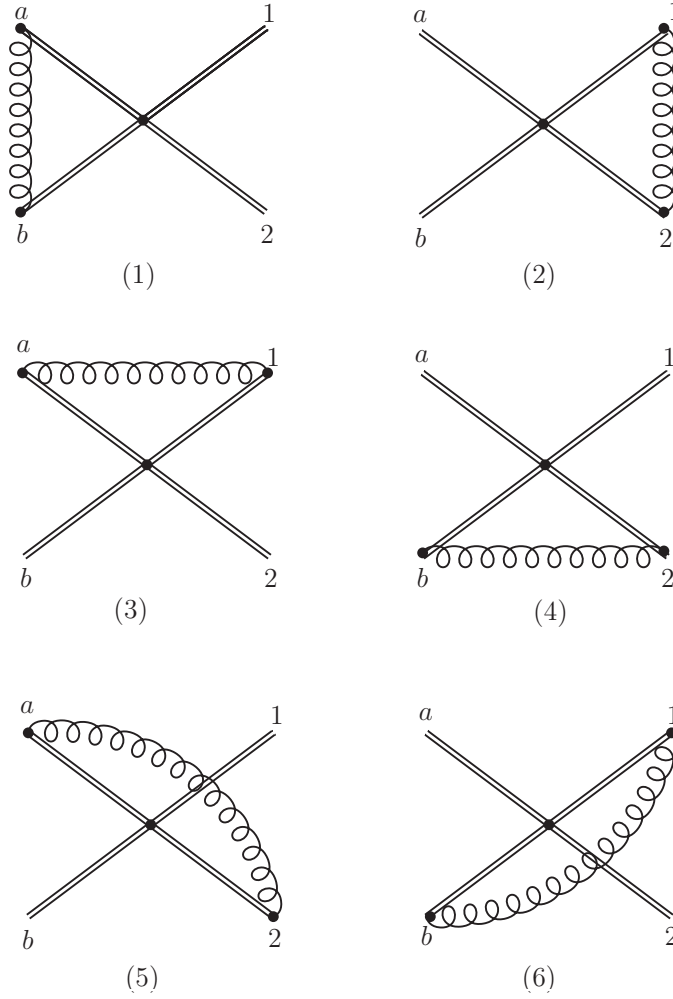


**Fig. 5.5.:** One loop eikonal vertex correction diagrams for partonic processes contributing to the soft anomalous dimension matrices [111]. The diagrams are *reduced* diagrams, in which all off-shell lines are contracted. The double lines symbolize eikonal lines.

where the superscript  $T$  indicates transposition. So, in order to derive the matrix of renormalization constants for a specific process, one is confronted with the calculation of vertex-correction-diagrams depicted in Fig. 5.5. For that, let us have a look at a generic vertex correction, in which a gluon is exchanged between partons with momenta  $p_i$  and  $p_j$ . As the soft function only couples to eikonal lines, one can use the Feynman rules for the eikonal approximation, as shown in Fig. 5.6. These do not depend on the full four-momenta  $p_i$  any more, but may be written with a dimensionless, light-like velocity vector  $\beta_i$  (defining the direction of Wilson lines at vertices  $w^{(f)}$ ), which is defined as in Eq. (4.16) by

$$\beta_i^\mu = \sqrt{\frac{2}{\hat{s}}} p_i^\mu. \quad (5.35)$$

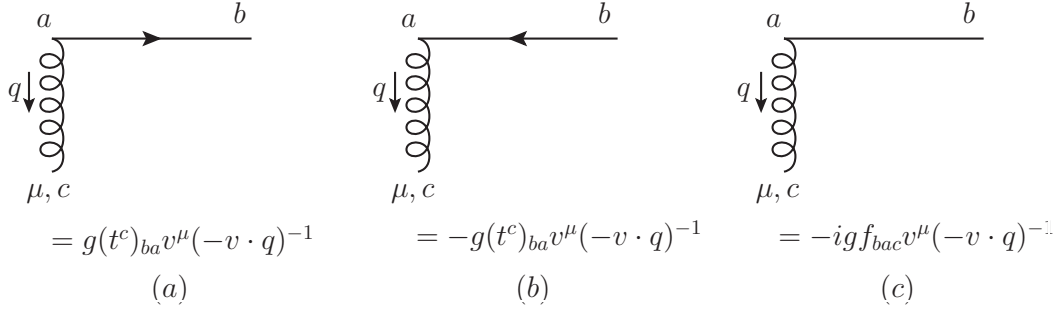


**Fig. 5.6.:** The Feynman rules in the eikonal approximation for a quark (a), antiquark (b) and gluon (c) eikonal line. [114]

We follow the notation of [111] to write the kinematic part of the one-loop vertex correction  $w_I^{(f)}$  as

$$w_{ij}^{(f)} = g^2 \int \frac{d^D q}{(2\pi)^D} D_{\mu\nu}(q) \frac{\Delta_i \beta_i^\mu}{\delta_i \beta_i \cdot q + i\epsilon} \frac{\Delta_j \beta_j^\nu}{\delta_j \beta_j \cdot q + i\epsilon} \quad (5.36)$$

Here,  $D_{\mu\nu}(k)$  is the gluon propagator. In axial gauge the propagator reads as

$$D^{\mu\nu}(k) = \frac{-i}{k^2 + i\epsilon} N^{\mu\nu}(k), \quad N^{\mu\nu}(k) = g^{\mu\nu} - \frac{n^\mu k^\nu + k^\mu n^\nu}{n \cdot k} + n^2 \frac{k^\mu k^\nu}{(n \cdot k)^2}, \quad (5.37)$$

where  $n$  denotes the gauge vector. Therefore we obtain

$$w_{ij}^{(f)} = g^2 \int \frac{d^D q}{(2\pi)^D} \frac{-i}{q^2 + i\epsilon} \left\{ \frac{\Delta_i \Delta_j \beta_i \cdot \beta_j}{(\delta_i \beta_i \cdot q + i\epsilon)(\delta_j \beta_j \cdot q + i\epsilon)} - \frac{\Delta_i \beta_i \cdot n}{(\delta_i \beta_i \cdot q + i\epsilon)} \frac{\mathcal{P}}{(n \cdot q)} \right. \\ \left. - \frac{\Delta_j \beta_j \cdot n}{(\delta_j \beta_j \cdot q + i\epsilon)} \frac{\mathcal{P}}{(n \cdot q)} + n^2 \frac{\mathcal{P}}{(n \cdot q)^2} \right\}. \quad (5.38)$$

Here,  $\mathcal{P}$  denotes the principal value,

$$\frac{\mathcal{P}}{(q \cdot n)^l} = \frac{1}{2} \left( \frac{1}{(q \cdot n + i\epsilon)^l} + (-1)^l \frac{1}{(-q \cdot n + i\epsilon)^l} \right). \quad (5.39)$$

Now we sort the contributions in Eq. (5.38) as follows

$$w_{ij}^{(f)} = \mathcal{S}_{ij} \left[ I_1(\delta_i \beta_i, \delta_j \beta_j) - \frac{1}{2} I_2(\delta_i \beta_i, n) - \frac{1}{2} I_2(\delta_i \beta_i, -n) \right. \\ \left. - \frac{1}{2} I_3(\delta_j \beta_j, n) - \frac{1}{2} I_3(\delta_j \beta_j, -n) + I_4(n^2) \right] \quad (5.40)$$

$\mathcal{S}_{ij} = \Delta_i \Delta_j \delta_i \delta_j$  is the overall sign. The next step is to evaluate the ultraviolet poles of the four integrals  $I_1 - I_4$ . The calculations are carried out in  $D = 4 - \epsilon$  dimensions. Let us

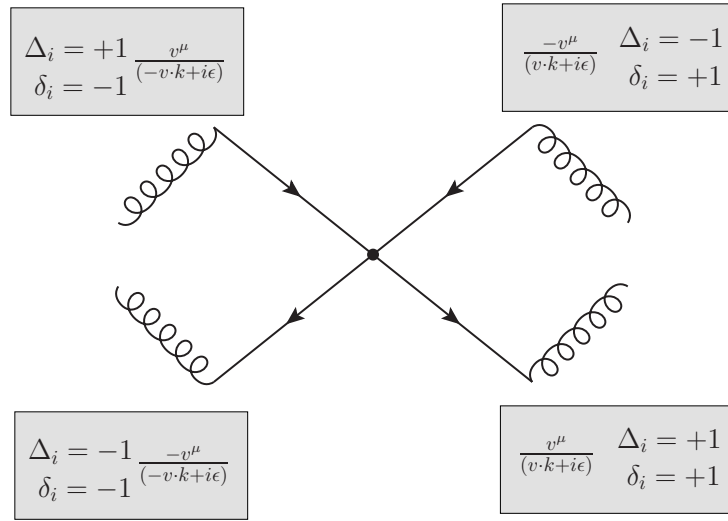


**Fig. 5.7.:** Feynman rules for eikonal lines in  $q\bar{q} \rightarrow q\bar{q}$  [111].  $v^\mu$  is a dimensionless four-vector which is proportional to the momentum  $p^\mu$  of the quark or antiquark, respectively. The gluon momentum  $k$  flows out of the eikonal lines. The color matrices at the vertices are the same as for the ordinary Feynman rules. The positive (negative) sign of  $\delta$  shows whether the 3-direction of the gluon momentum and  $v$  is the same (opposite). Furthermore,  $\Delta_i = 1$  corresponds to a quark and  $\Delta_i = -1$  to an antiquark.

start with the first integral,

$$I_1(\delta_i\beta_i, \delta_j\beta_j) = \frac{g^2}{\mathcal{S}_{ij}} \int \frac{d^D q}{(2\pi)^D} \frac{-i}{q^2 + i\epsilon} \frac{\Delta_i \Delta_j \beta_i \cdot \beta_j}{(\delta_i \beta_i \cdot q + i\epsilon)(\delta_j \beta_j \cdot q + i\epsilon)}. \quad (5.41)$$

Two different kinds of divergencies show up in this integral. On the one hand we have the ultraviolet divergence for  $q \rightarrow \infty$  and on the other hand the integral is also infrared divergent. The divergences will show itself as  $\frac{1}{\epsilon}$ -poles and have to be separated. We will come to this point later. Making use of Feynman parametrization

$$\frac{1}{ABC} = 2 \int_0^1 dx \int_0^{1-x} dy \frac{1}{[xA + yB + (1-x-y)C]^3} \quad (5.42)$$

we obtain

$$I_1(\delta_i\beta_i, \delta_j\beta_j) = -ig^2 \frac{\beta_{ij}}{\delta_i \delta_j} \frac{2}{(2\pi)^D} \int_0^1 dx \int_0^{1-x} dy \int \frac{d^D q}{[xq^2 + q \cdot (y\delta_i\beta_i + (1-x-y)\delta_j\beta_j) + i\epsilon]}, \quad (5.43)$$

where we defined

$$\beta_{ij} \equiv \beta_i \cdot \beta_j. \quad (5.44)$$

After a suitable translation in  $q_\nu$ , and a Wick rotation to Euclidian space  $q^0 \rightarrow iq_E^4$ ,  $q^2 \rightarrow -q_E^2$ , we arrive at

$$I_1(\delta_i\beta_i, \delta_j\beta_j) = -g^2 \frac{\beta_{ij}}{\delta_i\delta_j} \frac{2}{(2\pi)^D} \int_0^1 dx x^{-\frac{D}{2}} \int_0^{1-x} dy \int \frac{d^D q_E}{\left[ q_E^2 + \frac{(y\delta_i\beta_i + (1-x-y)\delta_j\beta_j)^2}{4x} - i\epsilon \right]^3} \quad (5.45)$$

Now the denominator in the last integral is in a form, which enables us to apply the master formula from [136] and calculate the  $q_E$ -integral. After substituting  $z := y/(1-x)$  we obtain

$$I_1(\delta_i\beta_i, \delta_j\beta_j) = -g^2 \frac{\beta_{ij}}{\delta_i\delta_j} \frac{2^{2\epsilon}}{4\pi^{\frac{D}{2}}} \Gamma(1 + \frac{\epsilon}{2}) \int_0^1 dx x^{-1+\epsilon} (1-x)^{-1-\epsilon} \times \int_0^1 dz [(z\delta_i\beta_i + (1-z)\delta_j\beta_j)^2]^{-1-\frac{\epsilon}{2}} \quad (5.46)$$

The integral in  $x$  contains UV singularities for  $x \rightarrow 1$  and IR singularities for  $x \rightarrow 0$ . As we are only interested in UV singularities, we separate them off:

$$\int_0^1 dx x^{-1+\epsilon} (1-x)^{-1-\epsilon} = \frac{1}{\epsilon} + \text{IR} \quad (5.47)$$

Therefore, we end up with

$$I_1^{\text{UV pole}} = \frac{\alpha_s}{\pi} \left[ \frac{2}{\epsilon^2} - \frac{1}{\epsilon} \left( \gamma_E + \ln(\delta_i\delta_j \frac{\beta_{ij}}{2}) - \ln(4\pi) \right) \right] \quad (5.48)$$

Next, we want to calculate the second integral in Eq. (5.38). As the second term of the sum in the definition of the principal value in Eq. (5.39) is easily obtained by the transformation  $n \rightarrow -n$  in the first term of the sum, it is sufficient to concentrate on the first one,

$$I_2(\delta_i\beta_i, n) = g^2 \mathcal{S}_{ij} \int \frac{d^D q}{(2\pi)^D} \frac{-i}{q^2 + i\epsilon} \frac{\Delta_i\beta_i \cdot n}{(\delta_i\beta_i \cdot q + i\epsilon)} \frac{1}{q \cdot n + i\epsilon}. \quad (5.49)$$

As before, we will make use of Feynman parametrization and a Wick rotation to solve the integral over  $q$ . We arrive at

$$I_2(\delta_i\beta_i, n) = -\frac{\alpha_s}{\pi} \Delta_i \mathcal{S}_{ij} (\beta_i \cdot n) \pi^{\frac{\epsilon}{2}} 2^{2\epsilon} \Gamma(1 + \frac{\epsilon}{2}) \int_0^1 dx x^{-1+\epsilon} (1-x)^{-1-\epsilon} \times \int_0^1 dz (2z(1-z)\delta_i\beta_i \cdot n + (1-z)^2 n^2)^{-1-\frac{\epsilon}{2}}. \quad (5.50)$$

The integral over  $x$  is the same as in Eq. (5.47) with a UV-singularity of  $\frac{1}{\epsilon}$ . Now we have to extract the singularities of the  $y$ -integral in Eq. (5.50). Replacing  $a \equiv \delta_i\beta_i \cdot n$  and  $b \equiv n^2$

it may be written as

$$I_y(a, b) = \int_0^1 dz (1-z)^{-1-\frac{\epsilon}{2}} (2za + (1-z)b)^{-1-\frac{\epsilon}{2}} \quad (5.51)$$

This integral is calculated analytically

$$I_y(a, b) = -\frac{b^{-1-\frac{\epsilon}{2}}}{\epsilon} \text{hypergeom} \left( \left[ 1, 1 + \frac{\epsilon}{2} \right], \left[ 1 - \frac{\epsilon}{2} \right], -\frac{2a-b}{b} \right), \quad (5.52)$$

where the hypergeometric function is defined as

$$\text{hypergeom}([n_1, n_2, \dots, n_p], [d_1, d_2, \dots, d_q], z) = \sum_{k=0}^{\infty} \frac{z^k}{k!} \frac{\prod_{i=1}^p \text{pochhammer}(n_i, k)}{\prod_{j=1}^q \text{pochhammer}(d_j, k)}, \quad (5.53)$$

in terms of the pochhammer function,

$$\text{pochhammer}(z, a) = \frac{\Gamma(z+a)}{\Gamma(z)}. \quad (5.54)$$

We simplify the result for  $I_y(a, b)$ :

$$\begin{aligned} I_y(a, b) &= -\frac{b^{-1-\frac{\epsilon}{2}}}{\epsilon} \frac{\Gamma(1-\frac{\epsilon}{2})}{\Gamma(1+\frac{\epsilon}{2})} \sum_{k=0}^{\infty} c^k \frac{\Gamma(1+\frac{\epsilon}{2}+k)}{\Gamma(1-\frac{\epsilon}{2}+k)} \\ &= -\frac{b^{-1-\frac{\epsilon}{2}}}{\epsilon} \frac{\Gamma(1-\frac{\epsilon}{2})}{\Gamma(1+\frac{\epsilon}{2})} \sum_{k=0}^{\infty} c^k [1 + \epsilon(\Psi(k+1) + \gamma_E) + \mathcal{O}(\epsilon^2)] \end{aligned} \quad (5.55)$$

We rearrange the second term in the sum

$$\sum_{k=0}^{\infty} c^k (\Psi(k+1) + \gamma_E) = \sum_{k=0}^{\infty} c^k \sum_{i=1}^k \frac{1}{i} = \sum_{i=1}^{\infty} \frac{c^{i-1}}{i} \sum_{k=0}^{\infty} c^k = \sum_{i=1}^{\infty} \frac{c^i}{i} \frac{1}{1-c} = -\frac{\ln(1-c)}{1-c} \quad (5.56)$$

Using this identity we obtain,

$$I_y(a, b) = -\frac{1}{a\epsilon} + \frac{\ln(\frac{4a^2}{b})}{2a} + \mathcal{O}(\epsilon), \quad (5.57)$$

what finally allows us to extract the UV-poles in Eq. (5.50). One ends up with

$$I_2^{\text{UV pole}} = \delta_j \Delta_j \frac{\alpha_s}{2\pi} \left( \frac{2}{\epsilon^2} - \frac{1}{\epsilon} \left[ \gamma_E + \ln \left( \frac{(\beta_i \cdot n)^2}{n^2} \right) - \ln(4\pi) \right] \right). \quad (5.58)$$

We showed explicitly how to calculate the UV-singularities of the integrals  $I_1$  and  $I_2$  in Eq. (5.40). The remaining integrals may be calculated analogously. Collecting all of them,

we have

$$\begin{aligned}
I_1^{\text{UV pole}} &= \frac{\alpha_s}{\pi} \left[ \frac{2}{\epsilon^2} - \frac{1}{\epsilon} \left( \gamma_E + \ln(\delta_i \delta_j \frac{\beta_{ij}}{2}) - \ln(4\pi) \right) \right] \\
I_2^{\text{UV pole}} &= \frac{\alpha_s}{2\pi} \left( \frac{2}{\epsilon^2} - \frac{1}{\epsilon} [\gamma_E + \ln(\nu_i) - \ln(4\pi)] \right) \\
I_3^{\text{UV pole}} &= \frac{\alpha_s}{2\pi} \left( \frac{2}{\epsilon^2} - \frac{1}{\epsilon} [\gamma_E + \ln(\nu_j) - \ln(4\pi)] \right) \\
I_4^{\text{UV pole}} &= -\frac{\alpha_s}{\pi} \frac{1}{\epsilon},
\end{aligned} \tag{5.59}$$

where

$$\nu_i = \frac{(\beta_i \cdot n)^2}{|n|^2}. \tag{5.60}$$

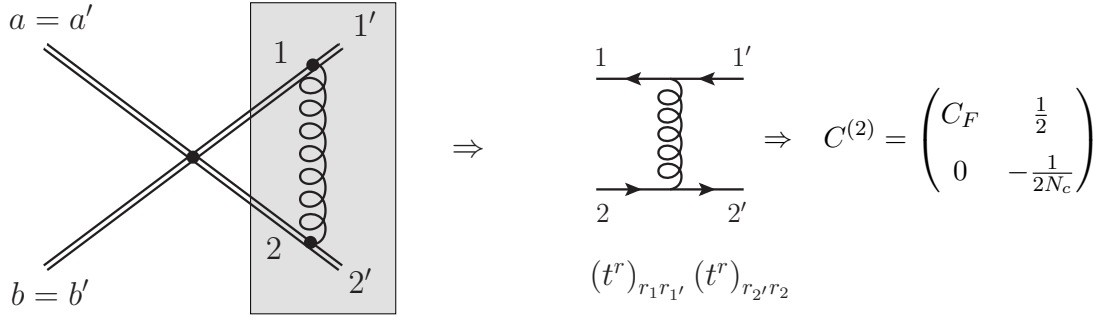
Note that the double poles have to cancel in the sum in Eq. (5.40), as at the end of each first-order calculation only  $1/\epsilon$ -poles can appear, which are then cured by adding counterterms. We end up with

$$w_{ij}^{(f)} = -\mathcal{S}_{ij} \frac{\alpha_s}{\pi\epsilon} \left[ \ln \left( \frac{\delta_i \delta_j \beta_{ij}}{2} \right) - \frac{1}{2} \ln(\nu_i \nu_j) + 1 \right] \tag{5.61}$$

What now is left to do, is to calculate the color decomposition into the basis color structures for each of the contributing diagrams. This gives the different entries of the matrix of renormalization constants. Then the anomalous dimension matrix can be directly deduced by the relation in Eq. (4.43)

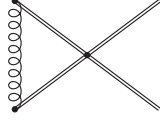
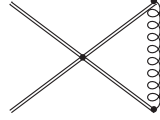
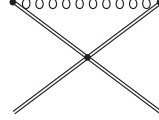
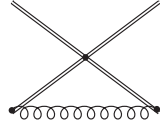
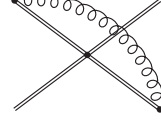
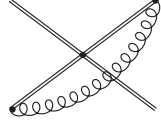
$$\Gamma_S(g) = -\frac{g}{2} \frac{\partial}{\partial g} \text{Res}_{\epsilon \rightarrow 0} Z_S(g, \epsilon) \tag{5.62}$$

It is instructive to study with an explicit example how the anomalous dimension is created step-by-step. Therefore, we will present details of the calculation of the anomalous dimension matrix of quark-antiquark production through quark-antiquark annihilation. The procedure is as following: For each color vertex of the reduced diagrams in Fig. 5.5 one considers its one loop correction. Then, one calculates the color decomposition of the resulting ultraviolet divergences. This may be done by calculating the resulting color decomposition after adding a gluon-exchange for each basis vector. This gives a matrix in color space for each color vertex in Fig. 5.5. They dictate the generic color flow for each one loop correction. Then these color matrices are combined with the respective ultraviolet poles from its kinematic parts (which have been calculated before and are given by Eq. (5.61)). This gives the counterparts, which in turn allow to deduce the anomalous dimension matrix. This procedure just depends on which partons are involved, but is independent of the underlying hard (LO) process. Consequently, the anomalous dimension



**Fig. 5.8.:** Illustration of the procedure to calculate the color decomposition of the one loop vertex correction in the reduced diagram (2) in Fig. 5.5.

**Table 5.3.:** The table shows for each reduced diagram in Fig. 5.5 the matrix, which represents the modification of the “Born-color structure” caused by the addition of a gluon exchange between two quark lines.

  <div style="display: flex; justify-content: space-around; margin-top: 5px;"> <span>(1)</span> <span>(2)</span> </div>	  <div style="display: flex; justify-content: space-around; margin-top: 5px;"> <span>(3)</span> <span>(4)</span> </div>	  <div style="display: flex; justify-content: space-around; margin-top: 5px;"> <span>(5)</span> <span>(6)</span> </div>
$C^{(1),(2)} = \begin{pmatrix} C_F & \frac{1}{2} \\ 0 & -\frac{1}{2N_c} \end{pmatrix}$	$C^{(3),(4)} = \begin{pmatrix} -\frac{1}{2N_c} & \frac{1}{2} \\ \frac{1}{2} & -\frac{1}{2N_c} \end{pmatrix}$	$C^{(5),(6)} = \begin{pmatrix} -\frac{1}{2N_c} & 0 \\ \frac{1}{2} & C_F \end{pmatrix}$

matrices are not specific to the individual channels. For instance, the anomalous dimension matrices are identical for the processes  $q_j \bar{q}_j \rightarrow q_j \bar{q}_j$ ,  $q_j \bar{q}_j \rightarrow q_k \bar{q}_k$ , and  $q_j \bar{q}_k \rightarrow q_j \bar{q}_k$ . In the end the combination with the hard matrix  $H$  of each process will project out the adequate color terms of the one loop correction for each channel.

To be specific, let us consider the reduced diagram (2) in Fig. 5.5. For the Born process we choose the basis in color space as follows

$$\begin{aligned} c_1 &= \delta_{r_a r_b} \delta_{r_1 r_2}, \\ c_2 &= \delta_{r_a r_2} \delta_{r_b r_1}. \end{aligned} \tag{5.63}$$

After a generic gluon exchange between two quark lines, the colors of two (initial or final) partons may change. As shown in Fig. 5.8, let  $r_{a'}$ ,  $r_{b'}$ ,  $r_{1'}$  and  $r_{2'}$  denote the color of the

partons after the one loop correction, respectively. The basis is then chosen to be

$$\begin{aligned} c'_1 &= \delta_{r_a' r_{b'}} \delta_{r_{1'} r_{2'}}, \\ c'_2 &= \delta_{r_a' r_{2'}} \delta_{r_{b'} r_{1'}}. \end{aligned} \quad (5.64)$$

Compared to the color structure of the Born process, the vertex correction term adds the term,

$$\delta_{r_a r_{a'}} \delta_{r_b r_{b'}} (t^r)_{r_1 r_{1'}} (t^r)_{r_2' r_2} \quad (5.65)$$

in color space. Starting with the basis vector  $c_1$  (from the Born term) we are summing over the intermediate colors  $r_1, r_2$ . Making use of the Fierz-identity,

$$(t^r)_{ij} (t^r)_{kl} = \frac{1}{2} \delta_{il} \delta_{jk} - \frac{1}{2N_c} \delta_{ij} \delta_{kl}, \quad (5.66)$$

we obtain

$$\begin{aligned} \sum_{r_1, r_2} c_1 \delta_{r_a r_{a'}} \delta_{r_b r_{b'}} (t^r)_{r_1 r_{1'}} (t^r)_{r_2' r_2} &= \sum_{r_1, r_2} \delta_{r_a' r_{b'}} \delta_{r_1 r_2} \left( \frac{1}{2} \delta_{r_1 r_2} \delta_{r_{1'} r_{2'}} - \frac{1}{2N_c} \delta_{r_1 r_{1'}} \delta_{r_2 r_{2'}} \right) \\ &= C_F \delta_{r_a' r_{b'}} \delta_{r_{1'} r_{2'}} = C_F c'_1. \end{aligned} \quad (5.67)$$

The vertex correction to the second basis vector  $c_2$  gives

$$\begin{aligned} \sum_{r_1, r_2} c_2 \delta_{r_a r_{a'}} \delta_{r_b r_{b'}} (t^r)_{r_1 r_{1'}} (t^r)_{r_2' r_2} &= \sum_{r_1, r_2} \delta_{r_a' r_{b'}} \delta_{r_1 r_2} \left( \frac{1}{2} \delta_{r_1 r_2} \delta_{r_{1'} r_{2'}} - \frac{1}{2N_c} \delta_{r_1 r_{1'}} \delta_{r_2 r_{2'}} \right) \\ &= \frac{1}{2} \delta_{r_2' r_{1'}} \delta_{r_a' r_{b'}} - \frac{1}{2N_c} \delta_{r_a' r_{2'}} \delta_{r_{b'} r_{1'}} = \frac{1}{2} c'_1 - \frac{1}{2N_c} c'_2. \end{aligned} \quad (5.68)$$

Thus the linear transformation, which describes the modification of the “Born-color structure” caused by an additional gluon exchange between the two outgoing quark lines, may be represented by the matrix

$$C^{(2)} \equiv \begin{pmatrix} C_F & \frac{1}{2} \\ 0 & -\frac{1}{2N_c} \end{pmatrix}. \quad (5.69)$$

Analogously the color decomposition of the other five vertex corrections in Fig. 5.5 may be derived. All results are summed up in Table 5.3.

The next step is to combine the color decomposition of each vertex correction with the UV-poles of its kinematic part, which we derived in Eq. (5.61). The sum of all these contributions gives, with an additional minus sign (counter terms), the matrix of renormalization



constants  $Z_S^{q\bar{q} \rightarrow q\bar{q}}$

$$\begin{aligned}
Z_{S,11}^{q\bar{q} \rightarrow q\bar{q}} &= -\frac{1}{\epsilon} \frac{\alpha_s}{\pi} C_F \left[ \ln \left( \frac{\beta_{12}\beta_{ab}}{4} \right) - \frac{1}{2} \ln(\nu_a \nu_b \nu_1 \nu_2) + 2 - 2\pi i \right] + \frac{1}{N_c} Z_{S,21}^{q\bar{q} \rightarrow q\bar{q}} \\
Z_{S,21}^{q\bar{q} \rightarrow q\bar{q}} &= -\frac{1}{\epsilon} \frac{\alpha_s}{2\pi} \ln \left( \frac{\beta_{a2}\beta_{b1}}{\beta_{a1}\beta_{b2}} \right) \\
Z_{S,12}^{q\bar{q} \rightarrow q\bar{q}} &= -\frac{1}{\epsilon} \frac{\alpha_s}{2\pi} \left[ \ln \left( \frac{\beta_{ab}\beta_{12}}{\beta_{a1}\beta_{b2}} \right) - 2\pi i \right] \\
Z_{S,22}^{q\bar{q} \rightarrow q\bar{q}} &= -\frac{1}{\epsilon} \frac{\alpha_s}{\pi} C_F \left[ \ln \left( \frac{\beta_{a2}\beta_{b1}}{4} \right) - \frac{1}{2} \ln(\nu_a \nu_b \nu_1 \nu_2) + 2 \right] + \frac{1}{N_c} Z_{S,12}^{q\bar{q} \rightarrow q\bar{q}}. \quad (5.70)
\end{aligned}$$

Eq. (5.62) relates the matrix of renormalization constants to the anomalous dimension matrix, which thus results in (see also [110, 111])

$$\begin{aligned}
\Gamma_{S,11}^{q\bar{q} \rightarrow q\bar{q}} &= \frac{1}{\epsilon} \frac{\alpha_s}{\pi} C_F \left[ \ln \left( \frac{\beta_{12}\beta_{ab}}{4} \right) - \frac{1}{2} \ln(\nu_a \nu_b \nu_1 \nu_2) + 2 - 2\pi i \right] - \frac{1}{N_c} \Gamma_{S,21}^{q\bar{q} \rightarrow q\bar{q}} \\
\Gamma_{S,21}^{q\bar{q} \rightarrow q\bar{q}} &= \frac{1}{\epsilon} \frac{\alpha_s}{2\pi} \ln \left( \frac{\beta_{a2}\beta_{b1}}{\beta_{a1}\beta_{b2}} \right) \\
\Gamma_{S,12}^{q\bar{q} \rightarrow q\bar{q}} &= \frac{1}{\epsilon} \frac{\alpha_s}{2\pi} \left[ \ln \left( \frac{\beta_{ab}\beta_{12}}{\beta_{a1}\beta_{b2}} \right) - 2\pi i \right] \\
\Gamma_{S,22}^{q\bar{q} \rightarrow q\bar{q}} &= \frac{1}{\epsilon} \frac{\alpha_s}{\pi} C_F \left[ \ln \left( \frac{\beta_{a2}\beta_{b1}}{4} \right) - \frac{1}{2} \ln(\nu_a \nu_b \nu_1 \nu_2) + 2 \right] - \frac{1}{N_c} \Gamma_{S,12}^{q\bar{q} \rightarrow q\bar{q}}. \quad (5.71)
\end{aligned}$$

Now we follow the formalism in [114] and express the anomalous dimension matrix in terms which depend on ratios of the Mandelstam variables (defined in Eq. (6.6)):

$$\begin{aligned}
T &\equiv \ln \left( \frac{-\hat{t}}{\hat{s}} \right) + i\pi \\
U &\equiv \ln \left( \frac{-\hat{u}}{\hat{s}} \right) + i\pi \quad (5.72)
\end{aligned}$$

Furthermore the gauge dependence for each parton  $i$  in process  $f$  is summarized in separate functions

$$\mathcal{G}_i^{(f)}(\nu_i) = C_i \frac{\alpha_s}{\pi} \left[ -\frac{1}{2} \ln(\nu_i) - \frac{1}{2} \ln 2 + \frac{1}{2} - \frac{1}{2} \pi i \right], \quad (5.73)$$

with  $C_i = C_F$  ( $C_A$ ) for a quark (gluon). As the gauge-dependent terms only occur in diagonal elements, the anomalous dimension matrix is typically written as

$$\left( \Gamma_S^{(f)} \right)_{mn} = \left( \Gamma_{S'}^{(f)} \right)_{mn} + \left( \sum_{i=a,b,1,2} \mathcal{G}_i^{(f)}(\nu_i) \right) \delta_{mn}. \quad (5.74)$$

With the choice of a suited gauge in Eq. (5.73),  $\Gamma_{S'}^{(f)}$  reduces to  $\Gamma_S^{(f)}$ . We will also call  $\Gamma_{S'}^{(f)}$

anomalous dimension matrix.

Let us now turn again to the quark-antiquark annihilation process. We have  $\beta_{ab} = \beta_{12} = 1$ ,  $\beta_{a1} = \beta_{b2} = -\hat{t}/\hat{s}$ , and  $\beta_{1b} = \beta_{2a} = -\hat{u}/\hat{s}$ . Then the anomalous dimension matrix may be written as,

$$\Gamma_{S'}^{q\bar{q} \rightarrow q\bar{q}} = \begin{pmatrix} -\frac{U-T}{N_c} & -T \\ U-T & 2C_F U + \frac{T}{N_c} \end{pmatrix} \quad (5.75)$$

This result of course depends on the one hand on our initial choice of basis ( $B$ ) in the two-dimensional color space in Eq. (5.63),

$$\begin{aligned} c_1^B &= \delta_{r_a r_b} \delta_{r_1 r_2}, \\ c_2^B &= \delta_{r_a r_2} \delta_{r_b r_1}, \end{aligned} \quad (5.76)$$

and on the other hand on the labeling conventions (and the order of) the participating partons in Eq. (5.20). For some reasons, however, another choice of basis ( $B'$ ), namely Eq. (5.21) (see also in Table 5.2)

$$\begin{aligned} c_1^{B'} &= \delta_{r_a r_1} \delta_{r_b r_2} \\ c_2^{B'} &= -\frac{1}{2N_c} \delta_{r_a, r_1} \delta_{r_b, r_2} + \frac{1}{2} \delta_{r_a, r_b} \delta_{r_1, r_2} \end{aligned} \quad (5.77)$$

and labeling  $q(p_a) + \bar{q}(p_b) \rightarrow q(p_1) + \bar{q}(p_2)$  (interchanging the outgoing quark and antiquark) turned out to be more common in the literature [114, 126]. The change-of-basis matrix  $T_{B'}^B$  from the set of basis vectors ( $B$ ) to the new basis ( $B'$ ) (vice versa,  $T_B^{B'}$ ) is given by

$$T_{B'}^B = \begin{pmatrix} 1 & \frac{1}{N_c} \\ 0 & 2 \end{pmatrix}, \quad T_B^{B'} = \begin{pmatrix} 1 & -\frac{1}{2N_c} \\ 0 & \frac{1}{2} \end{pmatrix}. \quad (5.78)$$

Then the anomalous dimension matrix with respect to the basis set ( $B'$ ) is given by  $T_{B'}^B \Gamma_{S'} T_B^{B'}$ . Interchanging  $U$  and  $T$  due to the change of quark and antiquark in the notation gives

$$\Gamma_{S'}^{q\bar{q} \rightarrow q\bar{q}}|_{B'} = \begin{pmatrix} 2C_F T & -\frac{C_F}{N_c} U \\ -2U & -\frac{1}{N_c} (T - 2U) \end{pmatrix}, \quad (5.79)$$

which, together with the anomalous dimension matrices of all the other processes, are collected in Table C.1, Table C.2 or may be found in [114, 126]. All of these are needed for the resummation of the resolved processes of hadron production.

## 6. Rapidity-dependent threshold resummation for high- $p_T$ hadron production

Before we start, please note that parts of this chapter have already been published in [31].

With the resummation formalism established in Sec. 4, we can now address high- $p_T$  hadron production in the photoproduction reaction  $\gamma N \rightarrow hX$ . Especially for fixed-target kinematics as for the lepton-nucleon scattering experiment COMPASS at CERN (see Fig. 6.1), typically transverse momenta are such that the variable  $x_T = 2p_T/\sqrt{s}$  (with  $\sqrt{s}$  the center-of mass energy) is relatively large. It turns out that the partonic hard-scattering cross sections relevant for  $\gamma N \rightarrow hX$  are then largely probed in the “threshold”-regime, where the initial photon and parton have just enough energy to produce the high-transverse momentum parton that subsequently fragments into the hadron, and its recoiling counterpart. Relatively little phase space is then available for additional radiation of partons. In particular, gluon radiation is inhibited and mostly constrained to the emission of soft

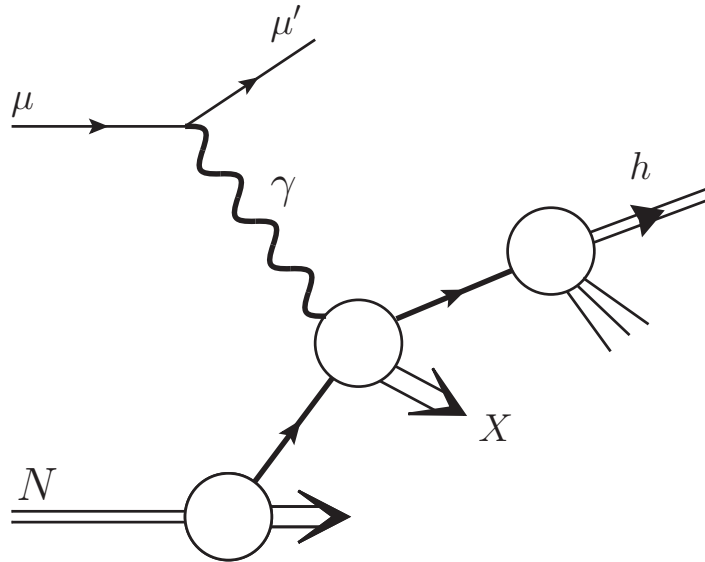


**Fig. 6.1.:** Photoproduction in lepton-nucleon scattering. The virtual photon is required experimentally to have low virtuality

and/or collinear gluons. As we have seen in the Drell-Yan process, the cancellation of infrared singularities between real and virtual diagrams then leaves behind large double- and single-logarithmic corrections to the partonic cross sections. These logarithms appear for the first time in the next-to-leading order (NLO) expressions for the partonic cross sections and also show up at higher orders of perturbation theory. When the threshold regime dominates, it is essential to take into account the large logarithms to all orders. The resummation of these large logarithms is performed in this case similar to the threshold resummation technique discussed in Sec. 4. For single-hadron production in  $pp \rightarrow hX$  in the fixed-target regime, the resummation has been carried out in [26], and substantial effects were observed that lead to an enhancement of the cross section. The same was found for the related dihadron production process  $pp \rightarrow h_1 h_2 X$  [27].

For the photoproduction reaction  $\gamma N \rightarrow hX$ , comparisons with experimental data of the lepton-nucleon scattering experiment COMPASS at CERN to NLO calculations [29] showed that the NLO cross section underpredicts the data by far. As the next-to-leading order correction is of the same order of the LO cross section, one expects also for this reaction large corrections from higher order threshold logarithms. Thus the aim of this work was to provide the resummed cross section for this case. In order to take also rapidity cuts, dictated by the experimental setup, into account, we additionally include rapidity dependence in our resummation scheme. For that, we extend the previous work [26], using the techniques developed in [27].

In the first part of this chapter we recall the basic framework for photoproduction of a hadron. In the next section we present details of threshold resummation valid for this process and describe the technique that enables us to get a resummed expression for fixed rapidity of the observed hadron. In the following phenomenological chapter we want to compare our rapidity-dependent result to that of the fully rapidity-integrated resummed approach in the previous work [26]. Therefore, we work out in Sec. 6.3 how to derive the fully-rapidity-integrated resummed approach in [26] starting with our rapidity-dependent result and point out which approximations have to be made.

## 6.1. Technical framework

We consider the unpolarized cross section for the semi-inclusive process

$$\ell N \rightarrow \ell' h^\pm X, \quad (6.1)$$

where a lepton beam scatters off a nucleon target  $N$  producing a hadron  $h$  with transverse momentum  $p_T$  and pseudorapidity  $\eta$  in the final state. The basic concept that links the experimentally measurable quantities to theoretical predictions obtained with perturbative calculations is the factorization theorem. It states that large momentum-transfer reactions

may be split into long-distance factors, the universal parton distribution functions, and short-distance factors reflecting the hard interactions of the partons. Thus we may write the unpolarized rapidity dependent differential cross section for the process in Eq. (6.1) as the following convolution [24, 137]:

$$\frac{p_T^3 d\sigma}{dp_T d\eta} = \sum_{a,b,c} \int_{x_\ell^{\min}}^1 dx_\ell \int_{x_n^{\min}}^1 dx_n \int_x^1 dz \frac{\hat{x}_T^4 z^2}{8v} f_{a/\ell}(x_\ell, \mu_{fi}) f_{b/N}(x_n, \mu_{fi}) D_{h/c}(z, \mu_{ff}) \frac{\hat{s} d\hat{\sigma}_{ab \rightarrow cX}}{dv dw}. \quad (6.2)$$

The sum in Eq. (6.2) extends over all possible partonic channels with  $\hat{\sigma}_{ab \rightarrow cX}$  denoting the associated partonic hard scattering cross section. In addition to the renormalization scale  $\mu_r$ , the factorization of the hadronic cross section requires the introduction of two further scales: the factorization scales  $\mu_{fi}, \mu_{ff}$  for the initial and final states, respectively. All scales are arbitrary but should be take of the order of the hard scale to minimize scale dependence. One usually chooses them to be equal, typically  $\mu_r = \mu_{fi} = \mu_{ff} = p_T$ . The parton distributions of the lepton and the nucleon,  $f_{a/\ell}(x_\ell, \mu_{fi})$ ,  $f_{b/N}(x_n, \mu_{fi})$ , are evolved to the factorization scale and depend on the respective momentum fractions  $x_{\ell,n}$  carried by partons  $a$  and  $b$ .  $D_{h/c}(z, \mu_{ff})$  denotes the parton-to-hadron fragmentation function. The lower bounds in the integrations over the various momentum fractions in Eq. (6.2) read:

$$x_\ell^{\min} = \frac{x_T e^\eta}{2 - x_T e^{-\eta}}, \quad x_n^{\min} = \frac{x_T e^{-\eta}}{2 - \frac{x_T}{x_\ell} e^\eta}, \quad x = \frac{x_T \cosh \hat{\eta}}{\sqrt{x_n x_\ell}}. \quad (6.3)$$

Here  $\hat{\eta}$  and  $\hat{x}_T$  are the partonic counterparts to the pseudorapidity  $\eta$  and the hadronic scaling variable  $x_T = 2p_T/\sqrt{s}$ ,

$$\hat{\eta} = \eta + \frac{1}{2} \ln \frac{x_n}{x_\ell}, \quad \hat{x}_T = \frac{x_T}{z \sqrt{x_\ell x_n}}. \quad (6.4)$$

It is common convention to introduce two variables  $v$  and  $w$ ,

$$v = 1 - \frac{\hat{x}_T}{2} e^{-\hat{\eta}}, \quad w = \frac{1}{v} \frac{\hat{x}_T}{2} e^{\hat{\eta}}, \quad (6.5)$$

and to rewrite the partonic cross section in terms of this new set of variables. Furthermore we introduce the Mandelstam variables

$$\begin{aligned} \hat{s} &= x_n x_\ell S, \quad \hat{t} = (p_a - p_c)^2 = -\hat{s} \hat{x}_T e^{-\hat{\eta}}/2, \\ \hat{u} &= (p_b - p_c)^2 = -\hat{s} \hat{x}_T e^{\hat{\eta}}/2. \end{aligned} \quad (6.6)$$

The invariant mass of the unobserved partonic final state is

$$s_4 = \hat{s} + \hat{t} + \hat{u} = \hat{s} v (1 - w) = \hat{s} (1 - \hat{x}_T \cosh \hat{\eta}). \quad (6.7)$$

The partonic hard-scattering functions  $\hat{\sigma}_{ab \rightarrow cX}$  can be evaluated in QCD perturbation theory. They may each be written as an expansion in the strong coupling constant  $\alpha_s(\mu_r)$  of the form

$$\hat{\sigma}_{ab \rightarrow cX}(v, w) = \hat{\sigma}_{ab \rightarrow cX}^{(0)}(v, w) + \alpha_s(\mu_r) \hat{\sigma}_{ab \rightarrow cX}^{(1)}(v, w) + \mathcal{O}(\alpha_s^2). \quad (6.8)$$

Whenever a photon takes part in a hard scattering process as initial particle, one generally distinguishes two contributions, the so-called “direct” and “resolved” photon contributions,

$$d\sigma = d\sigma_{\text{dir}} + d\sigma_{\text{res}}. \quad (6.9)$$

Applying the Weizsäcker-Williams equivalent photon method to the lepton-to-parton distribution functions,  $f_{a/\ell}$  in Eq. (6.2) may be written as a convolution of a lepton-to-photon splitting function  $P_{\gamma\ell}$  and a parton distribution function  $f_{a/\gamma}$  of a photon:

$$f_{a/\ell}(x_\ell, \mu_f) = \int_{x_\ell}^1 \frac{dy}{y} P_{\gamma\ell}(y) f_{a/\gamma}(x_\gamma = \frac{x_\ell}{y}, \mu_f). \quad (6.10)$$

In the unpolarized case the splitting function is given by [138, 139]

$$P_{\gamma\ell}(y) = \frac{\alpha}{2\pi} \left[ \frac{1 + (1 - y^2)}{y} \ln \frac{Q_{\text{max}}^2(1 - y)}{m_\ell^2 y^2} + 2m_\ell^2 y \left( \frac{1}{Q_{\text{max}}^2} - \frac{1 - y}{m_\ell^2 y^2} \right) \right], \quad (6.11)$$

and describes the collinear emission of a quasi-real photon with momentum fraction  $y$  off a lepton  $\ell$  of mass  $m_\ell$ . The virtuality of the radiated photon is restricted to be less than  $Q_{\text{max}}$ , which is in turn constrained by the experimental setup.

In the direct case, the photon participates as a whole and parton  $a$  in Eq. (6.2) is an elementary photon. Consequently, we here have simply

$$f_{\gamma/\gamma}(x_\gamma, \mu_f) = \delta(1 - x_\gamma). \quad (6.12)$$

There are two basic partonic subprocesses in lowest order (LO), in which a photon and a parton from the initial nucleon give rise to the production of a hadron: photon-gluon-fusion  $\gamma g \rightarrow q\bar{q}$  and Compton scattering  $\gamma q \rightarrow qg$ . For each process, either of the final-state partons may hadronize into the observed hadron. As the processes are partly electromagnetic and partly due to strong interaction their cross sections are proportional to  $\alpha\alpha_s(\mu_r)$ , where  $\alpha$  represents the electromagnetic fine structure constant.

In addition, the photon exhibits also a hadronic structure in the framework of QCD. This is described by the resolved photon process. Unlike hadronic parton distributions, photonic densities may be decomposed into a purely perturbatively calculable “pointlike” contribution and a nonperturbative “hadron-like” part. While the pointlike contribution dominates at large momentum fractions  $x_\gamma$ , the latter dominates in the low-to-mid  $x_\gamma$

region and may be estimated via the vector-meson-dominance model [140, 141]. At lowest order there are the following resolved subprocesses:

$$\begin{aligned} qq' \rightarrow qq', \quad q\bar{q}' \rightarrow q\bar{q}', \quad q\bar{q} \rightarrow q'\bar{q}', \quad qq \rightarrow qq, \quad q\bar{q} \rightarrow q\bar{q}, \\ q\bar{q} \rightarrow gg, \quad gq \rightarrow qg, \quad qg \rightarrow gq, \quad gg \rightarrow gg, \quad gg \rightarrow q\bar{q}. \end{aligned} \quad (6.13)$$

Each of these is a pure QCD-process and therefore has a cross section quadratic in  $\alpha_s(\mu_r)$ . However, as the photon parton distributions are formally of order  $\alpha/\alpha_s(\mu_f)$ , the perturbative expansion of the direct and resolved contributions starts at the same order.

At LO where one has  $2 \rightarrow 2$  kinematics,  $w \equiv 1$ , and therefore,

$$\frac{\hat{s}d\hat{\sigma}_{ab \rightarrow cX}^{(0)}(v, w)}{dv dw} = \frac{\hat{s}d\hat{\sigma}_{ab \rightarrow cd}^{(0)}(v)}{dv} \delta(1 - w). \quad (6.14)$$

The numerous partonic NLO cross sections  $\hat{\sigma}_{ab \rightarrow cX}^{(1)}(v, w)$  have been computed in [19, 142]. They can be cast into the form

$$\frac{\hat{s}d\hat{\sigma}_{ab \rightarrow cX}^{(1)}(v, w)}{dv dw} = A(v)\delta(1 - w) + B(v) \left( \frac{\ln(1 - w)}{1 - w} \right)_+ + C(v) \left( \frac{1}{1 - w} \right)_+ + F(v, w). \quad (6.15)$$

Here the “+”-distributions are defined as follows:

$$\int_0^1 f(w)[g(w)]_+ dw = \int_0^1 [f(w) - f(1)]g(w)dw. \quad (6.16)$$

The function  $F(v, w)$  collects all remaining terms that do not contain any distributions. The terms in Eq. (6.15) associated with “+”-distributions yield large logarithmic first order corrections close to the threshold. These terms can be traced back to soft gluon emission and will also show up in all higher order corrections. For each new order of perturbations theory one is faced with two more powers of leading logarithmic contributions. To be specific, in the  $k$ th order in perturbation theory  $d\hat{\sigma}_{ab \rightarrow cX}^{(k)}(v, w)/dv dw$  contains logarithms of the form  $\alpha_s^k [\ln^{2k-1}(1 - w)/(1 - w)]_+$ , plus subleading terms with fewer logarithms. Depending on kinematics, these logarithmic terms have to be resummed order-by-order.

## 6.2. Rapidity-dependent resummed cross section

In this section we will provide the resummed differential cross section as a function of transverse momentum  $p_T$  and pseudorapidity  $\eta$  of the produced hadron.

### 6.2.1. Mellin moments and threshold region

Threshold resummation of soft gluon emissions is performed in Mellin- $N$  moment space. Taking Mellin moments transforms a convolution of a parton distribution function and the partonic cross section into a product of moments of the corresponding quantities. The threshold region  $w \rightarrow 1$  corresponds to large Mellin moments. Under this transformation, the large soft-gluon corrections showing up as “+”-distributions are translated into powers of logarithms  $\ln N$ . This logarithmic behavior colludes with the  $N$ -dependence of the parton distribution functions and the fragmentation function, which in moment space typically fall off as  $1/N^4$  or faster at large  $N$ .

The single-inclusive cross section we are interested in here depends on two kinematic variables,  $p_T$  and  $\eta$ . If the cross section is integrated over all rapidities, it becomes a function of  $x_T^2$ , and a single Mellin moment in  $x_T^2$  suffices to factorize it in terms of moments of parton distributions, fragmentation functions, and partonic cross sections [26]. After resummation the full Mellin expression is inverted, directly giving the desired hadronic cross section. Here, the integrations of the various functions in Eq. (6.2) are no longer convolutions in a strict sense, and a different technique needs to be used. A convenient possibility [27] is to use Mellin moments for only a part of the terms in Eq. (6.2). That is, one takes Mellin moments only of the product of fragmentation functions and the resummed partonic cross sections, performs a Mellin inverse, and convolutes the result with the parton distributions in  $x$ -space. Inclusion of the fragmentation functions in the Mellin moment expression guarantees that the integrand for the inverse Mellin transform falls off fast enough for the integral to show good numerical convergence. On the other hand, performing the convolution with the parton distributions in  $x$ -space provides full control over rapidity, since the partonic and hadronic rapidities are related by a boost along the collision axis that involves only the momentum fractions of the initial-state partons.

To be specific, starting from Eq. (6.2), we consider only the last integral and take moments in  $x^2$  (where  $x$  is the lower bound of the  $z$ -integral). The integral then factorizes into a product of moments:

$$\int_0^1 dx^2 (x^2)^{N-1} \int_x^1 dz \frac{\hat{x}_T^4 z^2}{8v} D_{h/c}(z, \mu_{ff}) \frac{\hat{s} d\hat{\sigma}_{ab \rightarrow cX}}{dv dw} \equiv D_{h/c}^{2N+3}(\mu_{ff}) \tilde{w}^{2N}(\hat{\eta}), \quad (6.17)$$

where the Mellin moments  $D_{h/c}^N(\mu_{ff})$  of the fragmentation function are defined as usual by

$$D_{h/c}^N(\mu_{ff}) = \int_0^1 dz z^{N-1} D_{h/c}(z, \mu_{ff}), \quad (6.18)$$



and where the hard scattering function  $\tilde{w}^N(\hat{\eta})$  is given in Mellin- $N$  moment space by

$$\tilde{w}^N(\hat{\eta}) = 2 \int_0^1 d\frac{s_4}{\hat{s}} \left(1 - \frac{s_4}{\hat{s}}\right)^{N-1} \frac{\hat{x}_T^4 z^2}{8v} \frac{\hat{s} d\hat{\sigma}_{ab \rightarrow cX}}{dv dw}. \quad (6.19)$$

We next take the Mellin inverse of the expression in Eq. (6.17) which is then convoluted with the parton distributions:

$$\frac{p_T^3 d\sigma}{dp_T d\eta} = \sum_{a,b,c} \int_0^1 dx_\ell \int_0^1 dx_n f_{a/\ell}(x_\ell, \mu_{fi}) f_{b/N}(x_n, \mu_{fi}) \int_C \frac{dN}{2\pi i} (x^2)^{-N} D_{h/c}^{2N+3}(\mu_{ff}) \tilde{w}^{2N}(\hat{\eta}). \quad (6.20)$$

This is mathematically equivalent to using Eq. (6.2) in the first place. However, once one uses a resummed hard-scattering function, it is much better from a computational point of view to use the procedure in (6.20) since the moments of the fragmentation functions tame the large- $N$  behavior of the factor  $\tilde{w}^{2N}$  so that the Mellin integral converges rapidly. In contrast, to carry out a convolution over  $z$  as in Eq.(6.2) would become very difficult for a resummed hard-scattering function, since the latter contains “+”-distributions with any power of a logarithm.

### 6.2.2. Rapidity-dependent resummation to next-to-leading logarithm

In analogy to the resummed expression in Chap. 4, the multigluon QCD amplitudes factorize also here to logarithmic accuracy. Furthermore, in Mellin space, also the phase space including the constraint of energy conservation factorizes. The resummed cross section in moment space factorizes into functions for each single participating parton, a function describing the hard scattering, and a soft function. This factorization is illustrated in Fig. 6.2. Note that in the case of hadron production discussed here, the situation is different from what was discussed in Chap. 4, in which we had an observed photon or a jet. In the case of hadron production one also has final-state collinear singularities, which are factorized into the fragmentation function. This gives a radiative factor ( $\Delta_c$ ) for the observed final-state parton, which is similar to that of the initial partons. The resummed cross section is given by [111–114]:

$$\tilde{w}_{ab \rightarrow cd}^{\text{resum},N}(\hat{\eta}) = \Delta_a^{N_a}(\hat{s}, \mu_{fi}) \Delta_b^{N_b}(\hat{s}, \mu_{fi}) \Delta_c^N(\hat{s}, \mu_{ff}) J_d^N(\hat{s}) \text{Tr} \left\{ H S_N^\dagger S S_N \right\}_{ab \rightarrow cd}, \quad (6.21)$$

where  $N_a = (-\hat{u}/\hat{s})N$  and  $N_b = (-\hat{t}/\hat{s})N$ . For completeness, we recall each of the functions. The resummed exponents for the initial-state partons  $a, b = q, \bar{q}, g$  in Eq. (6.21) read,

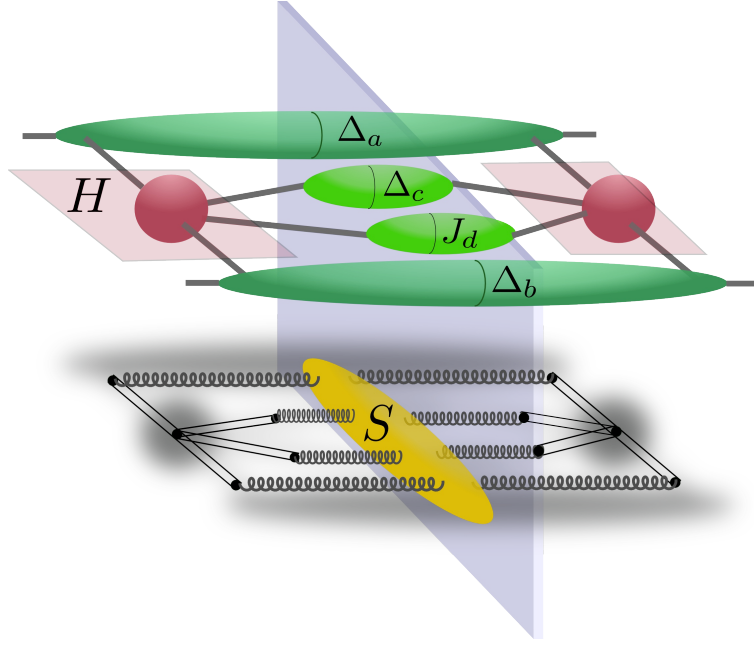


**Fig. 6.2.:** Schematic illustration of the factorization of the cross section close to threshold. The plane symbolizes the cut, which separates the amplitude and its complex conjugate. For each of the initial- and final-state partons there is a function ( $\Delta_{a,b,c}, J_d$ ) describing soft-gluon emissions off these partons. The hard-scattering part  $H$  is depicted as amplitude and its complex conjugate. It can be completely separated from the soft function  $S$ , shown in the lower part of the figure. The double lines represent eikonal lines.

in the  $\overline{\text{MS}}$  scheme:

$$\begin{aligned} \ln \Delta_i^N(M_i^2, \mu_{fi}) = & - \int_0^1 dz \frac{z^{N-1} - 1}{1-z} \left\{ \int_{(1-z)^2}^1 \frac{dt}{t} A_i[\alpha_s(tM_i^2)] + \bar{B}_i\left(\nu_i, \frac{M_i^2}{\hat{s}}, \alpha_s((1-z)^2 M_i^2)\right) \right\} \\ & - 2 \int_{\mu_r}^{M_i} \frac{d\mu'}{\mu'} \gamma_i(\alpha_s(\mu'^2)) + 2 \int_{\mu_{fi}}^{M_i} \frac{d\mu'}{\mu'} \gamma_{ii}(N, \alpha_s(\mu'^2)). \end{aligned} \quad (6.22)$$

Here  $M_i$  is a scale of order  $\sqrt{\hat{s}}$ . It was shown that the exponent is in fact independent of  $M_i$  at next-to-leading logarithmic (NLL) accuracy [72]. Furthermore, we have

$$\begin{aligned} A_i(\alpha_s) &= C_i[\alpha_s/\pi + (K/2)(\alpha_s/\pi)^2], \\ \bar{B}_i(\nu_i, M_i^2/\hat{s}, \alpha_s) &= C_i(\alpha_s/\pi)[1 - \ln(2\nu_i) + \ln(M_i^2/\hat{s})], \end{aligned} \quad (6.23)$$

where  $K = C_A[67/18 - \pi^2/6] - 5/9N_f$ ,  $C_i = C_q = C_F = 4/3$  for an incoming quark, and  $C_i = C_g = C_A = 3$  for a gluon.  $N_f$  denotes the number of flavors. The  $\nu_i$  are defined as

$$\nu_i \equiv \frac{(\beta_i \cdot n)^2}{|n^2|}, \quad (6.24)$$

with the parton velocity  $\beta_i^\mu = p_i^\mu \sqrt{2/\hat{s}}$  and an axial gauge vector  $n$ . Remember, that the  $\nu_i$  were introduced to make the factorization of the cross section manifest [28]. The gauge-

dependence they express will cancel in the final resummed cross section. The last two terms in Eq. (6.22) match the exponent to the chosen renormalization and factorization scale, respectively. The  $\gamma_i$  are the anomalous dimensions of the quark and gluon fields, and the  $\gamma_{ii}$  correspond to the logarithmic and constant terms of the moments of the diagonal Altarelli-Parisi splitting functions. To one loop order, one has

$$\begin{aligned}\gamma_q(\alpha_s) &= \frac{3}{4}C_F\frac{\alpha_s}{\pi}, & \gamma_{qq}(N, \alpha_s) &= -\left(\ln N - \frac{3}{4}\right)C_F\frac{\alpha_s}{\pi}, \\ \gamma_g(\alpha_s) &= b_0\alpha_s, & \gamma_{gg}(N, \alpha_s) &= -(C_A \ln N - \pi b_0)\frac{\alpha_s}{\pi},\end{aligned}\quad (6.25)$$

where  $b_0 = (11C_A - 4T_R N_f)/(12\pi)$ , with  $T_R = 1/2$ . We note that the large- $N$  behavior of the diagonal splitting functions and anomalous dimensions links the various terms in the exponent in Eq. (6.22) to each other,

$$\gamma_{ii}(N, \alpha_s) = -\ln \bar{N} A_i(\alpha_s) + \gamma_i(\alpha_s), \quad (6.26)$$

where  $\bar{N} = Ne^{\gamma_E}$  with the Euler constant  $\gamma_E$ .

For the direct processes, parton  $a$  is a photon and we have simply  $\Delta_\gamma^{N_a}(\hat{s}, \mu_{fi}) = 1$ . For the fragmenting parton  $c$  one has the same exponent as for the incoming partons  $\Delta_i^N(M_i^2)$  in Eq. (6.22), but with the final state factorization scale  $\mu_{ff}$  in place of the initial-state one.

The exponential function  $J_d^N$  in Eq. (6.21) contains collinear emission, both soft and hard, by the unobserved final-state jet that recoils against the observed parton. It is independent of factorization scale and is given by

$$\begin{aligned}\ln J_d^N(\hat{s}) &= \int_0^1 dz \frac{z^{N-1} - 1}{1-z} \left\{ \int_{(1-z)^2}^{(1-z)} \frac{dt}{t} A_d[\alpha_s(t\hat{s})] - \gamma_d[\alpha_s((1-z)\hat{s})] \right. \\ &\quad \left. - \bar{B}_d[\nu_d, 1, \alpha_s((1-z)^2\hat{s})] \right\} + 2 \int_{\mu_r}^{\sqrt{\hat{s}}} \frac{d\mu'}{\mu'} \gamma_d(\alpha_s(\mu'^2)),\end{aligned}\quad (6.27)$$

where  $A_d$ ,  $\gamma_d$  and  $\bar{B}_d$  are defined as in Eq. (6.23).

Finally, coherent soft gluon radiation among the jets is treated by the last term in Eq. (6.21). The functions  $H_{ab \rightarrow cd}$ ,  $\mathcal{S}_{N,ab \rightarrow cd}$  and  $S_{ab \rightarrow cd}$  are matrices in a space of color exchange operators [111, 112, 114], and the trace is taken in this color space. The  $H_{ab \rightarrow cd}$  are the hard-scattering functions. They are perturbative series in  $\alpha_s$ ,

$$H_{ab \rightarrow cd}(\hat{\eta}, \alpha_s) = H_{ab \rightarrow cd}^{(0)}(\hat{\eta}) + \frac{\alpha_s}{\pi} H_{ab \rightarrow cd}^{(1)}(\hat{\eta}) + \mathcal{O}(\alpha_s^2). \quad (6.28)$$

The LO contributions to the hard-scattering functions in the resolved-photon case are known with their full color dependence [111, 112, 114, 126], and the NLO terms have been

obtained in [143, 144]. The  $S_{ab \rightarrow cd}$  are soft functions and may be expanded as

$$S_{ab \rightarrow cd}(\hat{\eta}, \alpha_s) = S_{ab \rightarrow cd}^{(0)} + \frac{\alpha_s}{\pi} S_{ab \rightarrow cd}^{(1)}(\hat{\eta}, \alpha_s, \frac{\sqrt{\hat{s}}}{N}) + \mathcal{O}(\alpha_s^2). \quad (6.29)$$

Here, the Mellin- $N$  moment enters only in the argument of the running coupling [111]. Therefore, the  $N$ -dependence of the soft functions will show up at next-to-next-to-leading logarithmic order for the first time. The LO terms  $S_{ab \rightarrow cd}^{(0)}$  for the resolved contribution may be taken from [111, 112, 114], while the  $S_{ab \rightarrow cd}^{(1)}$  are not yet available in closed form. Contributions by soft gluons emitted at wide angles are resummed by the exponentials  $\mathcal{S}_{N, ab \rightarrow cd}(\hat{\eta}, \alpha_s)$ , which are evolved via the soft anomalous dimension matrices  $\Gamma_{ab \rightarrow cd}$ :

$$\mathcal{S}_{N, ab \rightarrow cd}(\hat{\eta}, \alpha_s) = \mathcal{P} \exp \left[ \int_{\mu_r}^{\sqrt{\hat{s}}/N} \frac{d\mu'}{\mu'} \Gamma_{ab \rightarrow cd}(\hat{\eta}, \alpha_s(\mu')) \right], \quad (6.30)$$

with  $\mathcal{P}$  denoting path ordering, and the soft anomalous dimensions can be expanded as follows:

$$\Gamma_{ab \rightarrow cd}(\hat{\eta}, \alpha_s) = \frac{\alpha_s}{\pi} \Gamma_{ab \rightarrow cd}^{(1)}(\hat{\eta}) + \mathcal{O}(\alpha_s^2). \quad (6.31)$$

For resummation to NLL accuracy one only needs the first-order terms, which may be found in [111, 112, 114] and have the structure

$$\left( \Gamma_{ab \rightarrow cd}^{(1)}(\hat{\eta}) \right)_{mn} = \left( \tilde{\Gamma}_{ab \rightarrow cd}^{(1)}(\hat{\eta}) \right)_{mn} + \delta_{mn} \sum_{k=a,b,c,d} \frac{C_k}{2} [-\ln(2\nu_k) + 1 - \pi i], \quad (6.32)$$

where one may see the gauge-dependent diagonal elements explicitly. As mentioned before, gauge-dependence cancels in the above expressions for the resummed cross section to next-to-leading-logarithmic accuracy.

Let us take a look at the first-order expansion of the trace part in Eq. (6.21) (see [27]):

$$\begin{aligned} \text{Tr} \left\{ H S_N^\dagger S S_N \right\}_{ab \rightarrow cd} &= \text{Tr} \left\{ H^{(0)} S^{(0)} \right\}_{ab \rightarrow cd} \\ &+ \frac{\alpha_s}{\pi} \text{Tr} \left\{ -[H^{(0)} (\Gamma^{(1)})^\dagger S^{(0)} + H^{(0)} S^{(0)} \Gamma^{(1)}] \ln N \right. \\ &\left. + H^{(1)} S^{(0)} + H^{(0)} S^{(1)} \right\}_{ab \rightarrow cd} + \mathcal{O}(\alpha_s^2). \end{aligned} \quad (6.33)$$

The trace of the product of the matrices  $H$  and  $S$  at lowest order reproduces the Born cross sections. As discussed in [27, 144], in order to obtain  $\text{Tr} \left\{ H S_N^\dagger S S_N \right\}$  fully to NLL accuracy one would need to implement the contributions from  $H^{(1)}$  and  $S^{(1)}$ , which is beyond the scope of this work. Following the approach of [26, 27], we use the approximation

$$\text{Tr} \left\{ H S_N^\dagger S S_N \right\}_{ab \rightarrow cd} \approx \left( 1 + \frac{\alpha_s}{\pi} C_{ab \rightarrow cd}^{(1)} \right) \text{Tr} \left\{ H^{(0)} S_N^\dagger S^{(0)} S_N \right\}_{ab \rightarrow cd}, \quad (6.34)$$

where the so-called “ $C$ -coefficients” are defined as

$$C_{ab \rightarrow cd}^{(1)}(\hat{\eta}) \equiv \frac{\text{Tr}\{H^{(1)}S^{(0)} + H^{(0)}S^{(1)}\}_{ab \rightarrow cd}}{\text{Tr}\{H^{(0)}S^{(0)}\}}. \quad (6.35)$$

This approximation becomes exact for color-singlet cases, and therefore in particular for the direct subprocesses which have only one color structure at Born level. The  $C$ -coefficients are constructed in such a way that the first order expansion of the resummed cross section reproduces all terms  $\propto \delta(1-w)$  in the NLO result.

### 6.2.3. Rapidity-dependent NLL exponents

The expression for the resummed partonic cross section in Eq. (6.21) is formally ill-defined for any value of  $N$ , as its exponents involve integrations of the running coupling over the Landau pole. However, it was shown that the divergencies showing up in Eq. (6.21) are subleading in  $N$  [100]. In return, a NLL expansion of the resummed formula is finite up to  $N$  reaching the first Landau pole at  $N_L = \exp(1/(2\alpha_s b_0))$ . We will return to this point later. We now rewrite the resummed exponents for soft gluon radiation off the incoming and outgoing partons in Eq. (6.21) as expansions to NLL accuracy using the perturbative expansions given in (6.23):

$$A_i(\alpha_s) = \frac{\alpha_s}{\pi} A_i^{(1)} + \left(\frac{\alpha_s}{\pi}\right)^2 A_i^{(2)} + \mathcal{O}(\alpha_s^3), \quad (6.36)$$

$$B_i(\alpha_s) = \frac{\alpha_s}{\pi} B_i^{(1)} + \mathcal{O}(\alpha_s^2), \quad (6.37)$$

$$\bar{B}_i(\alpha_s) = \frac{\alpha_s}{\pi} \bar{B}_i^{(1)} + \mathcal{O}(\alpha_s^2), \quad (6.38)$$

where  $B_i^{(1)} = -2\gamma_i^{(1)}$  with  $\gamma_i(\alpha_s) = \gamma_i^{(1)}\alpha_s/\pi + \mathcal{O}(\alpha_s^2)$ . The resulting exponents do not depend on the specific subprocess, but only on the type of parton and thus may be seen in this sense as ‘universal’ functions. The leading terms in the exponent are leading logarithms (LL) of the form  $\alpha_s^k \ln^{k+1} N$ , while subleading terms are down at least by one power of  $\ln N$ . We adopt the formalism of [145] and organize the logarithms in the exponentials in a way such that all leading logarithmic terms are collected in functions  $h_i^{(1)}$  and  $f_i^{(1)}$  for the observed and the unobserved partons, respectively. These functions are rapidity independent and hence are identical to the analogous functions in the rapidity-integrated exponents. Rapidity dependent terms first appear at NLL accuracy, where they yield additional terms when compared to the well-known rapidity integrated exponents of [26].

We further expand the resummed exponents for the observed partons  $i = a, b, c$  and

unobserved partons  $d$  to NLL accuracy:

$$\begin{aligned} \ln \Delta_i^{2N_i}(\hat{\eta}, \hat{s}, \mu_{fi}) = & \ln N h_i^{(1)}(\lambda) + h_i^{(2)}\left(\lambda, \frac{\hat{s}}{\mu_r^2}, \frac{\hat{s}}{\mu_{fi}^2}\right) - \frac{A_i^{(1)}}{\pi b_0} \ln\left(\frac{2N_i}{N}\right) \ln(1-2\lambda) \\ & - \frac{\bar{B}_i^{(1)}}{2\pi b_0} \ln(1-2\lambda), \end{aligned} \quad (6.39)$$

$$\begin{aligned} \ln J_d^{2N}(\hat{s}) = & \ln N f_d^{(1)}(\lambda) + f_d^{(2)}\left(\lambda, \frac{\hat{s}}{\mu_r^2}\right) - \frac{\bar{B}_d^{(1)}}{2\pi b_0} \ln(1-2\lambda) \\ & - \frac{A_d^{(1)}}{\pi b_0} \ln(2) (\ln(1-\lambda) - \ln(1-2\lambda)), \end{aligned} \quad (6.40)$$

where  $\lambda = \alpha_s b_0 \ln N$  and, as before,  $N_a = (-\hat{u}/\hat{s})N$  and  $N_b = (-\hat{t}/\hat{s})N$ . For the observed final-state parton we simply have  $N_c = N$ . Note that due to the NLL expansion of terms like  $\ln(1 - \alpha_s b_0 \ln(N_i)) \approx \ln(1 - 2\lambda) - \frac{2\alpha_s b_0}{1-2\lambda} \ln(N_i/N)$  explicit dependence on  $\hat{\eta}$  appears in Eq. (6.39). The functions  $h_i^{(k)}, f_i^{(k)}$  are known from resummation for the rapidity-integrated cross sections and are given by

$$h_i^{(1)}(\lambda) = \frac{A_i^{(1)}}{2\pi b_0 \lambda} [2\lambda + (1-2\lambda) \ln(1-2\lambda)], \quad (6.41)$$

$$\begin{aligned} h_i^{(2)}\left(\lambda, \frac{Q^2}{\mu_r^2}, \frac{Q^2}{\mu_a^2}\right) = & -\frac{A_i^{(2)}}{2\pi^2 b_0^2} [2\lambda + \ln(1-2\lambda)] - \frac{A_i^{(1)} \gamma_E}{\pi b_0} \ln(1-2\lambda) - \frac{A_i^{(1)}}{\pi b_0} \lambda \ln \frac{Q^2}{\mu_a^2} \\ & + \frac{A_i^{(1)} b_1}{2\pi b_0^3} \left[ 2\lambda + \ln(1-2\lambda) + \frac{1}{2} \ln^2(1-2\lambda) \right] \\ & + \frac{A_i^{(1)}}{2\pi b_0} [2\lambda + \ln(1-2\lambda)] \ln \frac{Q^2}{\mu_r^2}, \end{aligned} \quad (6.42)$$

and for the unobserved final-state parton

$$f_i^{(1)}(\lambda) = -\frac{A_i^{(1)}}{2\pi b_0 \lambda} [(1-2\lambda) \ln(1-2\lambda) - 2(1-\lambda) \ln(1-\lambda)], \quad (6.43)$$

$$\begin{aligned} f_i^{(2)}\left(\lambda, \frac{Q^2}{\mu_r^2}\right) = & -\frac{A_i^{(1)} b_1}{2\pi b_0^3} \left[ \ln(1-2\lambda) - 2\ln(1-\lambda) + \frac{1}{2} \ln^2(1-2\lambda) - \ln^2(1-\lambda) \right] \\ & + \frac{B_i^{(1)}}{2\pi b_0} \ln(1-\lambda) - \frac{A_i^{(1)} \gamma_E}{\pi b_0} [\ln(1-\lambda) - \ln(1-2\lambda)] \\ & - \frac{A_i^{(2)}}{2\pi^2 b_0^2} [2\ln(1-\lambda) - \ln(1-2\lambda)] + \frac{A_i^{(1)}}{2\pi b_0} [2\ln(1-\lambda) - \ln(1-2\lambda)] \ln \frac{Q^2}{\mu_r^2}. \end{aligned} \quad (6.44)$$

As before,  $b_0 = (11C_A - 4T_R N_f)/12\pi$ , and

$$b_1 = \frac{1}{24\pi^2} (17C_A^2 - 5C_A N_f - 3C_F N_f), \quad (6.45)$$

correspond to the first two coefficients of the QCD  $\beta$ -function.

The path-ordered matrix exponentiation of the soft anomalous dimension contribution in Eqs. (6.30), (6.31) proceeds<sup>16</sup> as described in [27, 146] and leads to the expansion of the integral in Eq. (6.30) at NLL,

$$\ln \mathcal{S}_{N,ab \rightarrow cd}(\hat{\eta}, \alpha_s) = \frac{\ln(1 - 2\lambda)}{2\pi b_0} \Gamma_{ab \rightarrow cd}^{(1)}(\hat{\eta}). \quad (6.46)$$

We use a numerical approach for the calculation of the matrix exponential, truncating its power series at a very high order. Finally, when all terms in the exponent are combined, the LL terms  $\alpha_s^k \ln^{k+1} N$  and the NLL terms  $\alpha_s^k \ln^k N$  in the exponent of Eq. (6.21) reproduce the three towers of logarithms  $\alpha_s^k \ln^{2k} N$ ,  $\alpha_s^k \ln^{2k-1} N$ , and  $\alpha_s^k \ln^{2k-2} N$  in the cross sections, up to the approximation concerning the  $C$ -coefficients discussed earlier. The  $C$ -coefficients for the direct part are given in the next subsection. As those for the resolved part are rather lengthy, we do not present them here; they can be obtained upon request from Prof. Dr. Schäfer.

#### 6.2.4. The direct contribution

Our discussion so far directly applies to the resolved-photon contributions. In the direct case, the resummation framework simplifies thanks to the fact that the LO processes have only three colored particles and hence only one specific color configuration. Nevertheless, a few remarks about the resummation for the direct part are in order, since this case has not been discussed in the previous literature in any detail.

For the direct processes the hard-scattering functions  $H_{\gamma b \rightarrow cd}$ , the soft functions  $S_{\gamma b \rightarrow cd}$ , and the anomalous dimensions are scalars in color space. This allows us to simplify Eq. (6.21):

$$\begin{aligned} \tilde{w}_{\gamma b \rightarrow cd}^{\text{resum}, N}(\hat{\eta}) &= \left(1 + \frac{\alpha_s}{\pi} C_{\gamma b \rightarrow cd}^{(1)}\right) \Delta_b^{N_b}(\hat{s}, \mu_{fi}) \Delta_c^N(\hat{s}, \mu_{ff}) J_d^N(\hat{s}) \hat{\sigma}_{\gamma b \rightarrow cd}^{(0)}(N, \hat{\eta}) \\ &\times \exp \left[ \int_{\mu_r}^{\sqrt{\hat{s}}/N} \frac{d\mu'}{\mu'} 2\text{Re} \Gamma_{\gamma b \rightarrow cd}(\hat{\eta}, \alpha_s(\mu')) \right], \end{aligned} \quad (6.47)$$

where we have defined the Mellin- $N$  moment of the Born cross sections as

$$\hat{\sigma}_{\gamma b \rightarrow cd}^{(0)}(N, \hat{\eta}) \equiv 2 \int_0^1 d\frac{s_4}{\hat{s}} \left(1 - \frac{s_4}{\hat{s}}\right)^{N-1} \frac{\hat{x}_T^4 z^2}{8v} \frac{\hat{s} d\hat{\sigma}_{ab \rightarrow cX}^{(0)}}{dv dw}. \quad (6.48)$$

<sup>16</sup>Path ordering becomes irrelevant for resummation at NLL.

The partonic Born cross sections for the three direct processes are given by

$$\frac{\hat{s}d\hat{\sigma}_{\gamma q \rightarrow qq}^{(0)}(v)}{\pi\alpha\alpha_s e_q^2 dv} = \frac{\hat{s}d\hat{\sigma}_{\gamma q \rightarrow gq}^{(0)}(1-v)}{\pi\alpha\alpha_s e_q^2 dv} = 2C_F \frac{1+(1-v)^2}{1-v}, \quad (6.49)$$

$$\frac{\hat{s}d\hat{\sigma}_{\gamma g \rightarrow q\bar{q}}^{(0)}(v)}{\pi\alpha\alpha_s e_q^2 dv} = \frac{v^2 + (1-v)^2}{v(1-v)}. \quad (6.50)$$

The soft anomalous dimensions for the direct processes may be derived from those for the prompt-photon production processes  $qg \rightarrow \gamma q$ , and  $q\bar{q} \rightarrow \gamma g$  [28, 72, 145, 147, 148]. The rapidity-dependent anomalous dimensions then read to first order:

$$\Gamma_{\gamma q \rightarrow qq}^{(1)}(\hat{\eta}) = \frac{C_F}{2} \left[ 2 \ln \left( \frac{-\hat{u}}{\hat{s}} \right) - \ln(4\nu_{q_a}\nu_{q_c}) + 2 \right] + \frac{C_A}{2} \left[ \ln \left( \frac{\hat{t}}{\hat{u}} \right) - \ln(2\nu_g) + 1 - \pi i \right], \quad (6.51)$$

$$\Gamma_{\gamma q \rightarrow gq}^{(1)}(\hat{\eta}) = \Gamma_{\gamma q \rightarrow qq}^{(1)}(\hat{\eta}) \Big|_{\hat{t} \leftrightarrow \hat{u}}, \quad (6.52)$$

$$\Gamma_{\gamma g \rightarrow q\bar{q}}^{(1)}(\hat{\eta}) = \frac{C_F}{2} \left[ -\ln(4\nu_q\nu_{\bar{q}}) + 2 - 2\pi i \right] + \frac{C_A}{2} \left[ \ln \left( \frac{\hat{t}\hat{u}}{\hat{s}^2} \right) + 1 - \ln(2\nu_g) + \pi i \right]. \quad (6.53)$$

With these first order terms of the anomalous dimensions, the integral in Eq. (6.47) can be written explicitly as an expansion to NLL accuracy:

$$\int_{\mu_r}^{\sqrt{\hat{s}}/2N} \frac{d\mu'}{\mu'} 2\text{Re}\Gamma_{\gamma b \rightarrow cd}(\hat{\eta}, \alpha_s(\mu')) = \frac{\Gamma_{\gamma b \rightarrow cd}^{(1)}(\hat{\eta})}{\pi b_0} \ln(1-2\lambda). \quad (6.54)$$

We recall that with only one color configuration present at Born level, the approximation in Eq. (6.34) becomes exact, and the  $C$ -coefficients for the direct processes may be derived by comparing the exact NLO calculation [149] to the first-order expansion of Eq. (6.47). Moreover, it can be checked that all double- and single-logarithmic terms  $\alpha_s \ln^2 N$ ,  $\alpha_s \ln N$  (including the rapidity-dependence of the latter) are correctly reproduced by the resummation formula.

The first order correction can be cast in the form Eq. (6.15),

$$\frac{\hat{s}d\hat{\sigma}_{ab \rightarrow cX}^{(1)}(v, w)}{dv dw} = A(v)\delta(1-w) + B(v) \left( \frac{\ln(1-w)}{1-w} \right)_+ + C(v) \left( \frac{1}{1-w} \right)_+ + F(v, w). \quad (6.55)$$



For quark production via Compton scattering, one has:

$$B(v) = S_{\gamma g}(4C_F - C_A) \quad (6.56)$$

$$C(v) = S_{\gamma g} \quad (6.57)$$

$$\begin{aligned} & \times \left[ -\frac{11}{12}C_A + \frac{N_f}{6} - C_F \left( \ln \frac{\mu_f^2}{\hat{s}} + \ln \frac{\mu_{fp}^2}{\hat{s}} \right) + (C_A - 2C_F) \ln(1-v) + 2(3C_F - C_A) \ln v \right] \\ A(v) = & \frac{C_F}{2(1-v)} \left\{ (C_A - 2C_F) \left[ (3-2v) \left( \ln^2 \frac{1-v}{v} + \pi^2 \right) + (1-2v) \ln^2(v) + 2(1-v) \ln \frac{1-v}{v^2} \right] \right. \\ & \left. + 6C_F \ln(1-v) \right\} \\ & + \frac{1}{4} S_{\gamma g} \left\{ C_F \left[ 6 \ln^2(1-v) - 20 \ln(1-v) \ln v + 22 \ln^2 v + 4 \ln(1-v) \ln \frac{\mu_f^2}{\hat{s}} \right. \right. \\ & \left. \left. - (3 + 4 \ln v) \left( \ln \frac{\mu_f^2}{\hat{s}} + \ln \frac{\mu_{fp}^2}{\hat{s}} \right) - 14 + 4\pi^2 \right] \right. \\ & \left. + C_A \left[ -3 \ln^2(1-v) + 10 \ln(1-v) \ln v - 9 \ln^2 v - \frac{5}{3} \pi^2 + \frac{4}{3} \right] \right. \\ & \left. + 4\pi b_0 \left( \frac{5}{3} + \ln \frac{\mu_r^2}{\hat{s}} - \ln v \right) \right\}, \quad (6.58) \end{aligned}$$

where  $S_{\gamma g} = 2C_F(1+(1-v)^2)/(1-v)$ . According to Eq. (6.19) the hard scattering function is given by

$$\tilde{w}(2N, \hat{\eta}) = 2 \int_0^1 d\left(\frac{s_4}{\hat{s}}\right) \left(1 - \frac{s_4}{\hat{s}}\right)^{2N-1} \frac{\hat{x}_T^4}{8v} \frac{\hat{s} d\sigma}{dv dw}. \quad (6.59)$$

Now we substitute:

$$m := 1 - \frac{s_4}{\hat{s}} \quad (= \hat{x}_T \cosh \hat{\eta}). \quad (6.60)$$

We may express  $v$  and  $w$  in terms of  $m$ :

$$v = 1 - \frac{\hat{x}_T}{2} e^{-\hat{\eta}} = 1 - m \frac{e^{-\hat{\eta}}}{2 \cosh \hat{\eta}} \quad (6.61)$$

$$w = \frac{1}{v} \frac{\hat{x}_T}{2} e^{\hat{\eta}} = \frac{1}{v} m \frac{e^{\hat{\eta}}}{2 \cosh \hat{\eta}}. \quad (6.62)$$

After this substitution we obtain:

$$\tilde{w}(2N, \hat{\eta}) = 2 \int_0^1 dm m^{2N-1} \frac{\hat{x}_T^4}{8v} \frac{\hat{s} d\sigma}{dv dw} = \frac{1}{4 \cosh^4 \hat{\eta}} \int_0^1 dm m^{2N+3} \frac{1}{v} \frac{\hat{s} d\sigma}{dv dw}. \quad (6.63)$$

The Mellin moments of functions arising in Eq. (6.63) are presented in Appendix B. After

taking Mellin moments one may extract the logarithmic dependence:

$$\tilde{w}(2N, \hat{\eta}) = \frac{\alpha\alpha_s^2}{4 \cosh^4 \hat{\eta}} \left[ \tilde{B} \ln^2 N + \tilde{C} \ln N + C_{q\gamma \rightarrow qg}(\hat{\eta}) + \mathcal{O}(\ln N/N) \right] \quad (6.64)$$

with

$$\begin{aligned} \tilde{B} &= \frac{1}{2}(4C_F - C_A)S_{\gamma g} \\ \tilde{C} &= \left[ \frac{11}{12}C_A - \frac{N_f}{6} + (4C_F - C_A)(\ln 2 + \gamma_E) + (C_A - 2C_F) \ln \frac{1 - A_v}{A_v} + C_F \ln \frac{\mu_f^2}{\hat{s}} + C_F \ln \frac{\mu_{fp}^2}{\hat{s}} \right] S_{\gamma g} \end{aligned} \quad (6.65)$$

and

$$\begin{aligned} C_{\gamma q \rightarrow qg}(\hat{\eta}) &= \frac{C_F}{2(1-v)} \left\{ (C_A - 2C_F) \left[ (3-2v) \left( \ln^2 \frac{1-v}{v} + \pi^2 \right) + (1-2v) \ln^2(v) \right. \right. \\ &\quad \left. \left. + 2(1-v) \ln \frac{1-v}{v^2} \right] + 6C_F \ln(1-v) \right\} \\ &\quad + \frac{1}{4}S_{\gamma g} \left\{ C_F \left[ 6 \ln^2 \frac{1-v}{v} + \frac{1}{2}(\rho_{q\gamma}^{(F)})^2 - 6 \ln[v(1-v)] \right. \right. \\ &\quad \left. \left. + \rho_{q\gamma}^{(F)} (3 - 2 \ln[v(1-v)]) + 8 \ln v \ln(1-v) + \rho_{q\gamma}^{(F)} \ln \frac{\mu_{fi}^2}{\hat{s}} \right. \right. \\ &\quad \left. \left. + \left[ -3 + 4(\gamma_E + \ln 2) \right] \ln \frac{\mu_{ff}^2}{\hat{s}} + \frac{16}{3}\pi^2 - \frac{19}{2} \right] \right. \\ &\quad \left. - C_A \left[ 3 \ln^2 \frac{1-v}{v} + \frac{1}{8}(\rho_{q\gamma}^{(A)})^2 + \rho_{q\gamma}^{(A)} \ln \frac{1-v}{v} + 2\pi^2 - \frac{4}{3} \right] \right. \\ &\quad \left. + 4\pi b_0 \left( \frac{5}{3} + \gamma_E + \ln 2 + \ln \frac{\mu_r^2}{\hat{s}} \right) \right\}, \end{aligned} \quad (6.66)$$

where  $S_{\gamma g} = 2C_F(1 + (1-v)^2)/(1-v)$  and

$$\rho_{q\gamma}^{(F)} = -3 + 4(\gamma_E + \ln[2(1-v)]), \quad (6.67)$$

$$\rho_{q\gamma}^{(A)} = 4(\gamma_E + \ln 2). \quad (6.68)$$

The  $C$ -coefficients are subject to LO-kinematics and therefore we have

$$v = 1 + \frac{\hat{t}}{\hat{s}} = \frac{e^{\hat{\eta}}}{2 \cosh \hat{\eta}}. \quad (6.69)$$

The  $C$ -coefficient for the production of a gluon, which then fragments into the observed

hadron, reads:

$$\begin{aligned}
C_{\gamma q \rightarrow gq}(\hat{\eta}) = & \frac{C_F}{2v} \left\{ (C_A - 2C_F) \left[ (1+2v) \left( \pi^2 + \ln^2 \frac{v}{1-v} \right) - (1-2v) \ln^2(1-v) \right. \right. \\
& \left. \left. + 2v \ln \frac{v}{(1-v)^2} \right] + 6C_F \ln v \right\} \\
& + \frac{1}{4} \tilde{S}_{\gamma g} \left\{ C_F \left[ 4 \ln^2 \frac{1-v}{v} + 2(\ln(1-v) - 3) \ln(1-v) \right. \right. \\
& \left. \left. + \rho_{q\gamma}^{(F)} \ln \frac{\mu_{fi}^2}{\hat{s}(1-v)} + \frac{1}{8} (\rho_{q\gamma}^{(F)})^2 + \frac{3}{2} \rho_{q\gamma}^{(F)} + \frac{11}{3} \pi^2 - \frac{29}{8} \right] \right. \\
& \left. - C_A \left[ \ln^2 \frac{1-v}{v} - \rho_{q\gamma}^{(A)} \ln \frac{\mu_{ff}^2}{\hat{s}} - \frac{1}{4} (\rho_{q\gamma}^{(A)})^2 - \rho_{q\gamma}^{(A)} \ln \frac{1-v}{v} + \frac{\pi^2}{3} \right] \right. \\
& \left. - 4\pi b_0 \ln \frac{\mu_{ff}^2}{\mu_r^2} \right\}, \tag{6.70}
\end{aligned}$$

where  $\tilde{S}_{\gamma g} = 2C_F(1+v^2)/v$ . Finally, for the photon-gluon fusion process, one finds

$$\begin{aligned}
C_{\gamma g \rightarrow q\bar{q}}(\hat{\eta}) = & -\frac{1}{8v(1-v)} \left\{ (C_A - 2C_F) \left[ (1+2v) \ln^2 v + (3-2v) \ln^2(1-v) \right. \right. \\
& \left. \left. + 2 \ln[v(1-v)] \right] + 6C_F(1-2v) \ln \frac{1-v}{v} \right\} \\
& + \frac{1}{4} S_{\gamma g} \left\{ -4\pi b_0 \ln \frac{\mu_{fi}^2}{\mu_r^2} + C_F \left[ \frac{1}{8} (\rho_{g\gamma}^{(F)})^2 + \ln[v(1-v)] (1 + \ln[v(1-v)]) \right. \right. \\
& \left. \left. - 2 \ln(1-v) \ln v + \frac{3}{2} \rho_{g\gamma}^{(F)} + \rho_{g\gamma}^{(F)} \ln \frac{\mu_{ff}^2}{\hat{s}} + \frac{5}{3} \pi^2 - \frac{29}{8} \right] \right. \\
& \left. + C_A \left[ \frac{1}{2} \ln^2[v(1-v)] + \ln[v(1-v)] (1 - \rho_{g\gamma}^{(A)}) \right. \right. \\
& \left. \left. - \ln v \ln(1-v) + \rho_{g\gamma}^{(A)} \ln \frac{\mu_{fi}^2}{\hat{s}} + \frac{1}{4} (\rho_{g\gamma}^{(A)})^2 + \frac{2}{3} \pi^2 \right] \right\}, \tag{6.71}
\end{aligned}$$

where now  $S_{\gamma g} = (v^2 + (1-v)^2)/(v(1-v))$  and

$$\rho_{g\gamma}^{(F)} = -3 + 4(\gamma_E + \ln 2), \tag{6.72}$$

$$\rho_{g\gamma}^{(A)} = 4(\gamma_E + \ln[2(1-v)]). \tag{6.73}$$

### 6.2.5. Inverse Mellin transform and matching procedure

Resummation takes place in Mellin- $N$  moment space, and one therefore needs an inverse Mellin transform to translate the result back into the physical space. As described in Sec. 6.2.1 (see Eq. (6.20)), our approach has been to place the Mellin- $N$  transformation in between the convolutions over the parton distribution functions and the fragmentation and

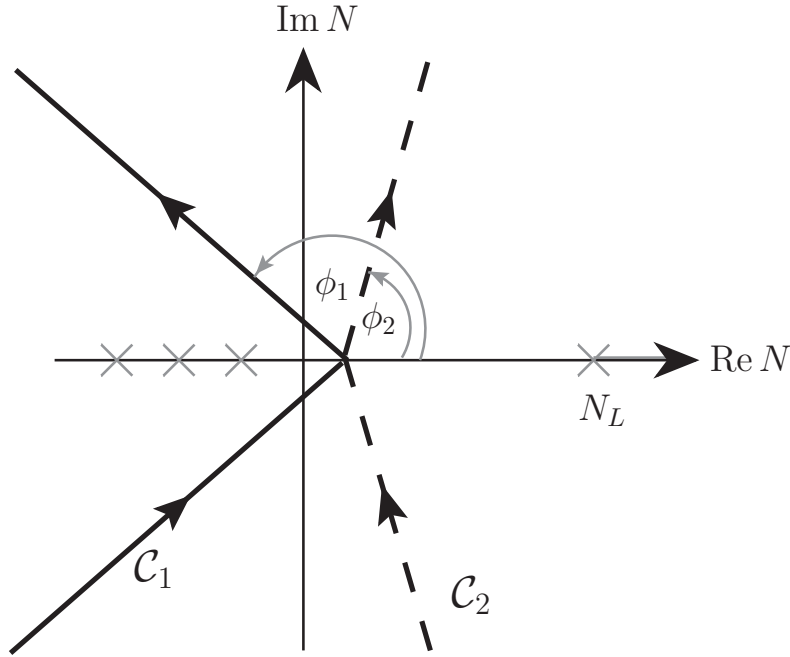


**Fig. 6.3.:** The two contours in Mellin- $N$  space for inverting the product of moments of the resummed partonic cross sections and the fragmentation functions. The crosses symbolize the poles of the fragmentation functions and LO cross sections on the real axis.  $N_L$  is the position of the leftmost Landau pole.

hard scattering functions. Therefore, the inverse Mellin transform that we need is given by

$$\sigma_D(x, \hat{\eta}) \equiv \int_C \frac{dN}{2\pi i} (x^2)^{-N} D_{h/c}^{2N+3}(\mu_{ff}) \tilde{w}^{\text{resum}, 2N}(\hat{\eta}). \quad (6.74)$$

The NLL expanded forms, Eqs. (6.39), (6.40), have singularities for  $\lambda = 1/2$  and  $\lambda = 1$ , known as Landau poles and corresponding to moments  $N_L = \exp(1/(2\alpha_s b_0))$  and  $N_L = \exp(1/(\alpha_s b_0))$ , respectively, that are located on the positive real axis in moment space. Therefore a prescription has to be found for dealing with these singularities. As discussed in Chap. 3, we follow the *minimal prescription* [100], according to which the contour for the inverse transformation runs between the first Landau pole  $N_L$  and the rightmost of all other poles of the integrand. This choice ensures that the perturbative expansion is an asymptotic series that has no factorial divergence [100]. Because of the branch cuts starting at the Landau poles to the right of the contour, the inverted  $\sigma_D(x, \hat{\eta})$  has support at  $x > 1$  [27, 100]<sup>17</sup>. Although the contribution from this unphysical region decreases exponentially

<sup>17</sup>A convenient parametrization of the contour in Eq. (6.74) is  $N = C + ze^{i\phi}$  (see Fig. 6.3). To obtain numerical convergence, the angle  $\phi$  has to be chosen in dependence of the value of  $x^2$ . While for  $x^2 < 1$  one has to choose  $\frac{\pi}{2} < \phi < \pi$ , on the other hand  $\phi < \frac{\pi}{2}$  is necessary for values  $x^2 > 1$ , such that the factor  $(x^2)^{-ze^{i\phi}}$  dampens the integrand.

with  $x$ , we find that it is not negligible for the kinematics of interest for phenomenology, even after subsequent convolution with the parton distributions. This possibly points to significant non-perturbative effects for the cross section and kinematic regime we consider here.

For our numerical computations, we choose the inverse Mellin contours  $\mathcal{C}_1$  (for  $x < 1$ ) and  $\mathcal{C}_2$  (for  $x > 1$ ) illustrated in Fig. 6.3 in the complex- $N$  plane. Bending the contours at non-zero angles with respect to the imaginary axis improves the numerical convergence of the integrals. The contour  $\mathcal{C}_2$  is still chosen to be rather steep, in order to avoid strong oscillations resulting from the branch cuts.

When using resummation to provide theoretical predictions of cross sections, one wants to make use of the best fixed-order theoretical calculation available, which in this case is NLO. Therefore, we “match” our resummed cross section to the NLO one. This is achieved by expanding the partonic cross sections to the first non-trivial order in  $\alpha_s$  ( $\mathcal{O}(\alpha_s^2)$  for the direct case,  $\mathcal{O}(\alpha_s^3)$  for the resolved one), subtracting the expanded result from the resummed one, and adding the full NLO cross section:

$$\begin{aligned} \frac{p_T^3 d\sigma^{\text{matched}}}{dp_T d\eta} &= \sum_{a,b,c} \int_0^1 dx_\ell \int_0^1 dx_n f_{a/\ell}(x_\ell, \mu_{fi}) f_{b/N}(x_n, \mu_{fi}) \\ &\quad \times \int_{\mathcal{C}} \frac{dN}{2\pi i} (x^2)^{-N} D_{h/c}^{2N+3}(\mu_{ff}) \left[ \tilde{w}_{ab \rightarrow cd}^{\text{resum}, 2N}(\hat{\eta}) - \tilde{w}_{ab \rightarrow cd}^{\text{resum}, 2N}(\hat{\eta}) \Big|_{\text{first-order}} \right] \\ &\quad + \frac{p_T^3 d\sigma^{\text{NLO}}}{dp_T d\eta}. \end{aligned} \quad (6.75)$$

This procedure allows to take into account the NLO calculation in full. The soft-gluon contributions beyond NLO are resummed to NLL.

### 6.3. Fully rapidity-integrated resummed cross section

In this section we want to derive the resummed formula for the fully rapidity-integrated cross section starting from the rapidity-dependent result, which we derived in the previous section. The fully rapidity-dependent resummed cross section was first implemented by [26] for the (resolved) processes in the context with neutral pion production in proton-proton collisions in collider and fixed-target regimes.

Thus, we integrate out the rapidity  $\eta$  in the rapidity-dependent cross section in Eq. (6.2)

$$\begin{aligned} p_T^3 \frac{d\sigma}{dp_T} &= \sum_{a,b,c} \int_{-\text{arccosh} \frac{1}{x_T}}^{\text{arccosh} \frac{1}{x_T}} d\eta \int_{x_\ell^{\min}}^1 dx_\ell \int_{x_n^{\min}}^1 dx_n \int_x^1 dz \frac{\hat{x}_T^4 z^2}{8v} \\ &\quad \times f_{a/\ell}(x_\ell, \mu_{fi}) f_{b/N}(x_n, \mu_{fi}) D_{h/c}(z, \mu_{ff}) \frac{\hat{s} d\hat{\sigma}_{ab \rightarrow cX}}{dv dw}. \end{aligned} \quad (6.76)$$

Interchanging the order of the integrals gives

$$p_T^3 \frac{d\sigma}{dp_T} = \sum_{a,b,c} \int_{x_T}^1 dz z^2 D_{h/c}(z, \mu_{ff}) \int_{\frac{x_T^2}{z^2}}^1 dx_n f_{b/N}(x_n, \mu_{fi}) \int_{\frac{x_T^2}{z^2 x_n}}^1 dx_\ell f_{a/\ell}(x_\ell, \mu_{fi}) \\ \times \int_{-\text{arccosh} \frac{1}{\hat{x}_T}}^{\text{arccosh} \frac{1}{\hat{x}_T}} d\hat{\eta} \frac{\hat{x}_T^4}{8v} \frac{\hat{s} d\hat{\sigma}_{ab \rightarrow cX}}{dv dw}. \quad (6.77)$$

Then the fully rapidity-integrated partonic cross section  $\Sigma_{ab \rightarrow cX}$  depends just on one kinematic variable, namely  $\hat{x}_T$ ,

$$\Sigma_{ab \rightarrow cX}(\hat{x}_T) \equiv \int_{-\text{arccosh} \frac{1}{\hat{x}_T}}^{\text{arccosh} \frac{1}{\hat{x}_T}} d\hat{\eta} \frac{\hat{x}_T^4}{8v} \frac{\hat{s} d\hat{\sigma}_{ab \rightarrow cX}}{dv dw}. \quad (6.78)$$

Having integrated out the rapidity, the large logarithmic first order corrections in form of the plus distributions  $[\ln(1-w)/(1-w)]_+$  and  $[1/(1-w)]_+$  in the NLO partonic cross section (6.15) show up in the rapidity integrated analogon  $\Sigma_{ab \rightarrow cX}^{(1)}(\hat{x}_T)$  as logarithmic terms  $\ln^2(1-\hat{x}_T^2)$  and  $\ln(1-\hat{x}_T^2)$ , which are singular at  $\hat{x}_T = 1$ . These terms potentiate at higher order corrections, such that in  $k$ th order one is faced with terms proportional to  $\alpha_s^k \ln^{2k}(1-\hat{x}_T^2)$  in  $\Sigma_{ab \rightarrow cX}^{(k)}(\hat{x}_T)$  [26].

The threshold logarithms are the larger, the closer the partonic scaling variable  $\hat{x}_T \rightarrow 1$ . Consider a fixed observed transverse momentum  $p_T$  at an experiment with center-of-mass energy  $s$ . This fixes the hadronic scaling variable  $x_T$ . Thus, according to Eq. (6.4) the threshold logarithms give particularly large contributions when the partonic momentum fractions are close to their lower bounds. Towards small momentum fractions, the parton distribution functions generally exhibit a steep rise. This enhances the effect of the threshold logarithms and makes it even important for situations in which one is not that close to the threshold region, i.e. in which the hadronic center-of-mass energy is much larger than the transverse momentum of the final state hadron [26].

### 6.3.1. Mellin moments and threshold region

As we did for the resummation of the rapidity-dependent resummed cross section, the resummation of the soft-gluon contributions for the rapidity-dependent resummed cross section is again carried out in Mellin- $N$  moment space. If the cross section is integrated over all rapidities, as we did in Eq. (6.77), it becomes a function of  $x_T^2$ , and a single Mellin moment in  $x_T^2$  suffices to factorize it in terms of moments of parton distributions, fragmentation functions, and partonic cross sections [26]. After resummation the full Mellin expression is inverted, directly giving the desired hadronic cross section.

Taking Mellin moments in the hadronic scaling variable  $x_T^2$ ,

$$\sigma^N \equiv \int_0^1 dx_T^2 (x_T^2)^{N-1} \frac{p_T^3 d\sigma(x_T)}{dp_T}, \quad (6.79)$$

yields

$$\sigma^N = \sum_{a,b,c} f_{a/\ell}^{N+1}(\mu_{fi}) f_{b/N}^{N+1}(\mu_{fi}) D_{h/c}^{2N+3}(\mu_{ff}) \hat{\sigma}_{ab \rightarrow cX}^N, \quad (6.80)$$

with

$$\begin{aligned} \hat{\sigma}_{ab \rightarrow cX}^N &\equiv \int_0^1 d\hat{x}_T^2 (\hat{x}_T^2)^{N-1} \Sigma_{ab \rightarrow cX}(\hat{x}_T^2) \\ &= \frac{1}{2} \int_0^1 dw \int_0^1 dv [4v(1-v)w]^{N+1} \frac{\hat{s} d\hat{\sigma}_{ab \rightarrow cX}^{(1)}(v, w)}{dv dw}, \end{aligned} \quad (6.81)$$

and where the Mellin moments of the parton distributions are defined by,

$$f^N(\mu) = \int_0^1 dx x^{N-1} f(x, \mu), \quad (6.82)$$

and the moments of the fragmentation functions are given as in Eq. (6.18). Recall that in the resolved processes,  $f_{a/\ell}(x_\ell, \mu_{fi})$  in turn is a convolution of a lepton-to-photon splitting function  $P_{\gamma\ell}$  and a parton distribution function  $f_{a/\gamma}$  of a photon, see Eq. (6.10). So, in case of the resolved processes the moments of the lepton-to-parton distribution functions are products of the moments of the lepton-to-photon splitting function  $P_{\gamma\ell}^N$  and the moments of the parton distribution functions of the photon:

$$f_{a/\ell}^N(\mu_{fi}) = P_{\gamma\ell}^N f_{a/\gamma}^N(\mu_{fi}). \quad (6.83)$$

Considering the Mellin moments (6.80) instead of the physical cross section of course changes nothing for the large soft-gluon corrections at threshold. The threshold limit corresponds to the limit  $N \rightarrow \infty$ , and the leading logarithms in  $(1 - \hat{x}_T)^2$  show up as terms proportional to  $\alpha_s^k \ln^{2k} N$ .

### 6.3.2. Moments of the Weizsäcker-Williams spectrum with cuts

Often specific experimental setups impose restrictions on the range of the momentum fraction  $y$  of the Weizsäcker-Williams spectrum. In this subsection we provide the moments of the spectrum taking into account certain bounds for the momentum fraction  $y$ ,

$$y_d \leq y \leq y_u. \quad (6.84)$$

These only have an effect on the Mellin moment of the Weizsäcker-Williams spectrum in Eq. (6.80). When taking Mellin moments we obtain

$$\tilde{P}_{\gamma l}^N = \int_0^1 y^{N-1} P_{\gamma l}(y) \theta(y - y_d) \theta(y_u - y) \equiv \frac{\alpha}{2\pi} (P^N(y_u) - P^N(y_d)), \quad (6.85)$$

with

$$P^N(x) = 2\tilde{P}^{N-1}(x) - 2\tilde{P}^N(x) + \tilde{P}^{N+1}(x) - \frac{2x^{N-1}}{N-1} + \frac{2x^N}{N} + \frac{2x^{N+1}}{N+1} \frac{m_l^2}{Q_{\max}^2} \quad (6.86)$$

and

$$\tilde{P}^N(x) = \frac{x^N}{N} \left[ \frac{1}{N} + \ln \frac{Q_{\max}^2(1-x)}{m_l^2 x^2} + \Phi(x, 1, N) \right], \quad (6.87)$$

where  $\Phi(x, a, v)$  denotes the Lerch transcendent and is defined by

$$\Phi(x, a, v) = \sum_{n=0}^{\infty} \frac{x^n}{(v+n)^a}. \quad (6.88)$$

Numerically the Lerch transcendent may be implemented by aborting this series at some order. We found that for our purposes, taking only the first 10 elements of the series, yields already a sufficiently good approximation.

### 6.3.3. Fully rapidity-integrated resummed cross section to NLL accuracy

Once the formula for the rapidity-dependent partonic resummed cross section is available, it is easy to derive the rapidity-integrated one. For that, let us recall the rapidity-dependent resummed cross section from (6.20) and (6.21),

$$\frac{p_T^3 d\sigma}{dp_T d\eta} = \sum_{a,b,c} \int_0^1 dx_\ell \int_0^1 dx_n f_{a/\ell}(x_\ell, \mu_{fi}) f_{b/N}(x_n, \mu_{fi}) \int_C \frac{dN}{2\pi i} (x^2)^{-N} D_{h/c}^{2N+3}(\mu_{ff}) \tilde{w}^{2N}(\hat{\eta}), \quad (6.89)$$

with  $x = x_T \cosh \hat{\eta} / \sqrt{x_n x_\ell}$  and

$$\tilde{w}_{ab \rightarrow cd}^{\text{resum}, N}(\hat{\eta}) = \Delta_a^{N_a}(\hat{s}, \mu_{fi}) \Delta_b^{N_b}(\hat{s}, \mu_{fi}) \Delta_c^N(\hat{s}, \mu_{ff}) J_d^N(\hat{s}) \text{Tr} \left\{ H S_N^\dagger S S_N \right\}_{ab \rightarrow cd}. \quad (6.90)$$

where  $N_a = (-\hat{u}/\hat{s})N$  and  $N_b = (-\hat{t}/\hat{s})N$ . We want to compare its Mellin- $N$ -moments directly to the ones of the fully rapidity-integrated cross section in Eq. (6.80). Therefore,



we take Mellin moments in  $x_T^2$ :

$$\begin{aligned}
& \int_0^1 dx_T^2 (x_T^2)^{N-1} \frac{p_T^3 d\sigma}{dp_T d\eta} = \sum_{a,b,c} \int_0^1 dx_T^2 (x_T^2)^{N-1} \int_C \frac{dN}{2\pi i} (x_T^2)^{-N} \\
& \times \int_0^1 dx_\ell x_\ell^N f_{a/\ell}(x_\ell, \mu_{fi}) \int_0^1 dx_n x_n^N f_{b/N}(x_n, \mu_{fi}) D_{h/c}^{2N+3}(\mu_{ff}) \cosh^{-2N} \hat{\eta} \tilde{w}^{2N}(\hat{\eta}) \\
& = \sum_{a,b,c} \int_0^1 dx_\ell x_\ell^N f_{a/\ell}(x_\ell, \mu_{fi}) \int_0^1 dx_n x_n^N f_{b/N}(x_n, \mu_{fi}) D_{h/c}^{2N+3}(\mu_{ff}) \cosh^{-2N} \hat{\eta} \tilde{w}^{2N}(\hat{\eta})
\end{aligned} \tag{6.91}$$

Integrating out the rapidity in the last two terms of Eq. (6.91) gives the corresponding Mellin- $N$ -moment for the fully rapidity-integrated partonic cross section

$$\hat{\sigma}_{ab \rightarrow cd}^{\text{resum}, N} = \int d\hat{\eta} \cosh^{-2N} \hat{\eta} \tilde{w}^{2N}(\hat{\eta}). \tag{6.92}$$

As we already mentioned before, the trace of the product of the lowest order hard and soft matrix,  $\text{Tr} \{HS\}_{ab \rightarrow cd}$ , gives the partonic Born cross section. So we rewrite

$$\text{Tr} \{HS_N^\dagger SS_N\}_{ab \rightarrow cd} = \frac{\text{Tr} \{HS_N^\dagger SS_N\}_{ab \rightarrow cd}}{\text{Tr} \{HS\}_{ab \rightarrow cd}} \hat{\sigma}_{ab \rightarrow cd}^{\text{Born}, N}(\hat{\eta}) \tag{6.93}$$

in order to explicitly separate the Born cross section from an additional multiplicative factor corresponding to the threshold resummation effects. To obtain the fully rapidity-integrated resummed cross section from this expression, it is sufficient to set  $\hat{\eta} = 0$  in the afore mentioned multiplicative factor. Let us have a more detailed look on where  $\hat{\eta}$ -dependence appears. We start with the jet functions  $\Delta_i$  and  $J_d$  in (6.90). All of them depend via the partonic center-of-mass energy

$$\hat{s} = 4p_T^2 \cosh^2 \hat{\eta} \tag{6.94}$$

on the partonic rapidity  $\hat{\eta}$ . In addition to that, the initial-state exponents  $\Delta_a$  and  $\Delta_b$  show an  $\hat{\eta}$ -dependence in their arguments  $N_a$  and  $N_b$ , respectively. Close to the threshold region, these are given by

$$N_a = \frac{e^{\hat{\eta}}}{2 \cosh \hat{\eta}} N, \quad N_b = \frac{e^{-\hat{\eta}}}{2 \cosh \hat{\eta}} N. \tag{6.95}$$

Setting  $\hat{\eta} = 0$  and defining  $Q^2 = 2p_T^2$  we obtain

$$\begin{aligned}\Delta_a^{2N_a}(\hat{s}, \mu_{fi})|_{\hat{\eta}=0} &= \Delta_a^N(Q^2, \mu_{fi}) + \frac{A_a^{(1)}}{2\pi b_0} \ln 2 \ln(1 - 2\lambda) \\ \Delta_b^{2N_b}(\hat{s}, \mu_{fi})|_{\hat{\eta}=0} &= \Delta_b^N(Q^2, \mu_{fi}) + \frac{A_b^{(1)}}{2\pi b_0} \ln 2 \ln(1 - 2\lambda) \\ \Delta_c^{2N_c}(\hat{s}, \mu_{ff})|_{\hat{\eta}=0} &= \Delta_c^N(Q^2, \mu_{ff}) - \frac{A_c^{(1)}}{2\pi b_0} \ln 2 \ln(1 - 2\lambda) \\ J_d^{2N}(\hat{s})|_{\hat{\eta}=0} &= J_d^N(Q^2) + \frac{A_d^{(1)}}{2\pi b_0} \ln 2 \ln(1 - 2\lambda),\end{aligned}\tag{6.96}$$

where as before  $\lambda = \alpha_s b_0 \ln N$ .

Next, we turn to the normalized terms in (6.93) collecting the contributions with the emission of soft gluons at wide angles. With  $\hat{\eta} = 0$  the matrices  $\Gamma_{ab \rightarrow cd}(\hat{\eta}, \alpha_s)$  in the exponentials  $\mathcal{S}_{N,ab \rightarrow cd}(\hat{\eta}, \alpha_s)$  in Eq. (6.30) may be diagonalized. This enables us to write the fraction of the traces in the form

$$\frac{\text{Tr} \left\{ H S_{2N}^\dagger S S_{2N} \right\}_{ab \rightarrow cd}}{\text{Tr} \left\{ H S \right\}_{ab \rightarrow cd}} \bigg|_{\hat{\eta}=0} = \sum_I G_{ab \rightarrow cd}^I \Delta_{(int)}^N(\tilde{D}_I \text{ } ab \rightarrow cd),\tag{6.97}$$

where in our notation  $\Delta_{(int)}^N(f)$  is the functional

$$\ln \Delta_{(int)}^N(\tilde{D}_I \text{ } ab \rightarrow cd) = \int_0^1 \frac{z^{N-1} - 1}{1 - z} \tilde{D}_I \text{ } ab \rightarrow cd(\alpha_s((1 - z)^2 Q^2))\tag{6.98}$$

with  $\tilde{D}_I \text{ } ab \rightarrow cd$  being a perturbative series in  $\alpha_s$ ,

$$\tilde{D}_I \text{ } ab \rightarrow cd(\alpha_s) = \frac{\alpha_s}{\pi} \tilde{D}_I^{(1)} \text{ } ab \rightarrow cd + \left( \frac{\alpha_s}{\pi} \right)^2 \tilde{D}_I^{(2)} \text{ } ab \rightarrow cd + \dots\tag{6.99}$$

Its coefficients  $\tilde{D}_I^{(1)} \text{ } ab \rightarrow cd, \tilde{D}_I^{(2)} \text{ } ab \rightarrow cd$  may be calculated from the matrices  $H_{ab \rightarrow cd}, S_{ab \rightarrow cd}$  and  $\Gamma_{ab \rightarrow cd}$  for each process. The  $I$  in the sum of Eq. (6.97) labels all possible color configurations. Each color configuration contributes with a weight  $G_{ab \rightarrow cd}^I$ . As we have a normalized contribution, we have  $\sum_I G_{ab \rightarrow cd}^I = 1$ .

Collecting our results of Eq. (6.96) and Eq. (6.97) we are now ready to write down the fully rapidity-integrated resummed partonic cross section in Mellin- $N$ -moment space:

$$\hat{\sigma}_{ab \rightarrow cd}^{\text{resum}, N} = C_{ab \rightarrow cd} \Delta_a^N \Delta_b^N \Delta_c^N J_d^N \left[ \sum_I G_{ab \rightarrow cd}^I \Delta_{(int)}^N(D_I \text{ } ab \rightarrow cd) \right] \hat{\sigma}_{ab \rightarrow cd}^{\text{Born}, N},\tag{6.100}$$

Note that we adopt the notation of [26] here, such that the functions  $D_I \text{ } ab \rightarrow cd$  are slightly different from the  $\tilde{D}_I \text{ } ab \rightarrow cd$  in Eq. (6.97). In [26] the  $D_I \text{ } ab \rightarrow cd$  were defined such that

**Table 6.1.:** Coefficients  $D_{i\ ab\rightarrow cd}^{(1)}$  and  $G_{i\ ab\rightarrow cd}$  for the fully rapidity-integrated resummed exponents of various resolved processes. Note that we adopt the notation in Ref. [26], in which terms in the exponents for the external partons proportional to  $\ln 2 \ln(1-2\lambda)$  were also absorbed in the definition of the coefficients. So, compared to their coefficients  $D_{i\ ab\rightarrow cd}^{(1)}$  in the exponents (see in Appendix of [26]), the  $D_{i\ ab\rightarrow cd}^{(1)}$  are shifted by a fixed term depending on the type of the participating partons. The weights  $G_{i\ ab\rightarrow cd}$ , however, are the same.

$q\bar{q} \rightarrow q\bar{q}$			$qq \rightarrow qq$	
$D_1^{(1)} = -\frac{10}{3} \ln 2, \quad D_2^{(1)} = \frac{8}{3} \ln 2$			$D_1^{(1)} = -4 \ln 2, \quad D_2^{(1)} = 0$	
$q_j \bar{q}_j \rightarrow q_j \bar{q}_j$	$q_j \bar{q}_j \rightarrow q_k \bar{q}_k$	$q_j \bar{q}_k \rightarrow q_j \bar{q}_k$	$q_j q_j \rightarrow q_j q_j$	$q_j q_k \rightarrow q_j q_k$
$G_1 = 5/21$	$G_1 = 1$	$G_1 = 1/9$	$G_1 = 9/11$	$G_1 = 1/3$
$G_2 = 16/21$	$G_2 = 0$	$G_2 = 8/9$	$G_2 = 2/11$	$G_2 = 2/3$

$q\bar{q} \rightarrow gg$	$gg \rightarrow q\bar{q}$	$qg \rightarrow qg$	$qg \rightarrow gq$	$gg \rightarrow gg$
$D_1^{(1)} = -10/3 \ln 2$	$D_1^{(1)} = 0$	$D_1^{(1)} = -14/3 \ln 2$	$D_1^{(1)} = -8 \ln 2$	$D_1^{(1)} = 0$
$D_2^{(1)} = 8/3 \ln 2$	$D_2^{(1)} = 6 \ln 2$	$D_2^{(1)} = 10/3 \ln 2$	$D_2^{(1)} = 0$	$D_2^{(1)} = -10 \ln 2$
		$D_3^{(1)} = -2/3 \ln 2$	$D_3^{(1)} = -4 \ln 2$	$D_3^{(1)} = 6 \ln 2$
$G_1 = 5/7$		$G_1 = 45/88$		$G_1 = 1/3$
$G_2 = 2/7$		$G_2 = 25/88$		$G_2 = 1/2$
		$G_3 = 18/88$		$G_3 = 1/6$

they absorb also the terms proportional to  $\ln 2$  in the initial- and final state exponents in Eq. (6.96):

$$D_{I\ ab\rightarrow cd}^{(1)} = \tilde{D}_{I\ ab\rightarrow cd}^{(1)} + \left( A_a^{(1)} + A_b^{(1)} - A_c^{(1)} + A_d^{(1)} \right) \ln 2. \quad (6.101)$$

We summarize the coefficients  $G_{ab\rightarrow cd}^I$  and  $D_{I\ ab\rightarrow cd}$  for all resolved processes in Table 6.1 (see [26]). In Eq. (6.100)  $\hat{\sigma}_{ab\rightarrow cd}^{\text{Born}, N}$  are the Mellin- $N$  moments of the fully rapidity-integrated Born cross section for the respective process. They are all listed in the appendix of [26] or may be calculated using the lowest order hard and the soft matrices given in Table C.1 and Table C.2,

$$\frac{\hat{s} d\hat{\sigma}_{ab\rightarrow cd}^{(0)}}{dvdw} = \pi \text{Tr} [H_{ab\rightarrow cd} S_{ab\rightarrow cd}] \delta(1-w). \quad (6.102)$$

We finish this section with an example. Let us consider the quark-antiquark scattering process  $q_j \bar{q}_k \rightarrow q_j \bar{q}_k$ . First we calculate the Mellin- $N$ -moment of the fully rapidity-

integrated Born cross section. The trace of the matrix product gives

$$\frac{\hat{s}d\hat{\sigma}_{q_j\bar{q}_k\rightarrow q_j\bar{q}_k}^{(0)}}{dvdw} = \pi \text{Tr} [H_{q_j\bar{q}_k\rightarrow q_j\bar{q}_k} S_{q_j\bar{q}_k\rightarrow q_j\bar{q}_k}] \delta(1-w) = \alpha_s^2 \pi \frac{N_c^2 - 1}{2N_c^2} \frac{\hat{s}^2 + \hat{u}^2}{\hat{t}^2} \delta(1-w) \quad (6.103)$$

Rewriting the Mandelstam variables in terms of  $v$  and  $w$  by using the relations (6.5) and (6.6) yields

$$\frac{\hat{s}d\hat{\sigma}_{q_j\bar{q}_k\rightarrow q_j\bar{q}_k}^{(0)}}{dvdw} = \alpha_s^2 \pi \frac{C_F}{C_A} \frac{1+v^2}{(1-v)^2} \delta(1-w), \quad (6.104)$$

and from that we may calculate  $\hat{\sigma}_{q_j\bar{q}_k\rightarrow q_j\bar{q}_k}^{\text{Born},N}$  through Eq. (6.81). As a result one obtains (see also [26]):

$$\begin{aligned} \hat{\sigma}_{q_j\bar{q}_k\rightarrow q_j\bar{q}_k}^{\text{Born},N} &= \frac{1}{2} \int_0^1 dv [4v(1-v)]^{N+1} \alpha_s^2 \pi \frac{C_F}{C_A} \frac{1+v^2}{(1-v)^2} \\ &= \alpha_s^2 \pi \frac{C_F}{3C_A} (5N^2 + 15N + 12) B\left(N, \frac{5}{2}\right), \end{aligned} \quad (6.105)$$

with  $B(x, y)$  denoting the *beta function*,

$$B(x, y) = \frac{\Gamma(x)\Gamma(y)}{\Gamma(x+y)}. \quad (6.106)$$

Next, we show how to derive the coefficients  $G_{q_j\bar{q}_k\rightarrow q_j\bar{q}_k}^I$  and  $D_{I q_j\bar{q}_k\rightarrow q_j\bar{q}_k}$ . For quark-antiquark scattering the space of color exchange operators is two-dimensional. Thus the soft, hard and anomalous dimension matrices are  $2 \times 2$ -matrices, which can be even diagonalized in the rapidity-dependent case. Taking the corresponding matrices from Table C.1 we obtain

$$\begin{aligned} &\frac{\text{Tr} \left\{ H_{q_j\bar{q}_k\rightarrow q_j\bar{q}_k} \exp \left( \frac{\ln(1-2\lambda)}{2\pi b_0} \Gamma_{q_j\bar{q}_k\rightarrow q_j\bar{q}_k}^\dagger \right) S_{q_j\bar{q}_k\rightarrow q_j\bar{q}_k} \exp \left( \frac{\ln(1-2\lambda)}{2\pi b_0} \Gamma_{q_j\bar{q}_k\rightarrow q_j\bar{q}_k} \right) \right\}}{\text{Tr} \left\{ H_{q_j\bar{q}_k\rightarrow q_j\bar{q}_k} S_{q_j\bar{q}_k\rightarrow q_j\bar{q}_k} \right\}} \\ &= G_{1 q_j\bar{q}_k\rightarrow q_j\bar{q}_k} \exp \left\{ \tilde{D}_{1 q_j\bar{q}_k\rightarrow q_j\bar{q}_k} \frac{\ln(1-2\lambda)}{2\pi b_0} \right\} + G_{2 q_j\bar{q}_k\rightarrow q_j\bar{q}_k} \exp \left\{ \tilde{D}_{2 q_j\bar{q}_k\rightarrow q_j\bar{q}_k} \frac{\ln(1-2\lambda)}{2\pi b_0} \right\} \end{aligned} \quad (6.107)$$

where

$$\begin{aligned}
G_{1\,q_j\bar{q}_k\rightarrow q_j\bar{q}_k} &= \frac{1}{2} + \frac{1}{\sqrt{d}} \left( \frac{C_A \ln(1-v)}{2} - \frac{\ln(v)}{C_A} \right) \\
G_{2\,q_j\bar{q}_k\rightarrow q_j\bar{q}_k} &= \frac{1}{2} - \frac{1}{\sqrt{d}} \left( \frac{C_A \ln(1-v)}{2} - \frac{\ln(v)}{C_A} \right) \\
\tilde{D}_{1\,q_j\bar{q}_k\rightarrow q_j\bar{q}_k} &= (4C_F - C_A) \ln(1-v) - 2(2C_F - C_A) \ln(v) - \sqrt{d} \\
\tilde{D}_{2\,q_j\bar{q}_k\rightarrow q_j\bar{q}_k} &= (4C_F - C_A) \ln(1-v) - 2(2C_F - C_A) \ln(v) + \sqrt{d}
\end{aligned} \tag{6.108}$$

with

$$d = C_A^2 \ln(1-v)^2 - 4 \ln(1-v) \ln(v) + 4 \ln(v)^2, \tag{6.109}$$

and where

$$v = 1 + \frac{\hat{t}}{\hat{s}} = \frac{e^{\hat{\eta}}}{2 \cosh \hat{\eta}}. \tag{6.110}$$

The conversion to the fully rapidity-integrated cross section is performed by setting  $\hat{\eta} = 0$ . This corresponds to  $v = \frac{1}{2}$ . Then we have

$$\begin{aligned}
G_{1\,q_j\bar{q}_k\rightarrow q_j\bar{q}_k} &= \frac{1}{9}, & G_{2\,q_j\bar{q}_k\rightarrow q_j\bar{q}_k} &= \frac{8}{9} \\
\tilde{D}_{1\,q_j\bar{q}_k\rightarrow q_j\bar{q}_k} &= -6 \ln 2, & \tilde{D}_{2\,q_j\bar{q}_k\rightarrow q_j\bar{q}_k} &= 0.
\end{aligned} \tag{6.111}$$

What is left to do now, is to add the terms proportional to  $\ln 2$  from Eq. (6.96) according to Eq. (6.101). In quark-antiquark scattering we have the coefficients

$$\begin{aligned}
D_{1\,q_j\bar{q}_k\rightarrow q_j\bar{q}_k} &= \tilde{D}_{1\,q_j\bar{q}_k\rightarrow q_j\bar{q}_k} + 2C_F \ln 2 = -\frac{10}{3} \ln 2 \\
D_{2\,q_j\bar{q}_k\rightarrow q_j\bar{q}_k} &= \tilde{D}_{2\,q_j\bar{q}_k\rightarrow q_j\bar{q}_k} + 2C_F \ln 2 = \frac{8}{3} \ln 2,
\end{aligned} \tag{6.112}$$

which are the ones presented in Table 6.1. For processes, in which gluons are involved, the soft anomalous dimension matrix are diagonalized after we have set  $\hat{\eta} = 0$ .

This example closes the section and also the chapter. We have studied the resummation of next-to-leading logarithmic threshold logarithms on the direct- and resolved-photon cross sections for the process  $\gamma N \rightarrow h + X$  at high transverse momentum of the hadron  $h$ . In order to take into account all relevant experimental cuts, we extended the rapidity-integrated resummed result [26] by fully including rapidity dependence, following the techniques developed in [27]. The basic idea was to treat only the partonic cross sections and the fragmentation functions in Mellin- $N$  moment space, and to keep the convolutions

with the parton distribution functions in  $x$ -space. Finally, we showed how to link the rapidity-dependent result to the fully rapidity-integrated result from the previous work [26].

## 7. Phenomenological studies: Hadron production at COMPASS

With our result for the rapidity-dependent resummed cross section from the previous chapter, we are now ready to turn to phenomenological studies. We will apply the developed formalism to the fixed-target lepton-nucleon scattering experiment COMPASS at CERN [29, 30]. There, produced charged hadrons were observed at high transverse momentum  $p_T$ . From the theoretical point of view the kinematics employed in this experiment is insofar challenging as the observed  $p_T$ -range is on the one hand relatively large (the hadronic scaling variable is  $x_T = 2p_T/\sqrt{s} \gtrsim 0.1$ , with  $\sqrt{s}$  the center-of-mass energy) such that the partonic hard-scattering is close to the partonic threshold, but on the other hand the observed  $p_T$ -range is that low that it is at the lowest end of the perturbative accessible range. Corresponding NLO calculations and their comparison to the experimental data [29] indicate, that the higher-order threshold logarithms have a large impact and are far from being negligible. Hence, a suitable theoretical prediction has to include these contributions, for instance via threshold resummation. In this chapter we will analyze the impact of the large logarithmic contributions to the partonic cross section associated with soft gluon emissions close to the threshold region. We, therefore, apply the rapidity-dependent threshold resummation formalism of Sec. 6.2 in the previous chapter. Then we compare our results directly to the experimental data. In the second part of this chapter we compare the phenomenological results of the fully rapidity-integrated resummed approach of the previous work [26] to the rapidity-integrated resummed cross section, which we integrate over the full kinematically allowed rapidity range. This allows to judge, whether rescaling the fully rapidity-integrated cross section by an appropriate ratio of NLO cross sections provides a suitable approximation for the rapidity-dependent resummed cross section.

Please note again that parts of the present chapter have already been published in [31].

### 7.1. Comparison of theoretical prediction to experimental data

Starting from Eq. (6.75) we now compare the resummed cross section to experimental hadron production data measured at the COMPASS experiment at CERN [29, 30]. In this fixed-target experiment muons with a mean beam energy of  $E_\mu = 160$  GeV were scattered

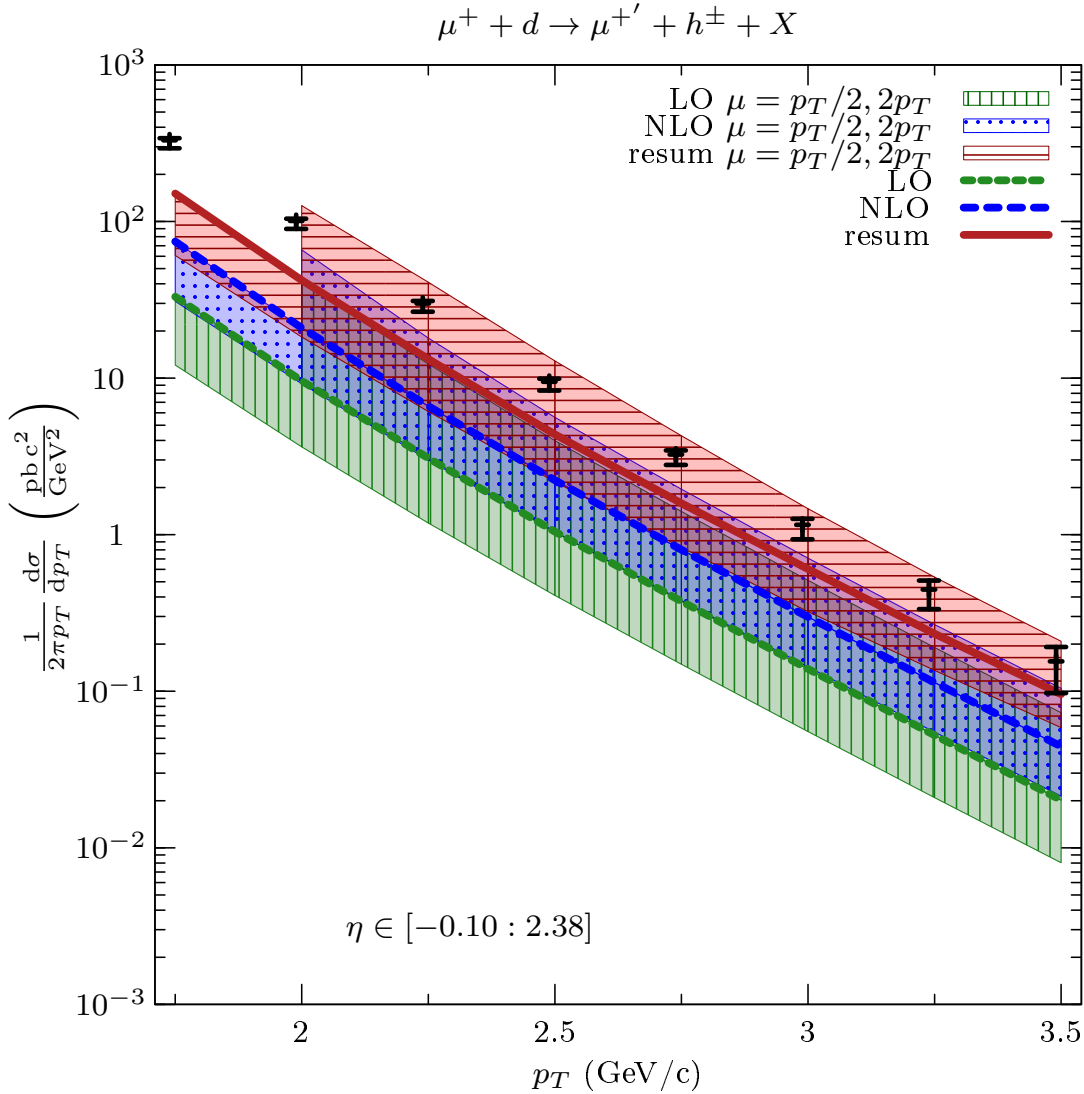


**Fig. 7.1.:** Comparison of the LO, NLO and resummed (“resum”) calculations to COMPASS data. The error bars shown for the experimental data are the quadratic sums of statistical and systematic uncertainties. In addition, there is a 10% normalization uncertainty due to the luminosity determination. For scale  $\mu = p_T/2$  we only show results for  $p_T \geq 2 \text{ GeV}$ .

off a deuteron target, corresponding to a lepton-nucleon center-of-mass energy of  $\sqrt{s} = 17.4 \text{ GeV}$ . Due to the detector acceptance the fraction  $y$  of the lepton momentum carried by the photon is restricted to the range  $0.2 \leq y \leq 0.8$ . For the COMPASS photoproduction studies the maximally allowed virtuality  $Q_{\text{max}}^2$  of the photons was  $Q_{\text{max}}^2 = 0.1 \text{ GeV}^2$ . The measured hadrons  $h^\pm$  were subject to the following kinematic cuts: the fraction  $z_{\text{cut}}$  of the virtual photon energy carried by the detected hadron had to be within the range  $0.2 \leq z_{\text{cut}} \leq 0.8$ . In addition, the scattering angle  $\theta$  of the observed hadron was constrained by  $10 \leq \theta \leq 120 \text{ mrad}$ , corresponding to  $2.38 \geq \eta \geq -0.1$  in pseudo-rapidity in the lepton-



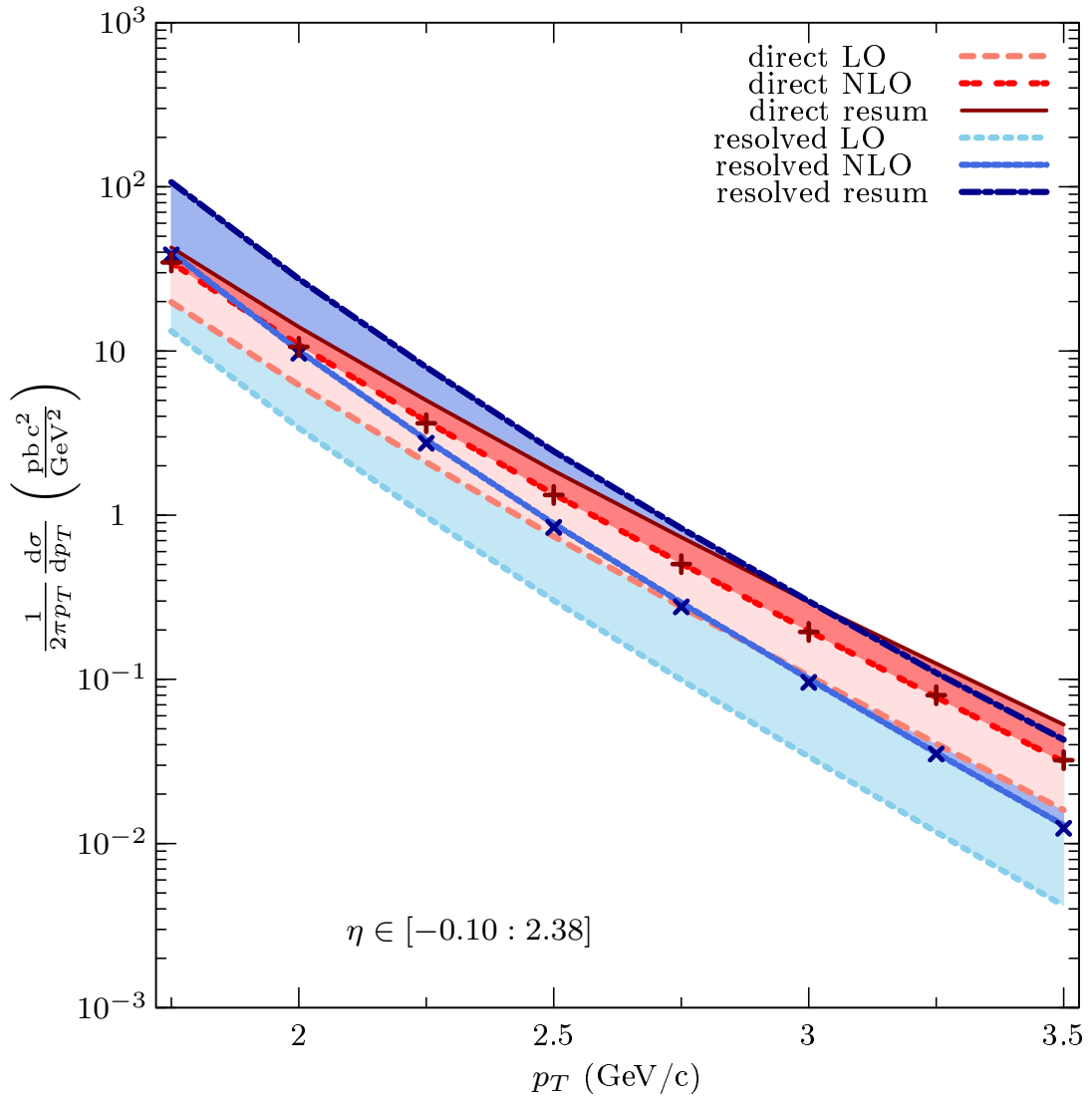


**Fig. 7.2.:** The direct contribution versus the resolved one in the  $\overline{\text{MS}}$  scheme for the photon's parton distributions. The crosses denote the first-order expansions of the direct and resolved resummed cross sections.

nucleon center-of-mass system.

In our calculations we use the CTEQ6M5 set of parton distribution functions for the nucleon [150] and the “Glück-Reya-Schienbein” (GRS) parton distribution functions of the photon [141]. For the fragmentation functions we use the “de Florian-Sassot-Stratmann” (DSS) set [151]. All scales in Eq. (6.75) are set equal,  $\mu = \mu_r = \mu_{fi} = \mu_{ff} = p_T$ . In order to investigate the scale dependence of our results, we will also show the results for  $\mu = p_T/2$  and  $\mu = 2p_T$ .

In Fig. 7.1 we present our results for the matched resummed cross section for photoproduction in  $\mu d \rightarrow h^\pm X$  for COMPASS kinematics and compare it to the experimental data

[29]. Note that the data are available down to low transverse momentum  $p_T = 1.2 \text{ GeV}$ , while we start our theoretical cross sections at  $p_T = 1.75 \text{ GeV}$  to make sure that application of perturbative methods is sensible. For all our calculations we have applied the cuts on the momentum fraction  $y$  in the Weizsäcker-Williams photon and on the photon's maximal virtuality given above. Moreover, thanks to our rapidity-dependent resummed approach, we are able to take into account the proper pseudo-rapidity cuts  $2.38 \geq \eta \geq -0.1$  as well as  $0.2 \leq z_{\text{cut}} \leq 0.8$  directly. Fig. 7.1 also shows the LO and the NLO cross section. One observes that the LO one is far below the data. The NLO corrections are huge, which indicates the importance of going beyond NLO and taking into account the threshold logarithms to all orders. The matched resummed cross section gives again a sizeable correction to the NLO result, enhancing the latter by a factor of about two. One observes that the resummed results agree with the data within the (admittedly, large) systematic error. Note that unfortunately for the kinematics discussed here the scale uncertainty of the resummed result is not really smaller than that of the LO or the NLO one.

Even if neither the direct contribution  $d\sigma_{\text{dir}}$  nor the resolved one  $d\sigma_{\text{res}}$  are individually measurable quantities, as both of them depend on the scheme chosen for the factorization of singular collinear parton emissions, it is instructive to consider both parts separately. The direct processes will generally dominate at high  $p_T$ . On the other hand, in contrast to the direct processes, the resolved ones have an additional intermediate particle generated by the photon. As this carries only a fraction  $x_\gamma$  of the photon momentum, less phase space is available for producing a high-momentum hadron. Therefore the resolved processes are on average closer to the partonic threshold, and thus we expect the threshold logarithms to have more impact than for the direct contribution. In addition, the resolved processes involve four colored partons, making them more likely to radiate soft gluons. Fig. 7.2 compares the direct and resolved contributions and the resummation effects on them. At lowest order the direct contribution exceeds the resolved one over the whole  $p_T$ -range considered. This changes already at NLO: Because of the large size of the NLO corrections in the resolved case, the resolved NLO cross section exceeds the direct NLO one at  $p_T \leq 2 \text{ GeV}$ . This trend continues for the resummed cross sections.

In order to see whether the large effects from soft-gluon resummation correctly give the dominant part of the cross section, we perform a consistency check. For each subprocess the resummed cross section (not the matched one) is expanded to NLO and compared to the corresponding full fixed-order NLO result. Fig. 7.3 shows that these expansions reproduce the NLO results very well for all processes, except for the relatively low  $p_T$  region ( $p_T < 5 \text{ GeV}$ ) of the channel  $gg \rightarrow q\bar{q}$  which, however, only makes a small contribution to the full cross section. The discrepancy in this particular case is due to terms not related to “+”-distributions which get more and more important at low  $p_T$ . In Fig. 7.4 one can see the process  $gg \rightarrow q\bar{q}$  for negatively charged hadrons at COMPASS kinematics. At

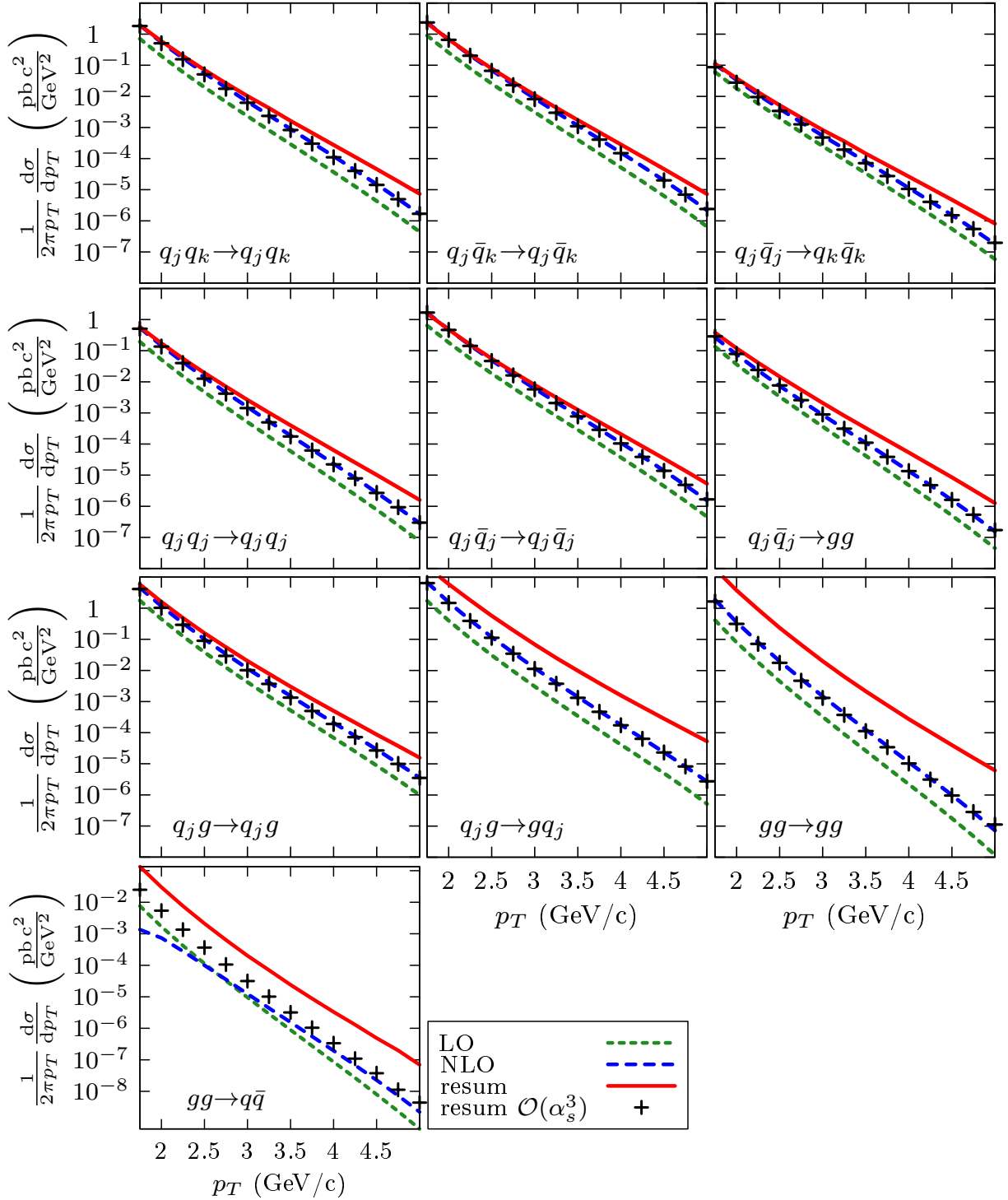


**Fig. 7.3.:** These plots, one for each of the resolved channels for the production of negatively charged hadrons  $\mu^+ + d \rightarrow \mu^{+'} + h^- + X$  at COMPASS kinematics, serve to compare the first order expansion of the resummed cross section (resum  $\mathcal{O}(\alpha_s^3)$ ) to the full NLO result. We plot also the LO and resummed curves, in order to show the soft-gluon effects and the contribution of each channel to the total resolved cross section.

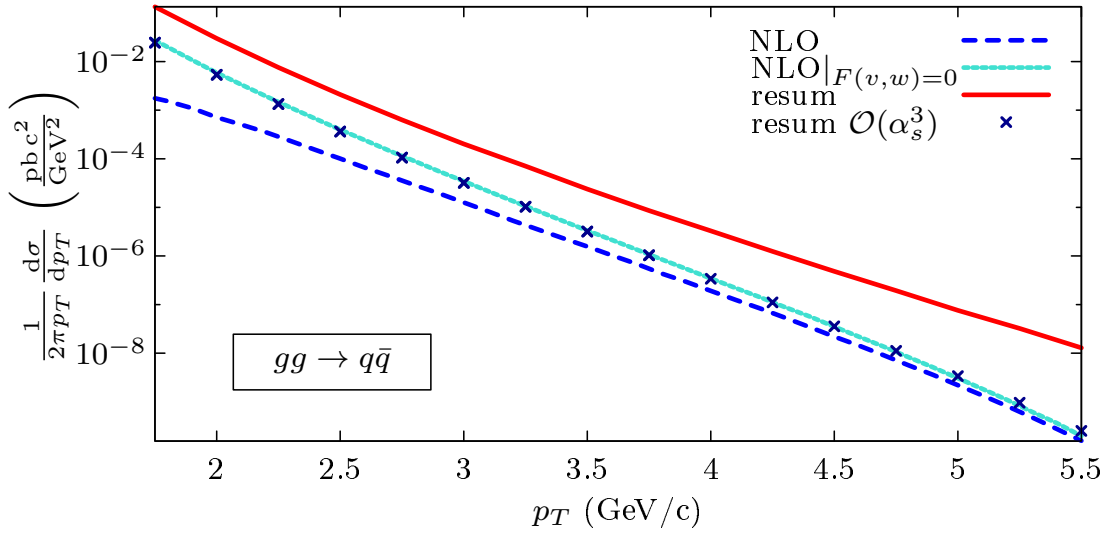


**Fig. 7.4.:** NLO, logarithmic and constant first order corrections at threshold ( $\text{NLO}|_{F(v,w)=0}$ ), resummed (resum) and first order expansion (resum  $\mathcal{O}(\alpha_s^3)$ ) of the resolved process  $gg \rightarrow q\bar{q}$  for the production of negatively charged hadrons at COMPASS kinematics. This process is the only one for COMPASS kinematics, in which the first order expansion of the resummed cross section seems not to be a good approximation for the full NLO result.

low  $p_T$  its full NLO result is up to a factor of 8 smaller than the first order expansion of the resummed cross section. With increasing transverse momentum and thus by coming closer to the threshold, the two curves approach each other. Fig. 7.4 shows, that when setting all terms at zero, which are subleading at threshold, that means  $F(v, w) = 0$  in Eq. (6.15), the resulting curve  $\text{NLO}|_{F(v,w)=0}$  coincides with the first order expansion. Thus the discrepancy is caused by the  $F(v, w)$  terms. However, due to the rather low numerical contribution of this channel, the total resummed cross section is not affected. Figure 7.2 also shows these comparisons, again separately for the direct and resolved contributions, where for each of the two we have combined all relevant subprocesses. As can be observed, the agreement of the expansion and the NLO result is excellent. This implies that the terms which are formally suppressed by an inverse power of the Mellin moment  $N$  near threshold indeed are insignificant. Thus one may safely assume that this will also be the case for higher-order corrections, so that the resummed cross section yields a good approximation to the all-order perturbative cross section.

We now investigate how the large enhancement of the NLL resummed cross section that we observed in Fig. 7.1 builds up order by order. We therefore expand the matched resummed formula beyond NLO and define the “soft-gluon  $K$ -factors”

$$K^{(n)} \equiv \frac{d\sigma^{\text{matched}}/dp_T|_{\mathcal{O}(\alpha_s^{1+n})}}{d\sigma^{\text{NLO}}/dp_T}. \quad (7.1)$$

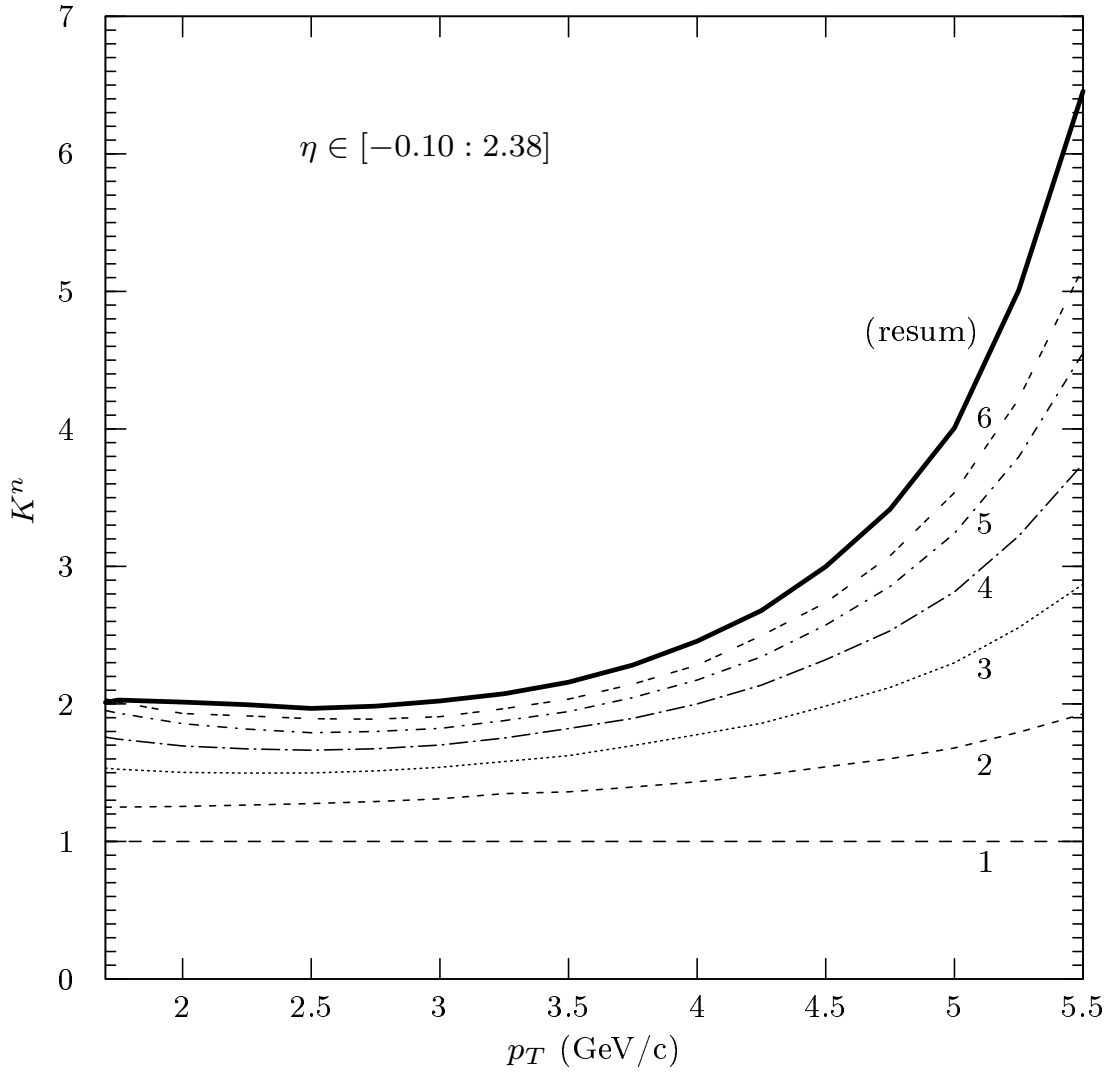


**Fig. 7.5.:** Soft-gluon “ $K$ -factors” relative to NLO, as defined in Eq. (7.1), for COMPASS kinematics. The numbers labeling the curves refer to the superscript  $n$  in  $K^{(n)}$  in Eq. (7.1).

In addition,  $K^{\text{resum}} \equiv K^{(\infty)}$  is defined as the ratio of the matched resummed cross section to the NLO one. Because of the matching procedure given by Eq. (6.75), the first-order expansion of the matched resummed cross section is identical to the full fixed order NLO result, and we have  $K^{(1)} = 1$ . Figure 7.5 shows  $K^{\text{resum}}$  along with the six lowest soft-gluon  $K$ -factors. One can see that they are almost flat for  $p_T \leq 3.5$  GeV but exhibit a dramatic enhancement for higher transverse momenta. Figure 7.5 also indicates that the series  $K^{(1)}, K^{(2)}, K^{(3)} \dots$  converges towards  $K^{\text{resum}}$ , which may be regarded as further evidence for the importance of resummation.

Next, we study the ratio of the production cross section for negatively charged hadrons over the one for positively charged hadrons. This ratio is also accessible at COMPASS.

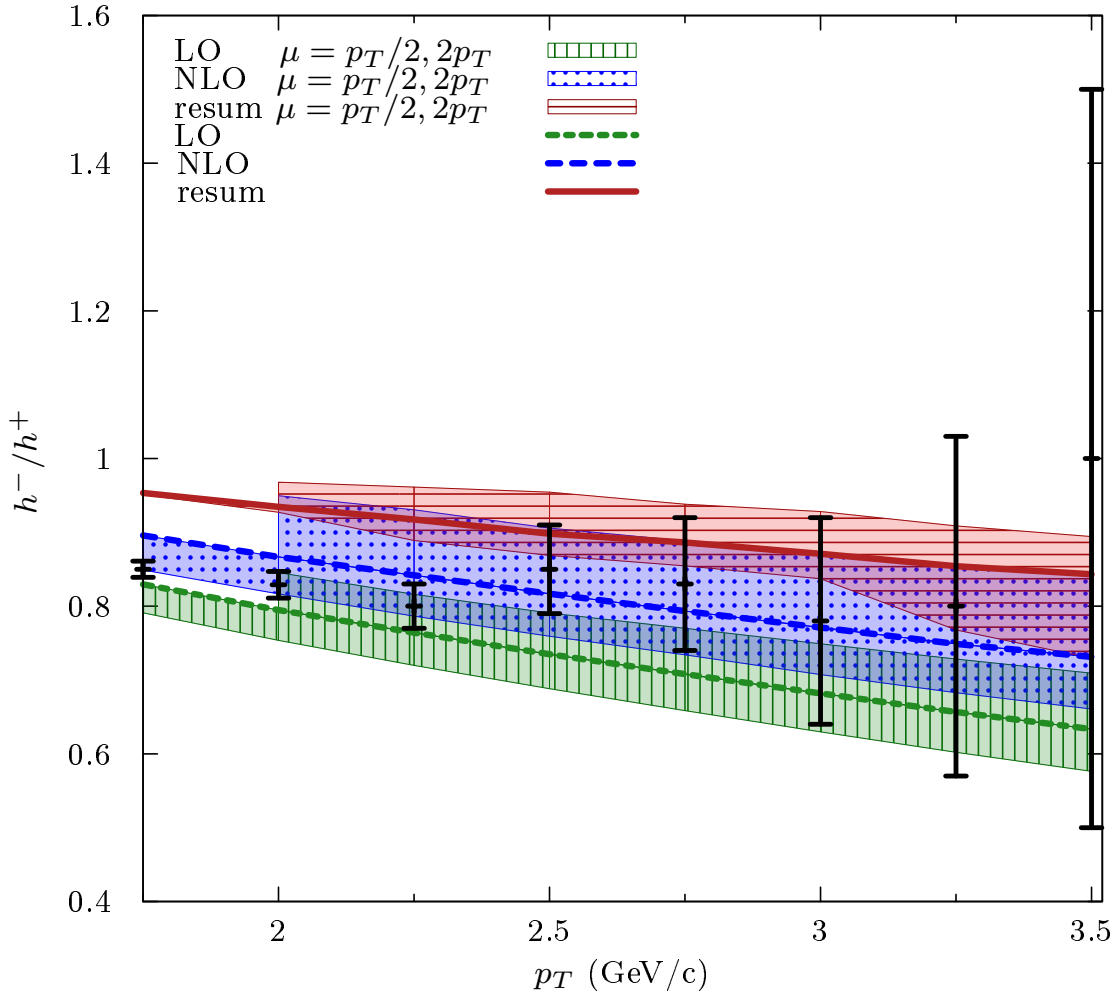


**Fig. 7.6.:** Ratio of production cross sections for  $h^-$  over  $h^+$ :  $d\sigma_{\mu^+d\rightarrow\mu^+h^-}/d\sigma_{\mu^+d\rightarrow\mu^+h^+}$ . The error bars of the experimental data are statistical only.

Figure 7.6 shows our calculation compared to the data. As expected, the production of positively charged mesons is preferred. This effect mostly stems from the QCD-Compton process  $\gamma q \rightarrow qg$  in the direct channel which couples to up quarks four times as strongly as to down quarks. This tendency is most distinct for LO and softens when going to NLO and to the NLL resummed cross section, since resolved higher-order contributions are gaining importance. Figure 7.6 shows that the resummed cross section somewhat overpredicts the charge ratio measured in experiment. We note, however, that we have obtained the scale uncertainty bands in the figure by simply dividing the  $h^-$  and  $h^+$  cross sections for a given scale. The true scale uncertainty on the ratio will likely be larger as one could, in principle, choose different scales in the computation of the two cross sections.

Finally, in Fig. 7.7 we investigate the dependence of the cross section on the photon energy fraction  $y$  in the Weizsäcker-Williams spectrum. We consider the double differential

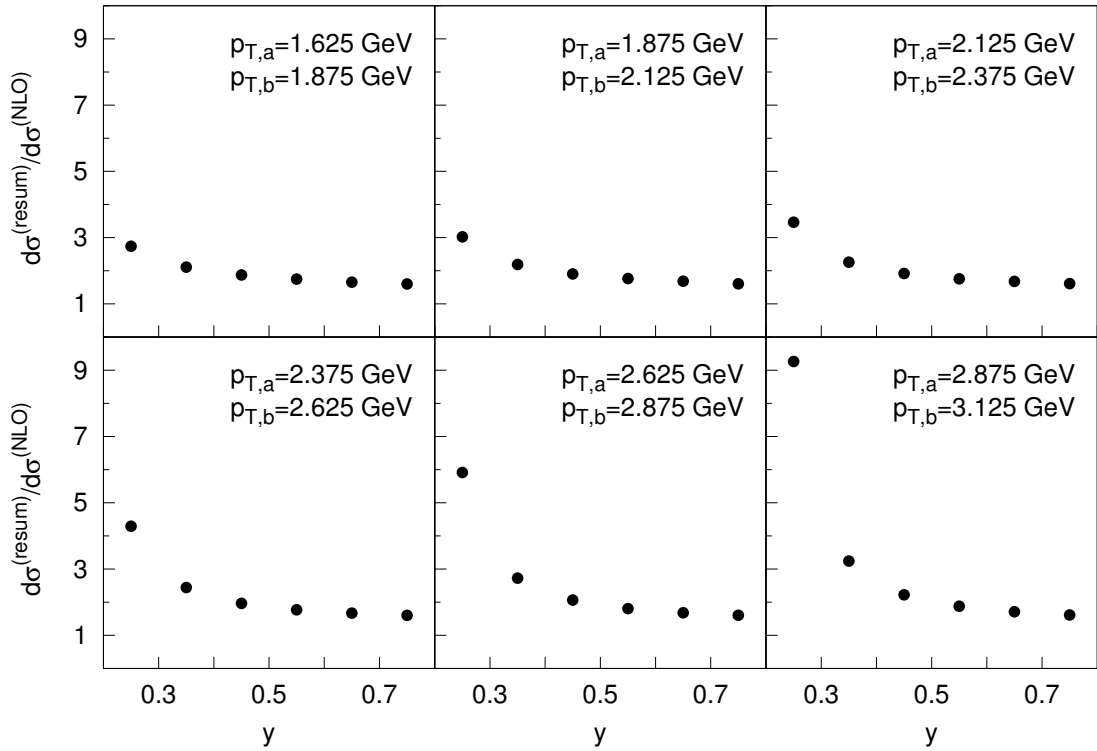


**Fig. 7.7.:** Ratios of the experimental data and NLO cross section, averaged over the ranges  $[y - 0.05 : y + 0.05]$  and integrated over various  $p_T$  bins.

cross section  $d^2\sigma/(dp_T dy)$  integrated over  $p_T$  bins and averaged over the ranges  $[y - 0.05 : y + 0.05]$ ,

$$\frac{1}{0.1} \int_{y-0.05}^{y+0.05} dy' \int_{p_{T,a}}^{p_{T,b}} \frac{d^2\sigma}{dp_T dy'} dp_T. \quad (7.2)$$

At fixed transverse momentum the phase space available for the production of additional partons is smaller, the smaller the photon energy fraction  $y$ . Therefore, for decreasing  $y$  one gets closer to partonic threshold, and one expects an increase of the cross section due to the impact of soft gluon emissions. This behavior is more pronounced at higher  $p_T$ . The quantity  $y$  is directly accessible in experiment, so we are able to compare the  $y$ -dependence of the experimental data to the theoretical calculation. This comparison is important to clarify the question whether hadron production at this kinematics is well-described by perturbative methods. Fig. 7.8 and Fig. 7.9 show the ratios of the experimental data to the NLO calculation and the resummed result, respectively. In the comparison with the NLO cross section, we observe a clear dependence on  $y$  with a strong increase of the ratio towards low  $y$ . This increase is stronger at higher  $p_T$ . This behavior is consistent with our previous considerations, as one is closer to the threshold region at higher  $p_T$  for a fix center-of-mass energy. Thus, here the soft gluon effects are expected to be larger.

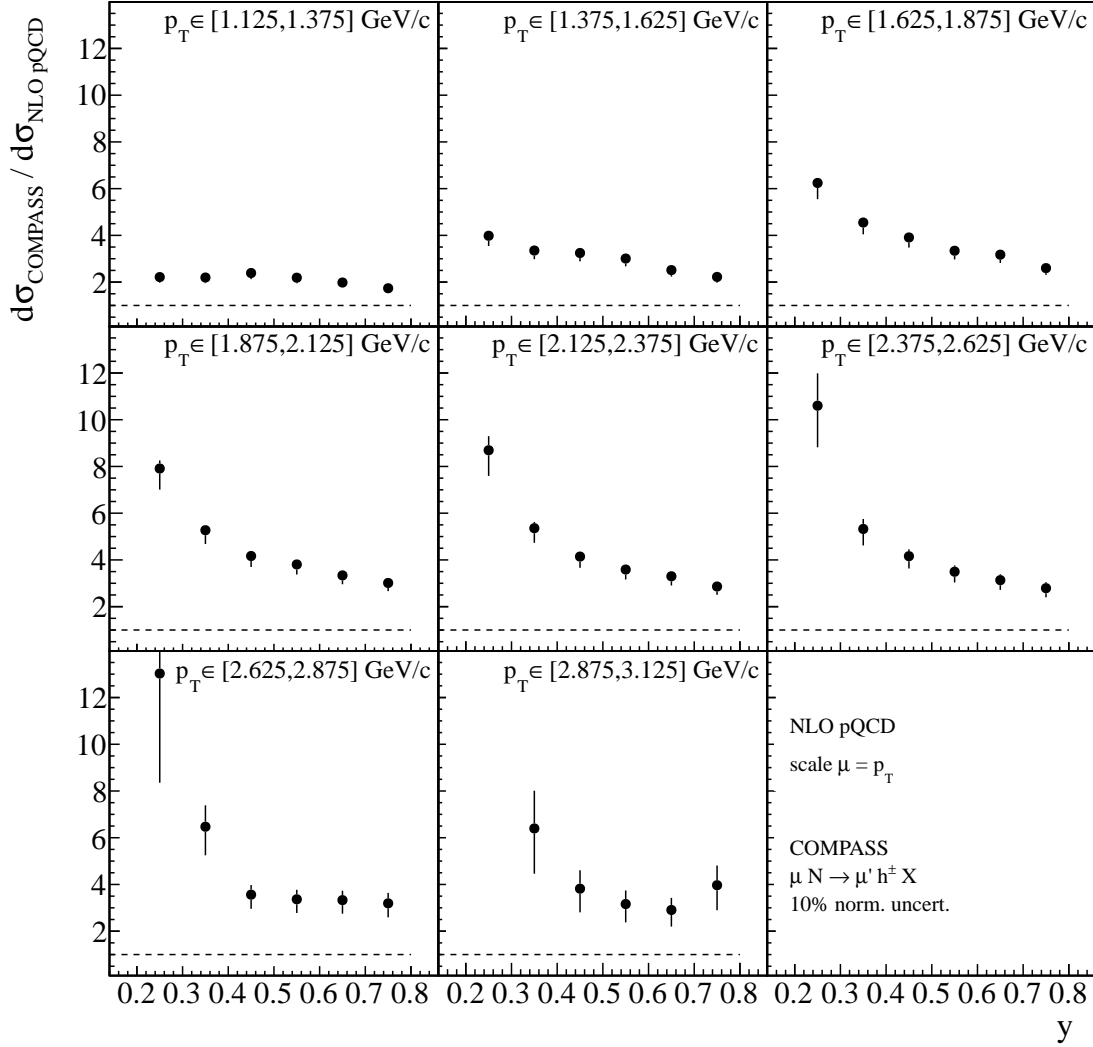


**Fig. 7.8.:** Ratios of the  $y$ -dependent resummed and NLO cross sections, integrated over various  $p_T$  bins. The cross sections are averaged over the ranges  $[y - 0.05 : y + 0.05]$ . The figures show a clear dependence on  $y$  with the overall trend that the cross section increases at low  $y$ . This behavior is more pronounced at higher  $p_T$ . We received this plot by private communication from members of COMPASS.



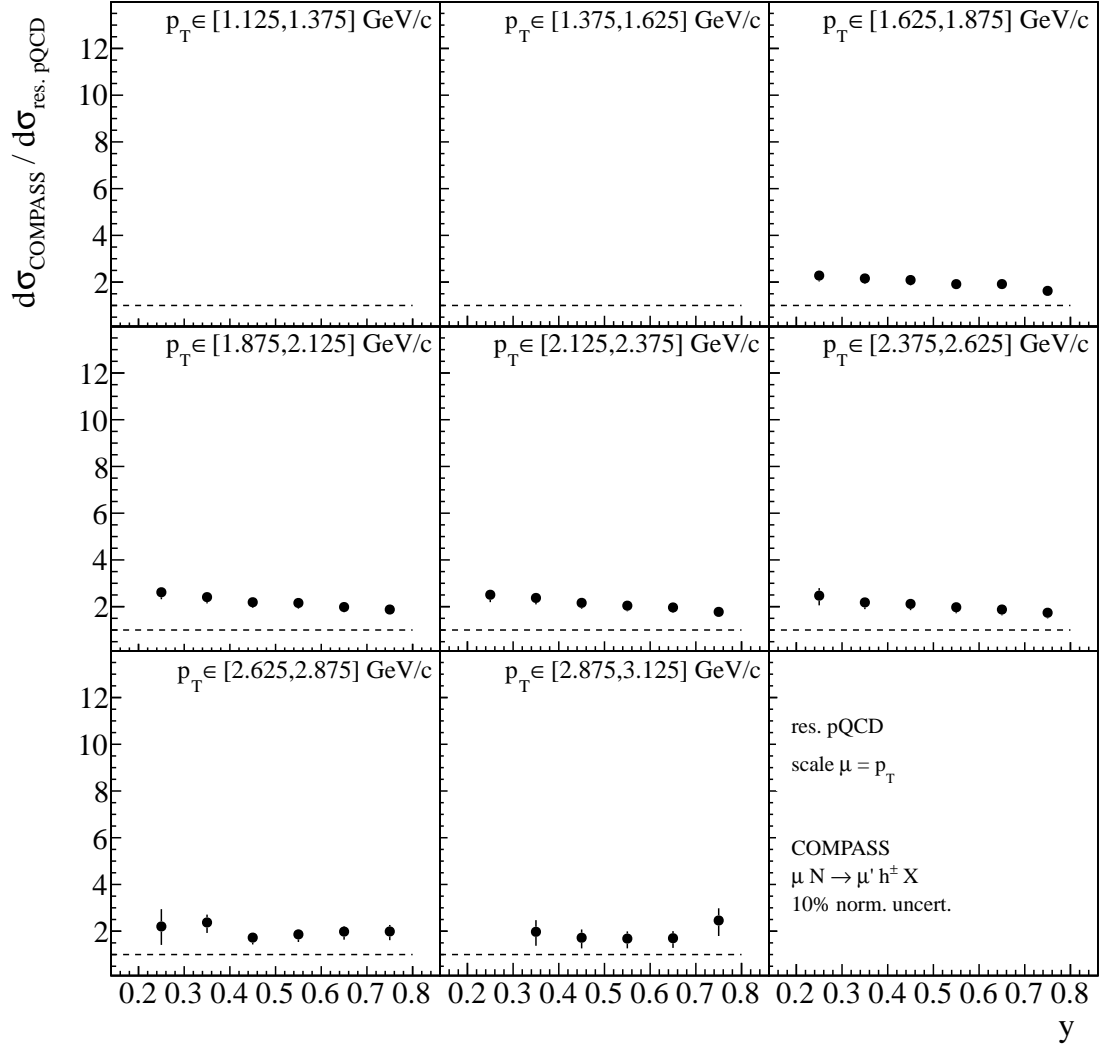


**Fig. 7.9.:** Ratios of the  $y$ -dependent resummed and NLO cross sections, integrated over various  $p_T$  bins. The cross sections are averaged over the ranges  $[y - 0.05 : y + 0.05]$ . The curves of all cross sections only show a slight  $y$ -dependence and are almost flat. We received this plot by private communication from members of COMPASS.

In Fig. 7.9 we take into account the impact of soft gluon emissions in the theoretical prediction. As a result we see that the  $y$ -dependence of the ratio has almost disappeared. This shows nicely that threshold resummation is really needed in the kinematical regime of COMPASS to explain the shape of the  $y$ -dependent cross section. Note that though the  $y$ -dependent part of the ratio of the experimental data to theoretical prediction is almost cured, the ratio is still roughly around the value two. This offset is independent of the given transverse momenta and showed up already in the  $y$ -integrated,  $p_T$ -dependent resummed cross section in Fig. 7.1. In this plot, however, we have seen, that the resummed results agree with the data within the systematic error.

## 7.2. Rapidity-dependent vs. rescaled fully rapidity-integrated resummation

In the last section we have seen that threshold effects become more important at higher transverse momentum  $p_T$ . A similar effect can be observed when one goes towards large rapidities for fixed  $p_T$ . High rapidities  $|\eta| \rightarrow \eta_{\max}$  correspond to the limit of phase space where the high momentum fraction  $x$  in the parton distribution functions are probed. Thus, large rapidities are expected to enhance resummation effects by far more than central rapidities. In previous studies, where rapidity dependence in resummation, has not been available, the following approximation was used to adopt the fully-rapidity integrated resummed cross section to the limited range of rapidity given by the experimental setup:

$$\left. \frac{d\sigma_{\eta\text{-match}}^{\text{resum}}}{dp_T} \right|_{-0.10 < \eta < 2.38} \equiv \frac{d\sigma_{\eta\text{-integrated}}^{\text{resum}}}{dp_T} \frac{\int_{-0.10}^{2.38} d\eta d\sigma^{\text{NLO}}/dp_T d\eta}{\int_{\text{all } \eta} d\eta d\sigma^{\text{NLO}}/dp_T d\eta} \quad (7.3)$$

That is, one rescales the fully rapidity-integrated cross section by an appropriate ratio of NLO cross sections [72]. As it was shown in [72], this approximation works fairly well for moderate  $\eta$ , since here threshold resummation mainly affects the normalization of the cross section, and less its shape in  $\eta$ . Before we will see how well this approximation works for the rapidity range covered by COMPASS kinematics, we study the full kinematically allowed  $\eta$  range, that is

$$|\eta| \leq \ln \left( \frac{1 + \sqrt{1 - x_T^2}}{x_T} \right). \quad (7.4)$$

In Fig. 7.10 we compare the fully rapidity-integrated resummed cross section  $d\sigma_{\eta\text{-integrated}}^{\text{resum}}/dp_T$  (6.100) from Sec. 6.3.3, with the rapidity dependent resummation formula  $d\sigma^{\text{resum}}/dp_T d\eta$  (6.21) from Sec. 6.2.2, which we integrated over all  $\eta$ . It is important to see that these two approaches actually are not identical. While in the first one the partonic rapidity, appear-

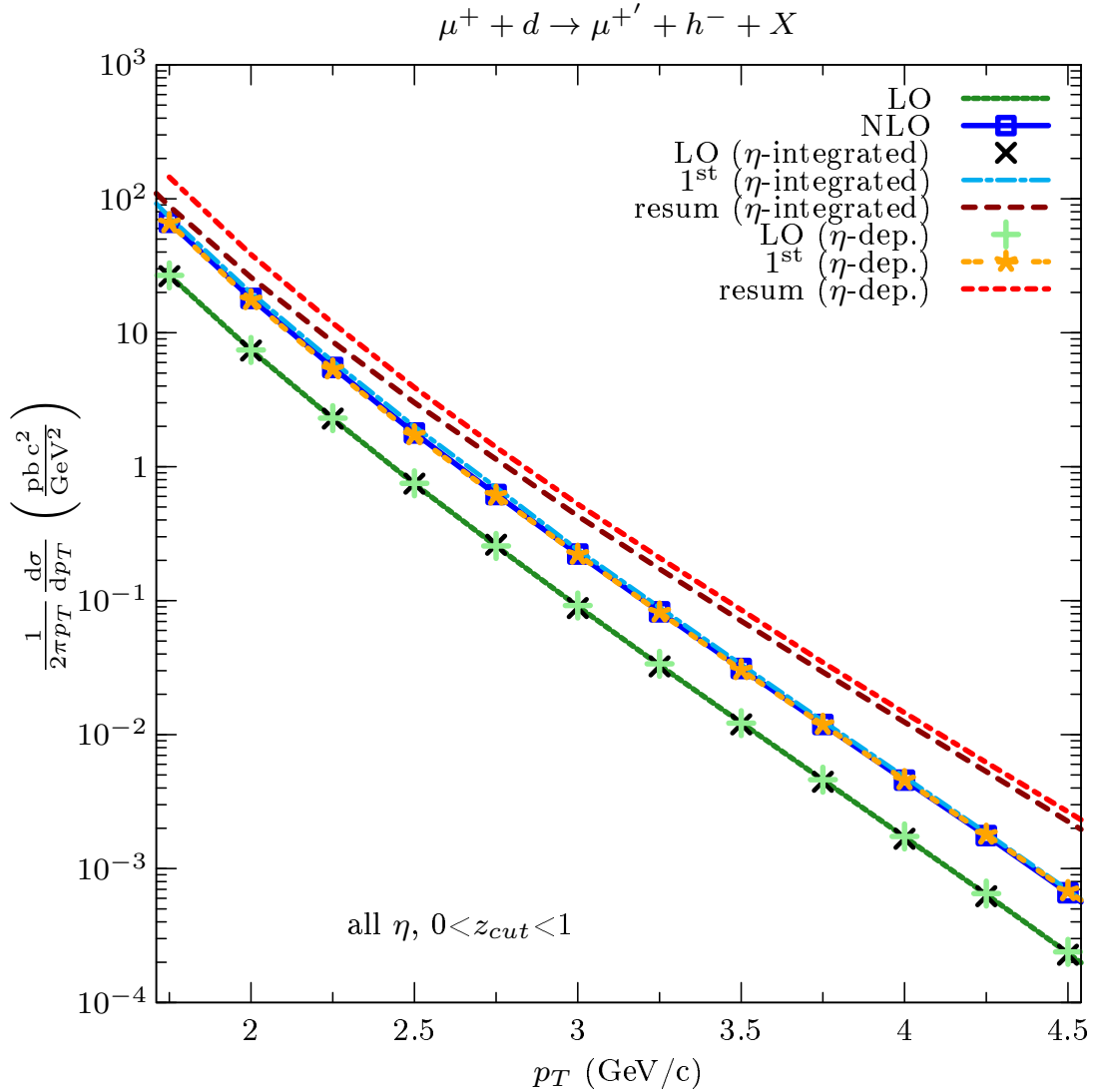


**Fig. 7.10.:** The figure shows the rapidity-dependent resummed result  $d\sigma^{\text{resum}}/dp_T d\eta$  (“resum ( $\eta$ -dep.)”) versus the fully rapidity-integrated one  $d\sigma_{\eta\text{-integrated}}^{\text{resum}}/dp_T$  (“resum ( $\eta$ -integrated)”), both in all kinematically allowed  $\eta$ . The full LO and NLO results serve to compare the zeroth and first order expansion of the rapidity-dependent and rapidity-integrated formula, respectively.

ing in the next-to-leading-log terms of the resummed exponents and in the  $N$ -independent  $C$ -coefficients, was simply set to zero  $\hat{\eta} = 0$ , the rapidity was integrated out correctly in the latter one,  $\int_{\text{all } \eta} d\eta d\sigma^{\text{resum}}/dp_T d\eta$ . In fact, we observe a quite substantial difference in our numerical studies in Fig. 7.10. Though this difference remains sizeable, it decreases for large  $p_T$  as one is closer to the threshold region, where the  $\hat{\eta}$ -independent leading-log terms get more and more important. This behavior can also be observed when one studies their respective first order expansions. While the first order expansion of  $d\sigma^{\text{resum}}/dp_T d\eta$  agrees excellently with the exact NLO result, the first order expansion of  $d\sigma_{\eta\text{-integrated}}^{\text{resum}}/dp_T$  is

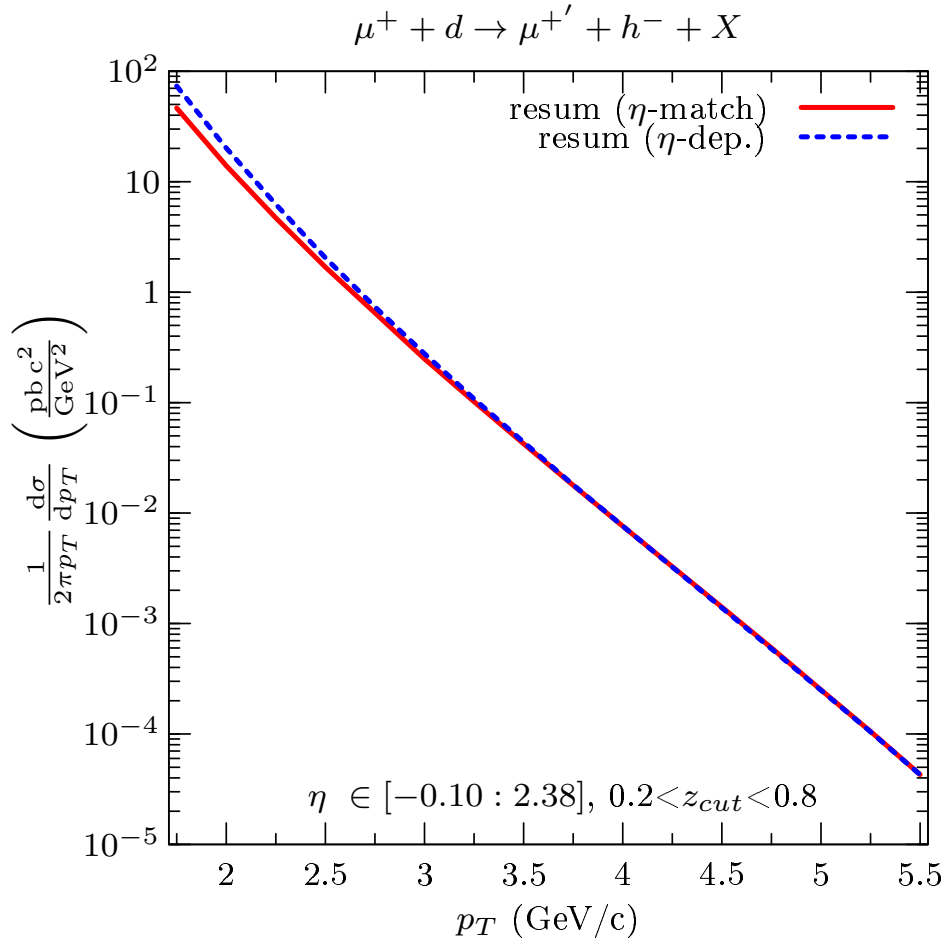


**Fig. 7.11.:** Comparison of the rescaled rapidity-integrated resummed cross section  $\frac{d\sigma_{\eta\text{-match}}^{\text{resum}}}{dp_T}$  in (7.3), labelled as “resum ( $\eta$ -match)”, to the rapidity-dependent resummed cross section  $\int_{-0.10}^{2.38} d\eta d\sigma^{\text{resum}}/dp_T d\eta$ , “resum ( $\eta$ -dep.)”, in the  $\eta$ -range covered by COMPASS kinematics.

slightly above the full NLO cross section at low  $p_T$ . For completeness, we also show the LO results. Apart from the fact, that they were numerically obtained in a different way<sup>18</sup>, they all agree analytically.

We now turn over to the limited rapidity range covered by COMPASS kinematics,

$$-0.10 \leq \eta \leq 2.38, \quad (7.5)$$

and compare the rescaled rapidity-integrated resummed cross section  $\frac{d\sigma_{\eta\text{-match}}^{\text{resum}}}{dp_T}$  in (7.3) to the rapidity-dependent resummed cross section  $\int_{-0.10}^{2.38} d\eta d\sigma^{\text{resum}}/dp_T d\eta$ . The results are presented in Fig. 7.11. We see that the difference of the results of the two formalisms gets

<sup>18</sup>In Fig. 7.10 “LO” was calculated completely in physical space, “LO ( $\eta$ -integrated)” was performed completely in Mellin- $N$ -space, and for “LO ( $\eta$ -dep.)” only the partonic cross section and the fragmentation function were calculated in Mellin- $N$ -space.

smaller and smaller for increasing  $p_T$  and they even agree well for  $p_T \geq 3.5$  GeV. So, for sufficiently high  $p_T$ , rescaling of the  $\eta$ -integrated resummed cross section is a fairly good approximation here. The question arises why this approach works well for high  $p_T$  in the  $\eta$ -range given by COMPASS kinematics, but not for the full kinematically allowed  $\eta$ . The reason lies in the arguments given above. The off-central  $\eta$ -region, which is not covered by COMPASS kinematics, receives particular large threshold corrections. The next figure 7.12 serves to illustrate this point.

We look at the rapidity dependence of the cross section at a fixed  $p_T$ . The resummed result  $d\sigma^{\text{resum}}/dp_T d\eta$  (“resum ( $\eta$ -dep.)”) is compared to

$$\frac{d\sigma_{\eta\text{-match}}^{\text{resum}}}{dp_T d\eta} \equiv \frac{d\sigma^{\text{NLO}}}{dp_T d\eta} \frac{\frac{d\sigma_{\eta\text{-integrated}}^{\text{resum}}}{dp_T}}{\int_{\text{all } \eta} d\eta \frac{d\sigma^{\text{NLO}}}{dp_T d\eta}}, \quad (7.6)$$

that is, the  $\eta$ -shape of the NLO cross section, which was rescaled by an  $\eta$ -independent constant. This constant was chosen to be the appropriate ratio of the fully rapidity-integrated resummed and NLO cross section. Fig. 7.12 shows the results for  $p_T = 3.5$  GeV. We see that for rapidities  $\eta \geq -0.10$ ,  $\sigma_{\eta\text{-match}}^{\text{resum}}$  is close to our final result, the rapidity-dependent resummed cross section  $\sigma^{\text{resum}}$ . Here, the soft-gluon corrections give almost the same percentage of the NLO result over the region  $\eta \geq -0.10$ . For rapidities  $\eta \leq -0.10$ , however, threshold effects get even more important, such that even the shape in  $\eta$  is changed. The resulting substantial difference to  $\sigma_{\eta\text{-match}}^{\text{resum}}$  explains why the two resummed formalisms in Fig. 7.10 still deviate from each other for high  $p_T$ .

Next, let us draw the attention to another point in Fig. 7.12. The plot also shows the first order expansion of the  $\eta$ -dependent resummed cross section, compared to the full NLO result. One may observe that the first order expansion excellently coincides with the full NLO result, except for central rapidities, where it is slightly below the exact cross section. This is due to the fact that threshold logarithms do not dominate as much as in the off-central regions.

We now want to study how things change if we move slowly away from the threshold region, meaning, we look at lower  $p_T$ . Therefore, in Fig. 7.13 we redo the same plot as in Fig. 7.12, but for  $p_T = 2$  GeV. The first order expansion still provides a good approximation for the exact NLO cross section. This is the basic requirement for the assumption that it also holds true for the resummed cross section.

However, comparing the plots for  $p_T = 3.5$  GeV and  $p_T = 2$  GeV, one change is clearly visible: In the latter one, there is a huge difference between the rescaled  $\eta$ -integrated cross section,  $\sigma_{\eta\text{-match}}^{\text{resum}}$ , and the  $\eta$ -dependent resummed result. This is the case for all rapidities. It is due to the fact, that  $\hat{\eta}$  was set to zero on the way to the derivation of the fully rapidity-integrated resummed cross section from the rapidity-dependent formula.

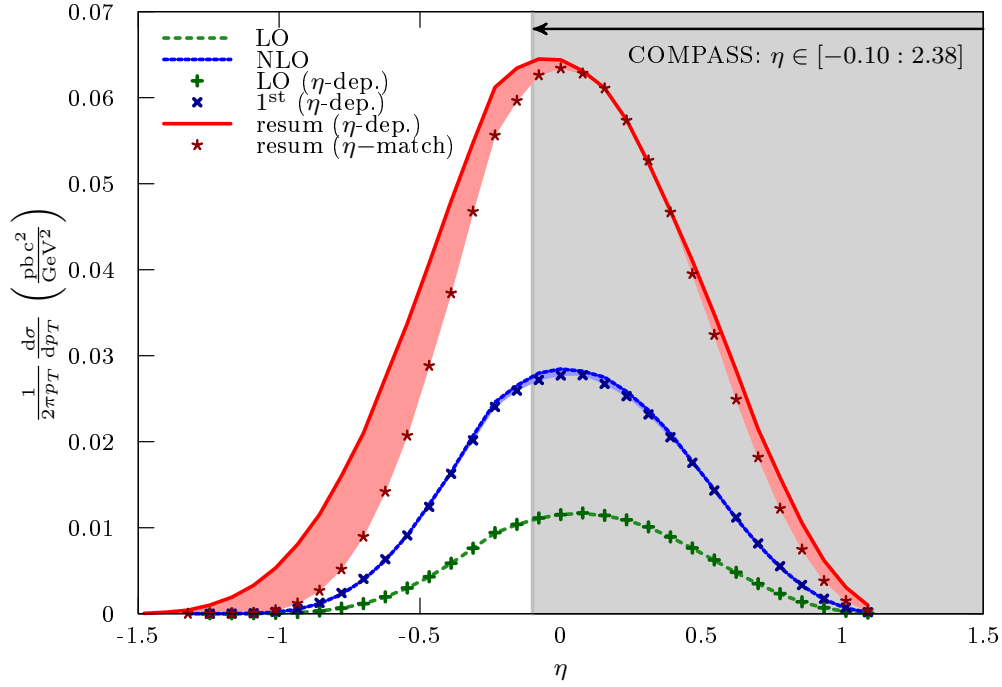


**Fig. 7.12.:** Rapidity dependence of the cross section for the hadron production process  $\mu^+ + d \rightarrow \mu^{+'} + h^- + X$  at fixed  $p_T = 3.5$  GeV. The resummed result  $d\sigma^{\text{resum}}/dp_T d\eta$  (“resum ( $\eta$ -dep.)”) is compared to the  $\eta$ -shape of the NLO cross section, which was rescaled by the ratio  $\frac{d\sigma^{\text{resum}}_{\eta\text{-integrated}}/dp_T}{\int_{\text{all } \eta} d\eta \frac{d\sigma^{\text{NLO}}}{dp_T d\eta}}$  (“resum ( $\eta$ -match)”). Furthermore, the zeroth (“LO ( $\eta$ -dep.)”) and first order (“1<sup>st</sup> ( $\eta$ -dep.)”) expansion of the  $\eta$ -dependent resummed cross section, as well as the full LO and NLO result are shown. The shaded region illustrates the  $\eta$ -range covered by COMPASS kinematics.

In order to see which impact an approximation of this kind may have, let us consider the rapidity-dependent cross section, in which we approximate the partonic center-of-mass energy in the arguments of the external parton exponents by

$$\hat{s} = 4p_T^2 \cosh^2 \hat{\eta} \approx 4p_T^2. \quad (7.7)$$

To be precise, in Fig. 7.14 we show

$$\begin{aligned} \frac{p_T^3 d\sigma^{\text{resum}}_{\eta\text{-approx.}}}{dp_T d\eta} &\equiv \sum_{a,b,c} \int_0^1 dx_\ell \int_0^1 dx_n f_{a/\ell}(x_\ell, \mu_{fi}) f_{b/N}(x_n, \mu_{fi}) \\ &\int_{\mathcal{C}} \frac{dN}{2\pi i} (x^2)^{-N} D_{h/c}^{2N+3}(\mu_{ff}) \tilde{w}_{\eta\text{-approx.}}^{2N}(\hat{\eta}), \end{aligned} \quad (7.8)$$

with

$$\tilde{w}_{\eta\text{-approx.}}^{\text{resum},N}(\hat{\eta}) = \Delta_a^{N_a}(4p_T^2, \mu_{fi}) \Delta_b^{N_b}(4p_T^2, \mu_{fi}) \Delta_c^N(4p_T^2, \mu_{ff}) J_d^N(4p_T^2) \text{Tr} \left\{ HS_N^\dagger SS_N \right\}_{ab \rightarrow cd}, \quad (7.9)$$

and where we used the same notation as in Eq. (6.21). As Fig. 7.14 shows, this approxi-

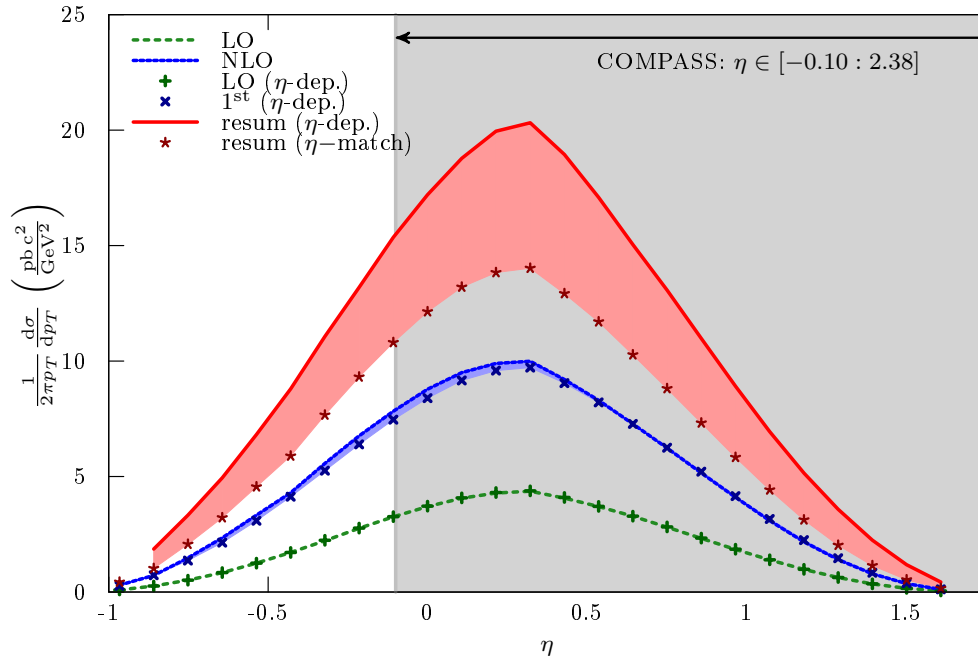


**Fig. 7.13.:** Same as in Fig. 7.12, but for  $p_T = 2 \text{ GeV}$ .

mation results in a drastical reduction of the resummed cross section. At large rapidities, where one is close to partonic threshold, it roughly corresponds to the rescaled cross section  $\sigma_{\eta\text{-match}}^{\text{resum}}$ . So, approximating  $\hat{s} \approx 4p_T^2$  has a large impact on the resummed cross section at relatively low  $p_T = 2 \text{ GeV}$ . This underlines the importance of having a  $\eta$ -dependent resummed cross section at these kinematics.

All in all, in the first part of our phenomenological studies we applied our theoretical prediction based on the soft-gluon resummation at fixed rapidity to the photoproduction process  $\mu^+ d \rightarrow \mu^{+'} + h + X$  at high transverse momentum of the hadron  $h$  for COMPASS kinematics. We observe an excellent agreement between the first order expansion of our resummed cross section and the full NLO one. We also find a significant enhancement of the resummed cross section over the next-to-leading order one, showing that the NLO calculations are likely not fully sufficient. Resummation also significantly improves the agreement between the data and theoretical predictions. The aim of the second part was to point out the differences of our new formalism, the rapidity-dependent resummed cross section versus the previous approach, that was, rescaling the fully rapidity-integrated resummed cross section by an appropriate ratio of NLO cross sections. In particular for relatively low  $p_T$  the rapidity-dependent resummed cross section yields sizable, non-negligible corrections.

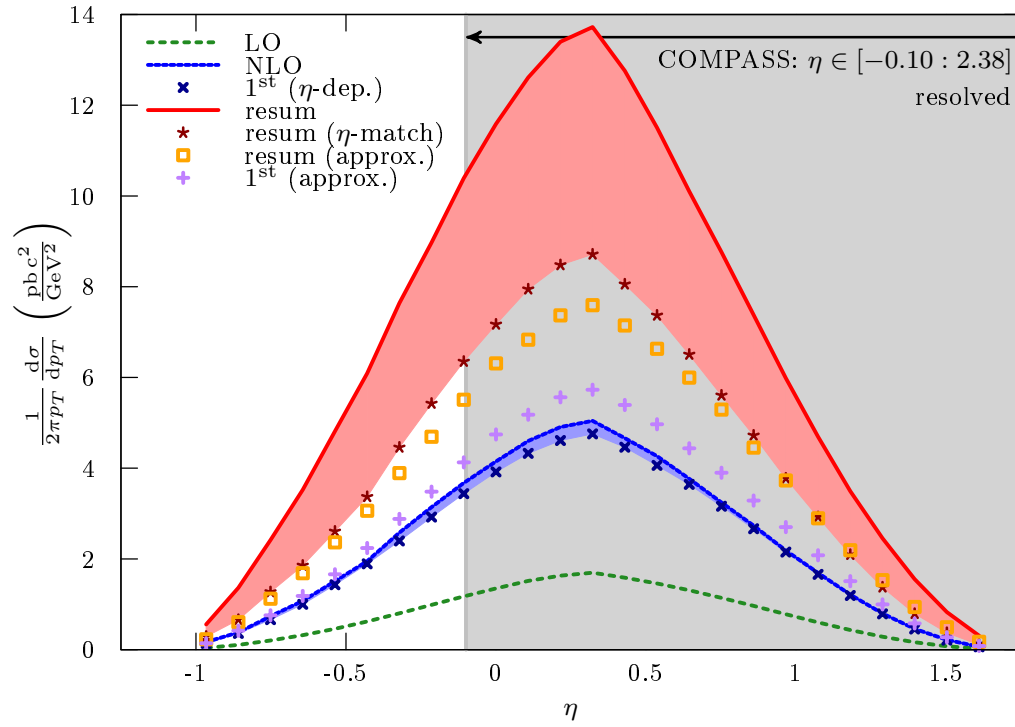


**Fig. 7.14.:** Same as in Fig. 7.12, but for  $p_T = 2 \text{ GeV}$  and for the resolved contribution only. The plot also shows the  $\eta$ -dependent resummed cross section  $\sigma_{\eta\text{-approx.}}^{\text{resum}}$  (see (7.8)), in which we replaced the partonic center-of-mass energy in the arguments of the external parton exponents by  $\hat{s} \approx 4p_T^2$ . In addition also its first order expansion “1<sup>st</sup> (approx.)” is plotted.



## 8. Summary and Conclusions

The goal of this thesis was to extend the unpolarized NLO cross section for inclusive-hadron photoproduction by including higher-order threshold logarithms up to NLL accuracy. This was done via a technique called threshold resummation. In order to provide reliable theoretical predictions a theoretical approach like this is essential for the fixed-target kinematics employed in the COMPASS experiment at CERN.

We started out with a short review of basic ideas in perturbative calculations, most notably regularization techniques and renormalization. This was followed by a part intended to recall some of the techniques used in the threshold resummation for the Drell-Yan process. We presented separate first order intermediate results for the real and the virtual gluon contribution in order to illustrate how the large logarithmic contributions associated with soft gluon emissions arise due to the imperfect cancellation of infrared singularities near the partonic threshold. In this kinematic region a resummed formula may be derived, which includes higher order terms in a systematic way. It turned out that close to the partonic threshold, the exponentiation of only a subset of all relevant Feynman diagrams of a specific order reproduces the dominant contributions of higher orders - up to a certain accuracy (which depends on the subset entering the exponent). We presented the resummed result summing up threshold logarithms up to NNLL accuracy.

So far, we restricted ourselves on the Drell-Yan process. Consequently, the next step was to outline how this procedure can be generalized to processes, in which four QCD-particles instead of two are involved in the lowest order hard scattering process. This is the case for the resolved processes of hadron production. Here, the situation is insofar more complicated than the Drell-Yan case as also color flow influences the threshold contributions. Nevertheless, resting on quite general factorization techniques it can be shown, that the threshold logarithms may be resummed. The current state of the art is NLL accuracy. The leading logarithmic terms associated with the soft and collinear gluon emissions of each external partons are identical to those in the Drell-Yan process - these just depend on the type of the corresponding parton. The greater complexity of hadron production manifests in the NLL terms first. To address these terms, matrices - the anomalous dimension matrices - occur in the resummed exponent to account for the color structure which is specific to each channel. An extra chapter was devoted to show how these anomalous dimension matrices may be derived.

The main task of this thesis has been to study the effects of next-to-leading logarithmic

threshold logarithms on the direct- and resolved-photon cross sections for inclusive-hadron photoproduction at high transverse momentum of the hadron  $h$ . There, the techniques resumming the soft-gluon effects of four QCD-particles mentioned above directly apply. As a new technical ingredient to resummation, we were able to fully include the rapidity dependence of the cross section in the resummed calculation and to account for all relevant experimental cuts. This was achieved by treating only the partonic cross sections and the fragmentation functions in Mellin- $N$  moment space, but keeping the convolutions with the parton distribution functions in physical space. This differs from the usual approach, in which all parts are calculated in Mellin- $N$  moment space first, and then the result is translated to physical space again.

In the last part of this work we applied the resummed expression for fixed rapidity of the observed hadron to a phenomenological analysis of the COMPASS experiment  $\mu^+d \rightarrow \mu^{+'} + h^\pm + X$ , in which the hadron  $h$  is observed at high transverse momentum  $p_T$ . For the kinematics employed in this experiment, we have found large higher-order soft-gluon QCD corrections. These are due to the fact that one is overall rather close to the threshold region, as shown by the relatively large value of the hadron's transverse momentum over the available center-of-mass energy  $\sqrt{s}$ , typically  $2p_T/\sqrt{s} \gtrsim 0.1$ . The threshold logarithms addressed by resummation strongly dominate the higher-order corrections. We have verified this by comparing the first-order expansion of our resummed cross section with the full NLO one, finding excellent agreement of the two. We have observed a significant enhancement of the resummed cross section over the next-to-leading order one. This shows that it is crucial to go beyond the NLO cross section. Resummation also significantly improves the agreement between the data and theoretical predictions and thus turns out to be a vital ingredient for the comparison between theory and experimental data.

In a future project, our calculations will be extended to the case of helicity asymmetries for this process. Previous NLO predictions observed significant differences in the  $K$ -factors (the ratio of higher order to LO cross sections) for unpolarized and polarized cross sections [152]. This makes the effect of threshold resummation on the helicity asymmetry particularly interesting. As far as the theoretical framework for that is settled, polarized COMPASS data can help to constrain the nucleon's spin-dependent gluon distribution at momentum fractions  $x \simeq 0.1 \div 0.3$ . However, even if this will add valuable information to the present knowledge, this experiment will probably not be able to resolve the proton's spin crisis. This requires new facilities as planned in the EIC project, which hopefully will be realized in future. With its anticipated capability to reach two orders of magnitude lower in parton momentum fraction than previously achieved and to enable new measurements to address also the quark and gluon orbital angular momenta in the nucleon [14], it surely would help to shed light on the mystery regarding the proton spin.

# A. Elements of QED and QCD: The Feynman rules

The Feynman rules provide an intuitive way of performing perturbation theory. In Feynman diagrams we differentiate between external lines, internal lines (propagators) and vertices at the intersection of three (or more) lines at one point. In the following we consider a fermion  $q$ , for example a quark. Its charge is given in units of the electron charge  $e$  by  $e_q e$ .

---

---

## *QED Feynman rules*

---

---

### Propagators

photon $A$	$\mu \text{ --- } \text{wavy line} \text{ --- } \nu$ $q$	$-i \frac{g_{\mu\nu} - (1 - \xi) \frac{q_\mu q_\nu}{q^2 + i\epsilon}}{q^2 + i\epsilon}$
fermion $\psi$	$i \text{ --- } \text{arrow} \text{ --- } j$ $p$	$i \frac{\not{p} + m}{p^2 - m^2 + i\epsilon} \delta_{ij}$

### Vertices

photon-fermion	$q \text{ --- } \text{dot} \text{ --- } q$ $\mu$	$-ie_q e \gamma_\mu$
----------------	---	----------------------

---

Here we adopted the convenient notation to denote combinations

$$a^\mu \gamma_\mu = a_\mu \gamma^\mu \equiv \not{a}. \quad (\text{A.1})$$

The Feynman rules given above provide us with truncated connected Green functions. In order to obtain transition matrix elements, we add the rule that external lines should be on their mass shell.

---



---

*QCD Feynman rules*


---



---

**Propagators**

gluon $A$	$a\mu \overset{q}{\text{-----}} b\nu$	$-i \frac{g_{\mu\nu} - (1-\xi) \frac{q_\mu q_\nu}{q^2 + i\epsilon}}{q^2 + i\epsilon} \delta_{ab}$
-----------	---------------------------------------	---

ghost $\chi$	$a \text{-----} \overset{k}{\text{-----}} b$	$\frac{i}{k^2 + i\epsilon} \delta_{ab}$
--------------	--	---

**Vertices**

quark-gluon	$\begin{array}{c} c\ \mu \\   \\ \text{-----} \text{-----} \text{-----} \\   \\ A \qquad B \end{array}$	$ig\gamma_\mu \left( \frac{\lambda^c}{2} \right)_{BA}$
-------------	---	--

ghost-gluon	$\begin{array}{c} c\ \mu \\   \\ \text{-----} \text{-----} \text{-----} \\   \\ b \qquad a \end{array}$	$gf_{abc}k^\mu$
-------------	---	-----------------

3-gluon	$\begin{array}{c} b\ \nu \\   \\ \text{-----} \text{-----} \text{-----} \\ \swarrow \quad \downarrow \quad \searrow \\ p_1 \quad p_2 \quad p_3 \\ a\ \mu \qquad c\ \lambda \end{array}$	$gf_{abc} [ g_{\nu\lambda}(p_3 - p_2)_\mu + g_{\mu\lambda}(p_1 - p_3)_\nu + g_{\nu\mu}(p_2 - p_1)_\lambda ]$
---------	---	--

4-gluon	$\begin{array}{c} a\ \mu \\   \\ \text{-----} \text{-----} \text{-----} \\ \text{-----} \text{-----} \text{-----} \\   \\ c\ \rho \qquad b\ \nu \\   \\ d\ \sigma \end{array}$	$-ig^2 [ f_{abe}f_{cde} (g_{\nu\sigma}g_{\rho\mu} - g_{\mu\sigma}g_{\rho\nu}) + f_{ace}f_{bed} (g_{\mu\sigma}g_{\rho\nu} - g_{\mu\nu}g_{\sigma\rho}) + f_{ade}f_{bce} (g_{\mu\nu}g_{\sigma\rho} - g_{\mu\rho}g_{\sigma\nu}) ]$
---------	--	--

---

The fermion and gauge boson propagators are in QCD the same as in QED, times an identity matrix in the gauge group space. Similarly, the polarization of external particles is treated the same as in QED, but each external particle also has an orientation in the group space.

Note, that the ghost-gluon vertex contains only the outgoing ghost momentum, but no incoming ghost momentum.

---



---

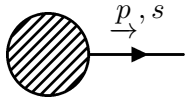
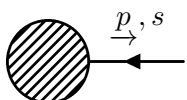
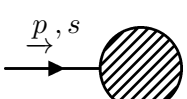
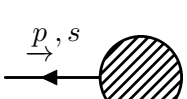
*Additional rules for external lines*

---

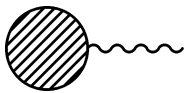



---

**Fermions (quarks)**

outgoing fermion		$\bar{u}(p, s)$
outgoing antifermion		$v(p, s)$
incoming fermion		$u(p, s)$
incoming antifermion		$\bar{v}(p, s)$

**Vector fields (photons/ gluons)**

outgoing vector		$\epsilon_{\lambda}^{\mu*}(k)$
incoming vector		$\epsilon_{\lambda}^{\mu}(k)$

---

A free fermion with mass  $m$  and spin  $s$  is described by a spinor  $u(p, s)$ , while an antifermion is denoted by  $\bar{v}(p, s)$ . In each case the energy, given by  $p_0 \equiv E_p = +\sqrt{\mathbf{p}^2 + m^2}$ , is positive. The spinors  $u(p, s)$  and the antiparticle spinors  $v(p, s)$  obey the Dirac equation

in the form

$$0 = (\not{p} - m)u(p, s) = \bar{u}(p, s)(\not{p} - m) \quad (\text{A.2})$$

$$= (\not{p} + m)v(p, s) = \bar{v}(p, s)(\not{p} + m). \quad (\text{A.3})$$

The spinors and antispinors are normalized in such a way that

$$\begin{aligned} \sum_{\text{spin}} \bar{u}(p, s)u(p, s) &= 2m \\ \sum_{\text{spin}} \bar{v}(p, s)v(p, s) &= -2m \end{aligned} \quad (\text{A.4})$$

and the projection operators are

$$\begin{aligned} u(p, s)\bar{u}(p, s) &= (\not{p} + m)\frac{1 + \gamma_5 \not{s}}{2} \\ v(p, s)\bar{v}(p, s) &= -(m - \not{p})\frac{1 + \gamma_5 \not{s}}{2}. \end{aligned} \quad (\text{A.5})$$

In computing unpolarized cross sections we often sum over the polarization states of a fermion. Due to the previous relations we obtain directly

$$\sum_s u(p, s)\bar{u}(p, s) = \not{p} + m \quad (\text{A.6})$$

$$\sum_s v(p, s)\bar{v}(p, s) = \not{p} - m. \quad (\text{A.7})$$

The spin vector  $s$  satisfies

$$\begin{aligned} s \cdot p &= 0 \\ s^2 &= -1, \end{aligned} \quad (\text{A.8})$$

and is generalized from its form in the rest frame of the particle  $s_\mu = (0, \mathbf{s})$ , where  $\mathbf{s}$  is the polarization vector with  $\mathbf{s} \cdot \mathbf{s} = 1$ .

A convenient basis for spin is the helicity basis, in which the spin is aligned parallel or antiparallel to the direction of motion. In this basis the spinor  $u_\lambda(p)$  is an eigenstate of the operator  $\frac{1}{2}\gamma_5 \not{s}$  with eigenvectors  $\lambda = \pm \frac{1}{2}$ . Here Eq. (A.4) and Eq. (A.4) yield [53]

$$\begin{aligned} \bar{u}_\lambda(p)u_{\lambda'}(p) &= 2m\delta_{\lambda, \lambda'} \\ \bar{v}_\lambda(p)v_{\lambda'}(p) &= -2m\delta_{\lambda, \lambda'}. \end{aligned} \quad (\text{A.9})$$

For unpolarized cross sections involving photons, one can replace

$$\sum_{\text{polarizations}} \epsilon_{\mu}^* \epsilon_{\nu} \rightarrow -g_{\mu\nu} \quad (\text{A.10})$$

Here  $\bar{u}_{\lambda}(p) = u_{\lambda}(p)^{\dagger} \gamma_0$ . *Dagger* “ $\dagger$ ” is used for hermitian conjugation and *asterisk* “ $*$ ” for complex conjugation.





## B. Mellin- $N$ moments of Plus-distributions

- $\boxed{1/(1-m)_+}$

$$\int_0^1 dm m^{N+1} \frac{1}{(1-m)_+} = -[\Psi(N+2) + \gamma_E] \quad (\text{B.1})$$

- $\boxed{\left(\frac{\ln(1-m)}{1-m}\right)_+}$

$$\int_0^1 dm m^{N+1} \left(\frac{\ln(1-m)}{1-m}\right)_+ = \frac{1}{2} [\Psi(N+2) + \gamma_E]^2 + \frac{\pi^2}{12} - \frac{1}{2} \Psi(1, N+2) \quad (\text{B.2})$$

- $\boxed{\ln(1-mA) \frac{1}{(1-m)_+}}$

$$\begin{aligned} \int_0^1 dm m^{N+1} \frac{\ln(1-mA)}{(1-m)_+} &= -\ln(1-A) [\Psi(N+1) + \gamma_E] - \frac{\ln(1-A)}{N+1} + \frac{2N^2 + 2N + 1}{N^2(N+1)^2} \\ &\quad + \frac{1}{AN(N+1)} - \left(\frac{1}{N} + \frac{1}{(N+1)A}\right) \text{LerchPhi}(A, 1, N) \\ &\quad + \sum_{i=1}^{\infty} \frac{A^i}{i} [\Psi(N+i) - \Psi(N)] \end{aligned} \quad (\text{B.3})$$

- $\boxed{\frac{1}{1-mA} \frac{1}{(1-m)_+}}$

$$\begin{aligned} \int_0^1 dm m^{N+2} \frac{1}{1-mA} \frac{1}{(1-m)_+} &= -\frac{1}{1-A} [\Psi(N+2) + \gamma_E] + \frac{1+AN}{(1-A)N(N+1)} \\ &\quad - (1+A) \text{LerchPhi}(A, 1, N+2) - \sum_{i=1}^{\infty} A^{i-1} [\Psi(N+i) - \Psi(N)] \end{aligned} \quad (\text{B.4})$$

$$\bullet \quad \boxed{\frac{1}{1-mA} \left( \frac{\ln(1-m)}{1-m} \right)_+}$$

$$\begin{aligned} \int_0^1 dm m^{N+1} \frac{1}{1-mA} \left( \frac{\ln(1-m)}{1-m} \right)_+ &= \frac{1}{1-A} \frac{1}{2} [\Psi(N+1) + \gamma_E]^2 + \frac{1}{1-A} \frac{\pi^2}{12} \\ &+ \frac{1}{2} \sum_{i=1}^{\infty} A^{i-1} [\Psi(N+i+1) - \Psi(N+1)]^2 \\ &+ \sum_{i=1}^{\infty} A^{i-1} [\Psi(N+i+1) - \Psi(N+1)] [\Psi(N+1) + \gamma_E] \\ &- \sum_{i=1}^{\infty} \frac{A^{i-1}}{2} \Psi(1, N+i+1), \end{aligned}$$

as

$$\begin{aligned} &- \frac{1}{2} \sum_{i=1}^{\infty} A^{i-1} [\Psi(i+1) + \gamma_E]^2 + \frac{1}{1-A} \sum_{i=1}^{\infty} \frac{A^{i-1}}{i} [\Psi(i+1) + \gamma_E] + \sum_{i=1}^{\infty} \frac{A^{i-1}}{2} \Psi(1, i+1) = \\ &= \frac{1}{1-A} \frac{\pi^2}{12} \end{aligned} \quad (\text{B.5})$$

$$\bullet \quad \boxed{\frac{\ln(1-mA)}{1-mA} \frac{1}{(1-m)_+}}$$

$$\begin{aligned} \int_0^1 dm m^{N+1} \frac{\ln(1-mA)}{1-mA} \frac{1}{(1-m)_+} &= -\frac{\ln(1-A)}{1-A} [\Psi(N) + \gamma_E] \\ &+ \sum_{i=1}^{\infty} A^i [\Psi(i+1) + \gamma_E] [\Psi(N+i+2) - \Psi(N)] \end{aligned} \quad (\text{B.6})$$

$$\bullet \quad \boxed{\frac{\ln(m)}{(1-mA)(1-m)}}$$

$$\begin{aligned} \int_0^1 dm m^{N+2} \frac{\ln(m)}{1-mA} \frac{1}{1-m} &= -\frac{1}{1-A} \Psi(1, N+1) + (1+A) \text{LerchPhi}(A, 2, N+2) \\ &- \frac{AN^2 + 2N + 1}{(1-A)N^2(N+1)^2} - \sum_{i=1}^{\infty} A^{i-1} [\Psi(1, N+i) - \Psi(1, N)] \end{aligned} \quad (\text{B.7})$$

$$\bullet \quad \boxed{\frac{\ln(m)}{(1-m)}}$$

$$\int_0^1 dm m^{N+1} \frac{\ln(m)}{1-m} = -\Psi(1, N+2) \quad (\text{B.8})$$

## C. Anomalous dimension-, soft- and hard-matrices

**Table C.1.:** Collection of anomalous dimension-, soft- and hard- matrices for the first part of processes [126]. We adopt the notation of [126]:  $T \equiv \ln\left(\frac{-\hat{t}}{\hat{s}}\right) + \pi i$ ,  $U \equiv \ln\left(\frac{-\hat{u}}{\hat{s}}\right) + \pi i$  (with the Mandelstam variables as in Eq. (6.6)).

$q\bar{q} \rightarrow q\bar{q}$		
$S = \begin{pmatrix} N_c^2 & 0 \\ 0 & \frac{(N_c^2-1)}{4} \end{pmatrix} \quad \Gamma_{S'} = \frac{\alpha_s}{\pi} \begin{pmatrix} 2C_F T & -\frac{C_F}{N_c} U \\ -2U & -\frac{(T-2U)}{N_c} \end{pmatrix}$		
$q_j \bar{q}_j \rightarrow q_j \bar{q}_j$	$q_j \bar{q}_j \rightarrow q_k \bar{q}_k$	$q_j \bar{q}_k \rightarrow q_j \bar{q}_k$
$H = \alpha_s^2 \begin{pmatrix} h_{11} & h_{12} \\ h_{12} & h_{22} \end{pmatrix}$ $h_{11} = \frac{2C_F^2}{N_c^4} \frac{\hat{t}^2 + \hat{u}^2}{\hat{s}^2}$ $h_{12} = \frac{2C_F}{N_c^3} \left( -\frac{\hat{t}^2 + \hat{u}^2}{N_c \hat{s}^2} + \frac{\hat{u}^2}{\hat{s}\hat{t}} \right)$ $h_{22} = \frac{1}{N_c^2} \left( \frac{2}{N_c} \frac{\hat{t}^2 + \hat{u}^2}{\hat{s}^2} + 2 \frac{\hat{s}^2 + \hat{u}^2}{\hat{t}^2} - \frac{4}{N_c} \frac{\hat{u}^2}{\hat{s}\hat{t}} \right)$	$H = \alpha_s^2 \begin{pmatrix} \frac{C_F^2}{N_c^2} h & -\frac{C_F}{N_c^2} h \\ -\frac{C_F}{N_c^2} h & \frac{1}{N_c^2} h \end{pmatrix}$ $h = \frac{2}{N_c^2} \frac{\hat{t}^2 + \hat{u}^2}{\hat{s}^2}$	$H = \alpha_s^2 \begin{pmatrix} 0 & 0 \\ 0 & h \end{pmatrix}$ $h = \frac{2(\hat{s}^2 + \hat{u}^2)}{N_c^2 \hat{t}^2}$
$qq \rightarrow qq$		
$S = \begin{pmatrix} \frac{(N_c^2-1)}{4} & 0 \\ 0 & N_c^2 \end{pmatrix} \quad \Gamma_{S'} = \frac{\alpha_s}{\pi} \begin{pmatrix} -\frac{T+U}{N_c} + 2C_F U & 2U \\ \frac{C_F}{N_c} & 2C_F T \end{pmatrix}$		
$q_j q_j \rightarrow q_j q_j$	$q_j q_k \rightarrow q_j q_k$	
$H = \alpha_s^2 \begin{pmatrix} h_{11} & h_{12} \\ h_{12} & h_{22} \end{pmatrix}$ $h_{11} = \frac{2}{N_c^2} \left[ \frac{\hat{s}^2 + \hat{u}^2}{\hat{t}^2} + \frac{1}{N_c^2} \frac{\hat{s}^2 + \hat{t}^2}{\hat{u}^2} - \frac{2}{N_c} \frac{\hat{s}^2}{\hat{t}\hat{u}} \right]$ $h_{12} = \frac{2C_F}{N_c^4} \left[ N_c \frac{\hat{s}^2}{\hat{t}\hat{u}} - \frac{\hat{s}^2 + \hat{t}^2}{\hat{u}^2} \right]$ $h_{22} = \frac{2C_F^2}{N_c^4} \frac{\hat{s}^2 + \hat{t}^2}{\hat{u}^2}$	$H = \alpha_s^2 \begin{pmatrix} h & 0 \\ 0 & 0 \end{pmatrix}$ $h = \frac{2(\hat{s}^2 + \hat{u}^2)}{N_c^2 \hat{t}^2}$	

**Table C.2.:** Same as Table C.1, but for the second part of processes.

$q\bar{q} \rightarrow gg$ and $gg \rightarrow q\bar{q}$	
$S = \begin{pmatrix} N_c(N_c^2 - 1) & 0 & 0 \\ 0 & \frac{(N_c^2 - 4)(N_c^2 - 1)}{2N_c} & 0 \\ 0 & 0 & \frac{N_c(N_c^2 - 1)}{2} \end{pmatrix}$	$\Gamma_{S'} = \frac{\alpha_s}{\pi} \begin{pmatrix} 0 & 0 & U - T \\ 0 & \frac{C_A}{2}(T + U) & \frac{C_A}{2}(U - T) \\ 2(U - T) & \frac{N_c^2 - 4}{2N_c}(U - T) & \frac{C_A}{2}(T + U) \end{pmatrix}$
$q\bar{q} \rightarrow gg$	$gg \rightarrow q\bar{q}$
$H = \alpha_s^2 \begin{pmatrix} h_{11} & h_{12} & h_{13} \\ h_{12} & h_{22} & h_{23} \\ h_{13} & h_{23} & h_{33} \end{pmatrix}$	$H = \frac{N_c^2}{(N_c^2 - 1)^2} \alpha_s^2 \begin{pmatrix} h_{11} & h_{12} & h_{13} \\ h_{12} & h_{22} & h_{23} \\ h_{13} & h_{23} & h_{33} \end{pmatrix}$
$h_{11} = \frac{1}{2N_c^4} \left( \frac{\hat{u}}{\hat{t}} + \frac{\hat{t}}{\hat{u}} \right), \quad h_{12} = N_c h_{11}, \quad h_{22} = N_c^2 h_{11}$ $h_{13} = -\frac{1}{2N_c^3} \frac{\hat{u}^2 - \hat{t}^2}{\hat{t}\hat{u}} - \frac{1}{N_c^3} \frac{\hat{u} - \hat{t}}{\hat{s}}, \quad h_{23} = N_c h_{13}, \quad h_{33} = \frac{1}{2N_c^2} \frac{\hat{s}^2}{\hat{t}\hat{u}} + \frac{4}{N_c^2} \frac{\hat{t}\hat{u}}{\hat{s}^2} - \frac{3}{N_c^2}$	
$qg \rightarrow qg$	
$S = \begin{pmatrix} N_c(N_c^2 - 1) & 0 & 0 \\ 0 & \frac{(N_c^2 - 4)(N_c^2 - 1)}{2N_c} & 0 \\ 0 & 0 & \frac{N_c(N_c^2 - 1)}{2} \end{pmatrix}$	$\Gamma_{S'} = \frac{\alpha_s}{\pi} \begin{pmatrix} (C_F + C_A)T & 0 & U \\ 0 & C_F T + \frac{C_A}{2}U & \frac{C_A}{2}U \\ 2U & \frac{N_c^2 - 4}{2N_c}U & C_F T + \frac{C_A}{2}U \end{pmatrix}$
$H = \alpha_s^2 \begin{pmatrix} h_{11} & h_{12} & h_{13} \\ h_{12} & h_{22} & h_{23} \\ h_{13} & h_{23} & h_{33} \end{pmatrix}$	
$h_{11} = -\frac{1}{2N_c^3(N_c^2 - 1)} \left[ \frac{\hat{t}^2}{\hat{s}\hat{u}} - 2 \right], \quad h_{12} = N_c h_{11}, \quad h_{22} = N_c^2 h_{11}$ $h_{13} = \frac{1}{N_c^2(N_c^2 - 1)} \left[ -1 - \frac{2\hat{s}}{\hat{t}} + \frac{\hat{u}}{2\hat{s}} - \frac{\hat{s}}{2\hat{u}} \right], \quad h_{23} = N_c h_{13}, \quad h_{33} = \frac{1}{N_c(N_c^2 - 1)} \left[ 3 - \frac{4\hat{s}\hat{u}}{\hat{t}^2} - \frac{\hat{t}^2}{2\hat{s}\hat{u}} \right]$	
$gg \rightarrow gg$	
$S = \begin{pmatrix} S_{3 \times 3} & 0_{3 \times 5} \\ 0_{5 \times 3} & S_{5 \times 5} \end{pmatrix} \quad \Gamma_{S'} = \begin{pmatrix} \Gamma_{3 \times 3} & 0_{3 \times 5} \\ 0_{5 \times 3} & \Gamma_{5 \times 5} \end{pmatrix}$	
$S_{3 \times 3} = \begin{pmatrix} 5 & 0 & 0 \\ 0 & 5 & 0 \\ 0 & 0 & 5 \end{pmatrix}, \quad S_{5 \times 5} = \begin{pmatrix} 1 & 0 & 0 & 0 & 0 \\ 0 & 8 & 0 & 0 & 0 \\ 0 & 0 & 8 & 0 & 0 \\ 0 & 0 & 0 & 20 & 0 \\ 0 & 0 & 0 & 0 & 27 \end{pmatrix}$	
$\Gamma_{3 \times 3} = \frac{\alpha_s}{\pi} \begin{pmatrix} 3T & 0 & 0 \\ 0 & 3U & 0 \\ 0 & 0 & 3(T + U) \end{pmatrix}, \quad S_{5 \times 5} = \begin{pmatrix} 6T & 0 & -6U & 0 & 0 \\ 0 & 3T + \frac{3U}{2} & -\frac{3U}{2} & -3U & 0 \\ -\frac{3U}{4} & -\frac{3U}{2} & 3T + \frac{3U}{2} & 0 & -\frac{9U}{4} \\ 0 & -\frac{6U}{5} & 0 & 3U & -\frac{9U}{5} \\ 0 & 0 & -\frac{2U}{3} & -\frac{4U}{3} & -2T + 4U \end{pmatrix}$	
$H = \alpha_s^2 \begin{pmatrix} 0_{3 \times 3} & 0_{3 \times 5} \\ 0_{5 \times 3} & H_{5 \times 5} \end{pmatrix}, \quad H_{5 \times 5} = \frac{1}{16} \begin{pmatrix} 9h_1 & \frac{9}{2}h_1 & \frac{9}{2}h_2 & 0 & -3h_1 \\ \frac{9}{2}h_1 & \frac{9}{4}h_1 & \frac{9}{4}h_2 & 0 & -\frac{3}{2}h_1 \\ \frac{9}{2}h_2 & \frac{9}{4}h_2 & h_3 & 0 & -\frac{3}{2}h_2 \\ 0 & 0 & 0 & 0 & 0 \\ -3h_1 & -\frac{3}{2}h_1 & -\frac{3}{2}h_2 & 0 & h_1 \end{pmatrix}$	
$h_1 = 1 - \frac{\hat{t}\hat{u}}{\hat{s}^2} - \frac{\hat{s}\hat{t}}{\hat{u}^2} + \frac{\hat{t}^2}{\hat{s}\hat{u}}$ $h_2 = \frac{\hat{s}\hat{t}}{\hat{u}^2} - \frac{\hat{t}\hat{u}}{\hat{s}^2} + \frac{\hat{u}^2}{\hat{s}\hat{t}} - \frac{\hat{s}^2}{\hat{t}\hat{u}}$ $h_3 = \frac{27}{4} - 9 \left( \frac{\hat{s}\hat{u}}{\hat{t}^2} + \frac{1}{4} \frac{\hat{t}\hat{u}}{\hat{s}^2} + \frac{1}{4} \frac{\hat{s}\hat{t}}{\hat{u}^2} \right) + \frac{9}{2} \left( \frac{\hat{u}^2}{\hat{s}\hat{t}} + \frac{\hat{s}^2}{\hat{t}\hat{u}} - \frac{1}{2} \frac{\hat{t}^2}{\hat{s}\hat{u}} \right)$	

# Bibliography

- [1] G. Aad et al. (ATLAS Collaboration), “A particle consistent with the Higgs boson observed with the ATLAS Detector at the Large Hadron Collider”, *Science* **338**, 1576 (2012).
- [2] G. Aad et al. (ATLAS Collaboration), “Observation of a new particle in the search for the Standard Model Higgs boson with the ATLAS detector at the LHC”, *Phys.Lett. B* **716**, 1 (2012), 1207.7214.
- [3] W. Gerlach and O. Stern, “Der experimentelle Nachweis der Richtungsquantelung im Magnetfeld”, *Zeitschrift für Physik* **9**, 349 (1922).
- [4] W. Gerlach and O. Stern, “Das magnetische Moment des Silberatoms”, *Zeitschrift für Physik* **9**, 353 (1922).
- [5] S. Goudschmidt and G. Uhlenbeck, “Spinning electrons and the structure of spectra”, *Nature* **117**, 264 (1926).
- [6] F. Hund, “Zur Deutung der Molekelspektren. II.”, *Zeitschrift für Physik* **43**, 805 (1927).
- [7] T. Hori, “Über die Analyse des Wasserstoffbandenspektrums im äußersten Ultraviolett”, *Zeitschrift für Physik* **44**, 834 (1927).
- [8] D. M. Dennison, “A note on the specific heat of the hydrogen molecule”, *Proc. R. Soc. Lond. A* **115** (1927).
- [9] M. Alguard, W. Ash, G. Baum, J. Clendenin, P. Cooper, et al., “Deep inelastic scattering of polarized electrons by polarized protons”, *Phys.Rev.Lett.* **37**, 1261 (1976).
- [10] G. Baum, M. Bergstrom, P. Bolton, J. Clendenin, N. de Botton, et al., “A new measurement of deep inelastic e p asymmetries”, *Phys.Rev.Lett.* **51**, 1135 (1983).
- [11] J. Ashman et al. (European Muon Collaboration), “A measurement of the spin asymmetry and determination of the structure function  $g(1)$  in deep inelastic muon-proton scattering”, *Phys.Lett. B* **206**, 364 (1988).

- [12] J. Ashman et al. (European Muon Collaboration), “An investigation of the spin structure of the proton in deep inelastic scattering of polarized muons on polarized protons”, Nucl.Phys. **B328**, 1 (1989).
- [13] R. Jaffe and A. Manohar, “The G(1) problem: fact and fantasy on the spin of the proton”, Nucl.Phys. **B337**, 509 (1990).
- [14] A. Accardi, J. Albacete, M. Anselmino, N. Armesto, E. Aschenauer, et al., “Electron Ion Collider: The next QCD frontier - understanding the glue that binds us all”, (2012), 1212.1701.
- [15] L. Gordon and W. Vogelsang, “Polarized and unpolarized isolated prompt photon production beyond the leading order”, Phys.Rev. **D50**, 1901 (1994).
- [16] C. Coriano and L. Gordon, “Polarized and unpolarized double prompt photon production in next-to-leading order QCD”, Nucl.Phys. **B469**, 202 (1996), hep-ph/9601350.
- [17] I. Bojak and M. Stratmann, “Photoproduction of heavy quarks in next-to-leading order QCD with longitudinally polarized initial states”, Nucl.Phys. **B540**, 345 (1999), hep-ph/9807405.
- [18] V. Ravindran, J. Smith, and W. van Neerven, “NLO differential distributions of massive lepton pair production in longitudinally polarized proton proton collisions”, Nucl.Phys. **B647**, 275 (2002), hep-ph/0207076.
- [19] B. Jäger, A. Schäfer, M. Stratmann, and W. Vogelsang, “Next-to-leading order QCD corrections to high-p(T) pion production in longitudinally polarized p p collisions”, Phys. Rev. **D67**, 054005 (2003), hep-ph/0211007.
- [20] B. Jäger, M. Stratmann, and W. Vogelsang, “Single inclusive jet production in polarized  $pp$  collisions at  $O(\alpha_s^3)$ ”, Phys.Rev. **D70**, 034010 (2004), hep-ph/0404057.
- [21] D. de Florian and W. Vogelsang, “Helicity parton distributions from spin asymmetries in W-boson production at RHIC”, Phys.Rev. **D81**, 094020 (2010), 1003.4533.
- [22] L. Silva (Compass Collaboration), “COMPASS results on gluon polarisation”, PoS **EPS-HEP2011**, 301 (2011).
- [23] E. Aschenauer, A. Bazilevsky, K. Boyle, K. Eyser, R. Fatemi, et al., “The RHIC spin program: achievements and future opportunities”, (2013), 1304.0079.
- [24] G. F. Sterman, “Summation of large corrections to short distance hadronic cross-sections”, Nucl. Phys. **B281**, 310 (1987).

- [25] S. Catani and L. Trentadue, “Resummation of the QCD perturbative series for hard processes”, Nucl.Phys. **B327**, 323 (1989).
- [26] D. de Florian and W. Vogelsang, “Threshold resummation for the inclusive-hadron cross-section in pp collisions”, Phys.Rev. **D71**, 114004 (2005), [hep-ph/0501258](#).
- [27] L. G. Almeida, G. F. Sterman, and W. Vogelsang, “Threshold resummation for di-hadron production in hadronic collisions”, Phys.Rev. **D80**, 074016 (2009), [0907.1234](#).
- [28] E. Laenen, G. Oderda, and G. F. Sterman, “Resummation of threshold corrections for single particle inclusive cross-sections”, Phys.Lett. **B438**, 173 (1998), [hep-ph/9806467](#).
- [29] C. Adolph et al. (COMPASS Collaboration), “Measurement of the cross section for high- $p_T$  hadron production in scattering of 160 GeV/c Muons off nucleons”, (2012), [1207.2022](#).
- [30] C. Höppner (COMPASS Collaboration), “First measurement of the cross section for the production of hadrons with high transverse momenta at COMPASS, and developments for particle tracking in high-rate experiments”, Technical U. Munich thesis (2012).
- [31] D. de Florian, M. Pfeuffer, A. Schäfer, and W. Vogelsang, “Soft-gluon resummation for high- $p_T$  inclusive-hadron production at COMPASS”, (2013), [1305.6468](#).
- [32] M. Pfeuffer, “QCD threshold resummation calculations”, Diplomarbeit, *University of Regensburg* (2008).
- [33] H. Fritzsch, M. Gell-Mann, and H. Leutwyler, “Advantages of the color octet gluon picture”, Phys.Lett. **B47**, 365 (1973).
- [34] D. Gross and F. Wilczek, “Asymptotically free gauge theories. 1”, Phys.Rev. **D8**, 3633 (1973).
- [35] S. Weinberg, “Nonabelian gauge theories of the strong interactions”, Phys.Rev.Lett. **31**, 494 (1973).
- [36] G. Dissertori, I. Knowles, and M. Schmelling, “High energy experiments and theory”, (2003).
- [37] L. Faddeev and V. Popov, “Feynman diagrams for the Yang-Mills field”, Phys.Lett. **B25**, 29 (1967).

- [38] C. Becchi, A. Rouet, and R. Stora, “Renormalization of gauge theories”, *Annals Phys.* **98**, 287 (1976).
- [39] J. Taylor, “Ward identities and charge renormalization of the Yang-Mills field”, *Nucl.Phys.* **B33**, 436 (1971).
- [40] A. Slavnov, “Ward identities in gauge theories”, *Theor.Math.Phys.* **10**, 99 (1972).
- [41] O. Tarasov, A. Vladimirov, and A. Y. Zharkov, “The Gell-Mann-Low function of QCD in the three loop approximation”, *Phys.Lett.* **B93**, 429 (1980).
- [42] T. van Ritbergen, J. Vermaseren, and S. Larin, “The four loop beta function in quantum chromodynamics”, *Phys.Lett.* **B400**, 379 (1997), [hep-ph/9701390](#).
- [43] S. Bethke, “The 2009 world average of  $\alpha(s)$ ”, *Eur.Phys.J.* **C64**, 689 (2009), [0908.1135](#).
- [44] D. Gross and F. Wilczek, “Ultraviolet behavior of nonabelian gauge theories”, *Phys.Rev.Lett.* **30**, 1343 (1973).
- [45] H. D. Politzer, “Reliable perturbative results for strong interactions?”, *Phys.Rev.Lett.* **30**, 1346 (1973).
- [46] F. Bloch and A. Nordsieck, “Note on the radiation field of the electron”, *Phys.Rev.* **52**, 54 (1937).
- [47] D. Yennie, S. C. Frautschi, and H. Suura, “The infrared divergence phenomena and high-energy processes”, *Annals Phys.* **13**, 379 (1961).
- [48] J. Grammer, G. and D. Yennie, “Improved treatment for the infrared divergence problem in quantum electrodynamics”, *Phys.Rev.* **D8**, 4332 (1973).
- [49] T. Kinoshita, “Mass singularities of Feynman amplitudes”, *J.Math.Phys.* **3**, 650 (1962).
- [50] T. Lee and M. Nauenberg, “Degenerate systems and mass singularities”, *Phys.Rev.* **133**, B1549 (1964).
- [51] C. Bollini and J. Giambiagi, “Dimensional renormalization: The number of dimensions as a regularizing parameter”, *Nuovo Cim.* **B12**, 20 (1972).
- [52] G. ’t Hooft and M. Veltman, “Regularization and renormalization of gauge fields”, *Nucl.Phys.* **B44**, 189 (1972).
- [53] R. Field, “Applications of perturbative QCD”, *Front.Phys.* **77**, 1 (1989).



- [54] M. E. Peskin and D. V. Schroeder, “An introduction to quantum field theory”, (1995).
- [55] W. A. Bardeen, A. Buras, D. Duke, and T. Muta, “Deep inelastic scattering beyond the leading order in asymptotically free gauge theories”, *Phys.Rev.* **D18**, 3998 (1978).
- [56] J. Christenson, G. Hicks, L. Lederman, P. Limon, B. Pope, et al., “Observation of massive muon pairs in hadron collisions”, *Phys.Rev.Lett.* **25**, 1523 (1970).
- [57] S. Drell and T.-M. Yan, “Massive lepton pair production in hadron-hadron collisions at high-energies”, *Phys.Rev.Lett.* **25**, 316 (1970).
- [58] J. Kubar-Andre and F. E. Paige, “Gluon corrections to the Drell-Yan model”, *Phys.Rev.* **D19**, 221 (1979).
- [59] G. Altarelli, R. K. Ellis, and G. Martinelli, “Large perturbative corrections to the Drell-Yan process in QCD”, *Nucl.Phys.* **B157**, 461 (1979).
- [60] K. Harada and T. Muta, “Full estimate of the higher order corrections to the Drell-Yan process in Quantum Chromodynamics”, *Phys.Rev.* **D22**, 663 (1980).
- [61] P. Ratcliffe, “Radiative corrections to the helicity asymmetries for the Drell-Yan process in QCD”, *Nucl.Phys.* **B223**, 45 (1983).
- [62] A. Weber, “Soft gluon resummations for polarized Drell-Yan dimuon production”, *Nucl.Phys.* **B382**, 63 (1992).
- [63] T. Gehrmann, “QCD corrections to the polarized Drell-Yan process”, (1997), [hep-ph/9710501](#).
- [64] B. Kamal, “QCD corrections to spin dependent Drell-Yan and a global subtraction scheme”, *Phys.Rev.* **D53**, 1142 (1996), [hep-ph/9511217](#).
- [65] W. Vogelsang and A. Weber, “Drell-Yan dimuon production with transversely polarized protons”, *Phys.Rev.* **D48**, 2073 (1993).
- [66] V. Barone, T. Calarco, and A. Drago, “Double spin transverse asymmetries in Drell-Yan processes”, *Phys.Rev.* **D56**, 527 (1997), [hep-ph/9702239](#).
- [67] R. Hamberg, W. van Neerven, and T. Matsuura, “A complete calculation of the order  $\alpha_s^2$  correction to the Drell-Yan  $K$  factor”, *Nucl.Phys.* **B359**, 343 (1991).
- [68] R. V. Harlander and W. B. Kilgore, “Next-to-next-to-leading order Higgs production at hadron colliders”, *Phys.Rev.Lett.* **88**, 201801 (2002), [hep-ph/0201206](#).

- [69] C. Anastasiou, L. J. Dixon, K. Melnikov, and F. Petriello, “Dilepton rapidity distribution in the Drell-Yan process at NNLO in QCD”, *Phys.Rev.Lett.* **91**, 182002 (2003), [hep-ph/0306192](#).
- [70] S. Catani, L. Cieri, D. de Florian, G. Ferrera, and M. Grazzini, “Vector boson production at hadron colliders: hard-collinear coefficients at the NNLO”, *Eur.Phys.J.* **C72**, 2195 (2012), [1209.0158](#).
- [71] V. Ravindran, J. Smith, and W. van Neerven, “NNLO corrections to massive lepton pair production in longitudinally polarized proton proton collisions”, *Nucl.Phys.* **B682**, 421 (2004), [hep-ph/0311304](#).
- [72] G. F. Sterman and W. Vogelsang, “Threshold resummation and rapidity dependence”, *JHEP* **0102**, 016 (2001), [hep-ph/0011289](#).
- [73] A. Vogt, “Next-to-next-to-leading logarithmic threshold resummation for deep inelastic scattering and the Drell-Yan process”, *Phys.Lett.* **B497**, 228 (2001), [hep-ph/0010146](#).
- [74] A. Djouadi, “The anatomy of electro-weak symmetry breaking. I: The Higgs boson in the standard model”, *Phys.Rept.* **457**, 1 (2008), [hep-ph/0503172](#).
- [75] S. Catani, D. de Florian, M. Grazzini, and P. Nason, “Soft gluon resummation for Higgs boson production at hadron colliders”, *JHEP* **0307**, 028 (2003), [hep-ph/0306211](#).
- [76] P. E. Reimer, “Exploring the partonic structure of hadrons through the Drell-Yan process”, *J.Phys.* **G34**, S107 (2007), [0704.3621](#).
- [77] J. C. Collins and D. E. Soper, “Parton distribution and decay functions”, *Nucl.Phys.* **B194**, 445 (1982).
- [78] G. F. Sterman, “Partons, factorization and resummation, TASI 95”, (1995), [hep-ph/9606312](#).
- [79] G. Altarelli and G. Parisi, “Asymptotic freedom in parton language”, *Nucl.Phys.* **B126**, 298 (1977).
- [80] M. Ahmed and G. G. Ross, “Polarized lepton -hadron scattering in asymptotically free gauge theories”, *Nucl.Phys.* **B111**, 441 (1976).
- [81] G. Curci, W. Furmanski, and R. Petronzio, “Evolution of parton densities beyond leading order: the nonsinglet case”, *Nucl.Phys.* **B175**, 27 (1980).

- [82] I. Antoniadis, C. Kounnas, and R. Lacaze, “Light gluinos in deep inelastic scattering”, Nucl.Phys. **B211**, 216 (1983).
- [83] R. Mertig and W. van Neerven, “The calculation of the two loop spin splitting functions  $P(ij)(1)(x)$ ”, Z.Phys. **C70**, 637 (1996), [hep-ph/9506451](#).
- [84] W. Vogelsang, “A rederivation of the spin dependent next-to-leading order splitting functions”, Phys.Rev. **D54**, 2023 (1996), [hep-ph/9512218](#).
- [85] W. Vogelsang, “The spin dependent two loop splitting functions”, Nucl.Phys. **B475**, 47 (1996), [hep-ph/9603366](#).
- [86] A. Hayashigaki, Y. Kanazawa, and Y. Koike, “Next-to-leading order  $q^{*2}$  evolution of the transversity distribution  $h(1)(x, q^{*2})$ ”, Phys.Rev. **D56**, 7350 (1997), [hep-ph/9707208](#).
- [87] S. Kumano and M. Miyama, “Two loop anomalous dimensions for the structure function  $h_1$ ”, Phys.Rev. **D56**, 2504 (1997), [hep-ph/9706420](#).
- [88] A. Vogt, S. Moch, M. Rogal, and J. Vermaseren, “Towards the NNLO evolution of polarised parton distributions”, Nucl.Phys.Proc.Suppl. **183**, 155 (2008), [0807.1238](#).
- [89] H. D. Abarbanel and C. Itzykson, “Relativistic eikonal expansion”, Phys.Rev.Lett. **23**, 53 (1969).
- [90] M. Levy and J. Sucher, “Eikonal approximation in quantum field theory”, Phys.Rev. **186**, 1656 (1969).
- [91] V. Sudakov, “Vertex parts at very high-energies in quantum electrodynamics”, Sov.Phys.JETP **3**, 65 (1956).
- [92] J. Gatheral, “Exponentiation of eikonal cross-sections in nonabelian gauge theories”, Phys.Lett. **B133**, 90 (1983).
- [93] J. Frenkel and J. Taylor, “Nonabelian eikonal exponentiation”, Nucl.Phys. **B246**, 231 (1984).
- [94] T. O. Eynck, E. Laenen, and L. Magnea, “Exponentiation of the Drell-Yan cross-section near partonic threshold in the DIS and  $\overline{\text{MS}}$  schemes”, JHEP **0306**, 057 (2003), [hep-ph/0305179](#).
- [95] J. Gracey, “Anomalous dimension of nonsinglet Wilson operators at  $O(1/N(f))$  in deep inelastic scattering”, Phys.Lett. **B322**, 141 (1994), [hep-ph/9401214](#).
- [96] W. van Neerven and A. Vogt, “Improved approximations for the three loop splitting functions in QCD”, Phys.Lett. **B490**, 111 (2000), [hep-ph/0007362](#).

- [97] S. Larin, T. van Ritbergen, and J. Vermaseren, “The next next-to-leading QCD approximation for nonsinglet moments of deep inelastic structure functions”, Nucl.Phys. **B427**, 41 (1994).
- [98] S. Larin, P. Nogueira, T. van Ritbergen, and J. Vermaseren, “The three loop QCD calculation of the moments of deep inelastic structure functions”, Nucl.Phys. **B492**, 338 (1997), [hep-ph/9605317](#).
- [99] A. Retey and J. Vermaseren, “Some higher moments of deep inelastic structure functions at next-to-next-to-leading order of perturbative QCD”, Nucl.Phys. **B604**, 281 (2001), [hep-ph/0007294](#).
- [100] S. Catani, M. L. Mangano, P. Nason, and L. Trentadue, “The resummation of soft gluon in hadronic collisions”, Nucl. Phys. **B478**, 273 (1996), [hep-ph/9604351](#).
- [101] I. Suslov, “Divergent perturbation series”, Zh.Eksp.Teor.Fiz. **127**, 1350 (2005), [hep-ph/0510142](#).
- [102] F. Dyson, “Divergence of perturbation theory in quantum electrodynamics”, Phys.Rev. **85**, 631 (1952).
- [103] J. K. Hunter, “Lecture Notes: Asymptotics”, (2004), URL <https://www.math.ucdavis.edu/~hunter/asymptotics/asymptotics.html>.
- [104] E. Sharpe, “Lecture Notes: Asymptotic series”, URL <http://www.phys.vt.edu/~ersharpe/spec-fn/app-d.pdf>.
- [105] H. Poincare, “On the irregular integrals of linear equations”, Acta Math. **8**, 295 (1886).
- [106] S. Catani, L. Trentadue, G. Turnock, and B. Webber, “Resummation of large logarithms in  $e^+e^-$  event shape distributions”, Nucl.Phys. **B407**, 3 (1993).
- [107] M. Beneke, “Renormalons”, Phys.Rept. **317**, 1 (1999), [hep-ph/9807443](#).
- [108] M. Beneke and V. M. Braun, “Power corrections and renormalons in Drell-Yan production”, Nucl.Phys. **B454**, 253 (1995), [hep-ph/9506452](#).
- [109] G. Oderda and G. F. Sterman, “Energy and color flow in dijet rapidity gaps”, Phys.Rev.Lett. **81**, 3591 (1998), [hep-ph/9806530](#).
- [110] J. Botts and G. F. Sterman, “Hard elastic scattering in QCD: leading behavior”, Nucl.Phys. **B325**, 62 (1989).
- [111] N. Kidonakis and G. F. Sterman, “Resummation for QCD hard scattering”, Nucl.Phys. **B505**, 321 (1997), [hep-ph/9705234](#).

- [112] N. Kidonakis, G. Oderda, and G. F. Sterman, “Threshold resummation for dijet cross sections”, Nucl. Phys. **B525**, 299 (1998), [hep-ph/9801268](#).
- [113] R. Bonciani, S. Catani, M. L. Mangano, and P. Nason, “Sudakov resummation of multiparton QCD cross-sections”, Phys.Lett. **B575**, 268 (2003), [hep-ph/0307035](#).
- [114] N. Kidonakis, G. Oderda, and G. F. Sterman, “Evolution of color exchange in QCD hard scattering”, Nucl. Phys. **B531**, 365 (1998), [hep-ph/9803241](#).
- [115] L. Landau, “On analytic properties of vertex parts in quantum field theory”, Nucl.Phys. **13**, 181 (1959).
- [116] G. F. Sterman, “An introduction to quantum field theory”, (1994).
- [117] H. Contopanagos, E. Laenen, and G. F. Sterman, “Sudakov factorization and resummation”, Nucl.Phys. **B484**, 303 (1997), [hep-ph/9604313](#).
- [118] E. Laenen and S.-O. Moch, “Soft gluon resummation for heavy quark electroproduction”, Phys.Rev. **D59**, 034027 (1999), [hep-ph/9809550](#).
- [119] T. O. Eynck, “Soft gluons and hard scales in QCD: Heavy quarks at finite and all orders”, Phdthesis (2003).
- [120] J. C. Collins and D. E. Soper, “Back-to-back jets in QCD”, Nucl.Phys. **B193**, 381 (1981).
- [121] J. C. Collins and G. F. Sterman, “Soft partons in QCD”, Nucl.Phys. **B185**, 172 (1981).
- [122] N. Kidonakis, “Resummation for heavy quark and jet cross-sections”, Int.J.Mod.Phys. **A15**, 1245 (2000), [hep-ph/9902484](#).
- [123] J. Kodaira and L. Trentadue, “Summing soft emission in QCD”, Phys.Lett. **B112**, 66 (1982).
- [124] H. Contopanagos and G. F. Sterman, “Normalization of the Drell-Yan cross-section in QCD”, Nucl.Phys. **B400**, 211 (1993).
- [125] H. Contopanagos and G. F. Sterman, “Principal value resummation”, Nucl.Phys. **B419**, 77 (1994), [hep-ph/9310313](#).
- [126] N. Kidonakis and J. F. Owens, “Effects of higher-order threshold corrections in high-E(T) jet production”, Phys. Rev. **D63**, 054019 (2001), [hep-ph/0007268](#).
- [127] M. Cacciari and S. Catani, “Soft gluon resummation for the fragmentation of light and heavy quarks at large x”, Nucl.Phys. **B617**, 253 (2001), [hep-ph/0107138](#).

- [128] S. Keppeler and M. Sjödal, “Orthogonal multiplet bases in  $SU(N_c)$  color space”, *JHEP* **1209**, 124 (2012), [1207.0609](#).
- [129] G. Dissertori, I. Knowles, and M. Schmelling, *Quantum Chromodynamics* (Oxford University Press Inc., New York, 2008).
- [130] J. Beringer et al. (Particle Data Group), “Review of particle physics (RPP)”, *Phys.Rev.* **D86**, 010001 (2012).
- [131] A. MacFarlane, A. Sudbery, and P. Weisz, “On Gell-Mann’s lambda-matrices, d- and f-tensors, octets, and parametrizations of  $SU(3)$ ”, *Commun.Math.Phys.* **11**, 77 (1968).
- [132] P. Cvitanovic, “Classics illustrated: Group theory. part 1”, (1984).
- [133] P. Cvitanovic, “Group theory: Birdtracks, Lie’s and exceptional groups”, (2008).
- [134] Y. Dokshitzer and G. Marchesini, “Soft gluons at large angles in hadron collisions”, *JHEP* **0601**, 007 (2006), [hep-ph/0509078](#).
- [135] G. Oderda, “Dijet rapidity gaps in photoproduction from perturbative QCD”, *Phys.Rev.* **D61**, 014004 (2000), [hep-ph/9903240](#).
- [136] A. Schäfer, “QCD script”, URL <http://homepages.uni-regensburg.de/~sca14496/schaefer.html>.
- [137] J. C. Collins, D. E. Soper, and G. F. Sterman, “Factorization for short distance hadron - hadron scattering”, *Nucl. Phys.* **B261**, 104 (1985).
- [138] S. Frixione, M. L. Mangano, P. Nason, and G. Ridolfi, “Improving the Weizsacker-Williams approximation in electron - proton collisions”, *Phys. Lett.* **B319**, 339 (1993), [hep-ph/9310350](#).
- [139] D. de Florian and S. Frixione, “Jet cross-sections in polarized photon hadron collisions”, *Phys.Lett.* **B457**, 236 (1999), [hep-ph/9904320](#).
- [140] G. A. Schuler and T. Sjöstrand, “Parton Distributions of the Virtual Photon”, *Phys. Lett.* **B376**, 193 (1996), [hep-ph/9601282](#).
- [141] M. Glück, E. Reya, and I. Schienbein, “Radiatively generated parton distributions of real and virtual photons”, *Phys. Rev.* **D60**, 054019 (1999), [hep-ph/9903337](#).
- [142] F. Aversa, P. Chiappetta, M. Greco, and J. P. Guillet, “QCD corrections to parton-parton scattering processes”, *Nucl. Phys.* **B327**, 105 (1989).

- [143] R. Kelley and M. D. Schwartz, “1-loop matching and NNLL resummation for all partonic 2 to 2 processes in QCD”, *Phys.Rev.* **D83**, 045022 (2011), 1008.2759.
- [144] S. Catani, M. Grazzini, and A. Torre, “Soft-gluon resummation for single-particle inclusive hadroproduction at high transverse momentum”, (2013), 1305.3870.
- [145] S. Catani, M. L. Mangano, and P. Nason, “Sudakov resummation for prompt photon production in hadron collisions”, *JHEP* **9807**, 024 (1998), hep-ph/9806484.
- [146] L. G. Almeida, G. F. Sterman, and W. Vogelsang, “Threshold resummation for the top quark charge asymmetry”, *Phys.Rev.* **D78**, 014008 (2008), 0805.1885.
- [147] N. Kidonakis and J. Owens, “Soft gluon resummation and NNLO corrections for direct photon production”, *Phys.Rev.* **D61**, 094004 (2000), hep-ph/9912388.
- [148] S. Catani, M. L. Mangano, P. Nason, C. Oleari, and W. Vogelsang, “Sudakov resummation effects in prompt photon hadroproduction”, *JHEP* **9903**, 025 (1999), hep-ph/9903436.
- [149] B. Jäger, M. Stratmann, and W. Vogelsang, “Longitudinally polarized photoproduction of inclusive hadrons beyond the leading order”, *Phys.Rev.* **D68**, 114018 (2003), hep-ph/0309051.
- [150] W. Tung, H. Lai, A. Belyaev, J. Pumplin, D. Stump, et al., “Heavy quark mass effects in deep inelastic scattering and global QCD analysis”, *JHEP* **0702**, 053 (2007), hep-ph/0611254.
- [151] D. de Florian, R. Sassot, and M. Stratmann, “Global analysis of fragmentation functions for pions and kaons and their uncertainties”, *Phys.Rev.* **D75**, 114010 (2007), hep-ph/0703242.
- [152] B. Jäger, M. Stratmann, and W. Vogelsang, “Longitudinally polarized photoproduction of inclusive hadrons at fixed-target experiments”, *Eur.Phys.J.* **C44**, 533 (2005), hep-ph/0505157.





# Acknowledgements

An dieser Stelle möchte ich all jenen meinen Dank aussprechen, die in verschiedenster Weise zur Entstehung dieser Arbeit beigetragen haben:

Meinem Doktorvater Prof. Dr. Andreas Schäfer dafür, dass er es mir ermöglichte an einem so spannenden Thema zu arbeiten. Von dessen wissenschaftlicher Kompetenz und außerordentlich guten Betreuung ich schon in meiner Diplomarbeit profitieren durfte und der mich auch jetzt während meiner Promotion in jederlei Hinsicht mit Rat und Tat unterstützte. Besonders hervorheben möchte ich, dass seine Tür für mich immer offen stand und er mir dann stets mit wertvollen Hinweisen weiterhelfen konnte. Durch die zahlreichen Forschungsreisen, Konferenzen und Workshops konnte ich viele interessante Themen kennenlernen und hervorragende Vorträge hören. Mein Dank gilt auch der pQCD-Gruppe für die wöchentlichen Treffen.

Prof. Dr. Werner Vogelsang für die großartige Zusammenarbeit. Durch seine große Erfahrung, sein umfangreiches Wissen und seine exzellenten Ideen wurde die Arbeit in großen Schritten vorangetrieben. Unvergessen bleiben die zahlreichen Besuche in Tübingen. Die vielen Diskussionen und Gespräche trugen dazu bei die mitunter komplexen Rechnungen zu meistern. Herzlichen Dank auch an den gesamten Lehrstuhl, bei dem ich mich immer sofort willkommen gefühlt habe.

Prof. Dr. Daniel de Florian sowohl für seine inhaltlichen Beiträge als auch für die Bereitstellung seines Codes und den MonteCarlo-Simulationen.

C. Höppner, B. Ketzer und den anderen COMPASS-Mitgliedern für die gute Zusammenarbeit.

Monika Maschek für ihre große Hilfe in allen organisatorischen Dingen und den Systemadministratoren für ihre Unterstützung bei Hard- und Software.

Meinen (ehemaligen) Kollegen Clemens Bauer, Matthias Aicher, Simon Heybrock, Florian Gruber und Matthias Kronseder, für all die Zeit die wir miteinander verbracht haben.

Meinen Eltern für ihre einzigartige Unterstützung, ihr Verständnis und ihre Ermunterungen, Danke vielmals! Meinen Geschwistern Thomas, Christine, Andreas, Matthias, Tobias und Florian für ihr Interesse und ihre Hilfe in verschiedensten Dingen.

Cynthia Karl für das Korrekturlesen der Arbeit und alles andere!

Der Studienstiftung des deutschen Volkes für die finanzielle Förderung während der Promotion. Zudem wurde diese Arbeit unterstützt vom “Bundesministerium für Bildung und Forschung” (BMBF).